

UNITED STATES DEPARTMENT OF THE INTERIOR  
GEOLOGICAL SURVEY

The Kola Superdeep Drill Hole by Ye. A. Kozlovskiy (1984):

A detailed summary

BY

James W. Clarke, Robert C. McDowell, John R. Matzko, Paul P. Hearn,  
Daniel J. Milton, Donald J. Percious, Dorothy B. Vitaliano, and  
Gregory Ulmishek

Open File Report 86-517

This report is preliminary and has not been reviewed for conformity with  
U.S. Geological Survey editorial standards and stratigraphic nomenclature.

**REPRODUCED FROM BEST AVAILABLE COPY**

1986

## PREFACE

In 1984 a book was published in the USSR that summarized in detail the results of the drilling and scientific studies up to that time of the Kola Superdeep Drill Hole on the Kola Peninsula. The bibliographic reference for this book is: Kozlovskiy, Ye. A., 1984, Kol'skaya sverkhglubokaya: Moscow, "Nedra," 490 p.

The U.S. Geodynamics Committee of the National Academy of Sciences asked the Academy's Continental Scientific Drilling Committee for a summary of this book. The request was transmitted to the U.S. Geological Survey, where the various chapters were summarized by the following persons:

Foreword, p. 4-18, James W. Clarke  
General geology, p. 19-65, Robert C. McDowell  
Rocks and rock-forming minerals, p. 66-101, John R. Matzko  
Geochemistry, p. 102-177, Paul P. Hearn  
Mineralization, p. 178-214, Daniel J. Milton  
Gases, organic matter, hydrogeology, p. 215-282, Donald J. Percious  
Geophysics, p. 283-327, James W. Clarke  
Magnetic properties, p. 328-374, Dorothy B. Vitaliano  
Drilling, p. 375-480, Gregory Ulmishek

A full translation of this book is being prepared by Springer Verlag. We hope that this review will so stimulate the reader's interest that he will avail himself of the opportunity to read the entire book when it is published.

We gratefully acknowledge the assistance of Juanita J. Page of Deep Observation and Sampling of the Earth's Continental Crust, Inc. and Teddy A. Clevenger of the U.S.G.S. for preparing the copy.

James W. Clarke  
Summary editor

## CONTENTS

	Page
Foreword -----	1
General geology -----	11
Rocks and rock-forming minerals -----	29
Geochemistry -----	37
Mineralization -----	75
Gases, organic matter, hydrogeology -----	91
Geophysics -----	137
Magnetic properties -----	147
Drilling -----	201

## ABSTRACT

Drilling of the Kola Superdeep well (SG-3) was begun in May, 1970 on the Kola Peninsula above the Arctic Circle in northwestern U.S.S.R. This book presents the main results of studies to its present depth of 11,600 m. The work is divided into three parts: geology, geophysics, and drilling.

Geology. The area of drill hole SG-3 is underlain by ancient igneo-metamorphic rocks of the Baltic shield. Archean crystalline basement is overlain by Proterozoic metamorphosed sedimentary and volcanic rocks.

The Archean consists of the Kola Series and is divided into two sequences: biotite-plagioclase and biotite-amphibole-plagioclase gneisses and amphibolites at the base, and biotite plagioclase and muscovite-biotite-plagioclase gneisses containing high-alumina minerals (sillimanite, kyanite, garnet) above.

The Proterozoic in drill hole SG-3 consists of metamorphosed tholeiitic metabasalt, metapyroxenite, metaperidotite, metatuffs, and a variety of metasedimentary rocks (sandstones, arkoses, carbonates) of the Pechenga Complex.

Drill hole SG-3 is located in the Pechenga copper-nickel sulfide district. The greatest concentrations of ore minerals were found in zones of pyrrhotite mineralization of the Pechenga Complex. Commercial-grade copper-nickel ore was found in the 1665-1830 m depth interval. Three types of ores are found in the Pechenga Complex: disseminated ores in altered peridotite, breccia ores in disturbed zones, and veinlet and disseminated ores in phyllites. Ultramafic intrusives are doubtless the source of copper-nickel ores.

The downward increase in temperature of metamorphism is accompanied by a transition from brittle to ductile deformation. However, one of the unexpected findings was a wide distribution at all depths of fissures with various mineral fillings. It was found that mineralized zones of crushing, cataclasis, fracturing, and low temperature hydrothermal alteration, including sulfide mineralization, extend to depths 3 or 4 times what had been expected.

Gas content of drilling mud and of cores was measured. Anomalous high concentrations of all components were detected down to 11,500 m. Methane content decreased with depth from 0.05% in the Proterozoic rocks to 0.03-0.01% in the Archean rocks. Helium content tends to increase with depth.

Drill hole SG-3 penetrates an ancient Proterozoic artesian basin. Gravitational water is distributed throughout the entire section of metamorphic rocks, marking the first time that ground water has been found under such conditions. This water is similar to deep metamorphosed marine connate water of ancient platforms and intermontane basins.

Ground water in the 0.8-7 km interval is of the sodium-chloride composition, salinities increasing with depth and reaching saturation in some intervals. Water in the 4.5-9 km interval is not connected hydraulically with the overlying zone; the water level immediately rose 80 m when this zone was penetrated. Below 7 km depth the water becomes calcium-chloride and calcium-sodium-chloride type. A constant inflow of water was observed during drilling.

Crustal development in the region of drill hole SG-3 was in two great cycles: the Archean (older than 2.6 billion years) including two stages: 1) sedimentation and volcanism, and 2) folding, metamorphism, and ultrametamorphism; and Proterozoic (2.6-1.1 billion years) including four stages: 1) subsidence of mobile belt, 2) andesite-basalt volcanism, 3) picrite basalt volcanism, and 4) folding and metamorphism.

The Conrad surface was not detected in the drill hole; a migmatitic plagioclase gneiss is present where the basaltic layer was expected. A continental crust comprising three layers is indicated: granite gneiss (0-15 km), granulite gneiss (15-30 km), and a protocrust (30-40 km). Extrapolation of geochemical trends down to 35 km suggests that the protocrust was formed from rocks close to sodic dacite in composition.

Geophysics. These investigations included well logging, density and porosity-permeability, acoustical properties, electrical properties, magnetic properties, radioactivity, heat flow, and mechanical properties.

The following logs were made in drill hole SG-3: acoustical, laterolog, resistivity, spectrometric-gamma, gamma, neutron, impulse neutron-neutron, magnetic, electrical potential, spectrometric neutron-gamma, gamma-gamma, selective gamma-gamma, thermal properties, caliper, vertical seismic profiling, and gas logs. At a depth of 11 km the variation in the length of the cable may be 20 m. This was compensated by adjusting logs to marker horizons.

Values of porosity of the Proterozoic meta-igneous and metasedimentary rocks are in the 0.4 to 0.6 percent range, and permeability is in the 0.3 to 1.2 md range. Archean gneisses have a porosity of 1% and permeability of 16 md.

The average longitudinal wave velocity with natural moisture for the Proterozoic metasediments is 5.67 km/s, and that for the Archean rocks is 3.99 km/s. The idea that velocity of rocks of the same composition increases with depth is not confirmed. Maximum values are found in the upper part of the section.

Magnetic susceptibility of the basaltic volcanics lies within a narrow range regardless of extent of metamorphism. Maximum values of this parameter are found for meta-trachybasalt schists and serpentized peridotites. Minimum values are characteristic of dolomites and quartzites.

Natural remanent magnetization in the Archean rocks is in general lower than in the Proterozoic rocks. Maximum values were recorded in serpentized peridotites of the Pechenga Complex.

The ratio of natural remanent magnetization to induced ( $Q$ ) ranges from 0.1 to 29 and correlates with the composition of the magnetic minerals.

Drill hole SG-3 is divided into three zones on a basis of magnetic characteristics. The depth interval 0-4586 m is a zone of sulfide mineralization, and the rocks are weakly magnetic except for the ultramafics. The 4586-5642 m depth interval corresponds with a zone of oxide mineralization and is characterized by higher magnetic susceptibility. The 5642-10,500 m depth interval is a zone of weakly magnetic rocks; concentrations of pyrrhotite and magnetite are small.

Radioactivity was measured both in the drill hole and on samples. Uranium and thorium content of rocks was determined in the laboratory. Data were also obtained on the average life time of thermal neutrons.

The geothermal gradient increases with depth from 1-1.1°C/100 m in the upper part of the Pechenga complex to 1.7-2°C/100 m in the lower part at a depth of 6000-7000 m.

The following physical properties were measured on core samples; static Young's modulus, static Poisson's ratio, compressive strength, tensile strength, hardness, plasticity, and abrasivity.

An abrupt decrease in longitudinal and transverse wave velocities and in rock density is observed at a depth of 4500 m. This coincides with the boundary between the greenschist and epidote-amphibolite metamorphic facies. The deep seismic interfaces are caused by secondary transformations leading to a change in physical properties rather than by lithologic variability of the rocks.

Various stress fields are recognized in the section. These suggest that there is a clearly expressed horizontal layering in the crust, related not to extensive horizontal displacements but to changes in local conditions and mechanisms of deformation of the various deep horizons.

Drilling. A turbo drill was used in the project. Calculations indicate a significant advantage of turbo drilling over rotary drilling at depths greater than 10 km. Rates of 100-200 rotations per minute appear optimum. Steel is used for the upper 1.5-2 km of the drill string; then aluminum.

Actual drilling time was 21.7 percent of total time at 0-2000 m, whereas it was only 3.1 percent at 10,000-11,500 m. Drilling rate ranged from 1.3 to 2.5 m/hour. A total of 3700.1 m of core was recovered.

## Foreword

The Communist Party of the Soviet Union and the Soviet Government at all stages of development of the state have given particular attention to strengthening the mineral resource base of the country and to improving exploration methods. For example, the economic plan for 1981-85 and on to 1990 confirms the importance of accelerated geological study of the country. This study naturally is affected by fundamental understandings of systematic distributions of mineral resources in the deep subsurface, by new scientific ideas, and by their implementation.

The present book addresses one of the most important problems of modern Earth Science - a study program of the deep subsurface. Spudding in the Kola Superdeep well marked the beginning of a new stage in the study of the Precambrian continental crust. The well is located in the northeast part of the Baltic shield in an area of junction of ore-bearing Precambrian structures typical of the basement of ancient platforms. The well is now at a depth of 12,000 m. It has passed through the entire Proterozoic section and a considerable part of the Archean. Drilling continues. The present work presents briefly the main results of studies to a depth of 11,600 m in three sections: geology, geophysics, and drilling.

The first part of the book examines the geology of the well site; core and the wall rock of the drill hole are described in detail. Then data are given on the petrography and geochemistry of the Precambrian complex, metamorphic zones, vertical ore zonality, faults, gases, organic matter, subsurface waters, and finally the evolution of the continental crust for about 3 billion years.

The second part treats geophysical studies of the Kola well: physical properties along the section and the nature of geophysical interfaces. Techniques for study of rock properties were developed.

The third part deals with the drilling process to a depth of 11,600 m. The scientific-methodological basis for the drilling is presented, and the drilling equipment is described. The technical-economic results of the drilling are interpreted. The main tendencies and variations in the drilling processes with depth are analyzed, as are means for improving the technology for further deepening of this unique well.

The importance of mineral resources in the modern world increases constantly. Oil, gas and atomic raw materials are required more and more as a source of energy. The use of aluminum and titanium, light metals, particularly molybdenum, and also manganese, chromium, and nickel are increasing. Agriculture requires phosphates and potassium minerals. Electronics and space technology cannot develop without using rare metals. Economic potential depends ever more on mineral resources, and these requirements continue to grow.

Exploration for new mineral resources has turned to the shelves of continents beneath the seas and the floor of the ocean. Depth of exploration on the continents has increased (fig. I.1). Oil and gas are produced from depths of 5 to 6 km. Some gold mines are at depths of more than 3 km. Even iron ore is worked at a depth of 1 km at Krivoy Rog, and ore reserves are extended to 2.5 km depth. Most new deposits now being found have no surface expression.

Study of the deep subsurface of the USSR can be divided into three stages. The first was during the Sixties when plans were made to drill to 10 to 15 km. The second was during the Seventies with experimental drilling in the Kola and Saatli superdeep wells. The third stage, beginning in 1981, is directed toward coordinated study of the crust and upper mantle of the entire country.

The objectives are the study of:

- a) Sedimentary cover of deep depressions on cratons
- b) Sedimentary section of geosynclines
- c) Composition and structure of the lower part of the granitic layer, nature

↳ of the Konrad discontinuity, and composition of the basaltic layer

- d) Nature of the M-discontinuity, composition of the upper layers of the upper mantle
- e) Processes of differentiation in the crust
- f) Magma chambers
- g) Solutions and gases in the crust
- h) Geothermal regime of the crust

1960-69. A group was organized that addressed "Study of the subsurface and superdeep drilling." It coordinated about 200 scientific and industrial agencies, 4 academicians and 15 corresponding members of the Academy of Sciences, USSR; 5 academicians and 6 corresponding members of Academies of the republics; 70 doctors; and 65 candidates [candidate is commonly equated with Ph.D.]. More than 80 conferences and 75 inquiry sessions were held. The Kola and Saatli sites were selected during this time.

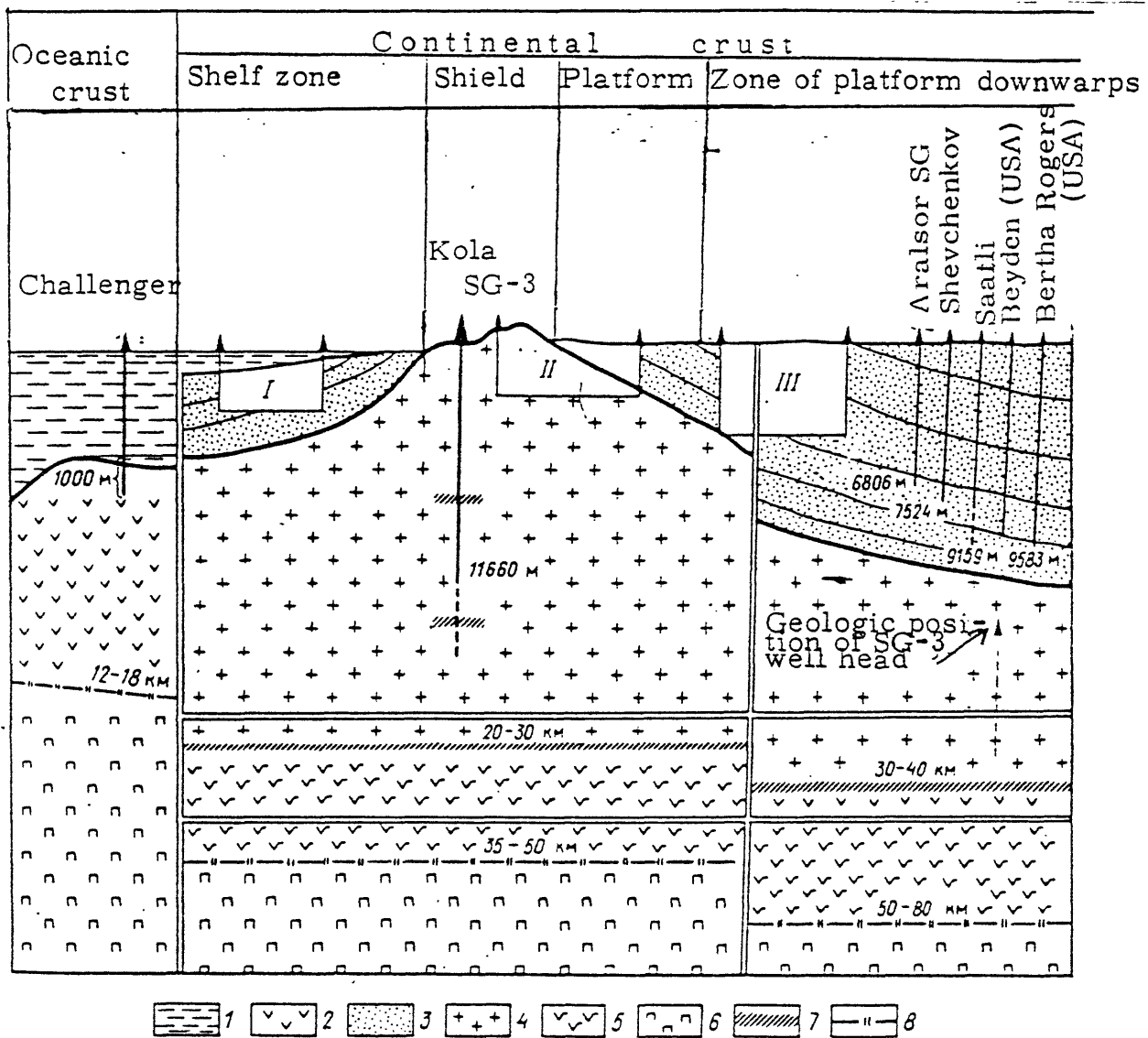


Figure I.1.--Schematic section of crust from deep drilling data.

Deep exploration drilling: I - in the shelf zone, II - for solid mineral resources, III - oil and gas wells.

1 - Hydrosphere; 2 - oceanic basalts; 3 - Phanerozoic sedimentary and sedimentary-volcanic rocks (age of 500 m.y.); 4 - Precambrian crystalline rocks of "granite" layer (age of 1,000-3,000 m.y. and more); 5 - rocks of continental "basaltic" layer; 6 - rocks of the mantle; 7 - high-velocity layer - Conrad discontinuity ( $v_p = 6.6-6.8 \text{ km/s}$ ); 8 - M-discontinuity ( $v_p = 8.0 \text{ km/s}$ ).

1970-80. The program for the Seventies included development of a model of the crust and mantle, new methods of predicting mineral deposits, compilation of resource assessment maps, and planning for exploration in favorable regions of the country. The program for 1976-80 included 198 projects directed toward solution of applied problems related to fundamental theoretical analysis of the deep subsurface.

The lead agency is the Ministry of Geology, and more than 150 scientific and industrial organizations are involved.

Drilling of Kola SG-3 (fig. I.2) was begun in May 1970. The purposes were:

- 1) Study of the deep subsurface of the nickeliferous Pechenga complex and Archean crystalline substrate of the Baltic shield.
- 2) Clarification of the geologic nature of seismic interfaces in the continental crust, and gaining new data on the thermal regime and on deep aqueous solutions and gases.
- 3) Obtaining information on the composition and physical properties of rocks, and study of the boundary between the granitic and basaltic layers of the crust.
- 4) Improvement and creation of new deep-drilling and geophysical-logging techniques.

By 1980 geophysical surveys had been completed in several of the regions; 18,000 km of deep-seismic-sounding had been run. The relief of the M-discontinuity and the pre-Riphean surface had been mapped in East Siberia. New information was obtained on the upper mantle for the East European and Siberian cratons and the platforms and foldbelts that surround them. Velocity sections to 400 km were compiled.

Kola Superdeep reached a depth of 10.7 km in 1980.

The composition and properties of the rocks were found to change systematically with depth. Vertical zonality in the metamorphic rocks was found to be different from the theoretical model.

Geothermal gradient was found to be steeper than, had been anticipated. The role of mantle and radiogenic sources in deep heat flow was determined.

The vertical geochemical section of the crust to a depth of 11.6 km disclosed a systematic variation with depth in the silicity and alkalinity of the rocks as well as in the behavior of metallic, rare, and radioactive elements.

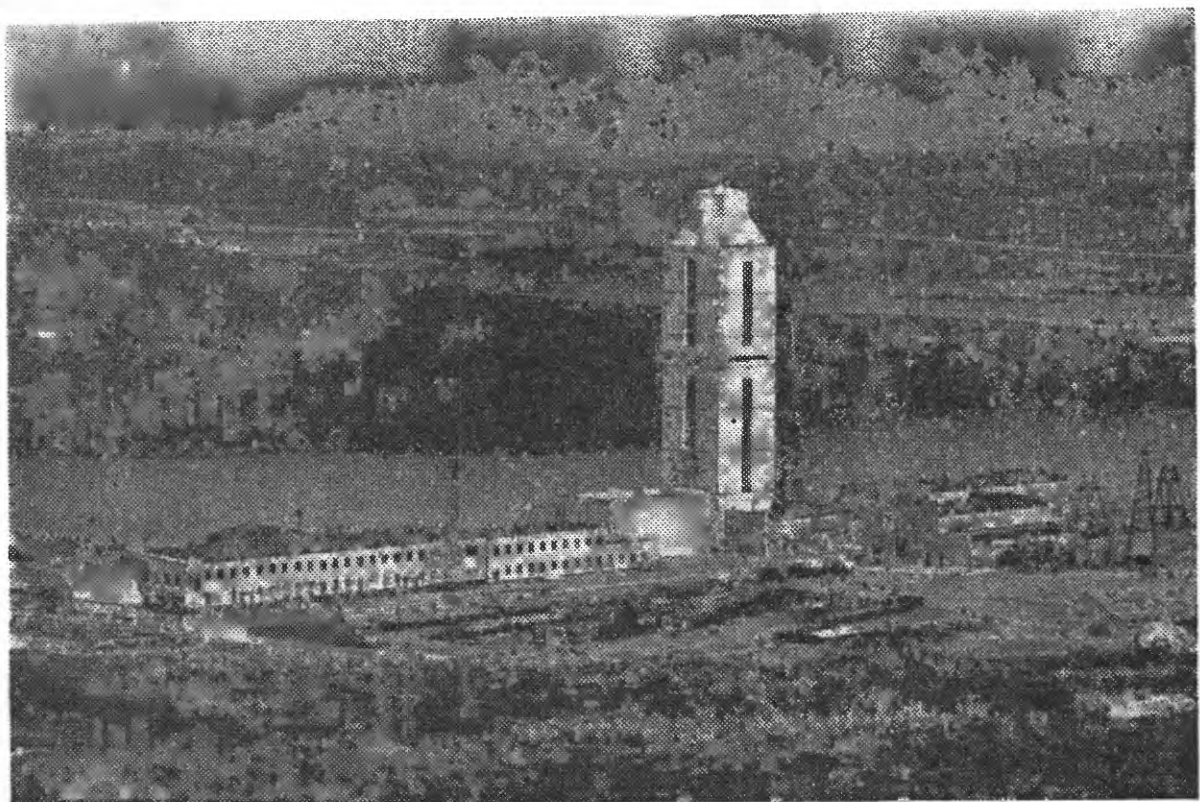


Figure I. 2. Kola superdeep, general view.

Commercial-grade copper-nickel ore was found in the 1665-1830 m interval. In the 6,500-9,500 m depth interval is a zone of copper-lead-nickel mineralization.

Unexpected was the occurrence at great depth of very porous, fractured rocks saturated by water. High permeabilities were also found. These disclosures are important for toxic waste disposal.

Kola Superdeep did not confirm the geophysical basaltic layer at 7,000-7,500 m depth; rather, dense Archean gneisses were present on through this level. This calls for a new look at the geophysics.

Yet another superdeep well, Saatli, was begun in 1977 in the Kura depression of Azerbaijan; it is on a long-known gravity high. The supposition was that this anomaly was due to a local uplift on the top of the basaltic layer. The hole passed through unconsolidated Cenozoic and upper Mesozoic sediments and then into a thick volcanic section apparently of Cretaceous age. These volcanic rocks are clearly the source of the gravity maximum.

Drilling rigs in world practice are rated for a lift capacity of 6-8 MN and a pump pressure of 50 mpa (mega-pascals). Depth, however, does not exceed 9,100-9,600 m. Greater depths do not seem possible. The Soviet rigs with less lift capacity (5 MN) and injection pressure (40 mpa) are capable of depths greater than 10 km.

New drilling equipment was designed by Uralmashzavod (figs. I.3, I.4).

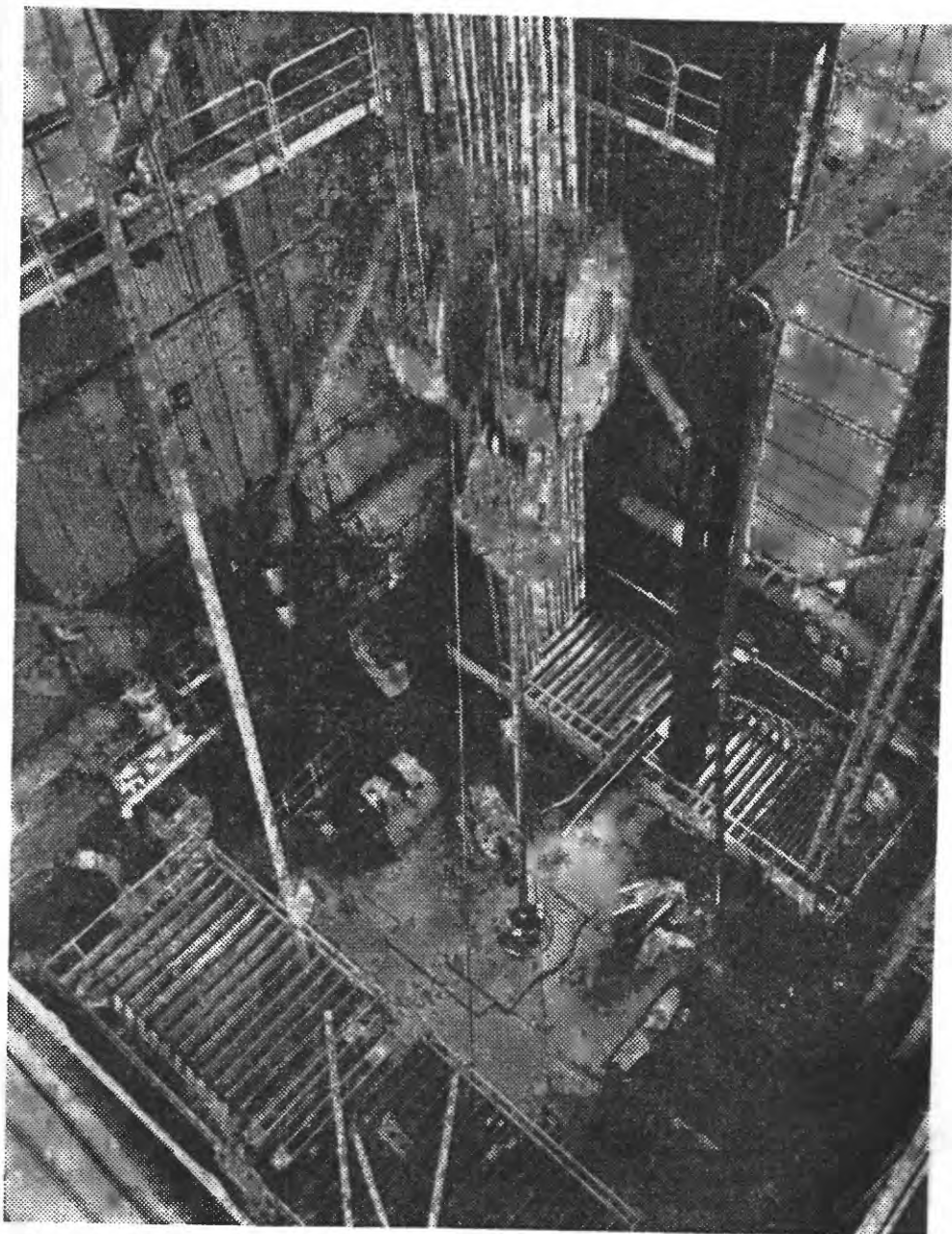
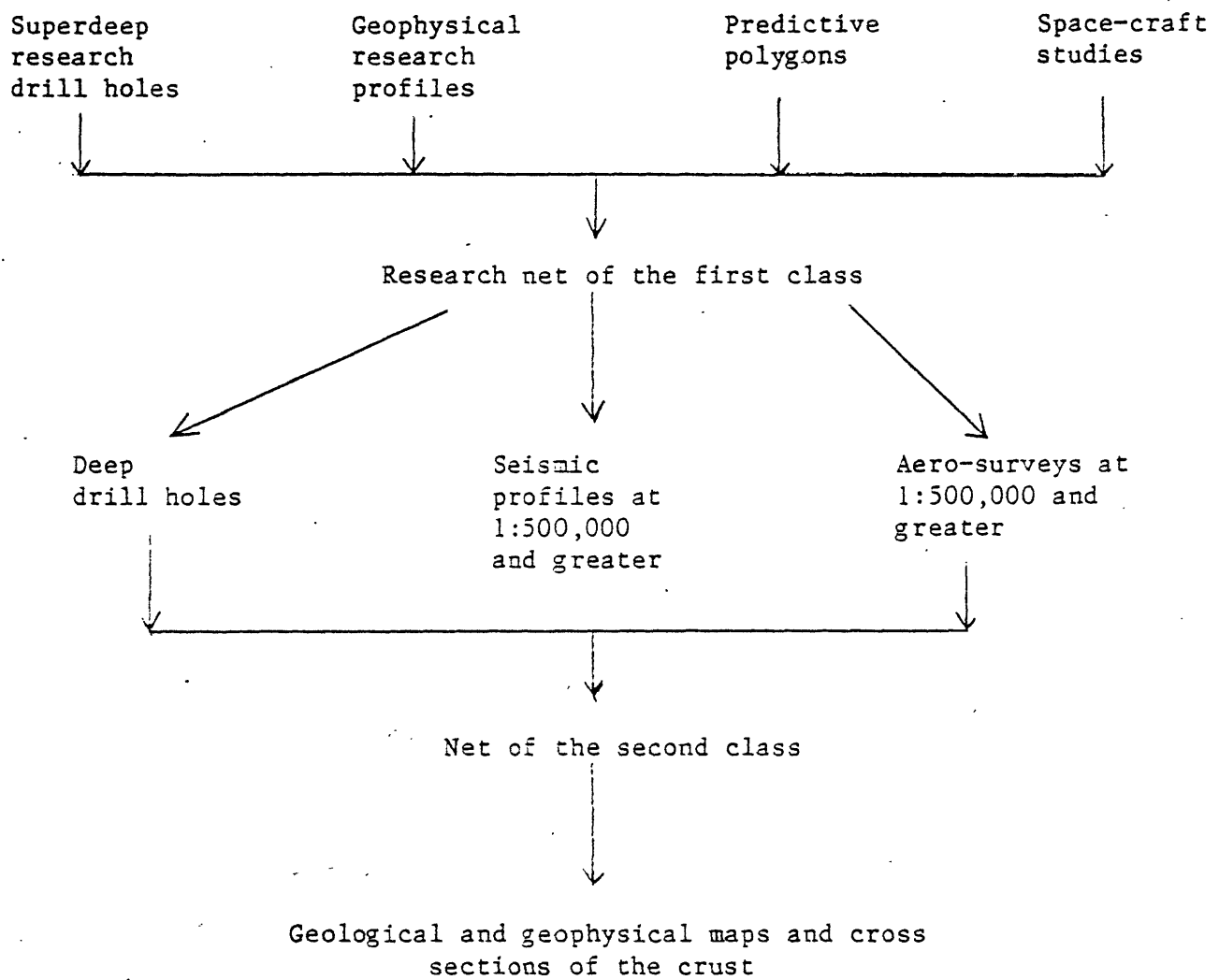


Figure I.3. Lowering of drill string into well.



Figure I.4. Core recovery.

1981-85. A new stage in the study of the deep subsurface began in the Eleventh Five Year Plan. A net of interrelated geophysical activities is to be set up:



Deep and superdeep drilling will be expanded. Drilling of the Kola and Saatli holes will continue. The Tyumen, Anastas'yev-Troitsk, and Ural superdeep (12-15 km) holes will be begun. Drilling will also begin on six deep holes: Three (Dnieper-Donets, North Caspian, Timan-Pechora) in oil patches and three (Muruntau, Noril'sk, and Krivorozh) in mining regions.

Kola Superdeep will reach 13,000 m during the Eleventh Five Year Plan and will intersect another geophysical interface, which may turn out to be the granite-basalt boundary. Saatli will be deepened to 11,000 m.

Drilling of the Tyumen superdeep hole will give information on the oil-gas potential of the Jurassic and pre-Jurassic section of the north of West Siberia. The Ural superdeep will yield information on a very large ore-bearing foldbelt.

At the time the Soviets were planning these operations, the Americans proposed an ocean drilling program. This program became international, and Soviet scientists participated. Thus, there are two programs: The Soviet on the continents and the international in the oceans, supplementing one another.

## General Geology

### GEOLOGY OF THE NORTHEAST PART OF THE BALTIC SHIELD

The Baltic Shield,  $1,140,000 \text{ km}^2$ , is the largest area of exposed crystalline basement of the East-European Platform. The Kola Peninsula occupies the northeast part of the Baltic Shield.

#### Geology of the Kola Peninsula

The Kola Peninsula is composed mainly of Precambrian crystalline rocks (Fig. I, 6) which extend into Finland, Sweden, and Norway. These rocks are Archean gneisses with metamorphosed sodic-calcic granitoids and Proterozoic metamorphosed sediments and volcanics. The Archean rocks have been dated as no less than 2700 m.y. and possibly as much as 3600 m.y. Mineral resources include iron, titanium, copper, nickel, rare-earth metals, pegmatites, apatite, nepheline, and others.

#### Subsurface Geology of the Kola Peninsula

The main source of data on the subsurface is from deep seismic sounding and seismic reflection studies. The average depth of the Mohorovicic discontinuity on the Kola Peninsula is 37 km with a range of 28 to 40 km (Fig. I, 7). The most important boundaries above the M-discontinuity are the Konrad discontinuity, at the top of the granulite-basite or basalt layer, and another at the top of the diorite layer.

#### Geology of the area of corehole SD-3

The area of the corehole is composed of ancient crystalline rocks, metamorphosed to various degrees, characteristic of Precambrian of the Baltic Shield (see Fig. I, 8. in pocket). Of continuing interest to geologists in this area are copper-nickel deposits associated with Proterozoic ultrabasic intrusions. The following Precambrian complexes are recognized in this area: Archean, forming the folded basement and in tectonic blocks; and Proterozoic, composed of metamorphosed sedimentary and volcanic rocks.

#### Archean

In the area of corehole SD-3 the Archean Kola Series is divided into two sequences: biotite-plagioclase and biotite-amphibole-plagioclase gneiss and amphibolite at the base, and biotite-plagioclase and muscovite-biotite-plagioclase gneiss with high-alumina minerals (staurolite, andalusite,

sillimanite, kyanite, garnet), and rarely interbeds of amphibolite, above. The lower sequence locally contains interbeds of magnetite-garnet-quartz feldspar schist and ferruginous quartzite, which are generally no more than 20-30 m thick. The gneisses are irregularly granitized locally with formation of migmatite. The rocks of the Kola Series are metamorphosed mainly to the amphibolite facies.

### Proterozoic

The Proterozoic section consists of sedimentary and volcanic rocks of the Pechenga and Varzug complexes and the Tundrov Series adjacent on the south. The Proterozoic rocks directly overlie folded Archean gneisses of the basement in a transgressive sequence with conglomerate at the base.

#### Results of deep geophysical studies in the area of corehole SD-3.

The first studies in the Soviet Union on the crust in shield areas were deep seismic sounding studies in the Kola Peninsula in 1960-1963 (Fig. I, 9). Crustal thickness in the vicinity of the corehole was shown to be about 40 km. The early seismic work showed a total thickness of 7-8 km for the sedimentary-volcanic rocks, and essentially no granitic layer. Reflection seismology was later used to determine the structure to depths of 10-15 km. A gravity survey was made in 1967-1969, which confirmed the conclusions of the seismic work.

The Kola superdeep corehole should answer many questions about the Baltic Shield and the crust in general, such as:

- 1) Stratigraphic subdivision of the Proterozoic and especially the Archean: age, thickness, structure.
- 2) Composition of the sedimentary-volcanic "superstructure" above the Archean basement.
- 3) Test the presence of deep ore horizons.
- 4) Sequence of metamorphic processes in the Precambrian.
- 5) Vertical zonation of hydrothermal mineralization.
- 6) Decrease in rock fracture with depth.
- 7) Gas emanations, and depth of water-bearing horizon, related to the preceding question.
- 8) Paleotemperatures and the present thermal gradient.
- 9) Lithostatic pressures with depth.
- 10) Nature of geophysical boundaries.

#### GEOLOGIC SECTION OF THE COREHOLE

The results of study of the core have been compiled in geologic and geophysical columnar sections (Fig. I, 10, 11, 12, 13). The hole penetrated the Pechenga sedimentary-volcanic complex and at 4700 m entered Archean gneisses, and at 7-8 km depth encountered the high-velocity layer, granulite-basite (Fig. I, 14).

#### Stratigraphic subdivision of the section

Tables I, 1, 2 present specific depths at which contacts were picked for the individual suites of the Pechenga Complex (Lower Proterozoic) and Kola Series (Archean).

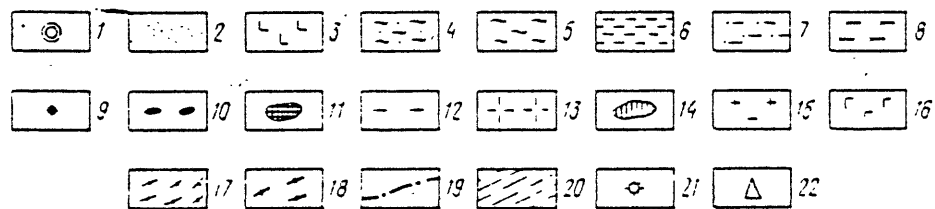
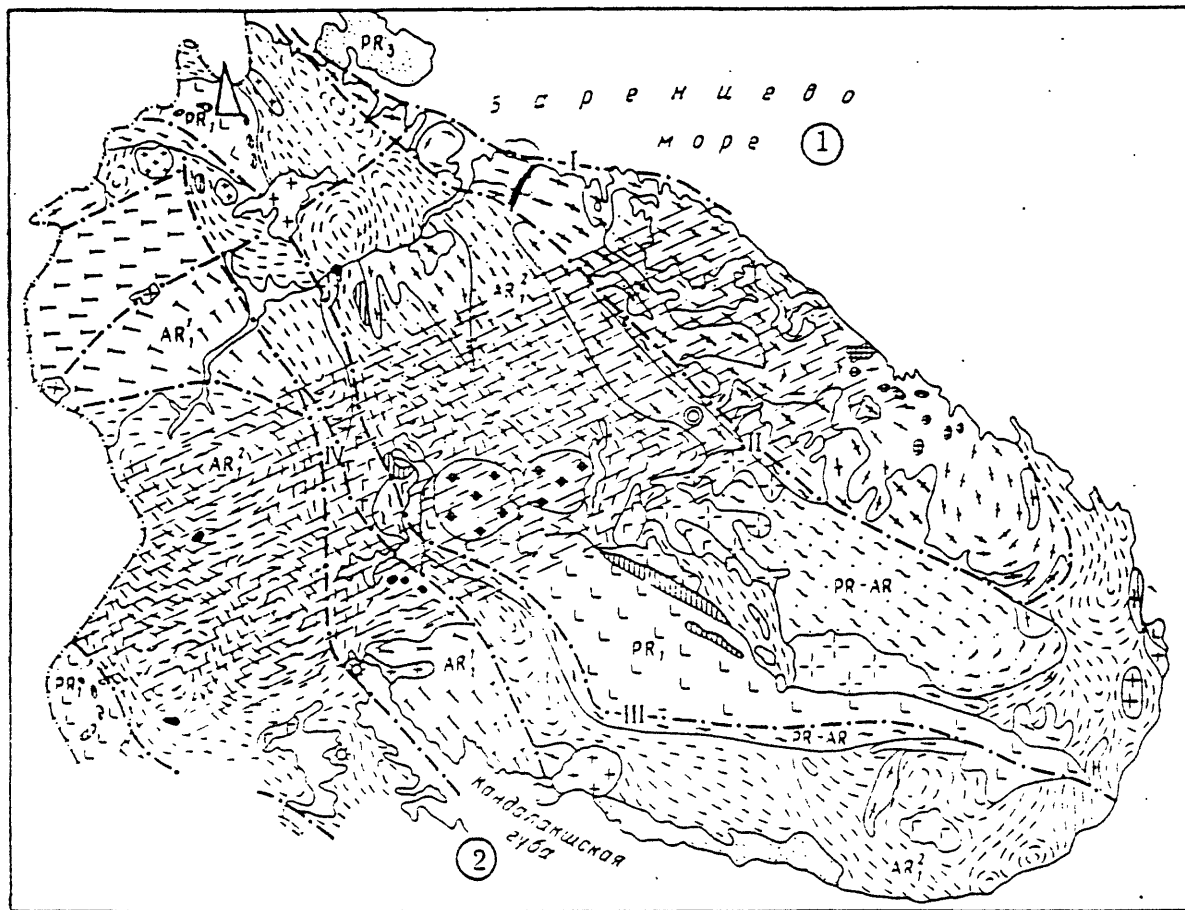


Figure I, 6

Fig. I, 6.--Geologic map of the Kola Peninsula. Paleozoic: 1) Upper Devonian and Lower Carboniferous, sedimentary-volcanic complex of the Kontozer structure. Upper Proterozoic; 2) formations of the Hyperboreal Series of the Rybach'ev Peninsula: conglomerate, sandstone, shale; Srednii Peninsula, Kil'dina and Terskaya Islands: quartzite, sandstone, variegated shale, dolomite. Lower Proterozoic: 3) Pechanga, Imandra-Varzug, and Kuolayarvin complexes: basic, medium, and ultrabasic lavas, tuffs, minor phyllite, siltstone, sandstone, dolomite, and conglomerate, metamorphosed mainly to greenschist facies. Lower Proterozoic-Upper Archean: 4) Keiva Series: aluminous, carbonaceous, micaceous, and other schists, quartzites, and sandstones, metamorphosed mainly to epidote-amphibolite facies; 5) Tundrov Series: amphibolitic, micaceous, aluminous schists and gneisses, amphibolite, ferruginous quartzites, metamorphosed mainly to epidote-amphibolite facies. Lower Archean, Kola Series: 6) biotite-plagioclase, biotite-amphibole-plagioclase, two-mica gneisses biotite-plagioclase gneiss with HAM (high-aluminum minerals), amphibolite; mainly amphibolite facies; 7) biotite-plagioclase gneiss with HAM, amphibolite, pyroxene-amphibolite-plagioclase gneiss and schist, ferruginous quartzite, mainly amphibolite facies; 8) granulite complex: cordierite-garnet-biotite-plagioclase gneiss pyroxene-amphibole-plagioclase gneiss and schist, amphibolite and migmatite, charnockite, enderbite, mainly in granulite facies. Intrusive and ultrametamorphic complexes: Middle Paleozoic (Upper Devonian): 9) silicic nepheline syenite complex; Lower Paleozoic: 10) basic, ultrabasic and alkaline rocks; Upper Proterozoic; 11) gabbro, diabase, granophyre; Lower Proterozoic; 12) granite, granodiorite; 13) alkaline granite syenite; 14) gabbro, gabbronorite, pyroxenite, peridotite, olivinite; Upper Archean; 15) granite, granite-migmatite; 16) gabbro-anorthosite, metagabbro-norite; Lower Archean; 17) granite, granite migmatite; 18) granodiorite, granite-gneiss, plagiogranite; 19) major faults (I. Karpinsk; II. Keiva-Uragub; III, Pechenga-Varzug; IV, Lapland-Kolvits); 20) zone of maximum Caledonian activity; 21) explosion vents; 22) Kola superdeep corehole

Key: 1) Barents Sea

2) Kandalak Bay

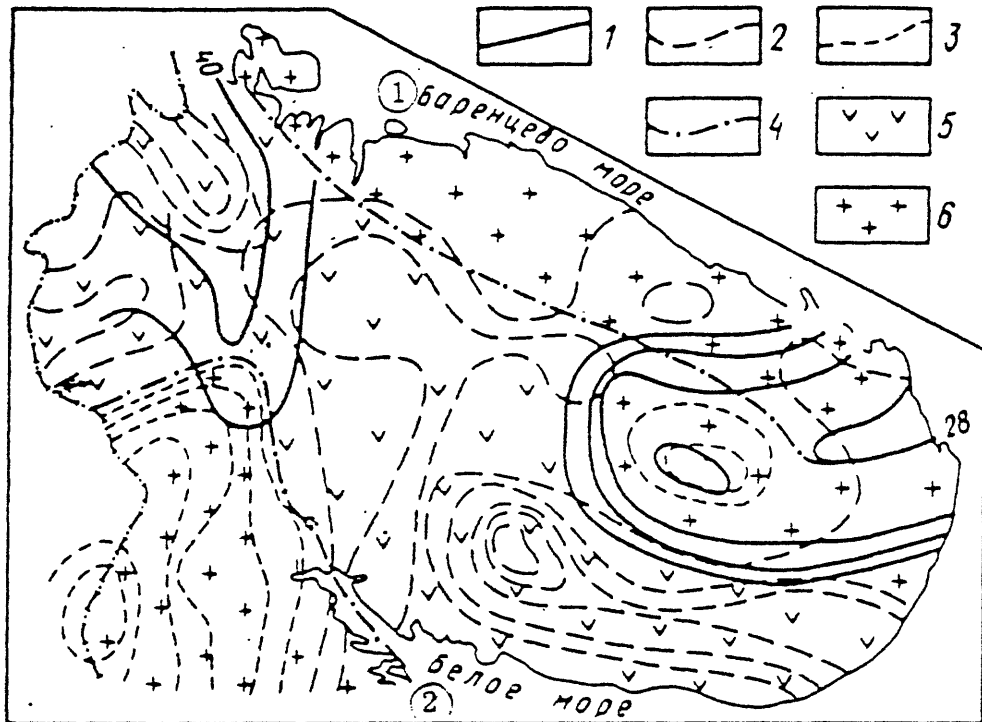


Fig. I, 7.--Subsurface geology of the Kola Peninsula. 1) contours on the M-discontinuity (in km); 2) isolines of increase in force of gravity field; 3) isolines of relative decrease in gravity force field; 4) major faults; 5) simatic crust; 6) sialic crust.

Key: ① Barents Sea

② White Sea

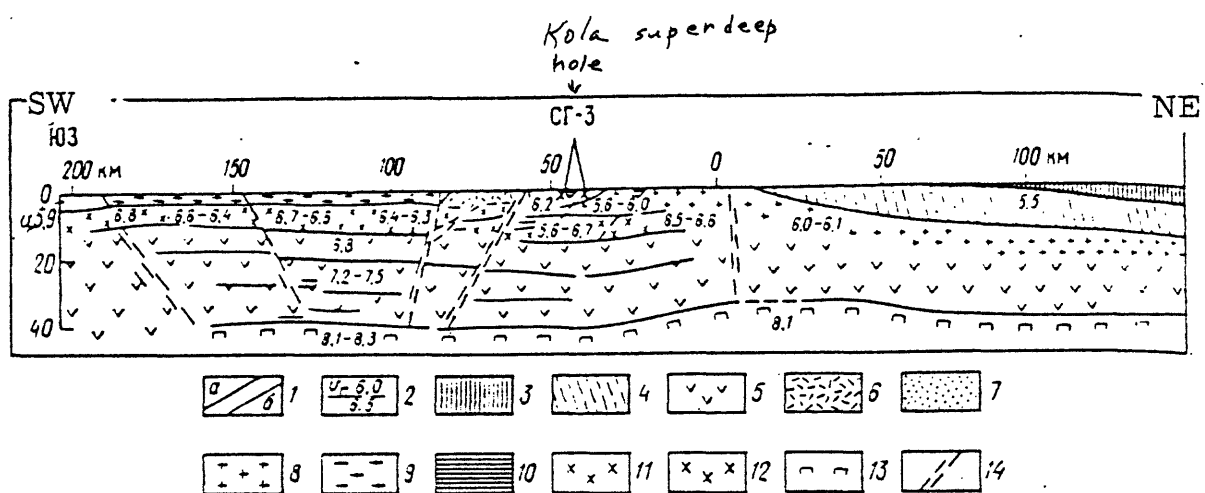
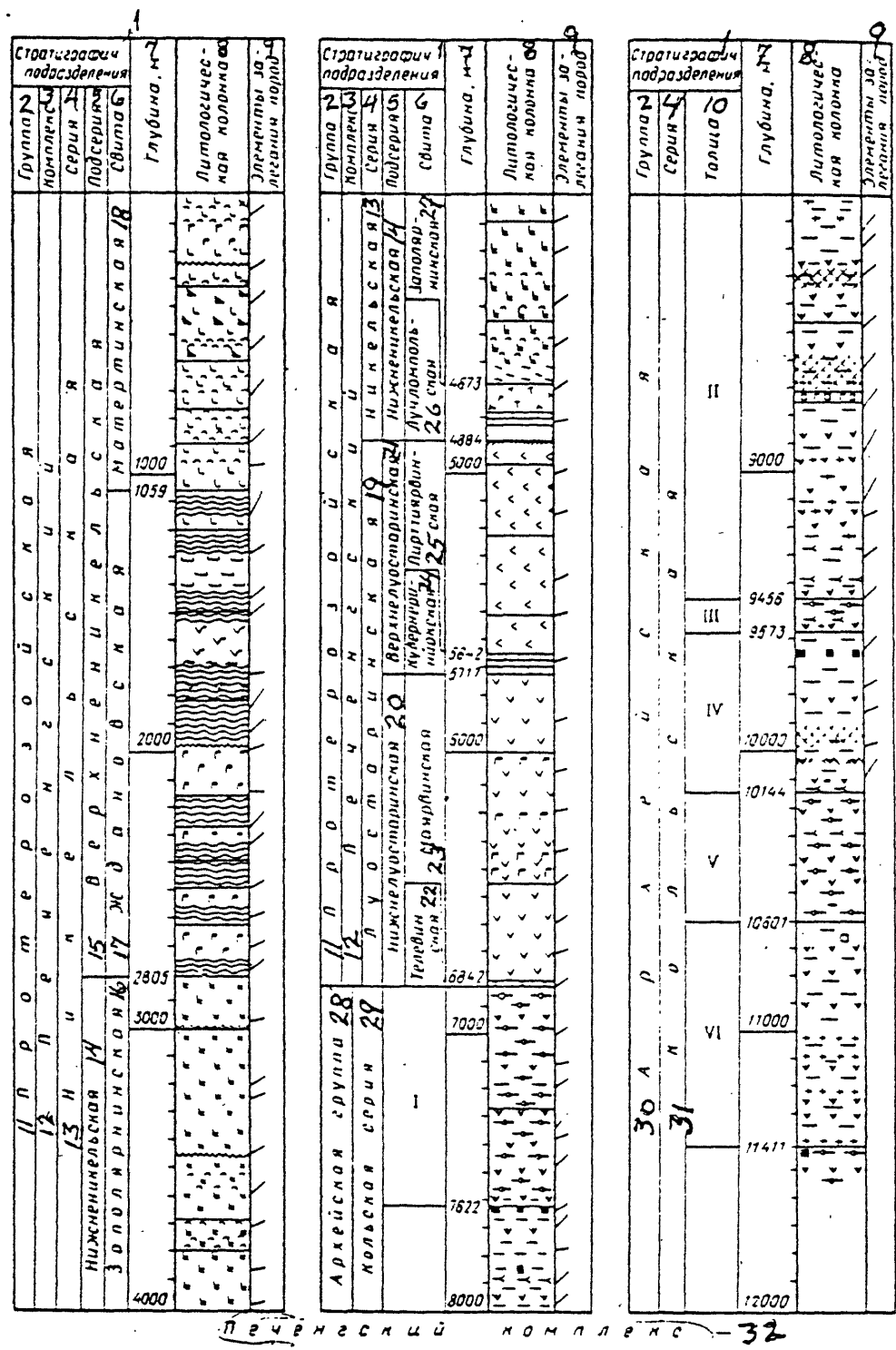


Fig. I, 9.--Seismic section of the crust along the profile Lovno-Pechenga-Barents Sea. 1) Average position of reference (a) and other (b) seismic boundaries; 2) velocity (upper, average; lower, boundary; km/sec); 3) Phanerozoic sedimentary rocks; 4) same, Riphean; 5) lower part of the "basaltic" layer; 6) schist and amphibolite; 7) gneiss complex; 8) gneiss, granite gneiss, granite; 10) basic and ultrabasic intrusions; 11) middle non-uniform part of the basaltic layer; 12) Pechenga sedimentary-volcanic series; 13) upper mantle; 14) fault.



Печерский комплекс - 32

A horizontal row of ten numbered boxes, each containing a small black outline of a shape for the student to draw over.

КОЛЬСКАЯ. СЕРИЯ 29

— 20 — 21 v v 22 — 23 + + 24 r r 25 — 26 ■ ■ 27 o o 28 x x 29

Fig. I, 10.--Columnar section of the Kola Superdeep corehole (SD-3). Pechenga complex: 1) augite diabase., 2) basic tuff; 3) pyroxenitic and picritic porphyrite; 4) rhythmically bedded phyllite, siltstone, sandstone, tuffite, and tuff; 5) rhythmically bedded sandstone with minor siltstone and phyllite; 6) actinolitized diabase; 7) amphibole and biotite-chlorite schist with ultrabasic tuff; 8) dolomite; 9) arkosic sandstone; 10) sericite schist (weathering rind); 11) meta-diabase, meta-andesite, meta-albitophyre, with banded lava, tuff, and greenschist; 12) dolomite, marble, and polymictic sandstone; 13) diabasic porphyrite, biotite-amphibole-plagioclase schist in andesite-basalt; 14) polymictic conglomerate, gravelite, sandstone; 15-18) intrusives; 15) andesitic porphyrite; 16) gabbro-diabase; 17) essexitic gabbro; 18) wehrelite; 19) sulfide copper-nickel ore. Kola series: 20) biotite-plagioclase gneiss, schist with HAM (high alumina minerals); 21) biotite-plagioclase and biotite-amphibole-plagioclase gneiss, schist; 22) amphibolite; 23) talc-biotite-actinolite schist (in ultrabasic rocks); 24-26) intrusives: 24) plagiomiccline granite, pegmatite; 25) metagabbro; 26) plagiogranite and dark migmatite; 27-29) ore; 27) magnetite; 28) titano-magnetite; 29) cataclastic and mylonitized zones. Sequences: I) muscovite-biotite-plagioclase gneiss with HAM (andalusite, staurolite, sillimanite, garnet); II) biotite-plagioclase and biotite-amphibole-plagioclase gneiss and amphibolite; III) muscovite-biotite-plagioclase gneiss with HAM (silliminate, garnet); IV) biotite-plagioclase and biotite-amphibole-plagioclase gneiss and amphibolite; V) muscovite-biotite-plagioclase gneiss with HAM (kyanite, sillimanite, garnet); VI) biotite-plagioclase gneiss and amphibolite

Key:	1) Stratigraphic subdivision	17) Zhdanov
	2) Group	18) Matertin
	3) Complex	19) Luostarin
	4) Series	20) Lower Luostarin
	5) Subseries	21) Upper Luostarin
	6) Formation	22) Televin
	7) Depth, m	23) Mayarvin
	8) Lithologic column	24) Kuvernerinuok
	9) Attitude of rock	25) Pirttiyarvin
	10) Sequence	26) Luchlompol
	11) Proterozoic	27) Zapolyarnin
	12) Pechenga	28) Archean Group
	13) Nickel	29) Kola Series
	14) Lower Nickel	30) Archean
	15) Upper Nickel	31) Kola

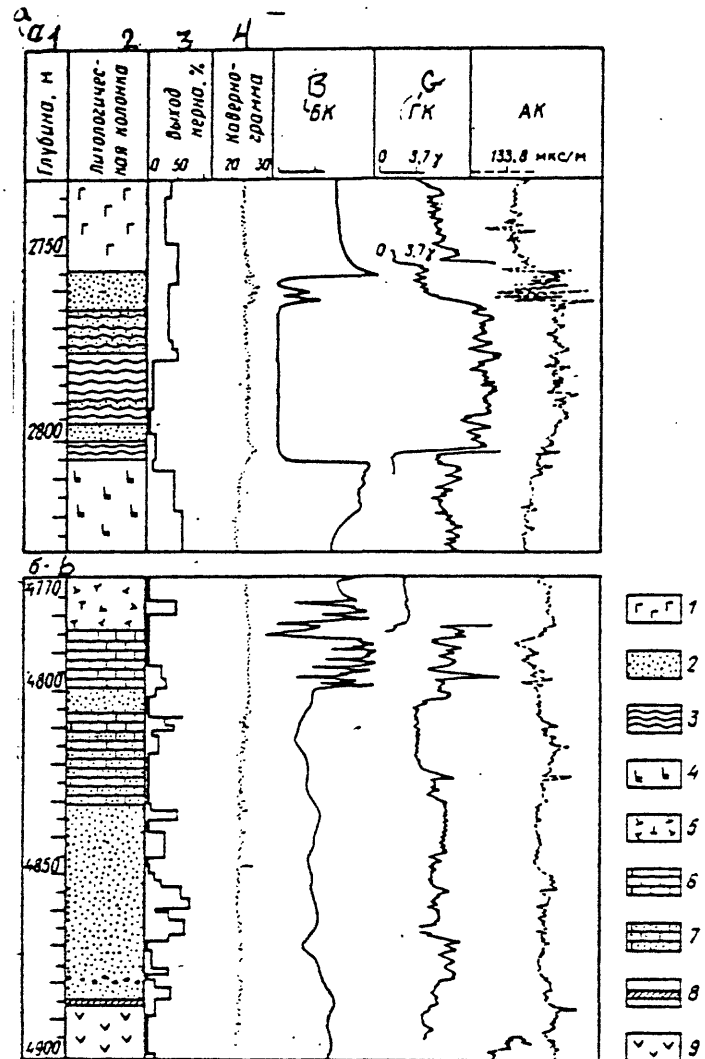


Fig. I, 11 --Parts of Kola corehole SD-3 in the intervals 2730–2830 m (a) and 4770–4900 m (b).

1) Gabbro-diabase; 2) sandstone; 3) phyllite; 4) diabase, actinolitized; 5) andesitic porphyry, 6) dolomite; 7) dolomitic sandstone; 8) sericitic schist (weathered rind); 9) schistose diabase.

Key: 1) Depth, M

2) Lithologic column

3) Amount of core, %

4) Calliper

Fig. I, 12.--Parts of the Kola corehole SD-3 in the intervals 10,550-10,640 m (a) and 11,360-11,460 m (b). 1-3) biotite-plagioclase gneiss; 1) with HAM, 2) with kyanite, sillimanite, garnet, 3) with garnet, sillimanite; 4) biotite-amphibole-plagioclase gneiss; 5) amphibolite; 6) talc-biotite-actinolite-schist (in ultrabasic rocks); 7) granite; 8) pegmatite.

Key: ① Depth, M

БК - Laterolog

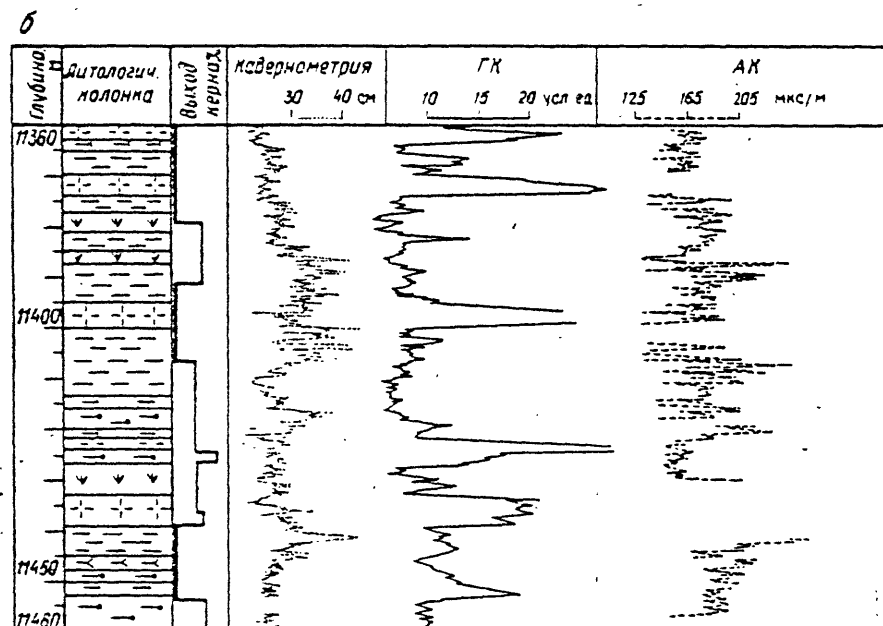
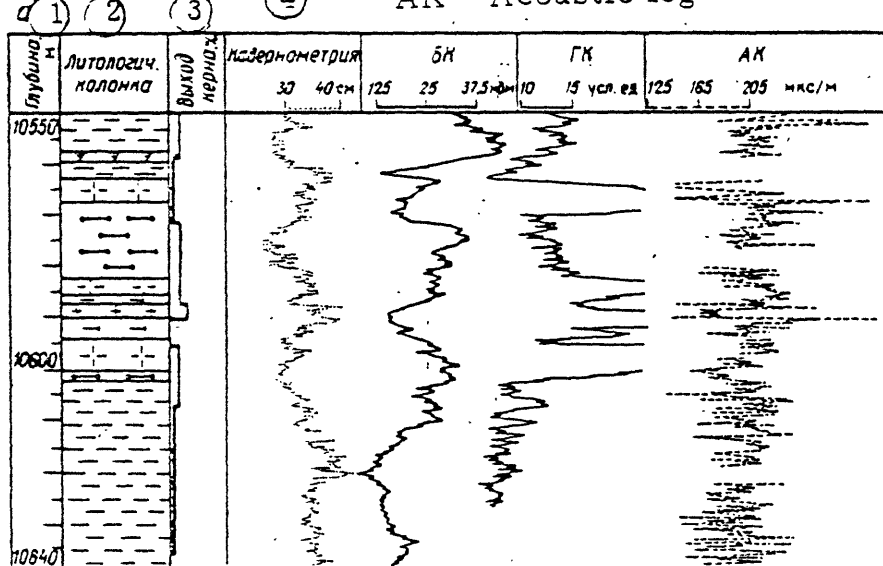
② Lithologic column

ГК - Gamma log

③ Amount of core, %

④ AK - Acoustic log

④ Calliper



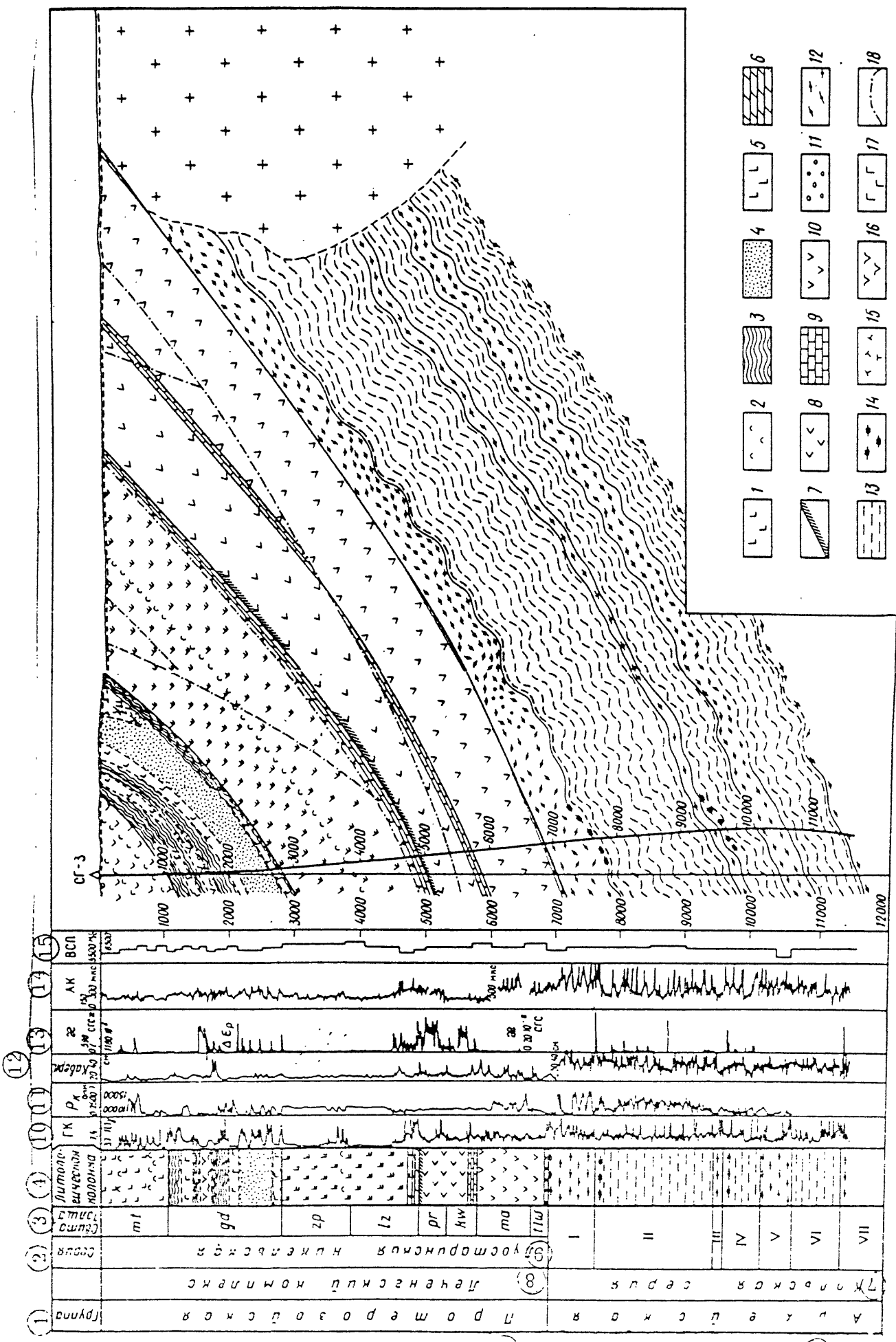
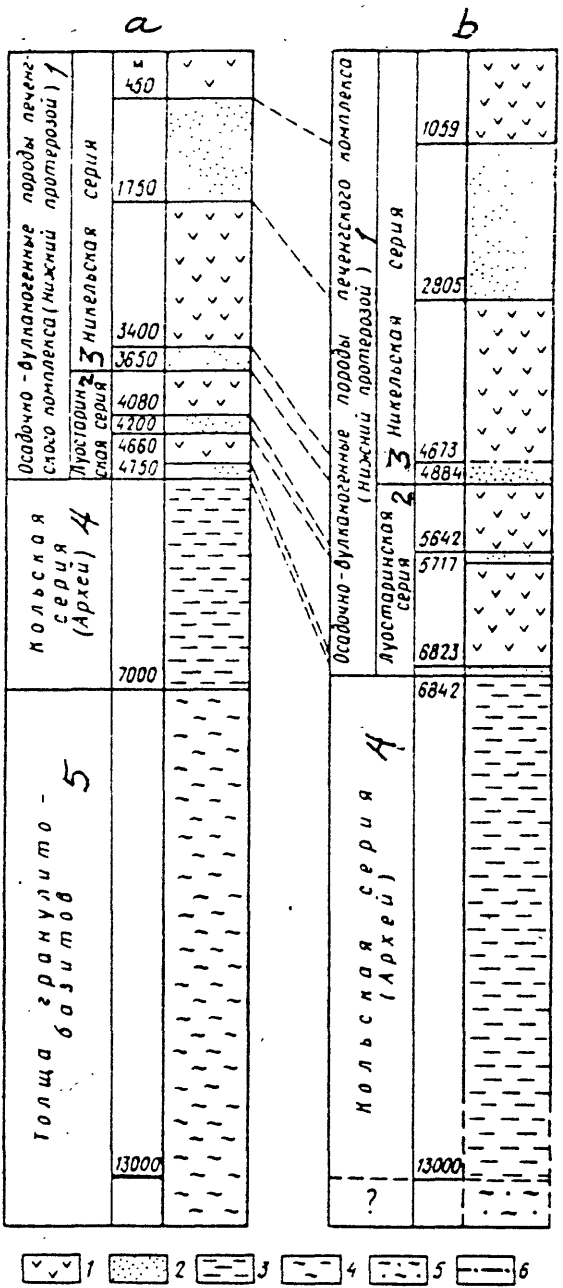


Fig. 1, 13

Fig. I, 13.--Geologic and geophysical section of Kola corehole SD-3.

1) Augite diabase with pyroxene and picrite porphyry interbeds;  
2) tuff and tuffite of basic composition; 3) phyllite, siltstone,  
with tuff interbeds; 4) rhythmically bedded sandstone with lesser  
siltstone and phyllite; 5) actinolitized diabase; 6) dolomite,  
arkosic sandstone; 7) sericit schist; 8) metadiabase; 9)  
dolomite, polymictic sandstone; 10) diabasic porphyry and  
schist; 11) polymictic conglomerate, gravelite; 12) biotite-  
plagioclase gneiss with HAM; 13) migmatized and granitized  
biotite-plagioclase gneiss; 14) magnetite-amphibolite schist; 15-  
18) intrusives: 15) andesitic porphyry, 16) wehrlite, 17) gabbro-  
diabase (dagger: granite), 18) fault. Sequences I, III, V, VII:  
muscovite-biotite-plagioclase gneiss with HAM (andalusite,  
staurolite, sillimanite, garnet) with amphibolite bodies;  
sequences II, IV, VI: biotite-plagioclase gneiss, biotite-  
amphibole-plagioclase gneiss and amphibolite.

Key:	(1) Group	(10) Gamma log
(2)	Series	(11) Resistivity log
(3)	Suite, sequence	(12) Caliper log
(4)	Lithologic column	(13) [?]
(5)	Archean	(14) Acoustical log
(6)	Proterozoic	(15) Vertical seismic profile (?)
(7)	Kola series	
(8)	Pechenga Complex	
(9)	Luostarin, Nickel	



**Fig. I, 14.** Comparison of the section at corehole SD-3 as projected from seismic studies (a) and from the core (b). 1) effusive rocks of mainly basic composition; 2) sedimentary rocks; 3) gneiss, granite gneiss, and amphibolite; 4) granulitic basalt; 5) gneiss and amphibolite in a high metamorphic facies; 6) fault.

**Key:** 1) Sedimentary-volcanic rocks of the Pechenga Complex (Lower Proterozoic)

- 2) Luostarin Series
- 3) Nickel Series
- 4) Kola Series (Archean)
- 5) Granulite-basite sequence

See next page for translation.

ТАБЛИЦА II  
СТРАТИГРАФИЧЕСКОЕ РАСЧЛЕНЕНИЕ ПЕЧЕНГСКОГО КОМПЛЕКСА  
(НИЖНИЙ ПРОТЕРОЗОЙ) ПО РАЗРЕЗУ СКВ СГ-3

1 Серия	2 Самта	3 Интервал бурения, м	4 Характеристика пород	5 Вертикальная толщина, м
22 Никольский	Матергин- ская (mt)  Жданов- ская (gd)	6 9—1059 1059—2803	7 Диабазы шаровых и массивных лав с подчиненными прослоями туфов, пикритовых и пироксеновых порфиритов  8 Тонкоритмичные алевролиты, филлиты с прослоями туфов и песчаников. Олигомиктовые и полимиктовые песчаники с прослоями конгломератов, филлитов и алевролитов	1050  1746
	Заполяр- нинская (zp)  Лучлом- польская (lz)	10 2805—4673 11 4673—4884	10 Актинолитизированные диабазы шаровых и массивных лав с подчиненными прослоями туфогенных пород 11 Доломиты, доломитовые песчаники, аркозовые песчаники с прослоями алевролитов	1863  211
		12	13	
23 Луостаринский	Пирттияр- винская (pr)  Куверне- ринийокская (kw)	14 4884—5642 15 5642—5717	14 Метадиабазы, метаандезиты, сланцы по диабазам и андезитам, в т. ч. полосчатым лавам 15 Тремолит-карбонатные сланцы, мраморизованные известняки, кварцито-песчаники	758  75
	Маярвии- ская (ma)  Телевин- ская (lw)	16 5717—6823 18 6823—6842	16 Амфибол-плагиоклазовые и биотит-амфибол-плагиоклазовые сланцы (по диабазам) 18 Метапесчаники и метагравелиты	1106  19
		20 21		

Table I, 1.--Stratigraphic subdivision of the Pechenga Complex (Lower Proterozoic) at corehole SD-3.

- Key: 1) Series  
2) Formation  
3) Interval  
4) Characteristics of the rock  
5) Vertical Thickness, m  
6) Matertin (mt)  
7) Diabase, spheroidal and massive lava with minor interbeds of tuff, picrite, and pyroxene porphyries.  
8) Zhanov (gd)  
9) Finely rhythmic siltstone, phyllite, with interbeds of tuff and sandstone. Oligomictic and polymictic sandstone with interbeds of conglomerate, phyllite, and siltstone.  
10) Zapolyarnin (zp)  
11) Actinolitized diabase, spheroidal and massive lava with minor interbeds of tuffaceous rocks  
12) Luchulompol' (lz)  
13) Dolomite, dolomititic sandstone, arkosic sandstone with interbeds of siltstone  
14) Pirttiyarvin (pr)  
15) Metadiabase, meta-andesite, schist in diabase and andesite, including banded lava  
16) Kuverneriniok (kw)  
17) Tremolite-carbonate schist. limestone marble, quartzose sandstone  
18) Mayarvin (ma)  
19) Amphibole-plagioclase and biotite-amphibole-plagioclase schist (in diabase)  
20) Televin (tlw)  
21) Metasandstone and metagravelite  
22) Nickel  
23) Luostarin

ТАБЛИЦА 12

СХЕМА СТРАТИГРАФИЧЕСКОГО РАСЧЛЕНЕНИЯ КОЛЬСКОЙ СЕРИИ  
(АРХЕЙ) ПО РАЗРЕЗУ СКВ. СГ-3

№ толщи	1 Интервал бурения, м	2 Характеристика толщ	3	4 Вертикальная мощность, м
I	6842—7622 <i>5</i>	Мусковит-биотит-плагиоклазовые гнейсы с ВГМ (андезит, ставролит, силиманин, гранат)		780
	6842—7271 <i>6</i>	Верхняя часть толщи — мусковит-биотит-плагиоклазовые гнейсы с ВГМ		430
	7271—7622 <i>7</i>	Нижняя часть толщи — мусковит-биотит-плагиоклазовые гнейсы с ВГМ и телами амфиболов		350
II	7622—9456 <i>8</i>	Биотит-плагиоклазовые и биотит-амфибол-плагиоклазовые гнейсы и амфиболиты		1830
	7622—8465 <i>9</i>	Верхняя часть толщи — биотит-плагиоклазовые гнейсы и амфиболиты преимущественно с куммингтонитом		840
	8465—9456 <i>10</i>	Нижняя часть толщи — биотит-плагиоклазовые, биотит-амфибол-плагиоклазовые гнейсы и амфиболиты		990
	9456—9573 <i>11</i>	Мусковит-биотит-плагиоклазовые гнейсы с ВГМ (силиманин, гранат)		120
IV	9573—10144 <i>12</i>	Биотит-плагиоклазовые гнейсы и амфиболиты		570
V	10144—10301 <i>13</i>	Мусковит-биотит-плагиоклазовые гнейсы с ВГМ (кианит, силиманин, гранат)		460
VI	10601—11416 <i>14</i>	Биотит-плагиоклазовые гнейсы		820
	11416—11862 <i>15</i>	Биотит-плагиоклазовые гнейсы с ВГМ (гранат, силиманин) и амфиболитов с гранатом		250

Table I, 2.--Stratigraphic subdivision of the Kola Series (Archean) at corehole SD-3.

- Key: 1) Sequence no.  
2) Interval, m  
3) Characteristics of the sequence  
4) Vertical thickness. m  
5) Muscovite-biotite-plagioclase gneiss with HAM (andalusite, staurolite, sillimanite, garnet).  
6) Upper part of sequence: muscovite-biotite-plagioclase gneiss with HAM  
7) Lower part of sequence: muscovite-biotite-plagioclase gneiss with HAM and amphibolite bodies  
8) Biotite-plagioclase and biotite-amphibole-plagioclase gneiss and amphibolite  
9) Upper part of sequence: biotite-plagioclase gneiss and amphibolite, principally with cummingtonite  
10) Lower part of sequence: biotite-plagioclase, biotite-amphibole-plagioclase gneiss and amphibolite  
11) Muscovite-biotite-plagioclase gneiss with HAM (sillimanite, garnet)  
12) Biotite-plagioclase gneiss and amphibolite  
13) Muscovite-biotite-plagioclase gneiss with HAM (kyanite, sillimanite, garnet)  
14) Biotite-plagioclase gneiss  
15) Biotite-plagioclase gneiss with HAM (garnet, sillimanite) and amphibolite with garnet

## Rocks and Rock-Forming Minerals

Volcanic, sedimentary and intrusive rocks, metamorphosed to varying degrees, as well as ultrametamorphic rocks, occur in the section penetrated by the SG-3 drillhole. The upper part of the section is represented by a Proterozoic metamorphosed sedimentary-volcanic complex and the lower part by an Archean polymetamorphic complex.

### Metamorphic and Intrusive Rocks of the Pechenga Complex

Basic volcanic rocks make up more than 70 percent of the Pechenga Complex, the remainder being composed of intermediate and ultramafic volcanics and tufogenic-sedimentary rocks. The latter includes tuffs, welded tuff breccias, conglomerates, gritstones, sandstones, siltstones, pelites, and carbonates. On the basis of mineral composition and paragenesis, the intensity of the regional metamorphism increases with depth, from prehnite-pumpellyite to epidote-amphibolite with local appearances of amphibolite facies.

### Volcanic Rocks

Diabasic volcanic rocks occur in the Matertin, Zapdyarnin, Mayarvin, Pirttiyarvin, and Zhdanov Formations.

Magmatic structures and minerals occur in the volcanic rocks in the upper part of the section, while a combination of primary magmatic features and neogenetic metamorphic structures and minerals occur in the middle part, and neogenetic metamorphic minerals, structures, and textures in the lower part of the section. The rocks are not uniformly metamorphosed, and the mineral composition is usually heterogeneous. Massive rock varieties yield to schistose varieties at depth.

Basalts are composed of pyroxene-augite and volcanic glass, with occasional laths of albitized plagioclase. Diabases are composed mainly of pyroxene-augite, salite, plagioclase, with rare hornblende and quartz.

The volcanic rocks in the section suggest two types of volcanic activity: trachy-andesite basalts (Mayarvin and Pirttiyarvin Formations), and picritic basalts higher up in the section (Zapolyarnin and Matertin Formations).

### Sedimentary-Rocks

Tufogenic-sedimentary rocks include tuffs, tuff breccias, and tuffites (Matertin, Zhdanov, Zapolyarnin and Pirttiyarvin Formations). Phyllite and

phyllitic shales, siltstones, sandstones, sedimentary breccias, carbonates, gritstones, and conglomerates are present in the Zhdanov Formation. Ore minerals here include pyrite, pyrrhotite, sphene, and leucoxene. The Luchlompol Formation contains widely developed arkosic sandstone, siltstone, conglomerate, gritstone, and carbonate. The rocks of this formation are enriched in hematite and magnetite. The carbonates are enriched in tourmaline, rutile, anatase, and apatite. The Kuverneriniok Formation contains quartzites, meta-sandstones, siltstones and carbonates. Some rock varieties are enriched in allanite. The Televin Formation includes conglomerates and micaceous sandstones. Carbonaceous matter is found in phyllite and siltstones of the Zhdanov Formation, tuffogenic rocks in the Matertin Formation, and sedimentary rocks of the Luchlompol and Kuverneriniok Formations.

#### Intrusive Rocks

Intrusive rocks include ultrabasites, gabbro-diabases, and andesite-dacite porphyry. The ultrabasites are werhlites and serpentinites; associated minerals are pyrrhotite, pentlandite, chalcopyrite, pyrite, magnetite, ilmenite, apatite, garnet, and chromite. Sulfide copper-nickel mineralization is found. Gabbro-diabases occur in the depth interval 93.3 to 2,754 m among rocks of the Matertin, Zhadonv, and Mayarvin Formations. Accessory and ore minerals are sulfides, magnetite, ilmenite, apatite, and sphene. There is also titanium (0.7%), chromium (0.02%), and vanadium (0.03%). Andesite-dacite porphyry occurs in the depth interval 4,673 to 4,784 m among rocks of the Luchlompol Formation.

#### Polymetamorphic Rocks of the Archean Complex

The Archean complex starts at a depth of 6842 m in the Kola Series, which is composed of gneisses with high-Al minerals, amphibolites, meta-ultramafites, granitized gneisses (plagio-granites, granites, pegmatites) and amphibolites. Small granite intrusions occur at 9,600 m.

#### Gneisses and Granitized Gneisses

Gneisses make up the larger part of the section penetrated. In the muscovite-biotite-plagioclase gneisses with high-Al minerals, the accessory minerals are apatite, magnetite, ilmenite, and zircon. The rock structure is lepidoheteroblastic, locally porphyroblastic. Biotite-plagioclase gneisses

with high-Al minerals have an insignificant admixture of Cr<sub>2</sub>O<sub>5</sub>, SrO, and BaO. Biotite is represented by three generations: Biotite from the granulite facies occurs at 10,222 m; biotite from the amphibolite facies occurs at all depths in the section in these rocks; and biotite from the epidote-amphibolite facies is also widely dispersed. Muscovite replaces biotite. Garnet occurs in two generations from the amphibolite facies and the epidote-amphibolite facies. Epidote is characteristic in biotite-plagioclase and granitized biotite-plagioclase gneisses, also forming two generations. Sphene also has two generations, the first being enriched in titanium.

#### Amphibolites

Three types of amphibolites are present in the drill-hole section. Hornblende amphibolite occurs along the entire section of the Archean. It is composed of hornblende with lesser amounts of plagioclase and biotite. Cummingtonite-hornblende-amphibolites are restricted mainly to biotite-plagioclase gneisses and alumina-amphibolites. The cummingtonite is replacing hornblende. The third type is an amphibolite transitional to hornblendite (ferruginous amphibolites). It is first noted at a depth of 8,465 m and is composed primarily of hornblende and plagioclase. At depths greater than 10,000 m garnet is present. The structure of the amphibolites is grano-nematoblastic.

#### Meta-ultramafites

The meta-ultramafites are ultrabasic rocks metamorphosed to actinolites and talc-actinolites. Actinolite is the most widespread and has an iron content of 22 to 23 percent (actinolite in talc-actinolite rocks has an even greater iron content). Actinolite is replaced by phlogopite, which is present in two varieties - iron-bearing (with a small admixture of titanium) and non-iron-bearing. The rock structure is lepidoblastic.

#### Rock Alterations in the Polymetamorphic Complex

In the Archean metamorphic structure, six processes are distinguished in the drillhole: Metamorphism of the granulite facies; regional metamorphism in the amphibolite facies contemporaneous with folding; retrogressive regional metamorphism in the epidote-amphibolite facies; regional granitization under the epidote-amphibolite facies - the formation of palgiognanites and granites together with gneisses by metasomatic means; local manifestation of

diaphthoresis in the greenschist facies along fracture zones; local low-temperature metamorphism along zones of cataclasis.

#### The Temperature of Metamorphism

To estimate the temperature of rock metamorphism, equilibrium pairs of minerals were used, which include amphibole-plagioclase; amphibole-biotite; garnet-biotite; muscovite-biotite; and plagioclase-potassium feldspar. The polymetamorphic Archean complex formed under a large range of temperatures. The temperature regime of metamorphism is: For the granulite facies, 1,000 to 1,200°C; for the amphibolite facies, 800 to 850°C (including regional metamorphism at 700 to 750°C); epidote-amphibole facies, 650 to 500°C (including granitization under the epidote-amphibole facies at 650 to 600°C).

#### Rock-Forming Minerals in the Subsurface Vertical Section

The age of the crust penetrated by the drillhole is 1.6 to 2.8+ b.y. The main rock types occurring in the Proterozoic section are metamorphosed magmatic rocks such as metabasalts (diabases and actinolite-diabases; apodiasitic-magnetite-amphibole-plagioclase schists; apodiasitic-amphibole-plagioclase schists), meta-andesites (apoandesitic magnetite-biotite-plagioclase schists), metapicrites, metagabbro, metawerhlite, and meta-sedimentary rocks (pelites, siltstones, sandstones, conglomerates, and carbonate rocks). The main rock types in the Archean are biotite-plagioclase gneisses, amphibolites, meta-ultramafites, plagiogranites, and granites. Biotite is found primarily in the Archean complex, at depths of 6,842 to 11,662 m. Garnets are found primarily in Archean gneisses. The composition and properties of the main types of rock-forming minerals of the metamorphic rocks were determined for their location in the drillhole's vertical section; this allows the possibility of estimating P-T conditions of the metamorphic rock at various stages of development.

ТАБЛИЦА I.4  
Table I.4

*Chemical composition of thin-stamped parts of the Reschovsky complex  
ХИМИЧЕСКИЙ СОСТАВ МИНЕРАЛОВ НА МЕТАБАЗИТОВ*

Diabase		Actinolite - diabase		Greenschist metasomatic facies		Apatite-Pumicite facies		Apatite-Plagioclase facies	
Диабаз		Диабаз активно-измененная		Зеленосланцевая фация метасоматизма		Апатит-амфиболовая фация метафорфизма		Апатит-плагиоклазовая фация метафорфизма	
Rock	Porphy.	Rock	Porphy.	Rock	Porphy.	Rock	Porphy.	Rock	Porphy.
Pyroxenite-Pumicite facies metamorphic facies	Sample 2305	Sample 9585	Sample 9508	Sample 9508	Sample 9508	Sample 19663	Sample 19663	Sample 21704	Sample 21704
Oxides	Rock	Porphy.	Actinolite Augite-Silicate	Actinolite Augite-Silicate	Actinolite Augite-Silicate	Plagioclase	Plagioclase	Plagioclase	Plagioclase
SiO <sub>2</sub>	47,70	48,90	47,42	54,98	64,11	49,49	49,25	62,56	54,04
TiO <sub>2</sub>	1,36	0,92	0,83	0,07	0	0,79	0,48	0,86	0,48
Al <sub>2</sub> O <sub>3</sub>	13,67	4,37	15,72	1,68	21,99	12,54	6,52	14,01	8,52
Fe <sub>2</sub> O <sub>3</sub>	2,01	3,05	3,23	1,41	—	6,66	3,16	1,15	4,09
FeO	12,01	10,50	9,70	1,27	—	8,91	14,59	—	13,02
MnO	0,20	0,25	0,17	0,18	—	0,17	0,35	0,15	0,30
MgO	7,00	14,66	7,00	15,97	—	6,62	10,66	—	5,72
CaO	6,30	16,20	9,50	12,84	3,13	9,65	11,11	5,32	11,88
Na <sub>2</sub> O	1,66	0,40	1,08	—	—	2,73	0,77	8,69	2,52
K <sub>2</sub> O	1,66	0,07	0,47	—	0,08	0,10	0,47	0,16	0,81
H <sub>2</sub> O-	0,22	—	—	—	—	—	—	—	0,19
He opn.	—	—	—	—	—	—	—	—	—
H <sub>2</sub> O <sup>+</sup>	—	—	—	—	—	—	—	—	—
P <sub>2</sub> O <sub>5</sub>	—	—	—	—	—	—	—	—	—
Summa	99,01	100,14	98,69	100,61	99,19	100,45	99,45	100,77	100,22

ПРИМЕЧАНИЯ. Аналитики: В. С. Ефимов, А. Б. Герман.  
Английский: Н. С. Беляев, Д. В. Герман

Pyroxene-bearing amphibolite (two-pyroxene-amphibole-plagioclase  
cognate schist)

Chemical composition of minerals from the main  
rock types of the Archean complex

Table 15  
ТАБЛИЦА 15

ХИМИЧЕСКАЯ СОСТАВ МИНЕРАЛОВ ИЗ ГЛАВНЫХ ТИПОВ ПОРОД АРХЕНСКОГО КОМПЛЕКСА

Oxides окислы	Гранулит-фации										Амфиболовые фации									
	Биотит-плагиоклазовый типа с ВГМ* и высоким содержанием железа					Биотит-плагиоклазовый типа с низким содержанием железа					Биотит-плагиоклаз-амфиболовый типа с кристаллическим стеклом					Биотит-плагиоклаз-амфиболовый типа с высоким содержанием железа				
	Биотит и обн. Biotite	Плагиоклаз 38-60% Plagioclase	Биотит 26-37% Biotite	Плагиоклаз 36-57% Plagioclase	Диопсид 36-65% Diopside	Гиперстен 36-65% Hypersthen	Диопсид 36-65% Diopside	Рутиловый пироксен и оливин Rutile pyroxene and olivine	Гранат и оливин Garnet and olivine	Биотит и обн. Biotite and olivine	Гранат и оливин Garnet and olivine	Биотит и обн. Biotite and olivine	Гранат и оливин Garnet and olivine	Биотит и обн. Biotite and olivine	Гранат и оливин Garnet and olivine	Биотит и обн. Biotite and olivine	Биотит и обн. Biotite and olivine	Гранат и оливин Garnet and olivine	Биотит и обн. Biotite and olivine	
SiO <sub>2</sub>	34,40	62,04	37,93	61,65	53,26	52,28	40,50	55,47	37,63	35,50	60,41	37,37	35,94	35,94	35,94	35,94	35,94	35,94	35,94	
TiO <sub>2</sub>	3,05	He обн.	2,36	He обн.	0,82	0,20	2,10	He обн.	1,88	He обн.	He обн.	1,94	He обн.	He обн.	He обн.	He обн.	He обн.	He обн.	He обн.	
Al <sub>2</sub> O <sub>3</sub> , Fe <sub>2</sub> O <sub>3</sub>	18,71	23,69	15,50	24,06	0,30	1,87	11,50	28,31	20,67	19,82	24,87	20,54	18,07	18,07	18,07	18,07	18,07	18,07	18,07	
FeO $\Sigma$ FeO	21,26	He обн.	19,56	"	He опр.	He опр.	19,77	6,79	0,83	1,14	He обн.	0,99	4,68	4,68	4,68	4,68	4,68	4,68	4,68	
MnO	0,43	"	0,28	"	0,06	0,14	0,38	He обн.	1,17	0,14	He обн.	1,26	0,22	0,22	0,22	0,22	0,22	0,22	0,22	
MgO	8,64	"	11,13	"	24,76	15,11	6,50	1,43	11,43	He обн.	1,27	8,74	8,74	8,74	8,74	8,74	8,74	8,74	8,74	
CaO	0,18	5,05	0,17	5,42	0,44	22,72	10,51	10,20	11,27	0,05	6,61	8,79	0,12	0,12	0,12	0,12	0,12	0,12	0,12	
Na <sub>2</sub> O	0,27	8,73	He обн.	8,71	He обн.	1,29	5,59	He обн.	0,30	7,86	He обн.	0,24	9,45	9,45	9,45	9,45	9,45	9,45	9,45	
K <sub>2</sub> O	9,25	0,13	9,77	0,12	0,08	0,08	0,17	0,19	He обн.	8,40	0,05	He обн.	8,89	8,89	8,89	8,89	8,89	8,89	8,89	
H <sub>2</sub> O-	He опр.	He опр.	He опр.	He опр.	He опр.	He опр.	He опр.	He опр.	He опр.	He опр.	He опр.	He опр.	He опр.	He опр.	He опр.	He опр.	He опр.	He опр.	He опр.	
H <sub>2</sub> O <sup>+</sup>	2,88	"	2,93	"	"	"	"	1,76	"	"	"	3,39	"	"	"	"	"	2,35	"	
n. n. n.	He опр.	"	He опр.	"	"	"	"	He опр.	"	"	"	He опр.	"	"	"	"	"	He опр.	"	
P <sub>2</sub> O <sub>5</sub>	"	"	"	"	"	"	"	He опр.	"	"	"	0,20	"	"	"	"	"	0,18	"	
F	"	"	"	"	"	"	"	He опр.	"	"	"	0,13	"	"	"	"	"	0,18	"	
Sum - O=2F	99,77	99,64	99,63	99,96	100,01	99,19	99,45	99,88	99,76	100,22	99,81	99,98	99,98	99,98	99,98	99,98	99,98	99,98	99,98	
Sum - Cумма																				

\* VGM = High-Aluminia-minerals

Table 1.5 *continued*  
ПРОДОЛЖЕНИЕ ТАБЛ. 1.5

Oxides Оксиды	Амфиболитовая фация				Биотит-амфиболитовая фация				Биотит-магноклазовая гнеc				Амфиболит-			
	Амфиболит- амфиболит		Амфиболит- амфиболит		Биотит-амфиболит с НГМ* и УСЛ**		Биотит- амфиболит		Биотит- амфиболит		Биотит- амфиболит		Биотит- амфиболит		Биотит- амфиболит	
SiO <sub>2</sub>	38,21	44,70	34,74	59,85	37,00	37,58	62,23	36,92	38,86	66,03	48,51	37,84	60,36			
TiO <sub>2</sub>	0,17	0,83	2,45	11,06	1,03	1,03	1,03	0,75	0,75	0,55	2,49					
Al <sub>2</sub> O <sub>3</sub>	21,03	10,79	19,50	24,81	20,99	16,18	23,21	20,90	17,02	21,44	7,79	17,53	24,58			
Fe <sub>2</sub> O <sub>3</sub>	0,85	4,60	He обн.	He опр.	He опр.	He опр.	He опр.	He опр.	He опр.	He опр.	4,14	He опр.	He опр.			
FeO	23,95	13,98	19,72	He опр.	He опр.	32,33	He опр.	12,32	30,90	10,96	"	9,70	"	"		
$\Sigma FeO$	0,58	0,27	0,04	He обн.	5,80	0,31	He обн.	8,23	0,09	He обн.	0,19	He обн.	He обн.			
MnO	3,96	9,74	10,31	2,04	17,99	0,23	4,54	1,75	16,15	He обн.	13,71	15,07	"			
MgO	10,98	11,59	0,36	7,06	1,85	0,23	4,54	1,37	0,09	2,67	12,66	0,50	6,32			
CaO	He обн.	1,33	0,20	7,72	He обн.	0,91	8,98	He обн.	0,19	9,80	0,40	0,17	7,40			
Na <sub>2</sub> O	He обн.	0,48	9,19	He обн.	9,07	0,08	He обн.	10,00	0,04	0,04	0,26	9,80	0,93			
K <sub>2</sub> O	He опр.	He опр.	He опр.	He опр.	He опр.	He опр.	He опр.	He опр.	He опр.	He опр.	He опр.	He опр.	He опр.			
H <sub>2</sub> O-	"	"	3,23	"	"	"	3,85	"	"	2,80	"	2,07	2,57	"		
H <sub>2</sub> O+	"	"	"	"	"	"	He опр.	"	"	He опр.	"	He опр.	He опр.	"		
n. n. n.	"	"	"	"	"	"	"	"	"	"	"	"	"	"		
P <sub>2</sub> O <sub>5</sub>	"	"	0,05	"	"	"	"	"	"	0,17	"	"	"	"		
F	"	"	100,37	"	"	"	"	"	"	99,72	0,07	99,98	99,98	99,48		
Сумма	"	"	0,02	99,74	99,44	100,01	100,12	99,04	100,07	99,65		99,98	99,98	99,59		
-O=2F	99,73	100,35														
Сумма																

Примечание. Аналитики А. В. Герман, К. К. Гумбар, Г. Ф. Петрова. — Note. Analysts: A. V. Germain, K. K. Gymbar, G. F. Petrova.

\* Номер образца.  
Sample number

Table I.6 Paleotemperatures of metamorphism, determined from mineralogical geothermometry

Породы Rocks	Sampl № опр. №	"Гранат-биотитовая ассоциация" равновесная парагенетическая ассоциация минералов Equilibrium paragenetic mineral association	Процессы предобразования пород processes	Темпера- тура, С Temperature, C
Биотит-плагиоклазо- вые гнейсы с высо- коглиноземистыми минералами  Biotite-plagioclase gneisses with high-alumina minerals	23 908 24 271 24 287 22 730	Garnet - biotite Гранат-биотит $K_{Mg}^{Pr}_{Cr} = 0,15; K_{Mg}^{Bi} = 0,49$  Garnet - biotite Гранат-биотит $K_{Mg}^{Pr}_{Cr} = 0,10; K_{Mg}^{Bi} = 0,50$  Garnet - biotite Гранат-биотит $K_{Mg}^{Pr}_{Cr} = 0,08; K_{Mg}^{Bi} = 0,49$ Мусковит-биотит Мусковит-биотит $K_{Na}^{Mu} = 19; K_{Na}^{Bi} = 5$	Региональный мета- морфизм. Эпидот- амфиболитовая фа- ния  As above. То же Регрессивный регио- нальный метамор- физм. Эпидот-амфи- болитовая фация  As above Гранитизация Granitization	600 600 550 550 650
Биотит-плагиоклазо- вые гнейсы  Biotite-plagioclase gneisses	26 431 26 339 24 301	Garnet - biotite, Гранат-биотит $K_{Mg}^{Pr}_{Cr} = 0,35; K_{Mg}^{Bi} = 0,62$  Garnet - biotite Гранат-биотит $K_{Mg}^{Pr}_{Cr} = 0,08; K_{Mg}^{Bi} = 0,56$  Мусковит-биотит Мусковит-биотит $K_{Na}^{Mu} = 22; K_{Na}^{Bi} = 9$	Региональный мета- морфизм; амфибо- литовая фация  As above Регрессивный ме- таморфизм; эпидот- амфиболитовая фа- ния  Гранитизация Granitization	800 700 500 650
Garnet-biotite- amphibole- plagioclase gneissos	23 873	Garnet - biotite, Гранат-биотит $K_{Mg}^{Pr}_{Cr} = 0,25; K_{Mg}^{Bi} = 0,54$	Региональный мета- морфизм; амфибо- литовая фация	750
Pyroxene-bearing amphibolites (relict two pyroxene- amphibole- plagioclase crystallizing schist).  Куммингтонитсодержащие амфиболиты Cummingtonite-bearing amphibolites	36 045 38 166	Saliite-hornblende Салит-роговая обманка $K_{Mg}^{Pr}_{Cr} = 0,54; K_{Mg}^{Cs} = 0,80$ Hypersthene-hornblende Гиперстен-роговая обманка $K_{Mg}^{Pr}_{Cr} = 0,70; K_{Mg}^{Pr}_{Cs} = 0,54$  Amporitite-hornblende Анортит-роговая обманка $K_{Ca}^{Pr} = 0,97; K_{Ca}^{Pr}_{Cs} = 0,82$	Региональный мета- морфизм; гранули- това фация  Regional metamorphism; granulite facies	1200 1100
Pyroxene-bearing amphibolites	37 615	Saliite-hornblende Салит-роговая обманка $K_{Mg}^{Cs} = 0,66; K_{Mg}^{Pr} = 0,43$	Региональный мета- морфизм; гранули- това фация	1000
Амфиболиты Amphibolites	24 945 26 176 38 133	Garnet-biotite Гранат-биотит $K_{Mg}^{Pr}_{Cr} = 0,22; K_{Mg}^{Bi} = 0,43$ Hornblende-plagioclase Роговая обманка-плагио- клас $K_{Mg}^{Pr}_{Cr} = 0,67; K_{Ca}^{Pr} = 0,57$ Hornblende-plagioclase Роговая обманка-плагио- клас $K_{Ca}^{Pr} = 0,79; K_{Ca}^{Pr}_{Cr} = 0,28$	Региональный мета- морфизм. Амфибо- литовая фация  To же As above  Регрессивный мета- морфизм, эпидот- амфиболитовая фа- ния	800 800 500

## Geochemistry and Environment of Formation of the Precambrian Complex

A systematic petrologic-geochemical study of the Precambrian complex in the Kola Superdeep borehole and the surroundings was conducted by the method of layer-by-layer synthesis and analysis, involving the documentation and testing of various rock types, delineated from core logs or from direct observation of cores and outcrops. At each level unaltered or only slightly altered metamorphic rocks were described together with the variability of migmatization or metasomatic alteration and all types of secondary veins. Intervals of similar rock types were organized into groups to establish their petrographic and geochemical characteristics, the parent rock type, and compositional variations due to differences in depth and the intensity of metamorphism.

A stratigraphic description of the SG-3 borehole and its correlation with the surrounding surface rocks was carried out: chemical trends related to magmatic or sedimentary differentiation, or metamorphic zonation were studied, and also the relationship between geochemical and the elastic-density characteristics of the rocks - in order to determine the nature of inhomogeneities of deep-crustal zones.

### A. Pechenga Complex

In the interval from 0-6842 m, the Proterozoic Complex is divided into 8 formations:

0-1059 m Materin formation

Tholeiitic metabasalts, including olivine, normal, and alkali-poor metabasalts, with minor metapicrites, metapyroxenites, and metaperidotites.

1059-2805 m zhdanov

Corresponds in both composition and structure to the Quaternary [sic] sedimentary strata exposed on the surface; broken down into four rhythmically layered members: 1) 2619-2805m gravelly sandy; 2) 2155-2619m sandy-silty; 3) 1203-2155m

	tuffaceous-silty 4) 1059-1203m
	tuffaceous-pelitic
2805-4673 m Zapoljarnin	Largely (95%) composed of tholeiitic basalts, including olivine basalts, normal and alkali-poor basalts, with subordinate meta-tuffs and metasedimentary layers.
4784-4884 m Luchlompol	
5642-5717 m Kuvernerinyiok	These formations are similar in structure and thickness: carbonates in the upper layers and meta-sandstones below; carbonate units are largely dolomites with minor sands; terrigenous units are arkosic meta-sandstones with minor dolomite.
4884-5642 m Pirttiyarvin	Meta-trachybasalts (32%), alkali-basalts (25%), trachyandesite basalts (25%), olivine and picrite basalts (10%), andesites and trachyandesites (7%).
5717-6823 m Mayarvin	Normal andesite basalts (97%)
6823-6842 m Televin	Intensely metamorphosed gravelly-plagioclase-rich sandstones

On the basis of geochemical data, two stages were delineated which show a sharp change in the geotectonic regime during the development of the Pechenga Complex. The Televin formation reflects only terrigenous processes; the Kuvernerinyiok and Luchlompol formations reflect terrigenous-chemogenic processes, and the Zhdanov formation - terrigenous processes with minor terrigenous-chemogenic processes.

#### B. Archean Complex

The Archean Complex is composed of plagiogneisses and migmatites (66%), amphibolites and amphibolite schists (30%), and granitoids (4%).

first stage (greater than 2.8 billion years) was characterized by the deposition of terrigenous and silicic-terrigenous-volcanogenic sediments (70% of the thickness of the SG-3 borehole), emplacement of tholeiitic basalts (23%) and the injection of comagmatic basite-ultramafic intrusives (7%). The second stage entailed metamorphism to the granulite stage, followed by retrograde metamorphism and ultrametamorphism to the andalusite-sillimanite stage. The metamorphism was accompanied by migmatization and the emplacement of veined granites (initial melt temperature 820-830°C) and pladio-pegmatites (initial melt temperature 810-675°C)

ТАБЛИЦА 1.7  
СРЕДНИЕ СОСТАВЫ МЕТАСАДОЧНО-ВУЛКАНОГЕННЫХ ПОРОД ПЕЧЕНГСКОГО КОМПЛЕКСА ИЗ РАЗРЕЗА СКВ. СГ-3 В ИНТЕРВАЛЕ 0-6842 м

b компоненты	с. Метасадочные породы									d. Метасаду шитник породы
	1	2	3	4	5	6	7	8	9	
L	N	A	H	A	H	H	H	A	H	
SiO <sub>2</sub>	71,62	74,46	74,76	52,64	49,36	15,41	57,71	53,92	44,97	43,93
TiO <sub>2</sub>	0,22	0,40	0,72	0,25	1,05	0,07	1,18	1,50	1,40	3,12
Al <sub>2</sub> O <sub>3</sub>	13,52	6,66	8,72	5,71	7,36	1,35	14,91	16,77	13,08	5,66
Fe <sub>2</sub> O <sub>3</sub>	0,72	0,89	4,20	0,79	0,85	0,08	1,93	1,77	2,42	2,90
FeO	3,13	7,05	1,79	1,60	7,20	0,43	10,19	10,52	15,83	11,99
MnO	0,03	0,06	0,05	0,05	0,49	0,08	0,07	0,05	0,16	0,14
Al <sub>2</sub> O	1,56	2,40	1,19	1,01	2,82	18,22	2,89	1,15	8,26	20,43
CaO	1,32	2,36	1,54	13,07	15,30	28,22	1,72	2,91	3,30	6,04
Na <sub>2</sub> O	3,63	0,64	0,54	0,59	1,00	0,15	1,99	1,89	1,34	0,42
K <sub>2</sub> O	2,85	0,62	4,69	2,67	0,70	0,19	2,48	3,49	0,08	0,06
P <sub>2</sub> O <sub>5</sub>	0,08	1,40	0,12	0,27	0,08	0,10	0,16	0,09	0,15	0,38
CO <sub>2</sub>	0,16	0,82	0,61	10,06	11,00	34,16	0,55	0,24	1,40	0,10
H <sub>2</sub> O <sup>-</sup>	0,10	0,20	0,04	0,09	0,14	0,11	0,12	0,18	0,38	0,34
H <sub>2</sub> O <sup>+</sup> +	0,66	1,39	0,59	1,18	1,20	0,95	3,76	5,30	5,18	6,32
+ п. п.										
S <sub>оргн</sub>	0,12	—	0,08	0,10	1,30	0,08	2,14	—	1,29	0,02
Li	34,0	29,3	8,6	26,8	21,0	16,8	39,9	43,8	32,5	14,5
Rb	71,0	25,6	93,8	73,6	25,8	38,0	72,2	97,9	26,2	12,7
Sr	80,0	59,7	26,4	49,4	162,0	73,8	46,4	15,4	26,3	13,4
Ba	575,0	106,2	705,5	333,3	113,1	320,0	165,3	283,3	61,8	10,0
B	9,0	38,6	16,4	32,0	29,3	83,8	33,6	40,0	10,5	16,0
Sc	50,0	12,2	21,8	21,5	12,5	11,6	11,9	17,9	4,1	7,6
Ga	27,5	13,6	15,7	20,7	12,7	7,0	19,2	24,5	19,6	10,6
La	22,9	21,9	33,4	17,4	—	3,8	23,4	—	53,0	—
Ce	64,1	37,6	65,6	36,5	—	11,3	44,3	—	66,7	—
Sm	3,7	5,4	5,7	2,0	—	0,70	7,1	—	9,8	—
Eu	1,0	1,3	1,8	0,70	—	0,30	1,5	—	1,4	—
Yb	—	2,8	2,4	1,5	—	—	—	3,0	—	—

**ПРОДОЛЖЕНИЕ ТАБЛ. I.7**

b Компоненты	с Метасиликатные породы									с Метаэффузионные породы			
	1	2	3	4	5	6	7	8	9	a	и	и	и
Lu	0,10	0,50	0,40	0,20	—	0,10	0,70	—	0,60	—	—	—	0,40
Th	12,9	2,9	6,1	8,0	—	1,2	4,2	—	4,8	—	—	—	5,5
U	3,7	2,0	1,7	0,20	—	0,40	2,5	—	3,3	—	—	—	—
Ge	0,50	2,4	0,46	1,1	1,9	0,33	2,6	2,0	2,3	1,9	0,79	2,0	2,0
Zr	85,0	64,0	71,0	98,9	70,2	34,4	70,3	94,0	64,1	48,9	50,0	71,3	71,3
Sn	3,1	5,2	3,4	3,5	4,2	3,0	32,7	5,2	5,8	4,1	3,0	5,7	5,7
Hf	6,3	3,0	4,5	10,7	—	1,8	3,2	—	4,7	—	—	—	2,5
Nb	5,2	7,0	4,0	4,4	5,3	2,0	5,7	7,7	4,9	3,9	2,4	7,9	7,9
F	290,0	586,0	504,1	819,4	526,7	1176,7	1071,1	720,0	817,5	—	—	—	—
Cu	10,0	119,0	6,5	48,7	104,8	12,8	162,3	130,0	222,9	307,8	242,5	329,5	329,5
Zn	26,9	191,5	51,4	78,9	137,2	24,9	199,8	230,8	213,5	253,9	30,0	209,1	209,1
Ag	0,09	0,05	0,02	0,05	0,06	0,05	0,08	0,07	0,10	0,01	0,10	0,19	0,19
Pb	20,8	16,3	21,3	15,6	17,0	16,4	20,6	22,2	11,7	4,4	11,0	6,6	6,6
Mo	1,8	4,2	0,69	1,2	3,3	0,88	7,0	5,0	10,1	1,9	1,2	3,0	3,0
V	69,5	190,4	190,2	108,9	161,0	49,7	233,6	255,4	247,5	136,3	250,0	241,5	241,5
Cr	37,2	150,6	240,0	138,9	195,8	79,8	209,7	202,8	367,6	958,0	220,0	254,7	254,7
Co	12,8	32,4	18,8	15,9	29,8	11,4	36,0	31,1	49,9	137,5	32,2	77,3	77,3
Ni	19,8	88,7	38,6	34,7	72,6	23,5	112,1	81,8	226,7	1080,4	59,0	181,7	181,7
f Число проб	4	128	73	9	32	8	259	24	17	28	4	39	39

Е ПРОДОЛЖЕНИЕ ТАБЛ. 1.7

Б Компоненты	10		11		12		13		14		15		16		17	
	L <sub>a</sub>	N <sub>a</sub>	A <sub>a</sub>													
SiO <sub>2</sub>	50,07	47,72	50,86	47,73	47,66	49,66	48,27	54,43	55,27	54,21	58,08					
TiO <sub>3</sub>	1,41	1,16	2,00	1,29	1,31	1,73	2,27	0,98	1,38	1,67	1,24					
Al <sub>2</sub> O <sub>3</sub>	11,98	13,93	12,83	12,81	2,80	6,25	14,46	13,55	11,40	14,79	13,42					
FeO <sub>3</sub>	5,74	3,04	4,34	11,71	11,30	8,81	5,94	1,84	1,85	4,26	2,08					
FeO	7,29	9,97	9,89	0,20	0,16	0,25	9,85	8,94	9,64	7,57	9,20					
MnO	0,20	0,19	0,16	0,20	0,16	0,25	0,23	0,16	0,12	0,13	0,14					
MgO	7,28	7,98	6,58	6,62	6,12	5,44	5,97	5,98	4,11	4,33	3,34					
CaO	7,83	9,98	6,20	9,23	10,35	5,84	4,83	7,92	6,40	4,43	6,35					
Na <sub>2</sub> O	3,56	2,20	3,03	2,46	0,60	5,26	4,09	3,14	2,65	4,13	3,19					
K <sub>2</sub> O	0,37	0,29	1,17	0,30	0,39	0,47	1,63	1,24	0,76	2,41	1,44					
P <sub>2</sub> O <sub>5</sub>	0,11	0,09	0,18	0,16	0,22	0,28	0,22	0,16	0,13	0,20	0,17					
CO <sub>2</sub>	2,33	0,21	0,23	0,50	0,32	0,43	0,18	0,30	2,39	0,48	0,05					
H <sub>2</sub> O <sup>-</sup>	0,08	0,13	0,14	0,18	0,20	0,09	0,12	0,13	0,06	0,22	0,09					
H <sub>2</sub> O <sup>+</sup> + +п. п. п.	3,54	3,24	2,37	3,74	5,26	2,02	2,23	1,63	4,22	1,84	1,42					
S <sub>о,6</sub> и	0,07	0,09	0,07	0,11	0,18	0,09	0,05	0,03	0,37	0,07	0,03					
Li	12,5	12,4	14,6	11,9	8,8	9,1	12,5	13,0	18,5	15,1	11,5					
Rb	16,0	6,9	31,8	7,6	12,3	14,2	37,5	40,2	8,8	57,5	41,7					
Sr	75,0	38,1	28,4	52,9	62,0	36,8	28,1	42,5	103,8	29,1	34,0					
Ba	300,0	85,7	75,0	67,0	54,0	223,5	195,9	255,0	87,5	443,1	190,0					
B	7,5	35,6	3,5	17,6	9,1	8,0	10,6	6,3	12,0	7,5	5,6					
Sc	13,0	13,0	6,3	14,4	13,0	11,2	9,2	4,3	6,8	5,2	5,8					
Ga	20,0	14,2	16,3	17,5	15,5	16,2	16,4	18,4	22,5	17,0	19,5					
La	—	9,4	—	12,4	6,2	17,7	30,5	19,9	40,0	34,9	30,5					
Ce	—	24,3	—	25,9	21,0	50,4	68,1	52,2	45,0	80,2	68,1					
Sm	—	3,8	—	5,3	4,2	5,8	5,5	3,9	5,9	5,4	5,5					
Eu	—	—	—	1,7	2,1	2,0	1,6	1,3	2,5	2,2	1,6					
Yb	—	—	—	3,2	2,7	3,4	2,9	1,9	2,3	2,8	2,9					

2 Приложение табл. I

Д Метафузулические породы

В Компоненты	Д Метафузулические породы						16	17
	10	11	12	13	14	15		
А	и	и	и	и	и	и	и	и
Iu	—	0,60	—	0,60	0,10	0,60	0,40	0,40
Th	—	0,80	—	1,2	2,0	5,7	5,1	4,8
U	—	0,20	—	0,20	1,1	1,5	—	5,7
Ce	0,05	0,90	0,79	0,93	0,08	0,74	0,70	0,60
Zr	70,0	41,4	51,6	51,6	49,0	53,8	48,8	45,0
Sn	3,0	5,7	2,7	4,6	3,2	3,0	54,6	64,0
Hf	—	2,1	—	2,3	2,0	3,5	2,8	2,9
Nb	0,50	3,2	2,4	3,0	1,8	0,62	1,0	1,9
F	—	82,0	480,0	120,2	158,0	46,9	205,9	73,6
Cu	150,0	153,7	266,6	202,7	202,5	76,2	164,0	64,0
Zn	30,0	118,5	88,4	131,3	122,0	40,0	62,4	55,0
Ag	0,01	0,12	0,05	0,05	0,02	0,02	0,03	0,02
Pb	13,0	16,8	18,0	11,0	8,9	14,5	21,0	23,5
Mo	1,0	0,72	0,70	1,08	0,95	0,98	1,1	0,87
V	95,0	260,8	221,7	301,9	240,5	182,3	520,6	222,6
Cr	620,0	155,1	238,4	83,9	97,2	207,3	116,1	216,7
Co	50,0	51,3	63,2	47,0	44,3	43,4	67,1	40,7
Ni	150,0	116,0	94,2	65,2	66,0	83,5	64,6	69,3
f Число проб	2	117	6	386	20	13	17	105
								4
								35
								18

1 — полевошпат-кариевые метапесчаники; 2 — аркотонные метапесчаники, с карбонатным цементом; 4 — песчанистые лопониты; 5 — металлеросечники с кальцитовым цементом и сульфидами; 6 — металлеросечники с сульфидами, в т. ч. с кальцитом и сульфидами; 7 — метатифтигиты, в т. ч. с кальцитом и сульфидами; 8 — металликриты; 9 — металликриты, в т. ч. с кальцитом и сульфидами; 10-13 — металликриты, пленокнаты, амфиболовые сланцы и вмикроболиты; 10 — оливинолиты (пикритоболлиты); 11 — металликриты, пленокнаты, амфиболовые сланцы и вмикроболиты биотитом; 12 — фенроболиты.

13 — инаконечочные биотиты, 14 — силикатные пропилиты, 15 — амфиболитовые пластины, 16 — амфиболиты, в т. ч. с магнетитом (также иллит), 17 — трахиандимитоболлиты, в т. ч. с кварцом, амфиболом, биотитом и пироксеном, 18 — пироксениты, в т. ч. с магнетитом (андезиты), 19 — породы пустотливой (л.) и никелевой (н.) серни. Составлены Петрохимических элементов промесей в г/г; прочерк — содержания не определены.

Table 1.7: a-Mean composition of metasedimentary and metavolcanic rocks of the Pechenga Complex from the SG-3 borehole in the interval 0-6842 m.

b-components

c-metasedimentary rocks

d-metavolcanic rocks

e-continuation of table 1.7

f-number of samples

g- 1) quartzo-feldspathic meta-sandstones; 2) arkosic meta-sandstones; 3) meta-sandstones and meta-siltstones with carbonate cement; 4) sandy dolomites; 5) meta-siltstones, some with carbonate cement and sulfide minerals; 6) meta-pelites, some with sulfide minerals; 7) meta-tuffites some with carbonate cement and sulfide minerals; 8) meta-picrites; 9) picritic meta-porphyrites (picrite basalts); 10-13) meta-diabases, plagioclase-amphibolite schists and amphibolites (10- olivine basalts; 11- basalts with some ferro-basalts; 12- alkali-poor basalts; 13- spilitized basalts); 14-16) biotite-amphibolite-plagioclase schists, some with magnetite; (14- trachybasalts; 15- andesitic basalts, with some pyroxene-olivine basalts, 16- trachyandesite basalts); 17) quartz-biotite-amphibole-plagioclase schists, some with magnetite (andesites); "L" and "N": rocks of the Luostarin (L) and Nickel (N) series. Content of major elements in weight percent; trace elements in grams/ton; dashes indicate element not detected.

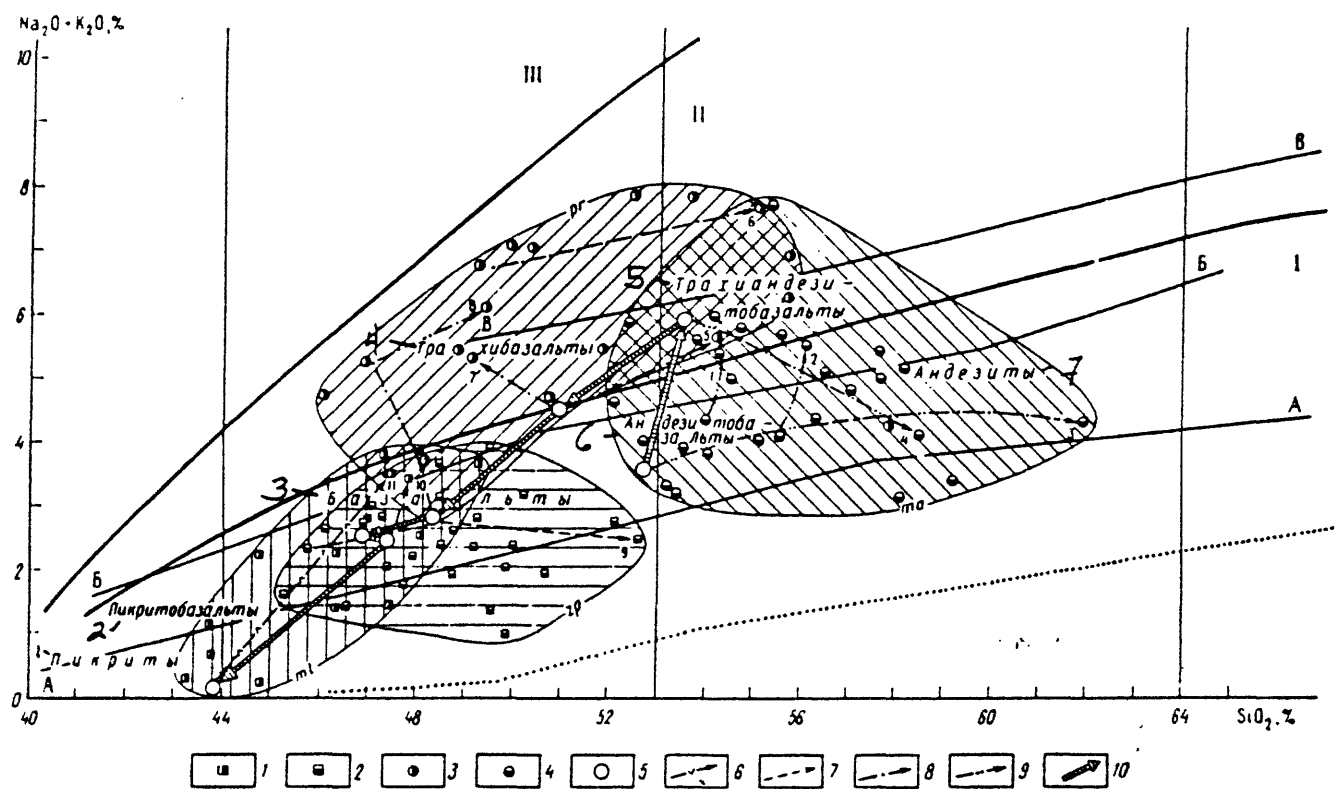


Figure 1.28 - Petrochemical types and differentiation trends of volcanic rocks of the Pechenga Complex:

1-4- Mean composition of meta-volcanic flows by formation: 1- Materin; 2- Zapolyarnin; 3- Pirttiyarvin; 4- Mayarvin; 5- compositions of the initial differentiates; 6-9- differentiation trends for the meta-volcanic rocks; 6- Materin; 7- Zapolyarnin; 8- Pirttiyarvin; 9- Mayarvin (numbers indicate the position of the volcanic series in the section, from top to bottom); 10- evolution of the composition of the initial differentiates during the formation of the Pechenga Complex. I- zone of rocks with normal alkali contents; II- subalkaline rocks; III- alkali-rich rocks. Differentiation trends for volcanic rocks of island arc series: A-tholeiitic, B- calc-alkaline, C-alkaline [62]. Numbers added to diagram:  
 1- picrites, 2-picrite basalts, 3- basalts, 4- trachybasalts, 5- trachy-andesite basalts, 6- andesite basalts, 7- andesites

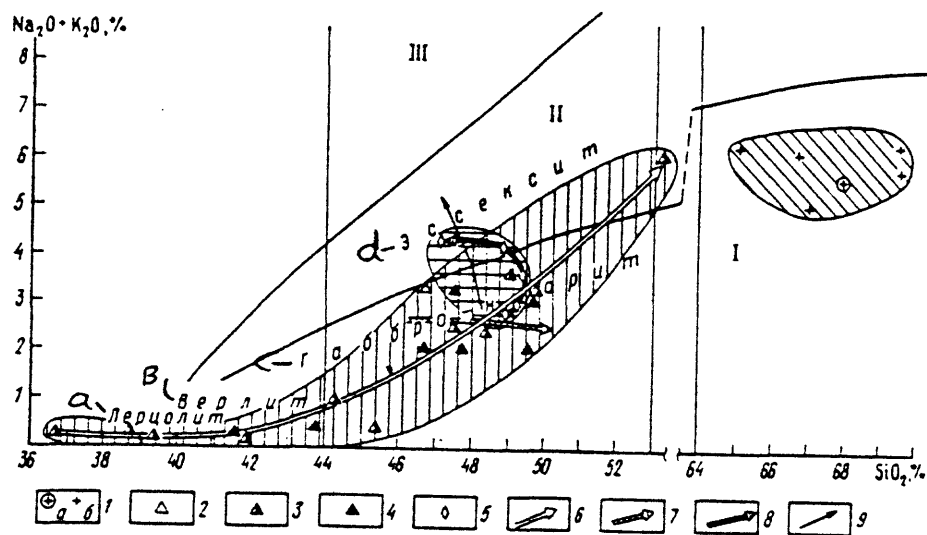


Figure I.29 Petrochemical types and differentiation trends of meta-intrusive rocks of the Pechenga Complex:

1-5 - mean composition of meta-intrusive rocks, grouped by formation:

1-Luchlompol (a- mean, b-individual compositions of the post-Materin Complex),

2- Materin, 3- Zhdanov, 4- Zapolyarnin, 5- Mayarvin, 6-8- differentiation trends for meta-intrusive rocks; complexes: 6- gabbro-werlite syn-Materin, 7- gabbro-diabase syn-Materin, 8- gabbro-diabase pre-Materin; 9- differentiation trend of metavolcanics of the Pirttiyarvin formation. For further information see figure 1.29.

a- Iherzolite, b- werlite, c- gabbro-norite, d- essexite

ТАБЛИЦА 1.8

α—СРЕДНИЕ СОСТАВЫ МЕТАИНТРУЗИВНЫХ ПОРОД ПЕЧЕНГСКОГО КОМПЛЕКСА  
ИЗ РАЗРЕЗА СКВ. СГ-3

б — Компоненты	1	2	3		4	5	6
	з	с	р	х	с	с	р
SiO <sub>2</sub>	37,85	42,99	48,77	47,60	46,93	52,30	67,81
TiO <sub>2</sub>	1,01	2,28	1,54	1,69	3,80	1,96	0,65
Al <sub>2</sub> O <sub>3</sub>	3,67	7,07	13,39	13,22	10,41	14,81	14,74
Fe <sub>2</sub> O <sub>3</sub>	7,51	4,44	2,26	3,02	2,47	2,17	1,73
FeO	10,38	12,25	12,83	12,08	14,74	11,05	3,19
MnO	0,20	0,19	0,24	0,22	0,21	0,19	0,07
MgO	26,17	18,12	6,74	6,24	7,82	2,64	2,10
CaO	3,20	4,58	8,22	8,88	5,44	4,38	2,45
Na <sub>2</sub> O	0,17	0,37	2,72	2,68	0,13	3,86	2,77
K <sub>2</sub> O	0,11	0,14	0,89	0,28	0,03	2,09	2,77
P <sub>2</sub> O <sub>5</sub>	0,15	0,30	0,14	0,15	0,33	0,56	0,21
CO <sub>2</sub>	0,47	0,20	0,14	0,56	0,04	0,26	0,41
H <sub>2</sub> O-	0,41	0,11	0,15	0,24	0,28	0,41	0,21
H <sub>2</sub> O <sup>+</sup>	8,77	7,13	2,04	3,67	7,55	3,39	1,43
+ п. п. п.							
S <sub>о</sub> бш	0,28	0,44	0,05	0,11	0,09	0,27	0,15
Li	8,9	12,5	10,2	19,2	36,5	15,1	26,2
Rb	13,3	8,6	27,1	9,7	5,0	42,7	115,5
Sr	5,0	13,0	17,7	33,9	12,5	67,6	47,2
Ba	13,5	23,5	108,0	75,3	10,0	256,7	425,9
B	67,7	12,8	6,9	14,6	9,2	18,6	24,0
Sc	4,7	6,5	4,5	13,0	9,0	2,0	5,0
Ga	5,7	7,5	18,6	13,9	11,5	28,1	22,7
La	12,0	17,3	10,4	12,5	—	41,8	39,4
Ce	21,0	32,0	32,4	15,4	—	51,3	96,9
Sm	2,4	4,3	4,1	5,6	—	12,6	7,6
Eu	0,60	1,1	1,6	1,4	—	2,8	1,5
Yb	2,0	1,8	1,9	2,9	—	3,5	5,0
Lu	0,40	0,30	0,70	0,50	—	0,60	0,50
Th	1,2	1,2	1,0	0,60	—	4,9	15,6
U	0,20	0,50	0,70	—	—	0,60	6,4
Ge	1,2	2,1	0,58	1,4	2,8	1,6	0,54
Zr	30,6	55,0	26,7	48,0	70,0	139,0	186,7
Sn	6,0	4,3	2,8	4,7	7,0	6,3	6,3
Hf	1,0	2,3	3,0	1,9	—	4,9	6,9
Nb	3,4	7,1	9,9	3,2	10,0	17,6	7,5
F	—	—	141,3	55,1	—	—	472,2
Cu	1022,3	237,9	192,7	22,7	400,0	54,8	17,9
Zn	190,7	160,3	94,7	144,6	215,0	396,2	35,4
Ag	0,27	0,03	0,05	0,03	0,03	0,01	0,14
Pb	15,6	5,0	17,6	10,0	4,5	8,5	35,4
Mo	4,9	2,1	0,93	1,36	1,5	5,6	1,0
V	183,9	184,1	280,7	362,0	160,0	48,0	74,7
Cr	1603,5	977,0	254,7	83,8	155,0	20,1	29,4
Co	207,7	90,3	58,1	50,1	40,5	20,5	17,8
Ni	2519,2	1121,6	147,3	103,0	115,0	17,7	12,5
— Число проб	26	34	16	128	3	39	27

1—2 — метаперидотиты, хлорит-серпентин-тальковые и хлорит-тремолитовые сланцы (1 — перидотиты, 2 — лерцолитоверлиты); 3—4 — метагаббро-диабазы, меланократовые плагиоклаз-амфиболовые сланцы и амфиболиты (3 — габбронориты, 4 — нориты); 5 — эсеккитовые метагаббро-диабазы, 6 — андезито-дацитовые метапорфириты; д. с. п — интрузивные комплексы (д — доматеринский, с — симматеринский, п — постматеринский). Содержания петрографических элементов даны в %, земногрунтовых примесей — в г/т; прочерк — содержания не определялись.

Table 1.8

a- Mean composition of meta-intrusive rocks of the Pechenga Complex from the SG-3 borehole.

b- components

c- number of samples

d- 1-2 - meta-peridotites, chlorite-serpentine-talc schists and chlorite-tremolite schists (1- lherzolites; 2- lherzolite-werlites); 3-4 - meta-gabbro-diabases, melanocratic plagioclase-amphibole schists and amphibolites (3- gabbro-norites, 4- norites); 5- essexite meta-gabbro-diabases; 6- andesite-dacite-meta-porphyrites; S, pr, po - intrusive complexes (Pr- pre-Materin, S- syn-Materin, po- post-Materin). Content of major elements given in weight percent; trace elements in grams/ton; dashes indicate element not detected.

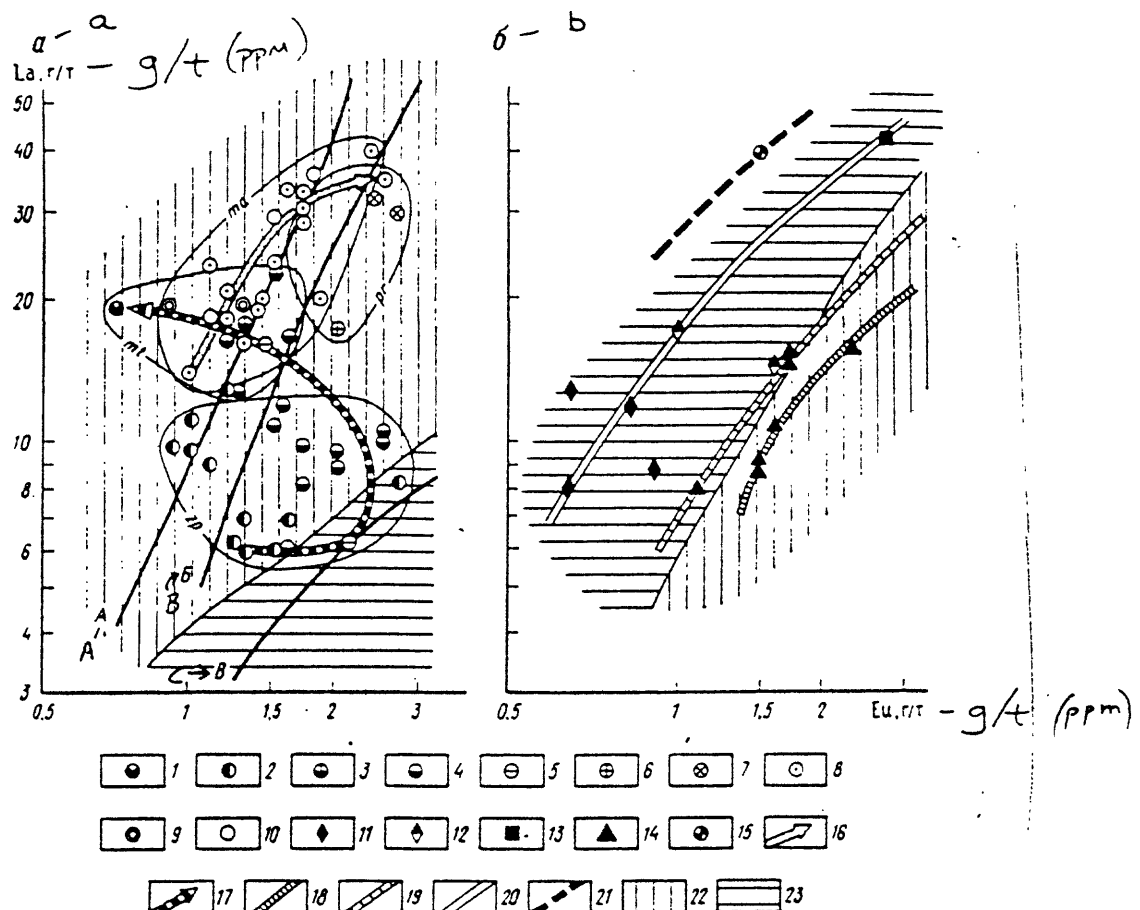


Figure 1.30 Distributional trends of rare-earth elements in meta-volcanic (a) and meta-intrusive rocks (b) of the Pechenga Complex.

1-10 - mean compositions of meta-volcanic rocks: 1- meta-picrite basalts; 2- olivine meta-basalts; 3- differentiated meta-basalts; 4- meta-basalts; 5- alkali-poor meta-basalts; 6- spilites; 7- meta-trachybasalts; 8- meta-andesite basalts; 9- meta-trachy-andesite basalts; 10- meta-andesites; 11-15 - mean composition of meta-intrusive rocks; 11- meta-lherzolites, meta-porphyrites; 12- meta-lherzolite-werlites; 13- essexite meta-gabbros; 14- meta-gabbro norites; 15- dacite meta-porphyrites; 16-17 - content of rare-earth elements in meta-volcanics of the first (16) and second (17) tectono-magmatic cycles; 18-21 - distribution of rare-earth elements in meta-intrusive rocks of the gabbro-diabase pre-Materin; (18) gabbro-diabase; (19) and gabbro-werlite syn-Materin; (20) and dacite-meta-porphyrite post-Materin; (21) Complexes; 22- field of continental and island-arc basalts (a) and differentiated trap intrusives; (b) 23- field of oceanic basalts; (a) and ultrabasites; (b) A-C trends of volcanic rocks, from [62]: A- island arcs and active continental margins, B- oceanic islands, and C- mid-ocean ridges.

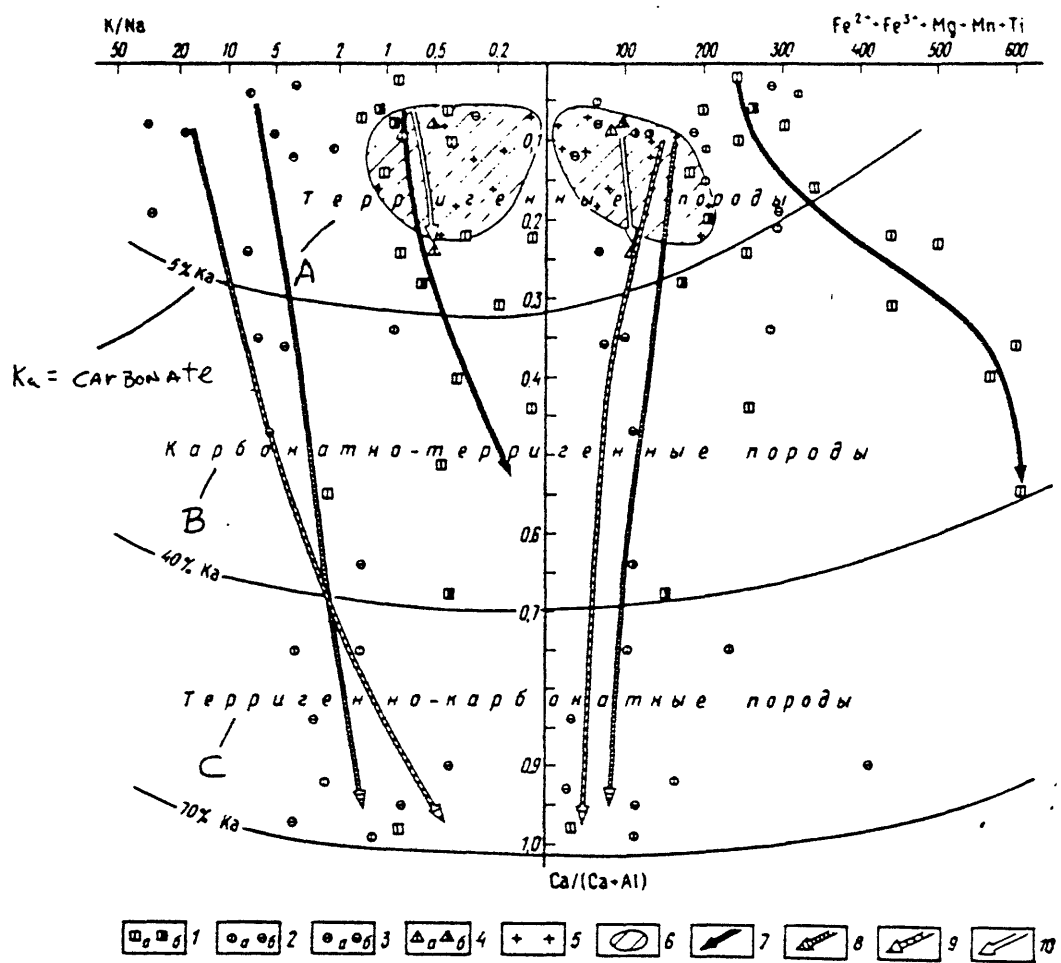


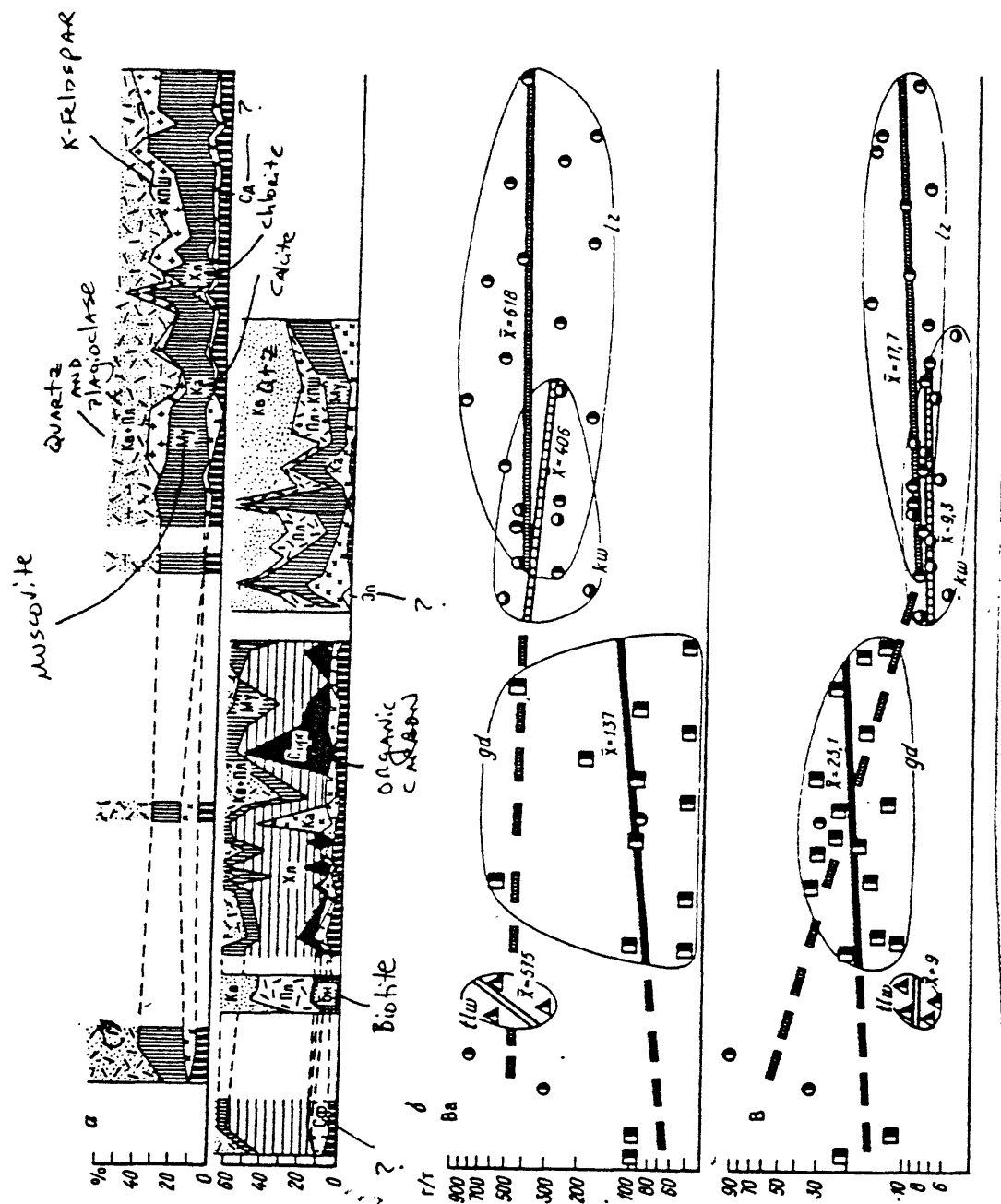
Figure I.31 Petrochemical differentiation trends for sedimentary rocks of the Pechenga Complex:

A- Terrigenous rocks

B- Carbonate-terrigenous rocks

C- Terrigenous-carbonate rocks

1-4 - composition of rocks from bore-hole SG-3 (a) and surrounding surficial rocks; (b) 1- Zhdanov formation; 2- Luchlompol formation; 3- Kuvernerinyok formation; 4- Televin formation; 5-6 - plagiogneisses of the Kola Complex (5) and their general distribution field (6); 7-10 - differentiation trends of sedimentary rocks of the Zhdanov (7), Televin (8), Kuvernerinyok (9), and Luchlompol (10) formations.



First part  
 of day 1.32

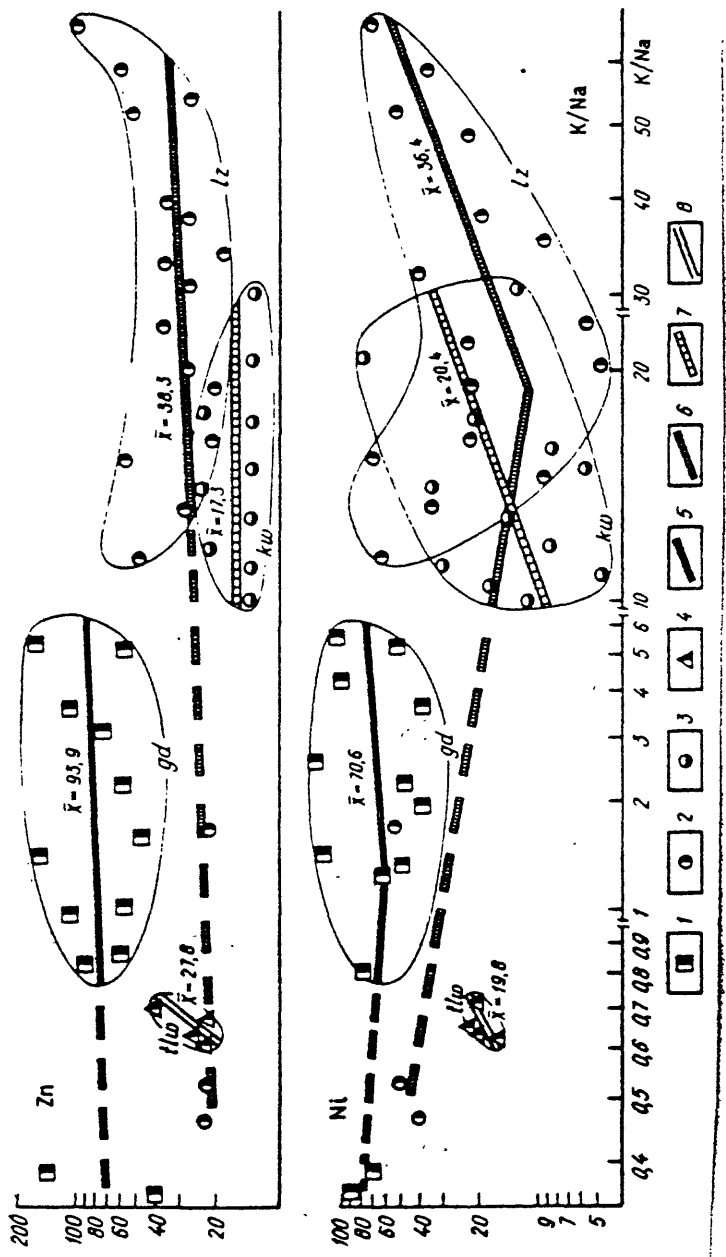


Figure 1.32 Lithologic composition (a, in percent) and geochemical trends of differentiation (b) for sedimentary rocks of the Pechenga Complex. Suites:  
 1- Zhdanov, 2- Luchlompol, 3- Kuvernerinyok, 4- Televin; 5-8 - geochemical trends.

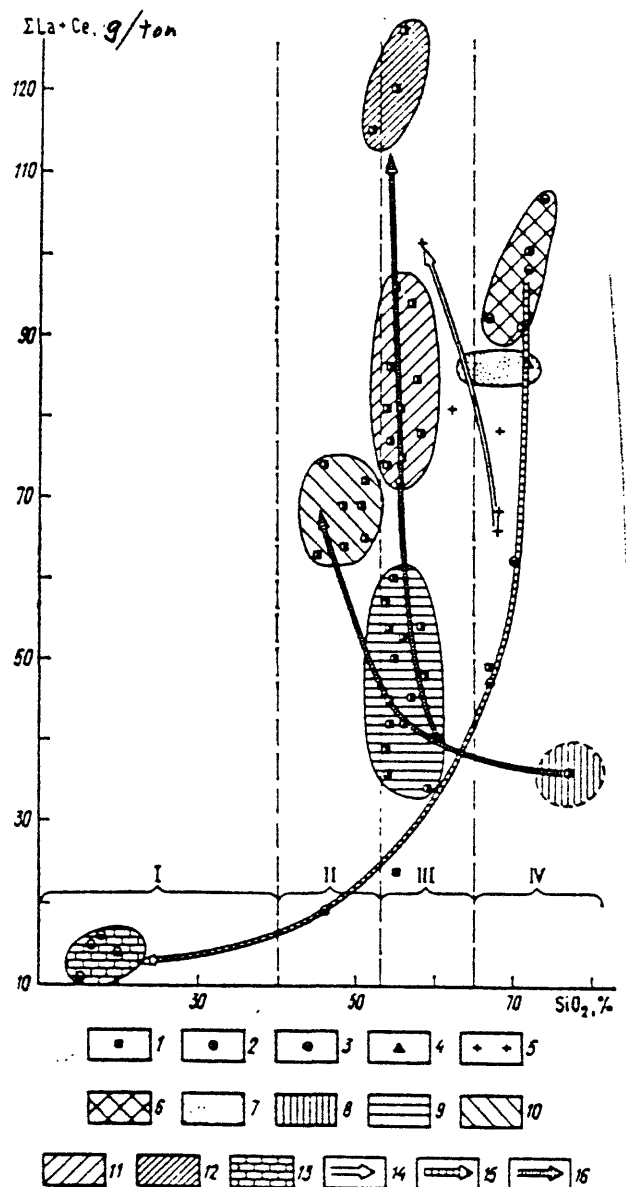
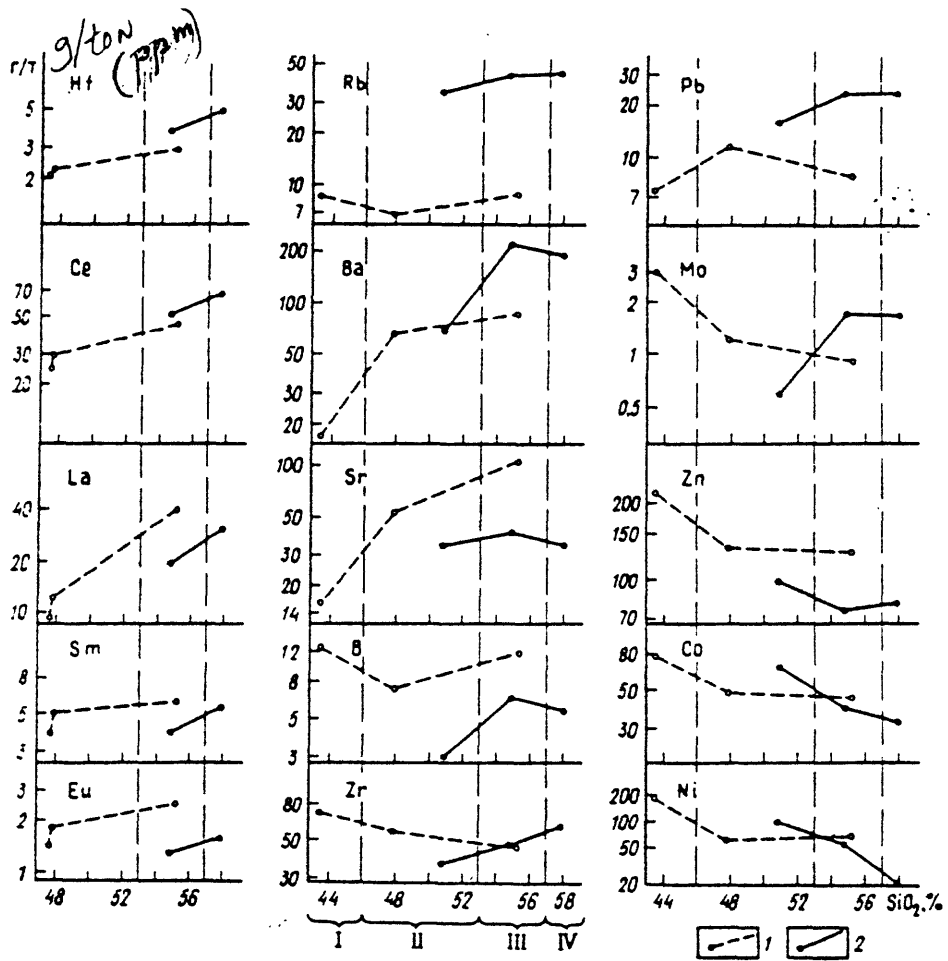


Figure I.33 Distributional trends for rare-earth elements in metasedimentary rocks of the Pechenga Complex. Formations: 1- Zhdanov, 2- Luchlompol, 3- Kuvernerinyok, 4- Televin, 5- gneisses and plagiogneisses of the Kola Complex; 6-13 - fields of metasedimentary rocks of the Pechenga Complex (6- arkosic meta-sandstones, 7- quartz-plagioclase meta-sandstones, 8- plagioclase-quartz meta-sandstones, 9- meta-siltstones, 10- meta-mudstones, 11- meta-siltstones with traces of tuffaceous material, 12- meta-tuffites, 13- sandy dolomites and limestones); 14-16 - rare-earth element trends in rocks of the Kola Complex (14), Luchlompol and Kuvernerinyok formations (15), and Zhdanov formation (16). I- sandy dolomites; II- silty-mudstones; III- silty sandstones; IV- sandstones.



**Figure I.34** Distribution of trace-elements in the major types of meta-volcanic rocks of the picrite-basalt (1) and andesite-basalt (2) stages of volcanism in the Pechenga Complex: I- meta-picrite basalts; II- meta-basalts; III- meta-andesite basalts; IV- meta-andesites.

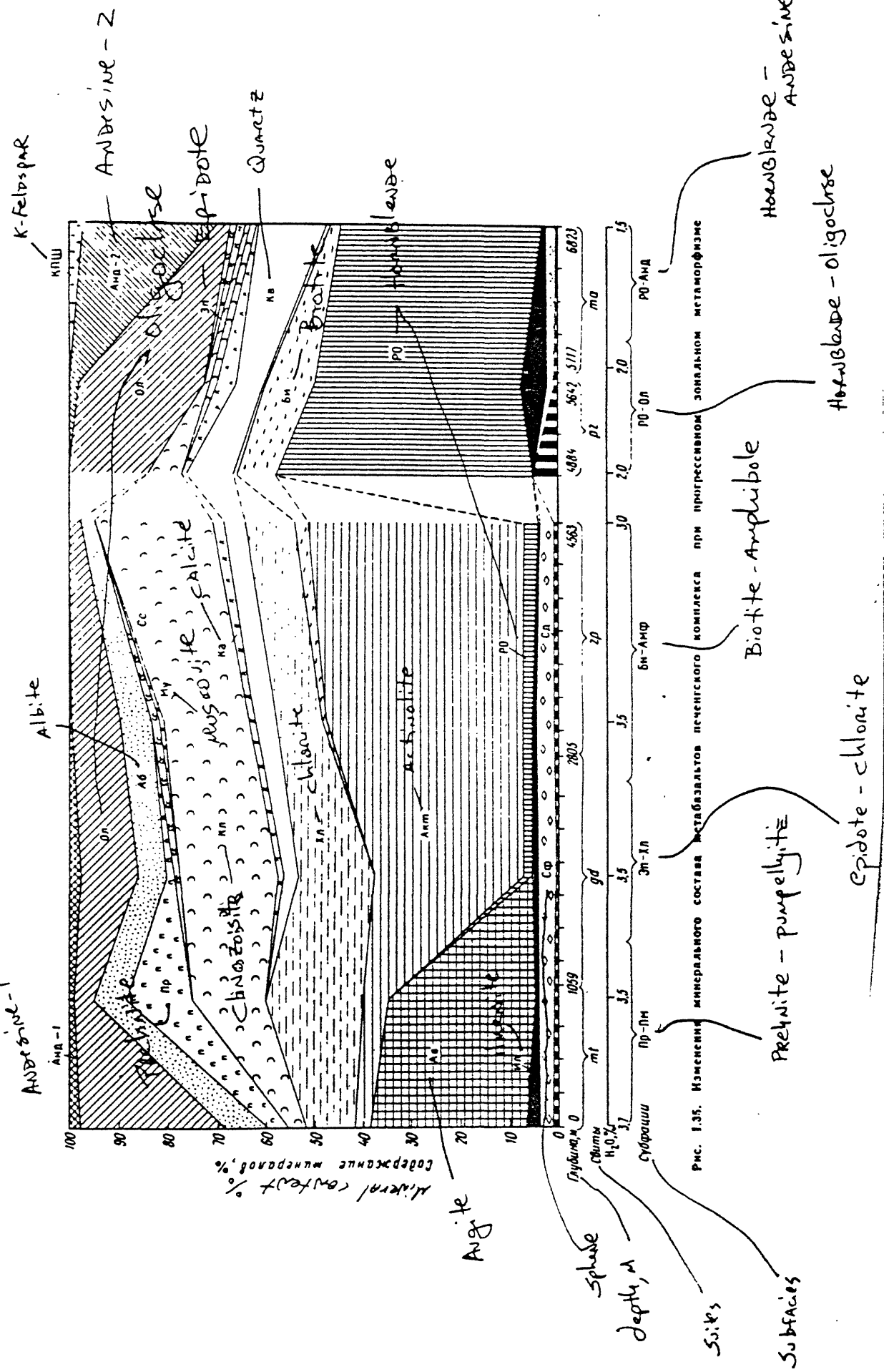
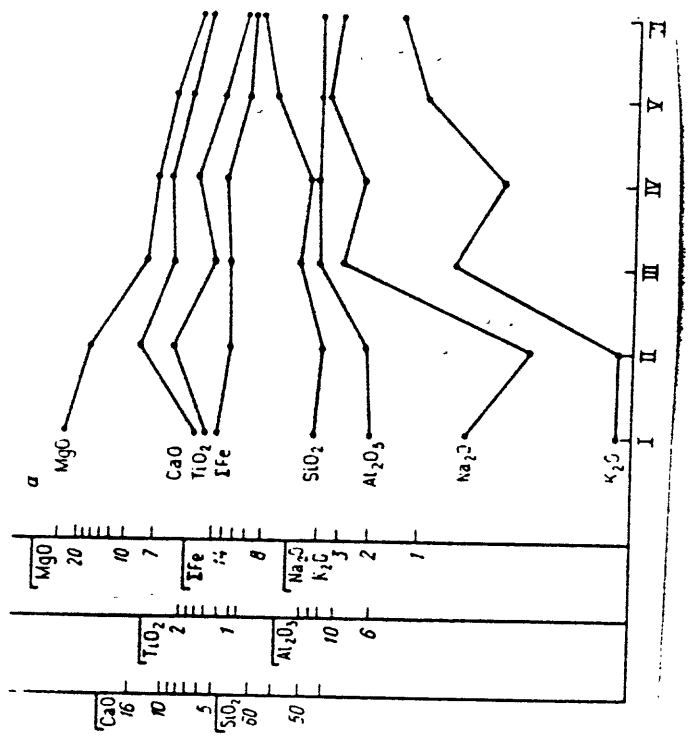


Figure 1.35 Variations in the mineralogy of meta-basalts of the Pechenga Complex within prograde metamorphic zones.



a

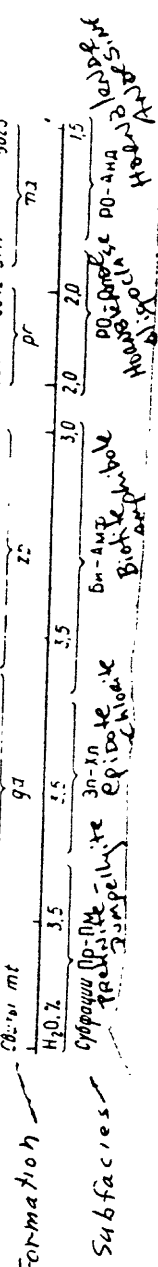
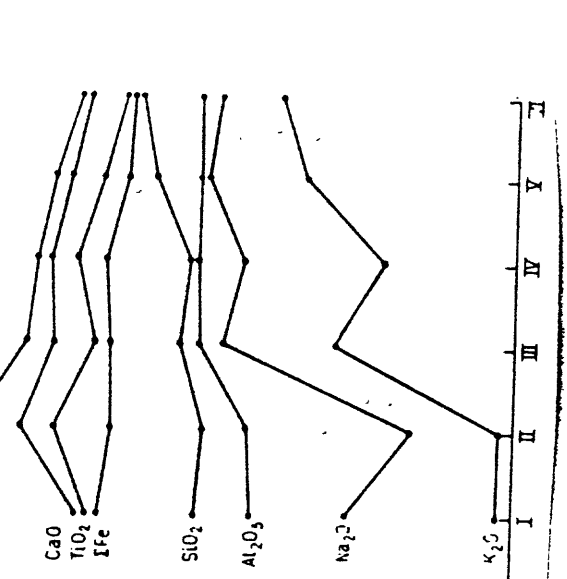


Figure 1.36 Distributional trends of major elements in various petrochemical types of meta-volcanic rocks (a) and meta-basalts of the normal series (b) with progressive metamorphism in the Pechenga Complex: I - meta-picrites; II - meta-picrite basalts; III - olivine meta-basalts; IV - meta-basalts; V - meta-andesite basalts; VI - meta-andesites.

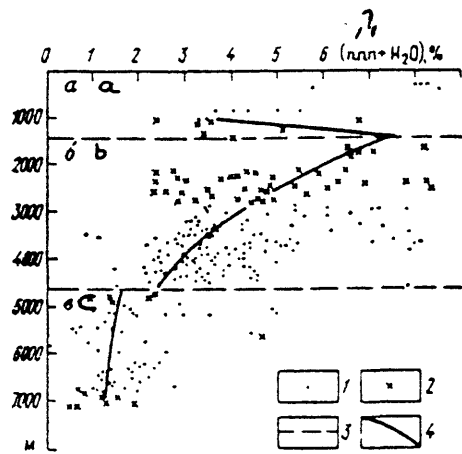


Figure I.37- Variation of water content with depth in zones of progressive metamorphism in rocks of the Pechenga Complex. 1- meta-volcanic rocks; 2- tuffaceous meta-sedimentary rocks; 3- facies boundaries (a- prehnite-pumpellyite; b- greenschist; c- epidote-amphibolite); 4- trend of variation for mean water content.

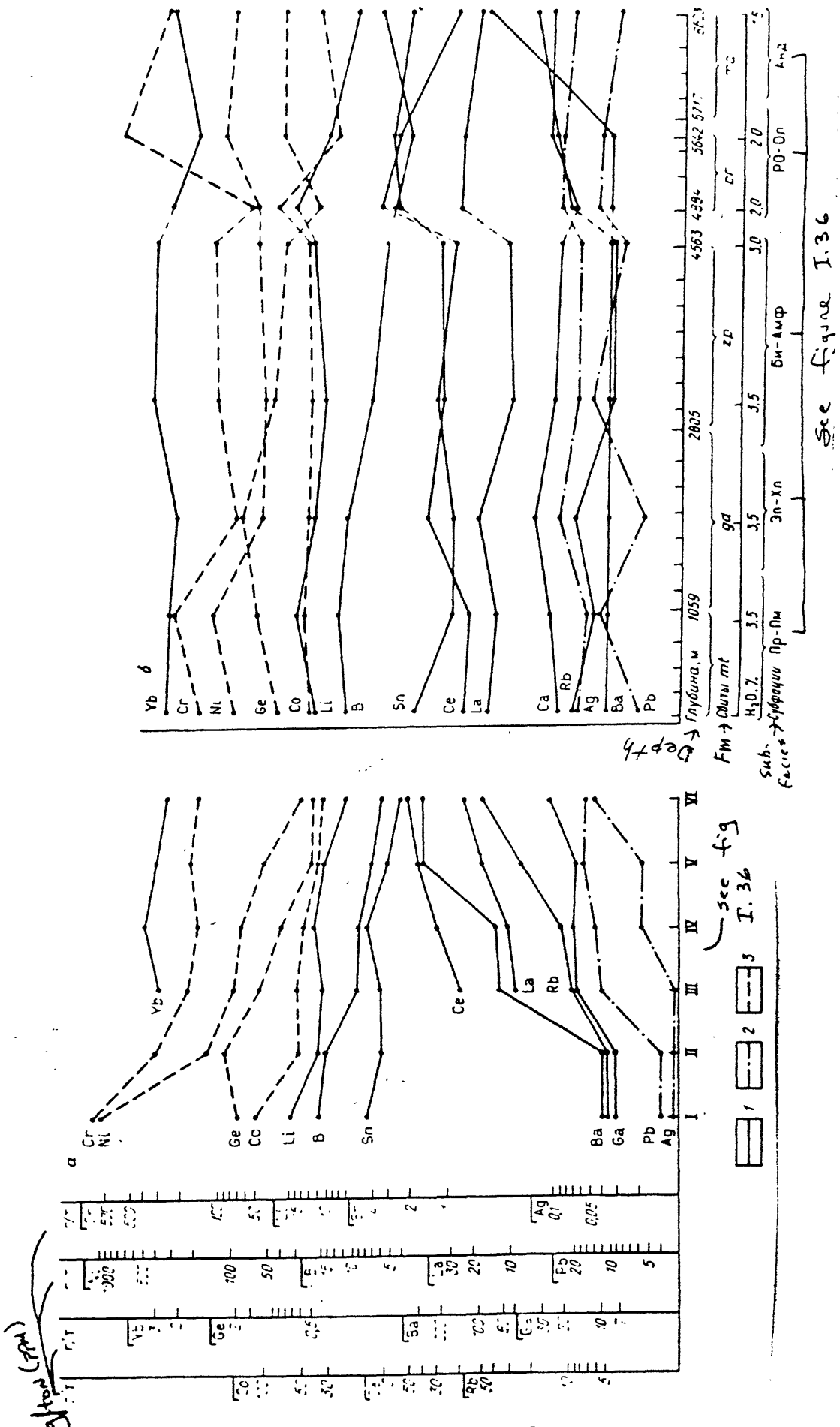
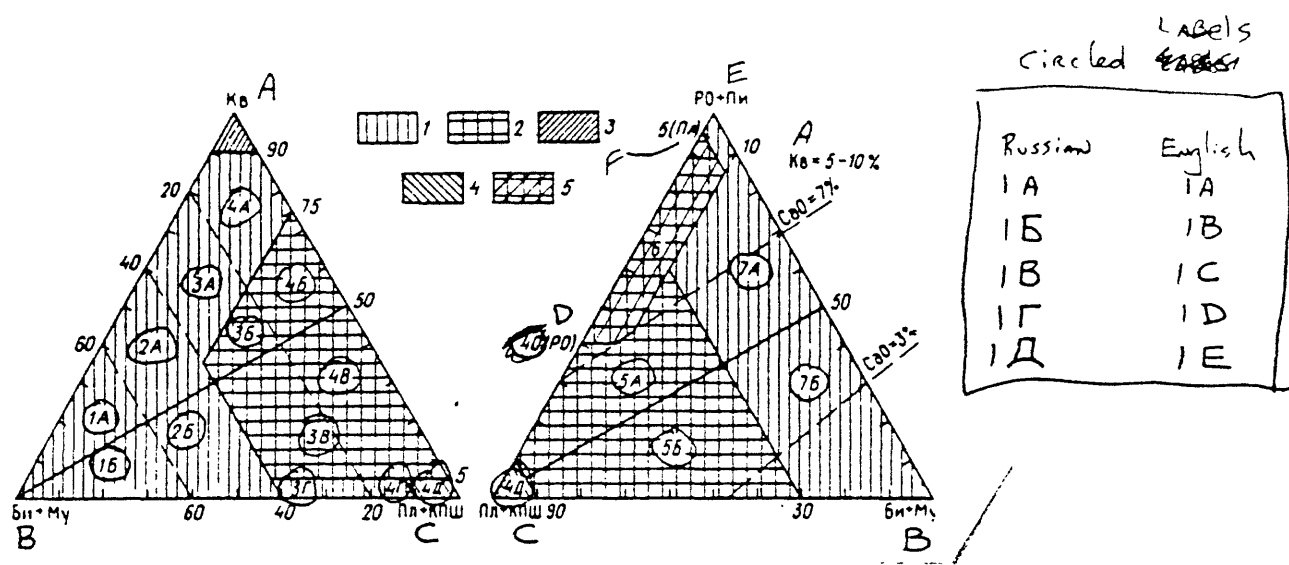


Figure I.38 - Distribution of lithophile (1), chalcophile (2), and siderophile (3) elements in various petrochemical types of meta-volcanic rocks (a) and in meta-basalts of the normal series (b) within zones of progressive metamorphism in the Pechenga Complex. See figure I.36 for additional designations.

Table I.9- Physical state and composition of metamorphic solutions at various stages of transformation in rocks of the Pechenga Complex. A - metamorphogenic rocks, isofacial folded veins; (1) B- folded retrograde veins

Table I.9 continued



**Figure I.39 Mineralogical classification of metamorphic rocks of the Kola Complex.** Rock groups: 1- schists; 2- gneisses and plagiogneisses; 3- quartzites; 4- K-feldspar rocks 5- amphibolites. Rock types: 1A, 1B- submicaceous schists (1A- feldspatho-quartzitic; 1B- quartzo-feldspathic); 2A, 2B- melanocratic micaceous schists (2A- feldspatho-quartzitic; 2B- quartzo-feldspathic); 3A-3D- melanocratic micaceous schists (3A-feldspatho--quartzitic; 3D- feldspathic); 3B - 3C - mesocratic gneisses and plagiogneisses (3B- feldspatho-quartzitic; 3C- feldspathic); 4A-4D - leucocratic schists (4A- feldspatho-quartzitic; 4D- feldspathic); 4B-4C - leucocratic gneisses and plagiogneisses (4B feldspatho-quartzitic; 4C- quartzo-feldspathic); 4E- feldspathic rocks (anorthosites); 5A- mica-amphibole (pyroxene) gneisses and plagiogneisses; 5B- amphibole-(pyroxene)-mica gneisses and plagiogneisses; 6- amphibolites; 7A-7B - amphibolite schists, hornblendites, pyroxenites (7A- mica-amphibole (pyroxene) schists; 7B- amphibole (pyroxene)-mica schists).

A: quartz

B: biotite + muscovite

C: plagioclase + K-feldspar

D: hornblende

E: hornblende + pyroxene

F: plagioclase

Table 1.10

## Nomenclature of Archean metamorphic and granitoid rocks from borehole SG-3

Груп. Группа	Суб Груп. Подгруппа	Тип Тип	(G) № подз. условное обозначение породы на рис. 1.10
Плагиогнейсы и гнейсы <i>Plagiogneisses &amp; gneisses</i>	<p><b>(A)</b> 1 Двуслюдяные сланцы и плагиогнейсы с ВГМ: гранатом, ставролитом, андалузитом, силиманитом (ВГМ)</p> <p><b>(B)</b> 1 Двуслюдяные сланцы и мелакратовые плагиогнейсы с ВГМ Мезократовые плагиогнейсы с ВГМ Лейкократовые плагиогнейсы с ВГМ</p>	<p><b>(B)</b> 1 Двуслюдяные сланцы и мелакратовые плагиогнейсы с ВГМ Мезократовые плагиогнейсы с ВГМ Лейкократовые плагиогнейсы с ВГМ</p>	1А, Б+2 А, Б 3Б, В 4В, В
	<p><b>2</b> Биотитовые плагиогнейсы и гнейсы</p> <p><b>3</b> Эпидот-биотитовые плагиогнейсы</p> <p><b>4</b> Роговообманково-биотитовые сланцы и плагиогнейсы</p>	<p><b>2</b> Лейкократовые биотитовые плагиогнейсы (<math>K_B &lt; 10\%</math> и <math>K_B &gt; 10\%</math>) Лейкократовые биотитовые гнейсы</p> <p><b>3</b> Лейкократовые эпидот-биотитовые плагиогнейсы Мезократовые эпидот-биотитовые плагиогнейсы</p> <p><b>4</b> Роговообманково-биотитовые сланцы Роговообманково-биотитовые плагиогнейсы</p>	4В 4В 4В 7Б 5Б
Амфиболиты и амфиболовые сланцы <i>Amphibolites and Amphibolite schists</i>	<p><b>(C)</b> 1 Амфиболиты</p> <p><b>2</b> Габбро-амфиболиты</p> <p><b>3</b> Амфиболовые сланцы</p>	<p><b>(D)</b> 1 Fe-Mg-амфиболиты Fe-амфиболиты Al-Mg-амфиболиты Si-амфиболиты</p> <p><b>2</b> Порфиробластические Fe-амфиболиты</p> <p><b>3</b> Актинолитовые сланцы Тальк-актинолитовые сланцы</p>	<b>(H)</b> 1 6 — биотитизированные разности
Гранитоиды <i>Granitoids</i>	<p><b>(E)</b> 1 Платиграниты</p> <p><b>2</b> Граниты</p> <p><b>3</b> Субщелочные граниты</p>	<p><b>(F)</b> 1 Платиграниты Платигнефматоиды</p> <p><b>2</b> Граниты Гранитные пегматоиды Гранодиориты</p> <p><b>3</b> Порфировидные граниты</p>	— — —

Key to Table I. 10

A)-1: two-mica schists and plagiogneisses with high-Al minerals: (garnet, staurolite, andalusite, sillimanite).

2: Biotite plagiogneisses and gneisses

3: Epidote-biotite plagiogneisses

4: Hornblende-biotite schists and plagiogneisses

B)

1: Two-mica schists and melanocratic plagiogneisses with high-Al minerals

Mesocratic plagiogneisses with high-Al minerals.

Leucocratic plagiogneisses with high-Al minerals.

2: Leucocratic biotite plagiogneisses (quartz less than 10%).

Leucocratic biotite gneisses

3: Leucocratic epidote-biotite plagiogneisses.

Mesocratic epidote-biotite plagiogneisses

4: Hornblende-biotite plagiogneisses

C)

1: Amphibolites

2: Gabbro-amphibolites

3: Amphibolite schists

D)

1: Fe-Mg-amphibolites

Fe-amphibolites

Al-Mg-amphibolites

Si-amphibolites

2: Porphyroblastic Fe-amphibolites

3: Actinolite schists

E) Talc-actinolite schists

1: Plagiogranites

2: Granites

3: Alkali-poor granites

F)

1: Plagiogranites

2: Plagiopegmatites

3: Granite porphyries

G) Field number as in Fig. 1.39; specific designation of rock also given in

Fig 1.39

H)

1: 6-biotitized varieties

2: A,B-ditto

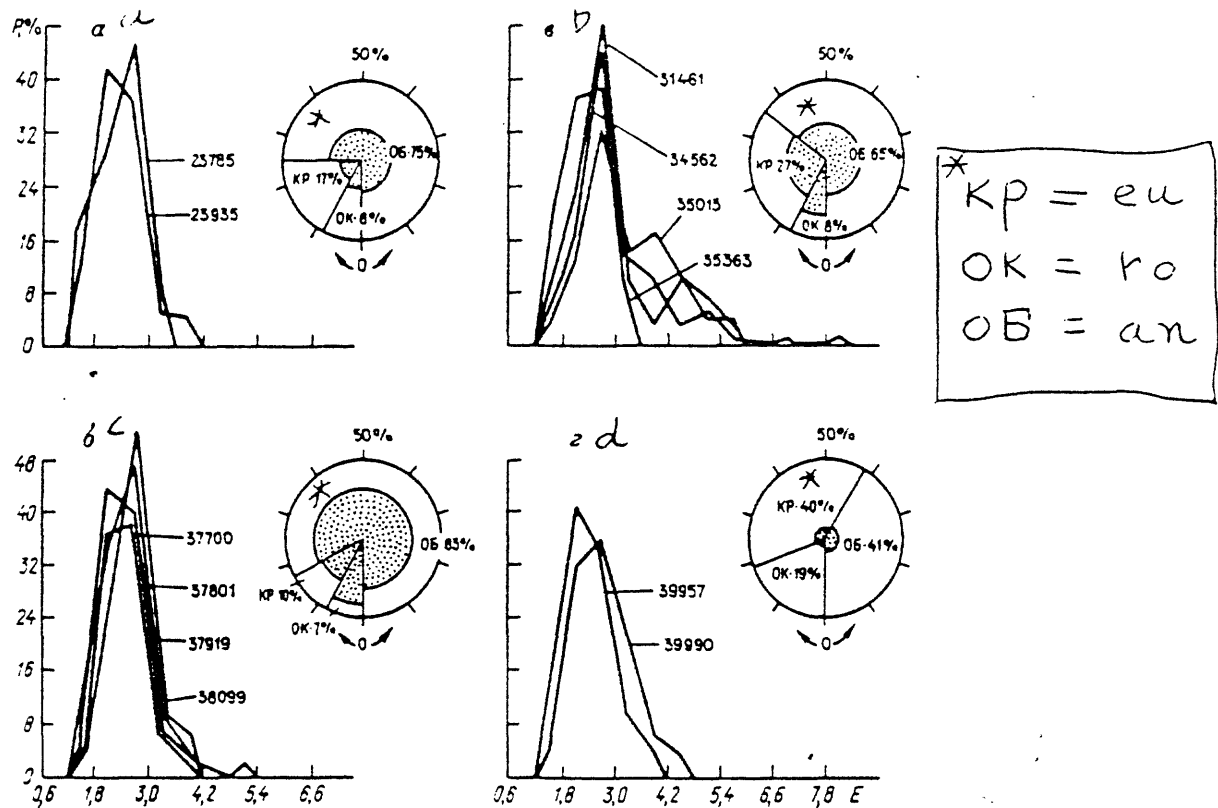


Fig. I.40 Histograms of elongation (E) and pie diagrams showing the distribution of euhedral (eu), rounded (ro), and angular (an) grains of accessory zircon in plagiogneisses of the Archean Complex. Two-mica schists and plagiogneisses with aluminum-rich minerals: a- series I; b- series III. Leucocratic biotite gneisses; c- series II; d- series IV. The relative proportion of opaque zircons is indicated by the stippled area; P,% - frequency of occurrence.

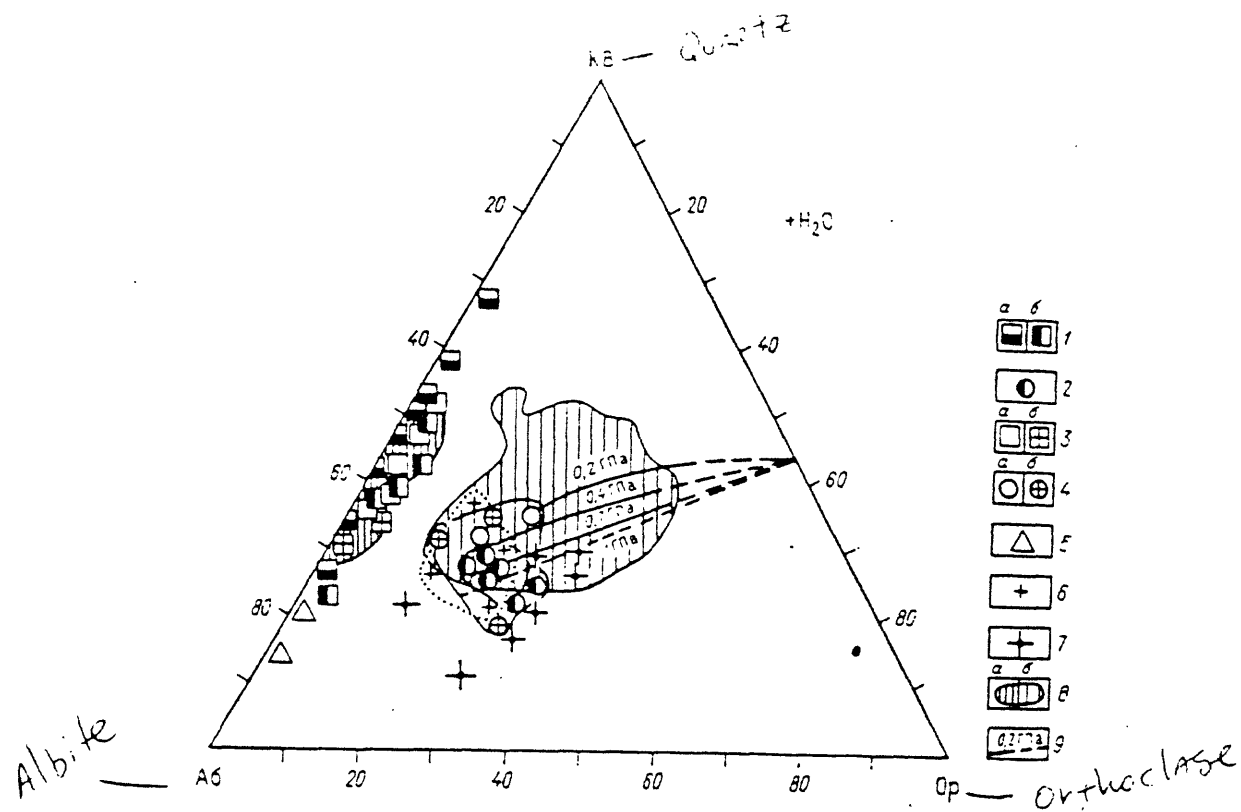


Fig. I.41 Modal composition of migmatites and granitoids of the Archean Complex plotted on the ternary diagram albite-quartz-orthoclase [19]:  
 1 - leucosomes of plagioclase migmatites and two-mica plagiogneisses and schists with high-Al minerals (a); and leucocratic biotite and epidote-biotite plagiogneisses (b); 2-leucosomes of microcline-plagioclase migmatites; 3-5 - Archean Complex granitoids: 3a - plagiogranites, 3b- plagiopegmatites; 4a- granites, 4b - granite pegmatoids; 5- granodiorites; late-folded granites; 7- porphyritic granites and pegmatites; 8-compositional field for plagiogranites, granodiorites (a) and granites (b); 9- projection of cotectic lines in the system quartz-albite-orthoclase-water at P<sub>H<sub>2</sub>O</sub> = 0.02, 0.04, and 0.07 giga-Pascals.

Table I. 11  
Average composition of rocks from SG-3 (6842-11,662 m)

Компоненты Component	Плагиогнейсы и гнейсы Plagiogneisses & gneisses									
	1	2	3	4	5	6	7	8	9	10
SiO <sub>2</sub>	62,01	63,99	69,02	64,22	70,48	70,96	65,05	62,28	64,33	51,25
TiO <sub>2</sub>	0,68	0,68	0,46	0,26	0,34	0,27	0,50	0,59	0,49	0,37
Al <sub>2</sub> O <sub>3</sub>	16,40	16,33	15,23	20,17	15,68	15,35	16,22	17,56	16,91	18,09
Fe <sub>2</sub> O <sub>3</sub>	1,23	0,87	0,47	0,48	0,51	0,55	1,14	0,57	1,02	1,82
FeO	5,71	5,55	4,14	1,79	2,18	1,59	3,19	4,54	3,47	6,90
MnO	0,07	0,07	0,05	0,02	0,03	0,04	0,06	0,05	0,05	0,11
MgO	3,47	2,88	1,79	0,58	0,88	0,65	1,85	1,94	1,84	8,04
CaO	1,74	1,99	2,07	2,42	2,09	1,68	4,22	4,00	4,57	4,23
Na <sub>2</sub> O	3,08	3,31	3,58	7,76	5,54	5,32	4,00	4,96	4,61	3,47
K <sub>2</sub> O	3,67	2,76	1,64	1,48	1,48	2,80	1,62	2,14	1,35	4,48
P <sub>2</sub> O <sub>5</sub>	0,07	0,09	0,08	0,08	0,11	0,07	0,13	0,13	0,12	0,08
CO <sub>2</sub>	0,20	0,15	0,16	0,16	0,16	0,39	0,17	0,16	0,16	0,17
H <sub>2</sub> O-	0,13	0,12	0,07	0,05	0,11	0,17	0,13	0,17	0,13	0,16
H <sub>2</sub> O+	0,90	0,67	—	0,07	0,26	0,30	0,28	0,19	0,16	0,48
п. п. п.	1,48	1,03	1,13	0,65	0,56	0,32	0,90	0,77	0,74	1,57
S	0,24	0,11	0,29	0,09	0,13	0,75	0,07	0,08	0,07	0,07
Li	51,1	44,6	21,8	9,8	15,7	17,9	57,0	33,2	29,0	30,1
Rb	185,7	131,6	82,2	34,0	54,4	95,2	126,5	123,4	77,6	122,5
Cs	6,9	7,1	2,6	1,1	1,8	1,0	1,9	3,9	—	4,5
Sr	85,0	110,4	158,9	186,0	218,2	212,0	208,5	258,8	233,5	249,4
Ba	534,3	295,3	230,0	400,7	403,9	558,9	232,0	421,0	395,3	303,1
B	6,0	6,4	7,7	8,2	8,1	8,3	6,2	6,3	6,9	5,6
Sc	16,8	14,1	8,8	2,2	2,6	3,2	13,9	11,3	11,6	15,8
Ga	32,1	23,8	20,6	29,3	29,0	29,9	30,2	33,9	27,1	20,6
La	26,0	24,0	24,0	25,0	23,0	25,0	14,0	17,0	—	25,0
Ce	54,0	47,0	51,0	44,0	46,0	44,0	26,0	28,0	—	25,0
Nd	13,0	17,0	—	14,0	19,0	13,0	13,0	13,0	—	17,0
Sm	4,0	3,5	3,4	2,1	2,1	2,3	2,8	2,8	—	3,4
Eu	1,2	1,2	1,0	0,81	0,78	0,72	1,1	1,2	—	1,3
Tb	0,67	0,59	0,62	0,22	0,26	0,19	0,49	0,39	—	0,90
Yb	1,8	1,8	1,9	0,38	0,40	0,21	1,7	1,1	—	2,7
Lu	0,25	0,27	0,29	0,06	0,06	0,05	0,30	0,22	—	0,34
Th	7,1	5,8	5,6	8,4	9,1	8,4	0,70	1,2	—	1,8
U	6,0	5,0	8,0	3,7	4,7	2,1	1,5	2,0	—	2,6
Ge	0,50	0,51	0,50	0,50	0,50	0,50	0,52	0,53	0,50	0,69
Zr	71,4	74,7	72,2	98,7	104,5	69,1	57,0	60,0	42,9	39,4
Sn	3,8	3,0	3,0	2,6	2,9	3,2	4,2	3,8	3,5	3,3
Hf	4,2	4,1	4,1	3,7	3,6	3,1	4,6	4,3	—	4,1
Nb	3,2	7,6	5,2	2,1	2,9	2,5	4,7	2,5	2,4	3,2
Ta	0,66	0,54	0,52	0,19	0,24	0,12	0,33	0,39	—	0,45
F	1152,8	872,5	244,4	197,3	172,9	169,2	583,5	509,4	312,1	931,9
Cu	40,4	89,4	50,9	25,3	15,7	17,3	83,4	26,7	29,2	48,3
Zn	145,7	89,6	52,2	35,7	43,1	44,5	71,1	115,3	95,0	90,3
Ag	0,03	0,08	0,05	0,03	0,05	0,06	0,11	0,05	0,04	0,07
Pb	21,8	31,6	17,9	20,7	21,7	31,0	20,9	20,2	25,1	21,4
Mo	1,1	1,6	1,3	0,77	0,81	0,80	1,5	0,98	0,80	1,0
V	112,8	115,5	76,9	31,0	32,8	33,7	139,2	130,4	88,9	156,4
Cr	216,7	150,7	99,3	37,7	31,6	43,1	95,4	44,0	97,1	160,9
Co	25,7	20,8	14,0	3,8	4,6	5,3	19,6	15,1	17,6	26,4
Ni	112,3	67,1	44,2	15,1	9,5	9,9	42,8	29,6	72,3	107,2
Число проб Number of samples	23	60	11	15	130	91	20	32	17	16

A: 1-3 - Two-mica plagiogneisses with high-alumina minerals (1- melanocratic, 2- mesocratic, 3- leucocratic); 4-5 - leucocratic biotite-plagioclase plagiogneisses (4- quartz content less than 10%, 5- quartz content more than 10%); 6- leucocratic biotite gneisses; 7-8 epidote-biotite plagiogneisses (7- leucocratic, 8- mesocratic); 9-10 - hornblende-biotite plagiogneisses (9-

Table I. 11 - continued

Amphibolite + amphibolite schists							Granitoids			
Амфиболиты и амфиболовые сланцы							Гранитоиды			
11	12	13	14	15	16	17	18	19	20	21
48,15	50,01	49,60	54,48	51,72	52,73	58,01	72,11	72,32	72,83	72,19
2,23	1,40	1,64	0,80	0,41	0,19	0,07	0,20	0,11	0,15	0,27
10,86	14,20	13,64	14,28	17,57	7,18	2,12	14,78	15,31	14,62	14,24
3,50	3,10	3,70	2,37	2,20	2,90	1,60	0,79	0,28	0,15	0,73
11,33	10,31	10,09	7,83	6,92	6,78	5,53	2,32	1,62	2,14	1,59
0,22	0,22	0,22	0,16	0,15	0,23	0,16	0,04	0,09	0,03	0,12
9,60	6,00	6,15	5,89	7,95	12,21	24,85	0,63	0,33	0,33	0,50
9,85	9,95	10,04	8,76	9,31	14,26	3,49	2,79	1,25	1,02	1,07
1,89	2,31	2,3	2,50	2,02	0,54	0,25	5,28	4,29	4,63	3,30
0,68	0,63	0,64	0,89	0,51	0,43	0,08	1,30	3,50	3,63	5,40
0,19	0,12	0,14	0,11	0,0	—	0,06	0,04	0,05	0,09	0,07
0,14	0,20	0,17	0,26	0,15	—	0,16	0,16	—	0,26	0,22
—	0,08	0,09	0,12	0,04	—	0,06	—	—	0,14	0,16
—	0,17	0,28	0,35	0,78	0,98	2,08	—	—	0,46	0,30
1,53	1,32	1,14	1,47	1,20	1,52	1,58	0,07	0,03	0,61	0,29
0,22	0,11	0,11	0,08	0,06	—	0,07	—	—	0,05	0,10
17,7	13,8	14,4	15,3	12,6	5,8	3,5	8,4	5,0	21,8	15,6
25,3	17,4	17,6	43,4	10,4	5,0	16,7	22,0	73,3	99,4	229,1
2,6	2,0	2,0	2,0	2,0	—	1,0	0,32	0,56	1,1	2,5
186,9	157,3	180,0	199,3	227,1	200,0	22,5	172,0	268,1	111,8	81,8
154,6	119,2	138,2	201,3	167,1	35,0	33,8	382,0	1085,6	310,0	342,6
6,8	6,3	5,9	7,0	4,7	7,0	4,5	7,7	11,1	8,8	8,3
44,0	37,3	36,9	31,8	32,9	9,0	5,2	3,3	1,7	6,1	2,6
21,3	20,9	23,5	19,6	22,1	20,0	8,2	21,0	26,7	25,6	31,0
29,0	12,0	13,0	14,0	7,0	—	0,97	33,0	6,0	4,0	62,0
58,0	27,0	27,0	28,0	12,0	—	5,0	64,0	9,0	8,0	138,0
—	12,0	14,0	15,0	8,0	—	10,0	22,0	7,0	5,0	54,0
8,3	3,8	4,1	3,1	1,2	—	0,55	3,9	0,66	1,0	8,6
2,7	1,4	1,5	1,1	0,58	—	0,18	0,87	0,64	0,39	0,62
0,99	0,73	0,80	0,59	0,35	—	0,10	0,51	0,14	0,54	0,97
2,0	2,5	2,5	2,0	1,7	—	0,39	0,44	0,20	0,48	1,1
0,25	0,35	0,45	0,34	0,31	—	0,05	0,15	0,04	—	0,15
2,2	1,9	1,5	2,0	1,5	—	1,0	18,0	1,7	3,2	41,2
2,4	2,0	2,0	2,2	2,0	—	2,6	2,0	1,0	9,1	5,6
1,0	0,75	0,77	0,57	0,50	1,0	1,8	0,50	0,50	0,50	0,50
73,1	68,7	58,7	55,8	27,5	5,0	7,5	114,0	43,3	61,2	81,5
5,9	2,9	5,6	3,4	2,3	6,0	2,2	2,7	3,8	3,2	4,1
5,5	2,6	2,6	2,9	1,1	—	0,30	4,1	1,6	2,7	6,0
5,5	3,2	3,5	4,6	—	3,0	1,5	8,3	2,4	7,8	4,8
1,8	0,53	0,51	0,34	0,27	—	0,10	0,16	0,06	1,2	0,40
590,8	428,5	273,1	556,8	212,1	1600,0	750,0	67,5	61,1	417,5	213,5
192,8	129,2	114,6	72,9	35,6	5,5	4,4	39,8	12,7	83,0	6,8
150,4	124,8	125,0	97,0	160,0	180,0	115,0	34,0	23,3	37,3	40,2
0,03	0,03	0,06	0,05	0,04	0,05	0,02	0,06	0,04	0,13	0,06
103,1	13,0	12,3	18,7	17,8	15,0	4,1	27,2	32,2	22,9	53,4
1,6	1,0	1,6	0,89	0,78	1,0	0,81	0,78	0,75	1,3	3,4
188,3	239,1	331,6	182,2	77,8	83,5	14,2	29,8	11,9	43,3	21,3
414,6	92,1	80,7	29,6	105,8	540,0	980,0	24,6	40,2	48,4	35,8
61,0	41,1	50,8	38,7	47,4	36,0	95,0	5,1	3,3	11,9	3,1
169,1	70,1	64,0	76,1	160,6	790,0	2175,0	7,2	8,1	26,1	12,1
26	68	101	60	15	4	4	5	15	16	34

mesocratic, 10- melanocratic); 11- Fe-Mg amphibolites; 12- Fe-amphibolites; 13- porphyroblastic Fe and Fe-Mg amphibolites; 14- Si-amphibolites; 15- Al-Mg amphibolites; 16- actinolite schists; 17- talc-actinolite schists; 18- plagiogranites; 19- granites; 20- granite pegmatoids; 21- porphyritic granites. Major-element content given in percent, trace elements in g/ton (ppm); dashes indicate element not detected.

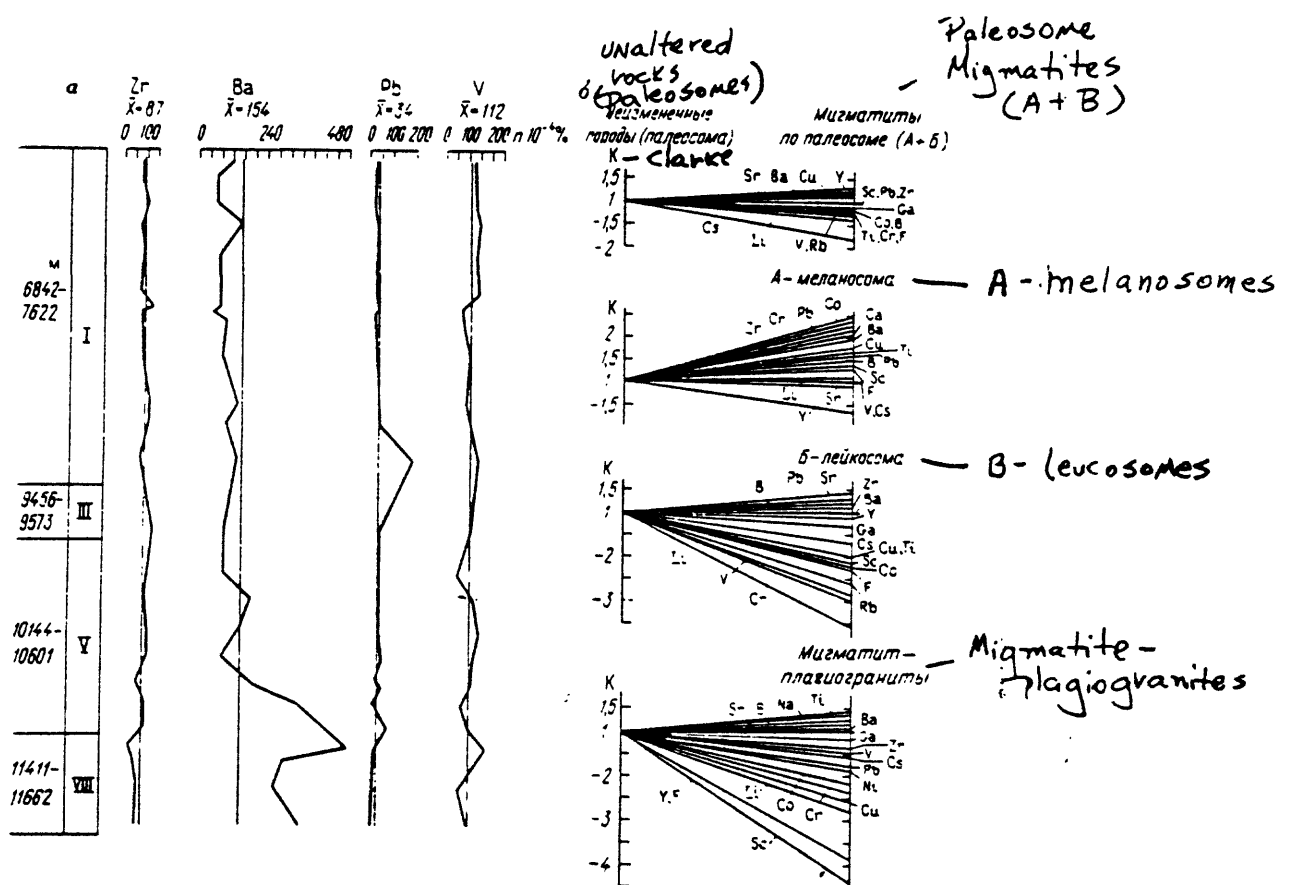


Fig. I.42 Distribution of trace elements in paleosomes of mesocratic plagiogneisses with high-alumina minerals for the Kola-Complex section (a) and associated migmatites (b)

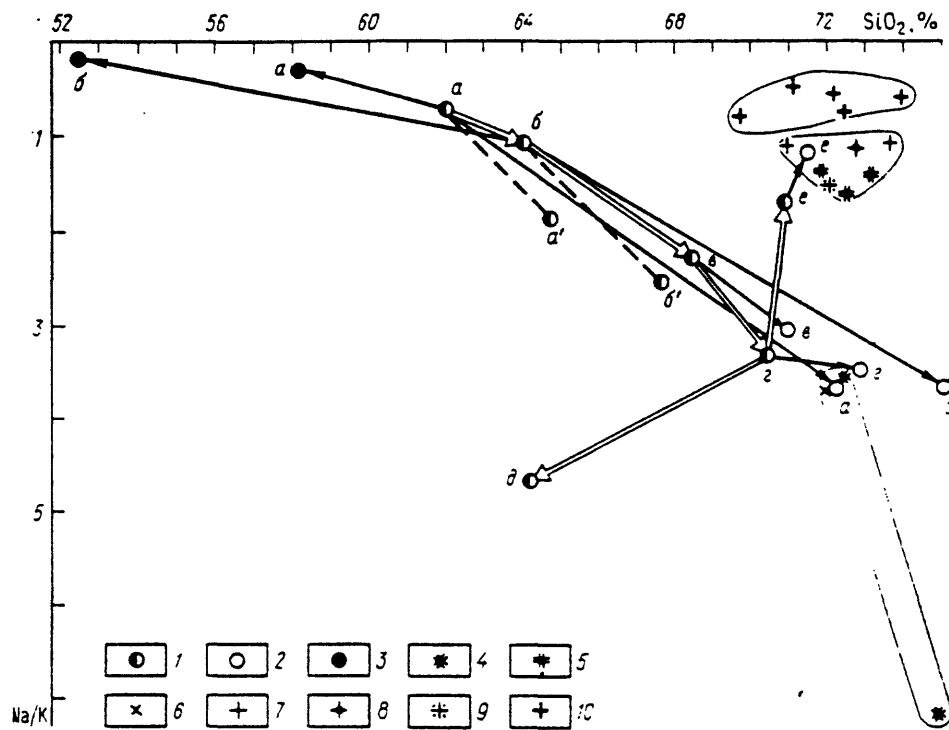
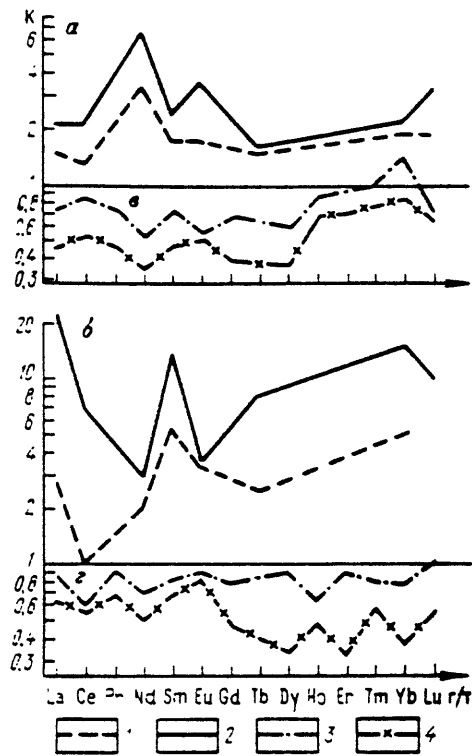
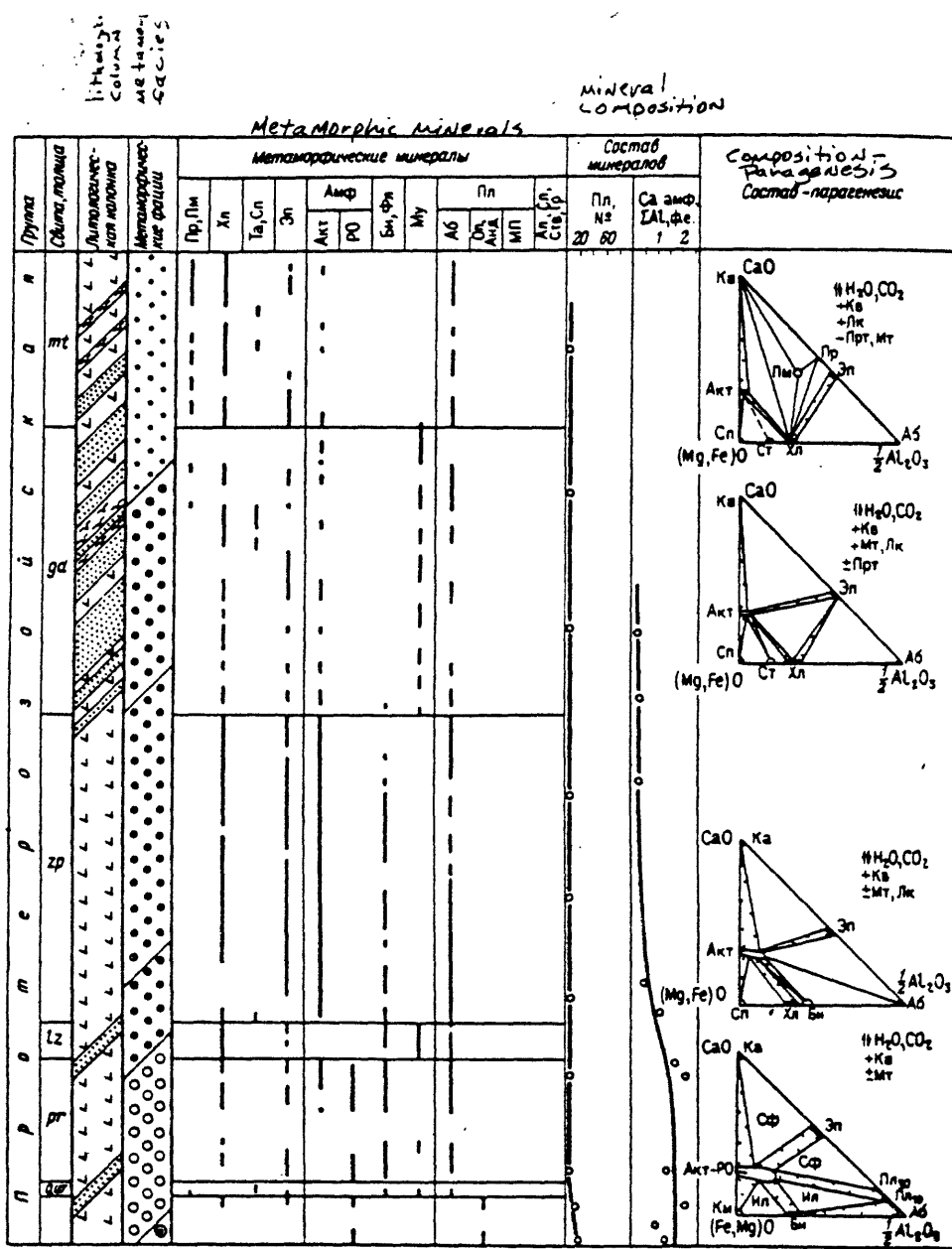


Fig. I.43 Chemical composition of migmatites and granites of the Archean Complex: 1-3 - migmatites (1-paleosomes, 2- leucosomes, 3- melanosomes) from two-mica schists with high-alumina minerals (a), mesocratic plagiogneisses with high-alumina minerals (b), leucocratic plagiogneisses with high-alumina minerals (c), leucocratic biotite plagiogneisses with more than 10% quartz (d), less than 10% quartz (e), and leucocratic biotite gneisses (f); 4-8 - granitoids (4- plagiogranites less than 1m thick; 5-granites less than 1m thick, 6- plagiogranites greater than 2m thick, 7- granites greater than 2m thick, 8- pegmatoids); 9- late-folded granites; 10- porphyritic granites; estimated composition of migmatites from two-mica schists with high-alumina minerals (a,) and mesocratic plagiogneisses with high-alumina minerals (b,)



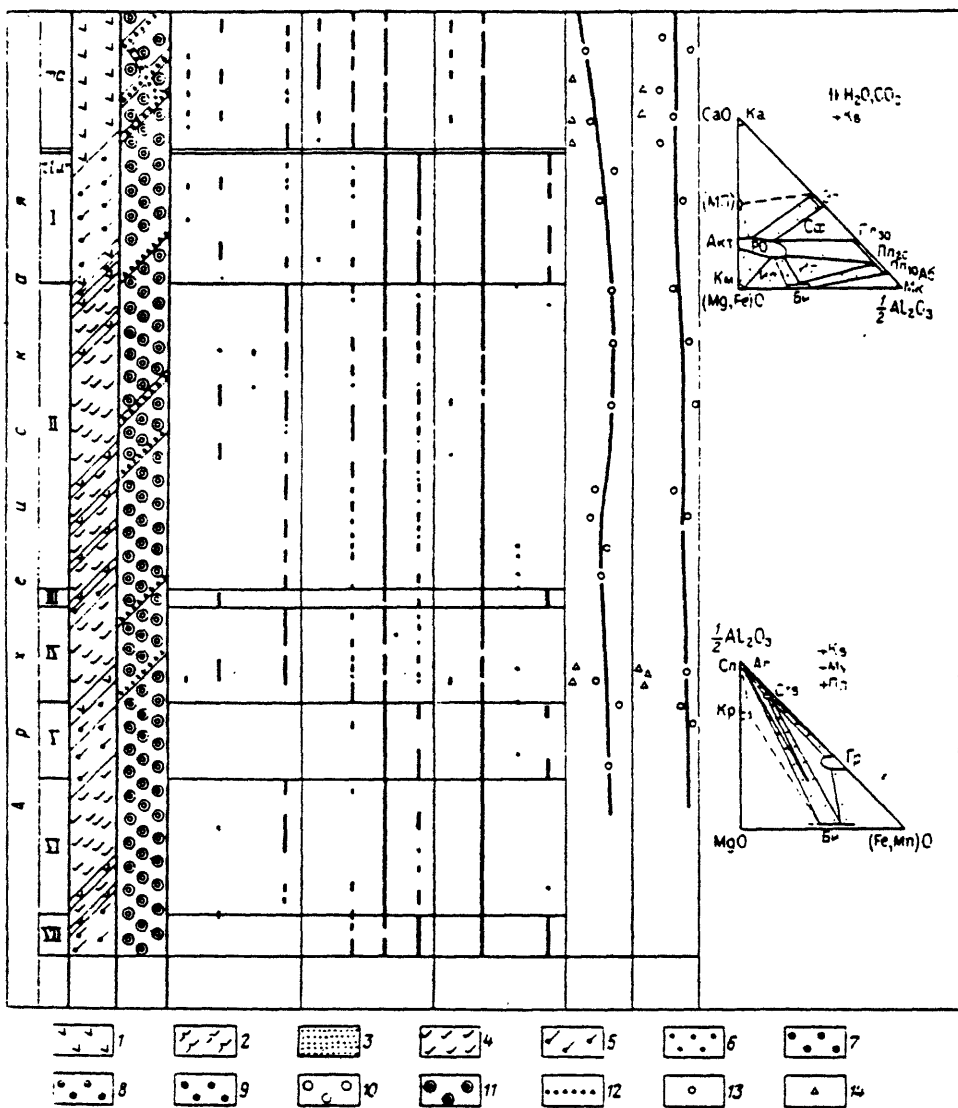
**Fig. I.44** Distribution of rare-earth elements in biotitized amphibolites (a), amphibolite schists (b), migmatized two-mica plagiogneisses with high-Al minerals (c), and leucocratic biotite plagiogneisses (d):  $K = \text{Bi}(M)/P$ , where  $\text{Bi}(m)$  is the content of REE in biotitized (Bi) or migmatized rocks; P is the REE content in the country rock (paleosome); the degree of biotitization is 1-5-25%, 2- 25-50%; 3- migmatites; 4- leucosomes.



First half of figure I.45

Fig. I.45 Vertical zonation of metamorphism in the section from borehole SG-3: 1-5 - metamorphic rocks (1- metabasites, meta-ultrabasites, 3- metasedimentary rocks, 4- biotite plagiogneisses, 5- sillimanite gneisses); 6-11 - progressive metamorphic facies: 6- prehnite-pumpellyite, 7-9 - greenschist (subfacies: 7- epidote-chlorite, 8- biotite-actinolite, 9- biotite-amphibolite), 10- epidote-amphibolite, 11- amphibolite; 12- retrograde greenschist facies; content of metamorphic minerals: 13- prograde, 14- retrograde stage. Mineral associations of metabasites are shown on the composition-paragenesis diagrams for the prehnite-pumpellyite, greenschist, and epidote-amphibolite facies; for the amphibolite facies the mineral associations of metabasites (above) and gneisses with high-Al minerals are shown.

ПР - Prehnit  
 ПМ - Pumpelly  
 ХЛ - chlorite  
 Та - talc  
 Сп - Spinel  
 ЭП - epidote  
 Амб - amphibole  
 АКТ - actinolite  
 РО - Hornblen  
 Би - Biotite  
 ФЛ - phlogopite  
 Му - muscovite  
 ПЛ - plagiocl  
 А6 - Albite  
 ОЛ - oligochock  
 АНД - andesite  
 АР - Apatite  
 Сп - Spinel  
 СТВ - Staurol  
 ГР - Garnet



Second half of figure I. 45

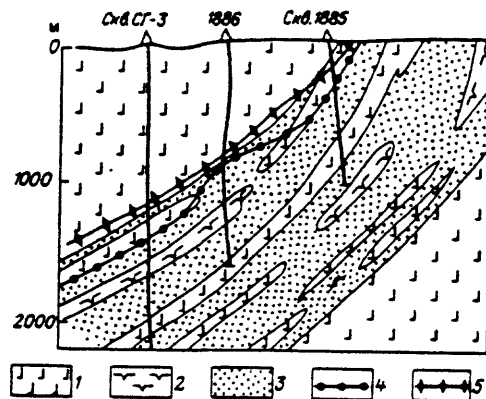


Fig. I.46 Lithological cross section for boreholes SG-3, 1886, and 1885: 1- metabasites, 2- meta-ultrabasites, 3- metasedimentary rocks, 4- boundary between prehnite-pumpellyite (above) and greenschist facies (below), 5- boundary for the replacement of clinopyroxene by actinolite.

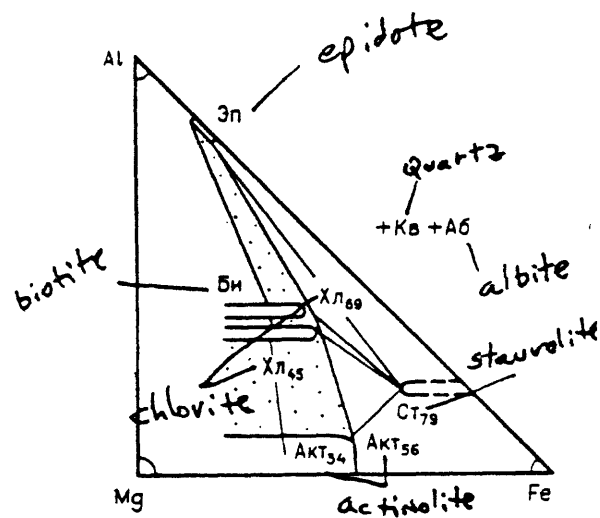


Fig. I.47 Compositional-paragenetic diagram for metabasites of the greenschist facies. Numbers near mineral abbreviations indicate the relative proportions of ferrous iron (ferrous/ferrous + ferric).

## MINERALIZATION

The major ore deposits of the northwestern Kola Peninsula belong to the Pechenga copper-nickel sulfide district. The majority occur in the Pechenga Complex, but some are in the Kola Group. In addition, there are iron quartzites, muscovite-bearing pegmatites, and hydrothermal lead-zinc veins.

Gorbunov established that the Pechenga deposits are spatially and genetically connected with mafic-ultramafic intrusives, having a primary metamorphism and hydrothermal activity that produced rich epigenetic ores. Most of the nickel intrusives are concentrated in the upper and lower parts of the Zhdanov Formation in two trends, Eastern and Western.

Transverse folding of the tuffaceous-sedimentary rocks and intrastratal disturbances play a role in localizing the nickel intrusives. The intrastratal disturbances usually affect the bottom portions of the mafic-ultramafic intrusives and control epigenetic brecciated ore bodies.

One of the main goals of the Kola Superdeep, located in the center of the Pechenga district, was to evaluate the potential for Cu-Ni ores at depth, and this has been accomplished. A previously unknown zone of ultramafics and Cu-Ni ores was drilled through in the middle Zhdanov Fm. Further drilling indicated mineralization of various types not only in the Pechenga Complex but in the underlying Kola Group.

Ore minerals were found in the entire section of the Kola Superdeep; pyrrhotite, chalcopyrite, pentlandite, magnetite, ilmenite, and leucoxene. Sulfides ranged from isolated grains to 50%. Greatest concentrations were in zones of pyrrhotite mineralization in the tuffaceous-sedimentary rocks of the Zhdanov Fm. This formation also hosts the ultramafic intrusives with the Cu-Ni mineralization. The deepest 3000 m of the Pechenga Complex contain less than 1% sulfides and only in the 6000-6835 m interval do sulfides reach 4%, where they include chalcopyrite. The sulfides form streaks of disseminated grains (from hundredths of a mm up to 2 mm), veinlets, pods and lenses, in which they are associated with quartz and calcite. Quantities are significantly higher in zones of cataclasis and phyllonitization.

Sulfides were found also in the Kola Group. Contents vary: in gneisses from isolated grains to 0.5% (1-2% in some specimens), in amphibolites 0.1 to 0.3% (3-5% in local segregations), and in meta-ultramafics 0.1 to 0.5%.  
15

Oxide mineralization also occurs through the entire depth, but more evenly distributed than the sulfides. Opaque oxides range from isolated grains up to 5-10%. They predominate over sulfides in the whole section, except in the Zhdanov Fm. They include magnetite, titanomagnetite, chrome spinal, ilmenite, rutile, hematite, and leucoxene. Magnetite is most important in the Proterozoic section; ilmenite, magnetite and rutile in the Archean. Rarer minerals were found -- see table 119. Types of mineralization found are:

- 1) Cu-Ni sulfide mineralization associated with the mafic-ultramafic intrusives in the Zhdanov Fm. and in metamafites and meta-ultramafics of the Kola Gp.
- 2) Fe-Ti mineralization in metamafites of the Kola Gp.
- 3) Fe-quartzites within the granite-gneisses of the Kola Gp.
- 4) Hydrothermal sulfide mineralization in retrograded shear zones in metamafites of the Pechenga Complex and in rocks of the Kola Gp. The first is of both theoretical and practical importance; the rest are of theoretical importance only.

#### CU-NI SULFIDE MINERALIZATION

##### CONDITIONS OF OCCURRENCE

(Details of occurrences mentioned above, mostly in the Pechenga Complex)

Types of ore and their Mineral Composition. In the Proterozoic complex there are three types of ore: disseminated ores in altered periodotite, breccia ores in disturbed zones, and veinlet and disseminated ores in phyllites. Lean ores in the periodotites have less than 2-3% sulfides and about 5-7% oxides but are upgraded by alteration to over 15% sulfide. Breccia ores run from 20 to 90% sulfides. Veinlet and disseminated ores in phyllite from 2 to 60%. Pyrrhotite is the dominant mineral in each, with subsidiary pentlandite and chalcopyrite. Considerable descriptive and analytical detail follows, but anything indicative of grades and bondages of copper and nickel is conspicuously absent.

## Genesis

The source of Cu-Ni ores was doubtless the ultramafic intrusives. Ni-rich pyrrohoite ores extend only 10.5 m from the contact of serpentinized peridotite into underlying phyllites. We suggest the surrounding tuffaceous-sedimentary rocks have a massive sulfide-type pyrite-pyrrhotite mineralization.

### Fe-Ti mineralization in metamafites.

Magnetite, ilmenite, and sometimes rutile occur through the whole section. They reach a high concentration in the Kola Group at 8711 m in schistose biotite amphibolite and metamorphosed gabbro.

### Fe-quartzite

Fe-quartzite (7635 m) has a banded texture, with biotite-quartz layers alternating with magnetite-rich layers. The magnetite runs 20-30% in 0.1-0.3 mm grains. One sample has accessory apatite, zircon, and allanite, which is not characteristic of banded iron formations, but the magnetite is chemically pure, which is characteristic of BIFs.

Hydrothermal sulfide mineralization in zones of retrograde metamorphism along fractures. These are found at depths of 6 to 10 km in both complexes. Sulfide mineralization is thinly disseminated or rarely in richer lenses and veins, and consists of pyrrhotite, pyrite and chalcopyrite, with rarer sphalerite, galena, bornite, molybdenite, argentopentlandite, and <sup>S</sup>iegnite, with various gangue minerals.

The Kola Superdeep confirms predictions on the presence of Cu-Ni sulfide ores at depth in the Pechenga District. It has been established that these ores are found in the same geologic environment as the other deposits of Pechenga, lying at the contact of metaperidotites with phyllites, complicated by zones of phyllonitization. In textural and structural characteristics, mineralogy and genesis, the ores are like those at the surface, indicating persistence to depth, with a significant fall-off at 2.5 km. An important find is the previously unknown zone of ultramafics and Cu-Ni ores in the middle of the tuffaceous-sedimentary rocks of the Zhdanov fm.

These findings change current ideas on the vertical zonation of endogenous mineralization in the ores, and clarify the occurrence of various types of mineralization at depth under conditions of varying age.

#### FRACTURES AND MINERALIZED FISSURES

All investigators have emphasized the importance of fracturing in the geology of the Pechenga region. Gorbunov et al., have established five stages in the history of the ore deposits:

- 1) Eruption of mafic volcanics and intrusion of gabbro-diabase sills;
- 2) Karelian folding and intrusion of mineralized mafic and ultramafics;
- 3) Change of stress directions leading to cross-folding;
- 4) Metamorphism of rocks and ores under conditions of brittle deformation;
- 5) Displacement of ore bodies along faults with the formation of clayey gouge.

Investigation of the Kola Superdeep core was not able to detect the entire history of fracturing as determined from surface exposures. However, it did offer the rare opportunity to investigate the internal structure of the fractures, the relation between metamorphism and faulting, and the vertical zonation and quantitative characteristics of mineralized fractures.

Systematic observation of the internal structure of fractures and the distribution of mineralized veins was carried out down to 7 km. This is for two reasons: 1) the homoclinal attitude of the beds of the Pechenga Complex and the reliable correlation of the sedimentary-volcanic beds with those cropping out at the surface, 2) the recovery of core in this interval by a straight core barrel, which guaranteed the preservation of the core "up-down" and its relative position within a single trip. At greater depths these data were intermittent, but still of interest.

#### Fractures and Dislocation Metamorphism

Dislocation metamorphism (alteration associated with faulting) was studied in the Kola Superdeep through the texture and structure of the rocks and the mineral associations including their fabric. (Fig. I-60). There are three groups of textures associated with dislocation metamorphism: banded-phyllitic for sandstones, siltstones and fine-grained tuffs; schistose for the metamorphic, pyroclastic and intrusive rocks, and finally cataclastic.

The fullest data were obtained from the Pechenga Complex, showing increasing intensity of deformation and recrystallization downward.

Down to 4340 m dislocation metamorphism was restricted to fairly narrow seams, the internal texture of which is determined basically by the original rock. Below this depth, original lithology becomes secondary, and all the rocks have undergone a process of schist formation, with a regular oriented fabric of metamorphic minerals.

## MINERALIZED FISSURES AND THEIR DISTRIBUTION WITH DEPTH.

One of the unexpected findings was the wide distribution at all depths of fissures with various mineral fillings. These were systematically studied. Doubtless unmineralized fractures exist, but the logging techniques were unable to spot these in the outside of the hole, and in the cores the only unmineralized fractures that could be confidently distinguished were those that were a consequence of the drilling and core-handling itself.

Mineralized fractures in the cores were divided into two classes each with two subclasses A) lithogenetic or premetamorphic (A-1 diaconitic fractures in the weakly metamorphosed sediments and A-2 contraction fractures in the diabase sills) and B) tectonic (B-1 associated with prograde and B-2 with retrograde metamorphism).

Fractures also classified by orientation: Series I) concordant with contacts and primary textural elements of the rock; Series II) High angle, almost perpendicular to same, transverse fractures; Series III) High angle, at angles less than 30-60° to same, diagonal fractures; Series IV) Slanting, with a thrust relationship to same.

Fractures were investigated in homogeneous intervals. The basic measurements were the number of fractures per meter of core and the total thickness of veins and veinlets per meter, as a whole and in each of the four series, as summarized in the various figures and tables.

## Discussion of Findings

In the early stages of the geologic development of a single region, the character of deformation varies in dependence on the geothermal regime, which in turn involves a more markedly zoning or a more uniform vertical profile. Under conditions of low heat flow, shallow-type fracturing may extend to great depths. It must be added that 10-11 km is the minimum depth of the zone of regressive dislocation metamorphism. Unfortunately, its geologic age, and the amount of cover eroded are not precisely known. Tentatively, 3-5 km may be taken as eroded, so the zone of crushing, fracturing and low-temperature mineralization in the Baltic Shield may originally have reached to 15 km.

### FRACTURING, PHYSICAL PROPERTIES AND ANISOTROPY OF THE ROCK

Fracturing in the cores was compared with bulk measurements of density, total porosity, natural moisture content, open porosity, and velocities of compressional and transverse waves in three mutually perpendicular directions. A clear connection was established between the progressive metamorphism and the thrust-slice displacements of the Pechenga Complex along conformable faults. It was established that the downward increase of the temperature of metamorphism is accompanied by the transition from brittle to ductile deformation, with the appearance of extensive oriented recrystallization and neocrystallization of minerals, and the development of anisotropy toward elastic waves.

Extensive statistical data <sup>were</sup> for the first time obtained on the distribution of mineralized fractures to a depth of 7 km. The important factors determining the frequency, orientation and mineralization of fractures were determined. It was found that mineralized zones of crushing, cataclasis, fracturing and low temperature hydrothermal alteration, including sulfide mineralization, extend to depths 3 or 4 times what had been supposed from general principles.

In distinction from the near-surface situation, there was established a direct correlation of the intensity of development of mineralized fractures not with the porosity of the rock but with the anisotropy of the elastic properties and the dispersion of the compressive waves.

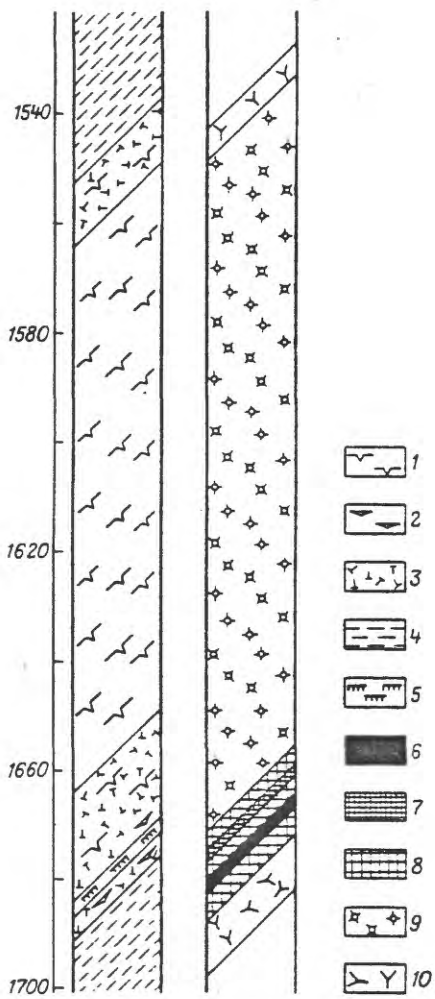


Fig I-51 structure of a nickeliferous intrusive in Superdeep 3, showing zonation of metaperiodotite and of Cu-Ni ore.

1. Massive metaperiodotites
2. Phyllonitized
3. Talcose
4. Schistose phyllite and siltstone
5. Phyllonitized
6. Breccia ore
7. Thickly disseminated ore
8. Thinly disseminated ore
9. Rich disseminated ore in metaperiodotites
10. Veinlet and disseminated ore in phyllites and siltstones.



Fig. 54

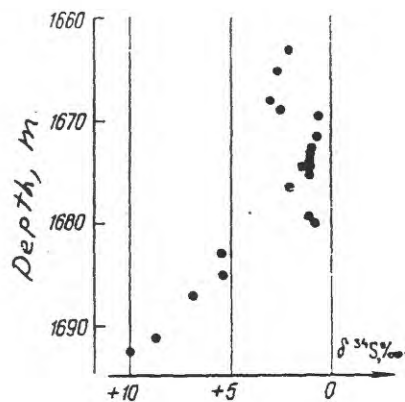


Fig. 55

Fig. I.54 Lamellar intergrowth of Pentlandite (white) in pyrrhotite (light gray) in meta-ultramafic, polished section, x20, 9674 m.

Fig. I.55 Isotopic composition of sulfur in sulfides of Cu-Ni ores



Fig. 56

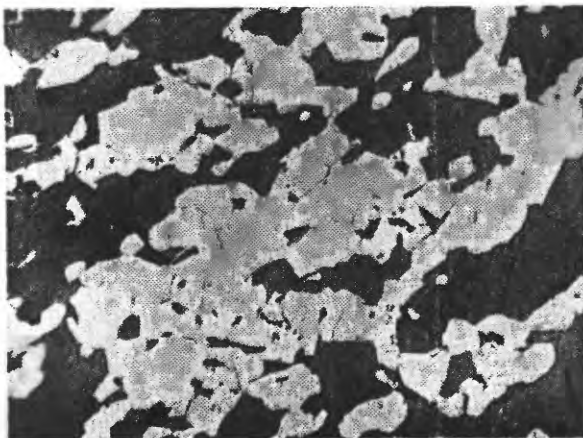


Fig. 57

Fig. I.56 Schistose texture of amphibolite with Fe-Ti mineralization (light-gray). Polished surface x9/10, 8711.5 m.

Fig. I.57 Banded magnetite, ilmenite and pyrrhotite in schistose amphibolite. Polished section x60, 8711 m.

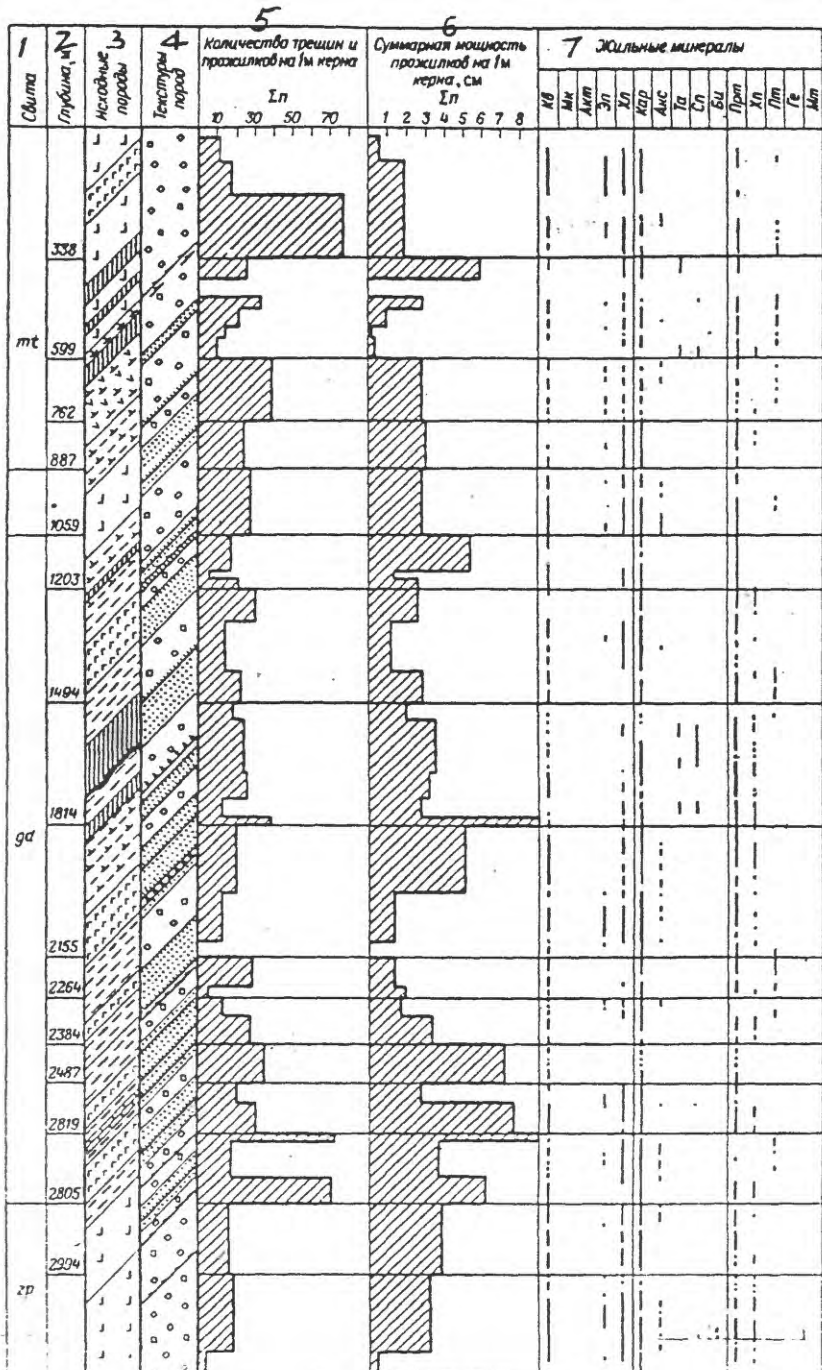


Fig. I 60. Distribution of fractures and mineralized fissures in SG-3.  
After Kazanskom and Smirnov. - Continued next page.

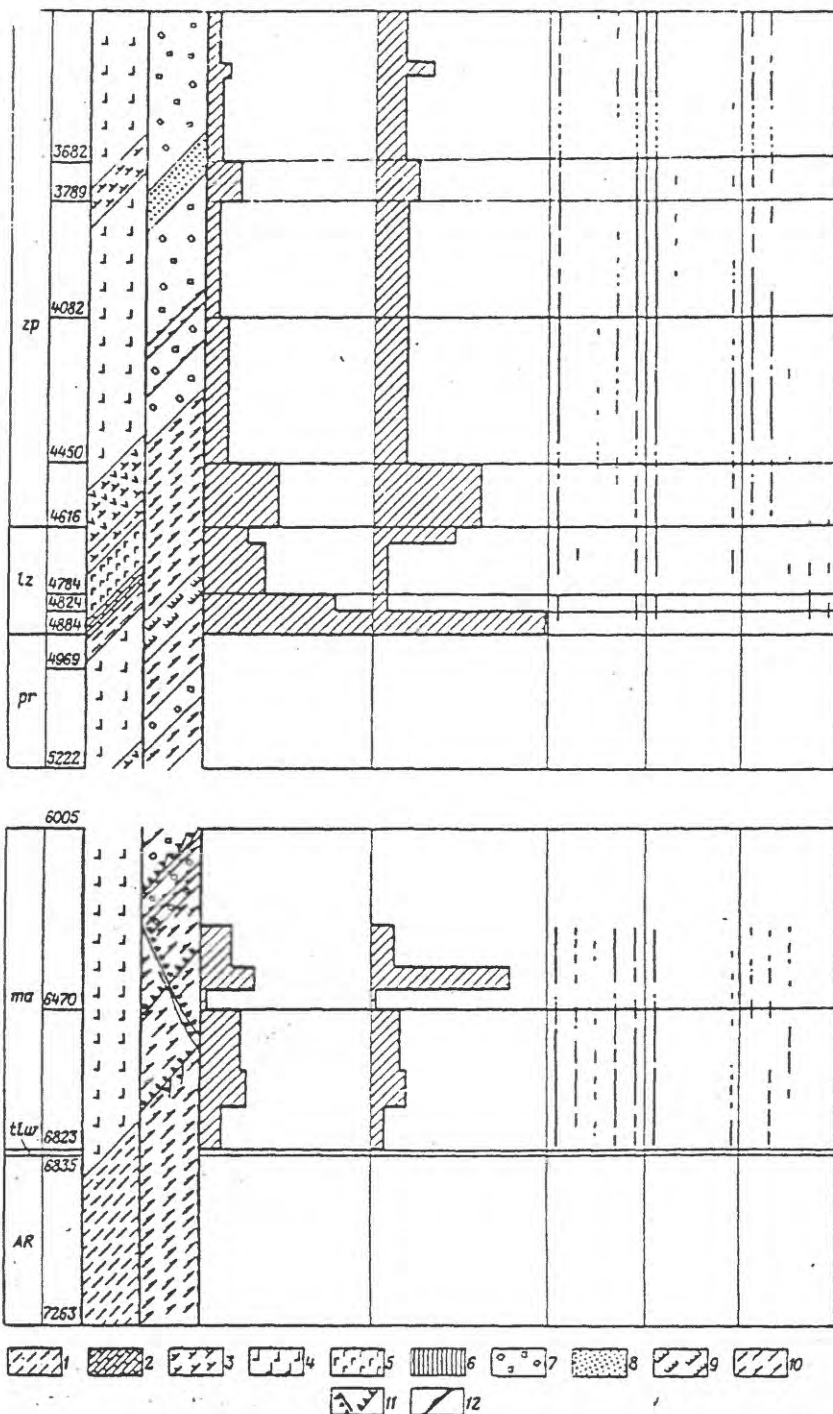
Original rocks:

- 1) sandstone, argillite
- 2) carbonates
- 3) mafic tuffs
- 4) mafic lavas
- 5) mafic intrusives
- 6) ultramafic intrusives

Rock textures:

- 7) massive and spherical relict
- 8) banded relict
- 9) banded-phyllitic
- 10) schistose
- 11) cataclastic
- 12) ore bodies

L. J. T. 60 continued



Column Headings: 1) Formation, 2) Depth, m, 3) Original rock, 4) Rock texture, 5) Fractures and veins per meter of core, 6) Total thickness of veins per meter of core, 7) vein minerals: quartz, microcline, actinolite, epidote, chlorite, carbonite, axinite, talc, sphene, biotite, pyrrhotite, chalcopyrite, pentlandite, magnetite.

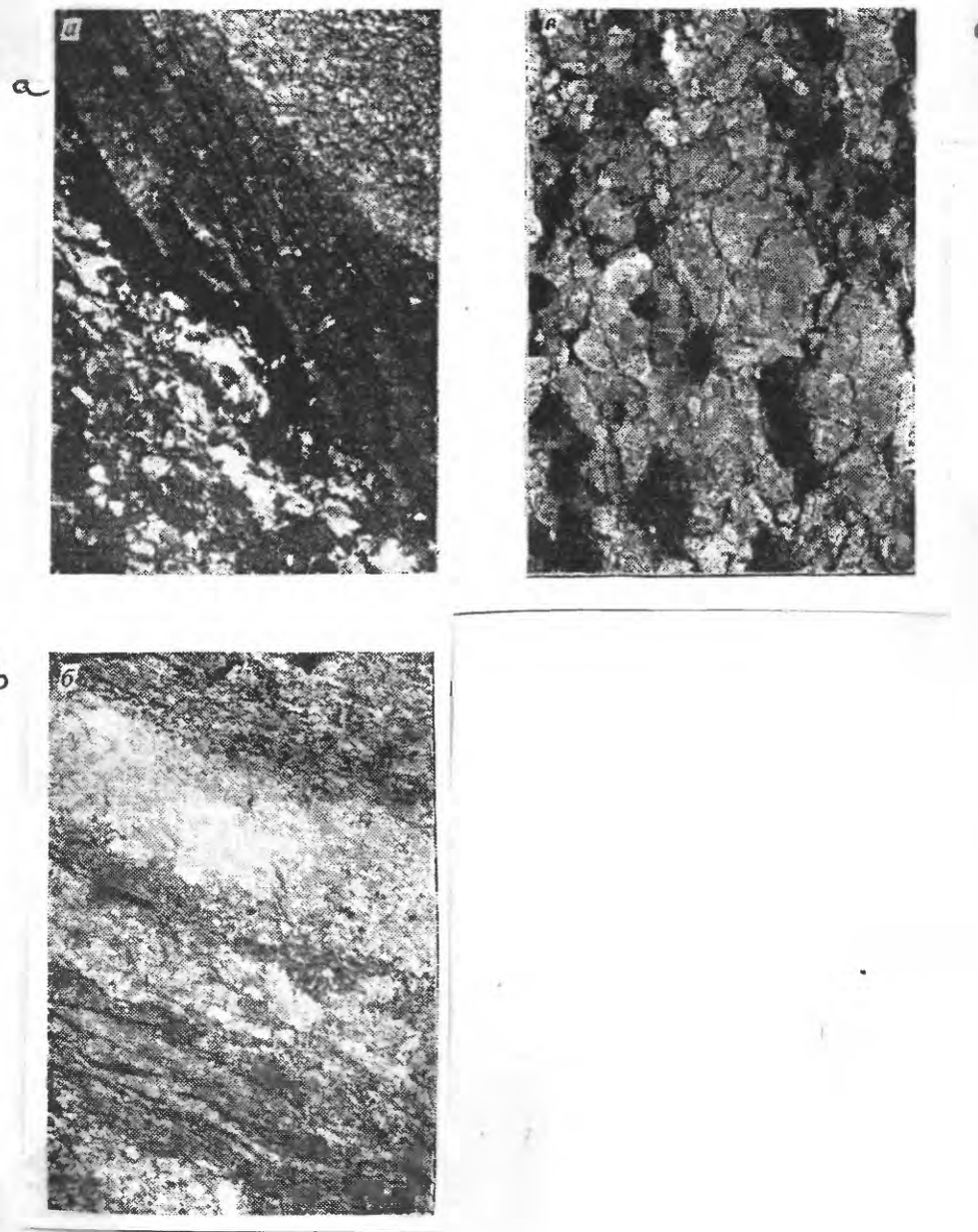


Fig. I.61 Change of texture of deformed rocks at depth; a) phyllitized siltstone, b) chlorite-actinolite cataclasite, c) biotite-amphibolite blastomylonite. x15.

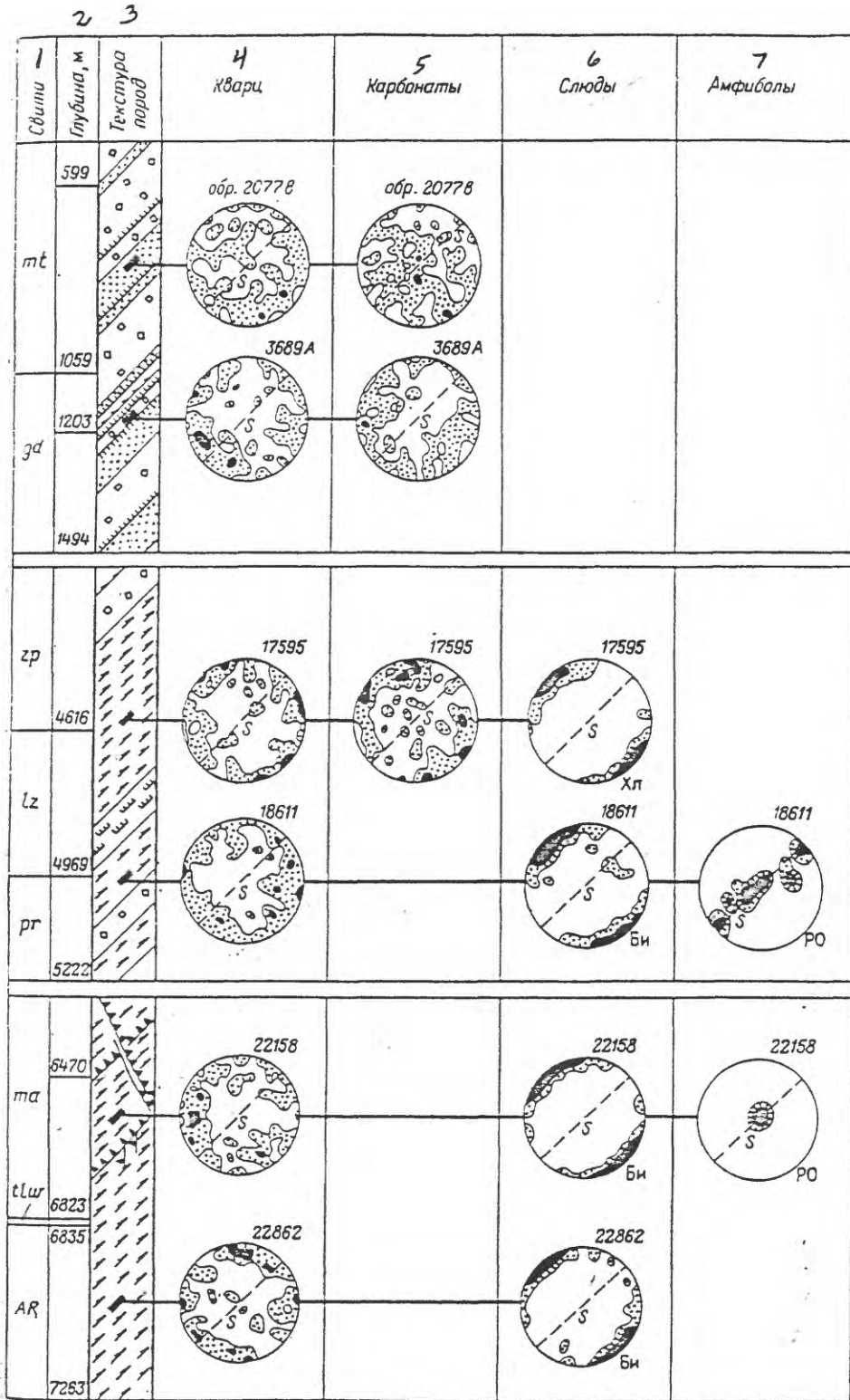


Fig. 1. 62 Orientation of minerals in the Luchlompol fracture zone. Black rectangles indicate specimens used to measure optic axes of quartz and carbonates, mica poles, and amphibole c axes. Contoured at 1 and 4%. S indicates schistosity, Columns: 1) Formation, 2) Depth, 3) Rock texture, 4) Quartz, 5) Carbonates, 6) Micas, 7) Amphiboles.

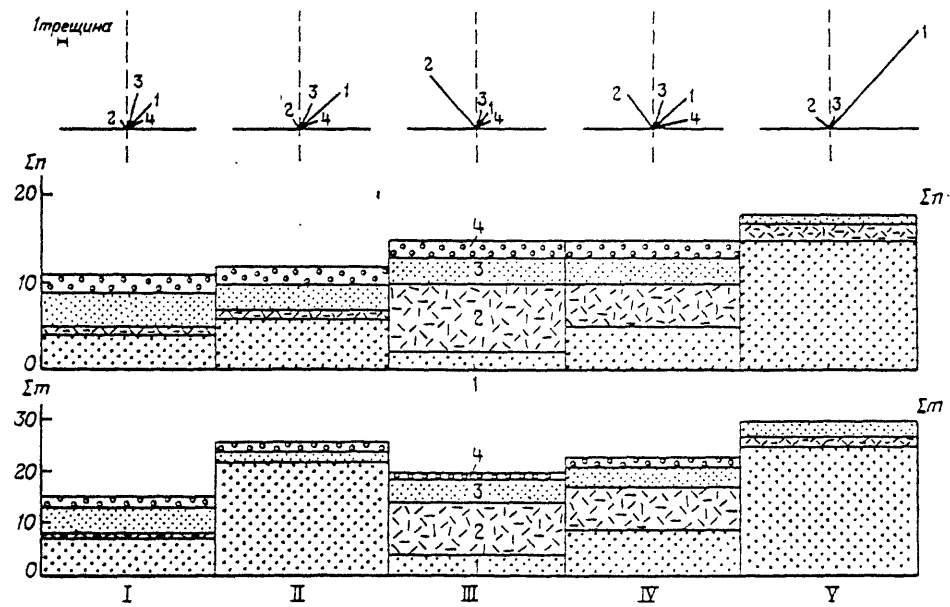


Fig. I.63 Influence of lithology on frequency of mineralized fractures and thickness of veins ( $\Sigma m$ ) in the four series of fractures. Rock types: I gabbro-diabase, II mafic tuffs, III peridotites, IV mafic lavas, V sedimentary

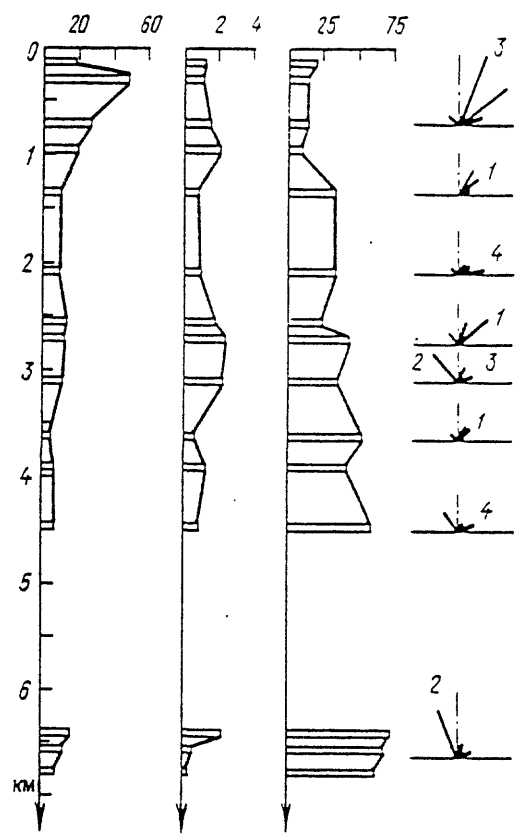


Fig I.64 Influence of depth on distribution of mineralized fractures in metabasites. a) Number of fractures per meter; b) Total thickness (cm) of veinlets per meter; c) percentage of shear fractures; d) distribution in groups 1-4.

## GASES, ORGANIC MATTER, and HYDROGEOLOGY

The results of studies of gases and organic matter is timely since one of the important problems that may be solved by drilling of Middle Proterozoic and Archean metamorphic complexes is the connection between hydrocarbon gases and other forms of organic matter in metamorphic rocks.

Organic matter is defined as dispersed reduced forms of carbon and carbonaceous matter and graphite, independent of origin; therefore, the symbol  $C_{org}$  is equally applicable for metasediments as well as for highly metamorphosed rocks.

Free gases of dispersed gas-producing zones, gases sorbed on grain surfaces, gases bound in cracks, and gas inclusions were studied. Gasometric determinations were made in drilling fluid and thereafter at different time intervals. The predominantly uncased hole (after 2 km) allowed the entire section to be tested. Gas content in closed pores and in extracted cores permitted calculation of the fraction of the total gas fraction in the drilling fluid.

### WELL GASOMETRY

Drilling fluid was sampled at the well head every 2-10m of drilling. The sampling probe was thermally degassed with a GBE degasifier (heated to 60-70°C), and the gas components were analyzed chromatographically.

Gasometry results of the drilling fluid are presented in Figure I.66 in cubic meters of gas per cubic meter of drilled rock. Anomalously high concentrations were detected for all components down to 11,500m. Helium was used to detect zones of gas permeability. Anomalously high gas shows stemmed from lithologic and structural-tectonic properties of the rocks (fractures, schist formation, sealing factors). A lithologic control on gas shows was established only in the Middle Proterozoic Zhdanov volcanic-sedimentary formation where the concentration of methane was characteristic for the metasediments and volcanic-sedimentary rocks at various intervals from 1050 to 2770 m.

Concentration of associated methane was anomalously high in the metasediments, but was less than 20% of the total concentration in the drilling fluid. Methane content decreased with depth to 0.05% in the Proterozoic complex, and to 0.03 - 0.01% in the Archean (7500 to 11,050m).

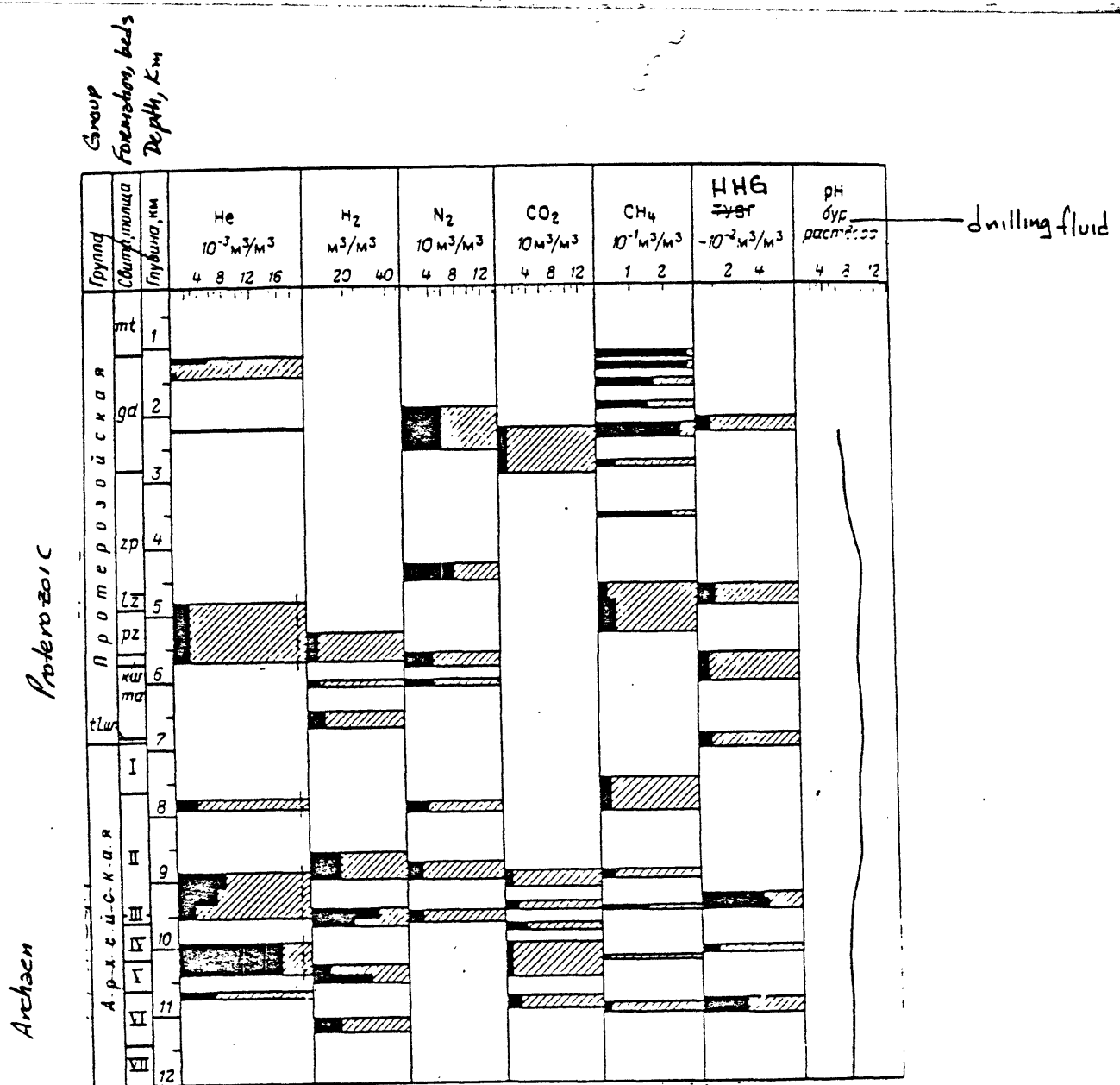


Figure I.66. Gasometric results of drilling fluid during drilling of CG-3 at intervals of anomalously high gas indications (cross hatched).

Given are mean values by interval (shaded), dotted lines signify intervals where He was detected during repeated gasometry of drilling fluid during breaks in drilling operations. Background concentrations are in cubic meters of gas per cubic meter of drilled rock: He - ..... , HHg -  $0.2 \times 10^{-2}$ .

Supersaturation of the drilling fluid by the gas components during drilling was observed in the Upper Proterozoic as a spontaneous release of gas from solution in various intervals from 1100 to 4570m. Anomalous heavy hydrocarbon gas (HHG) contents coincided with anomalous methane concentrations at various intervals, whereas their absolute and relative values in the total hydrocarbon gas concentration increased, especially after 8800m.

From repeated gas sampling of drilling fluid during drilling intervals, a number of intervals with increased gas shows indicated by helium could be classified as dispersed and gas permeable (4800-10,750m).

Helium content of the rock based on gasometry data from the drilling fluid is presented in Figures I.67 and I.68; this identifies the fraction of bound helium released from the rock during drilling, which did not exceed 10% in the fluid-permeable zones in the Proterozoic and ranged from 30 to 100% in the massive rock. In the Archean gas-permeable zones it ranged from 0.4 to 4%, and 10-40% in the relatively impermeable blocks.

The information content from the carbon dioxide after 8800 m is balanced against the addition of sodium carbonate to the drilling fluid at 8700m; however, the spikes of helium, nitrogen, hydrogen, methane, and HHG indicate that the carbon dioxide content is not simply due to contamination.

#### GASES IN ROCKS

Studies of gases in the closed rock pores in Kola Drillhole SG-3 are applicable in solving the following problems: establishing a relationship between the distribution of gases in ancient crystalline rocks of different origin and composition as a function of depth and geological setting; determining the role of the gaseous phase in the processes of endogenic ore formation and metamorphism from prehnite-pumpellyite to amphibolite facies with active granitization; establishing the gas fraction in closed pores relative to the gas content in the drilling fluid to identify fluid conducting zones and also the specific gas content of the rocks.

The principal characteristics of the helium and hydrocarbon gas (HG) distribution in SG-3 shown in Figures 1.67-70 are:

1. A decrease in total HG down to 4884 m; and subsequent stabilization of the average values with second order variations depending on rock type and classification as formation or strata. For example, the metasediments of the Zhdanov Formation are distinctly different from the extrusive and intrusive Proterozoic rocks; a strong reduction in HG for metasediments at the

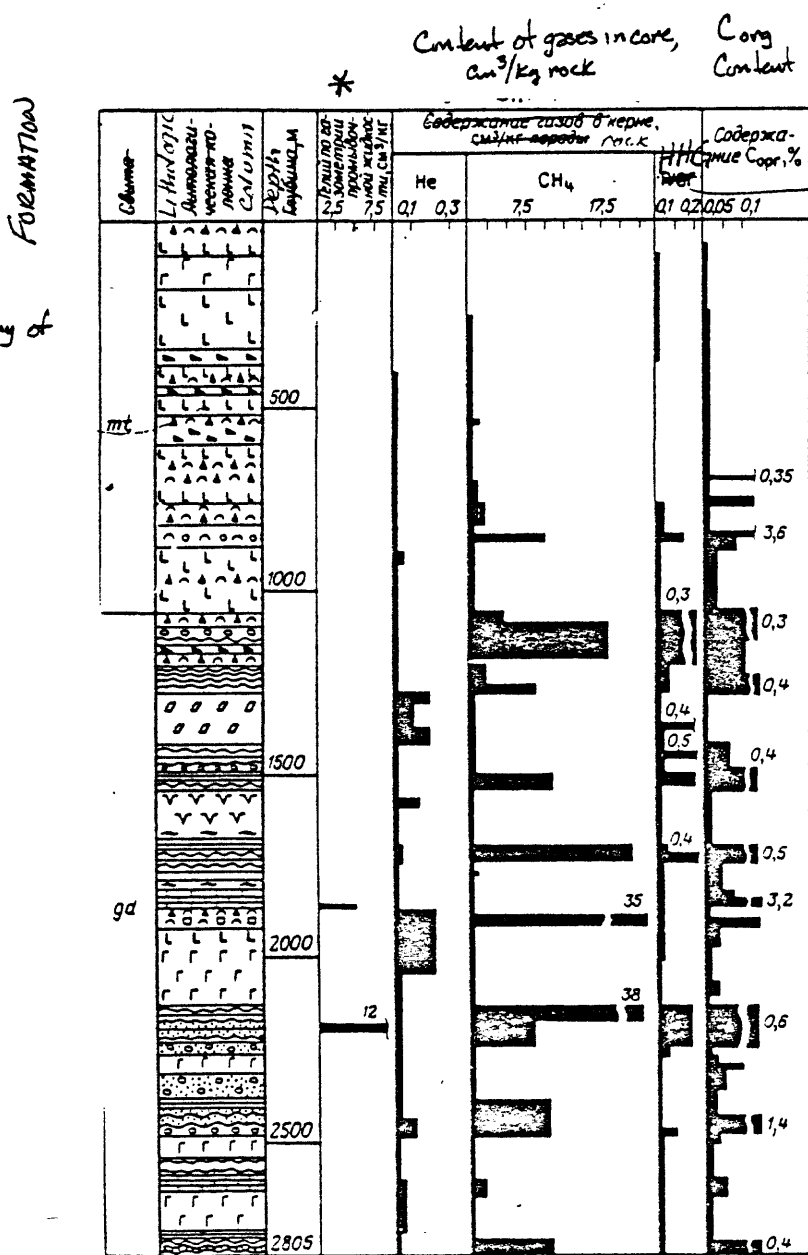
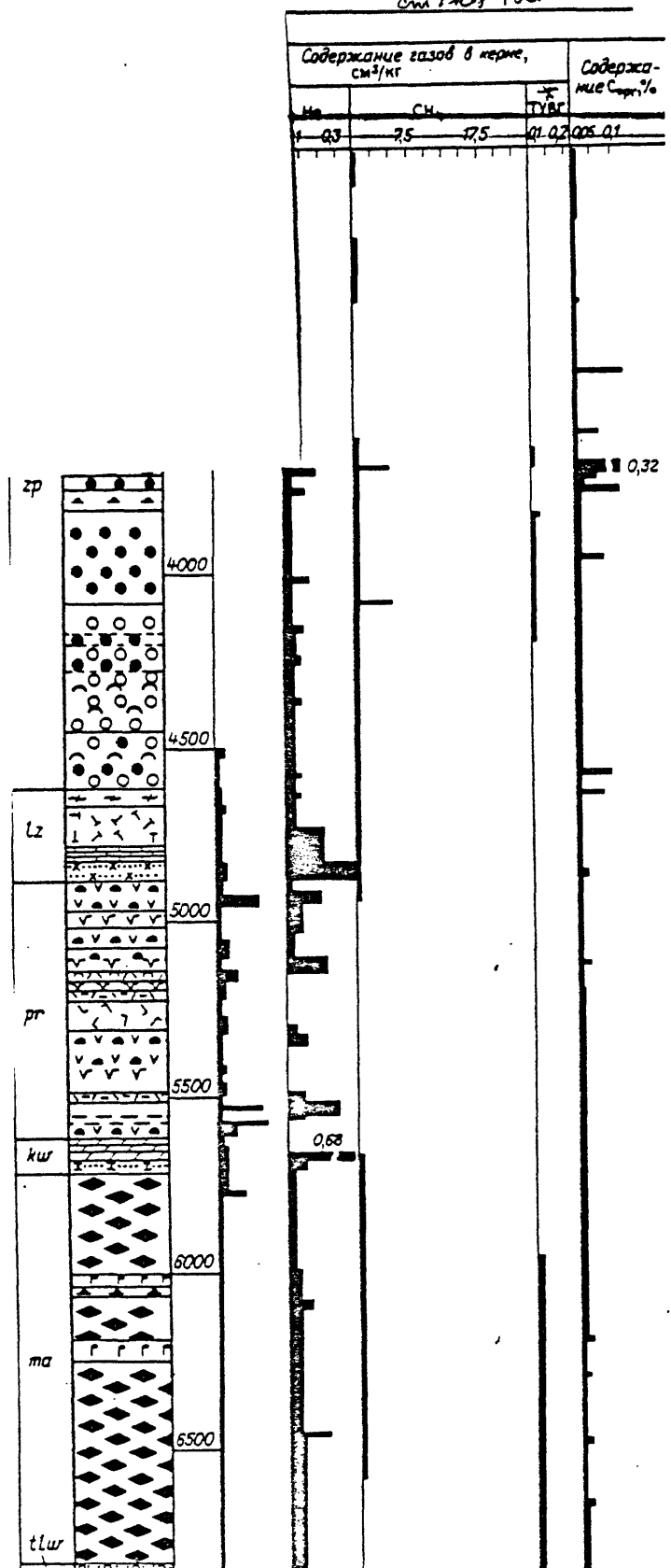


Figure I.67. Concentration of helium, methane, heavy hydrocarbon gases (HHG), and  $\text{C}_{\text{org}}$  in rocks of the Pechenga complex in section of Well CG-3: 1 - augitic diabases; 2 - pyroxenic and picritic porphyrites; 3 - basic pelitic and silty tuffs; 4 - basic psammitic tuffs; 5 - basic tuffaceous lava and lava breccias; 6 - tuffite; 7 - phyllite; 8 - siltstone; 9 - sandstone; 10 - conglomerate; 11 - sandstone conglomerate; 12 - quartzitic and arkosic sandstone; 13 - quartzite-sandstone and quartz-carbonate-mica schist; 14 - actinolitic diabase; 15 - spherolitic lava; 16 - diabase porphyrite; 17 - magnetite-plagioclase-amphibole schists and plagioclase-amphibole schist on metadiabase; 18 - magnetite-biotite-plagioclase schist with amphibole on andesitic porphyrite; 19 - basic and acidic altered tuffaceous lava; 20 - orthophyre; 21 - biotite-amphibole-plagioclase schist in andesitic basalt; 22 - magnetite-sericite-chlorite schist with carbonate; 23 - dolomite; 24 - metamorphosed dolomite, marble, carbonate-tremolitic schist; 25 - chlorite-serpentine-talc and talc-tremolitic rocks; 26 - gabbro-diabase; 27 - gabbro-diabase essexite; 28 - amphibolite with massive gabbro-diabase; 29 - andesitic porphyrite; 30 - pocket-streaky sulfide ore manifestations.

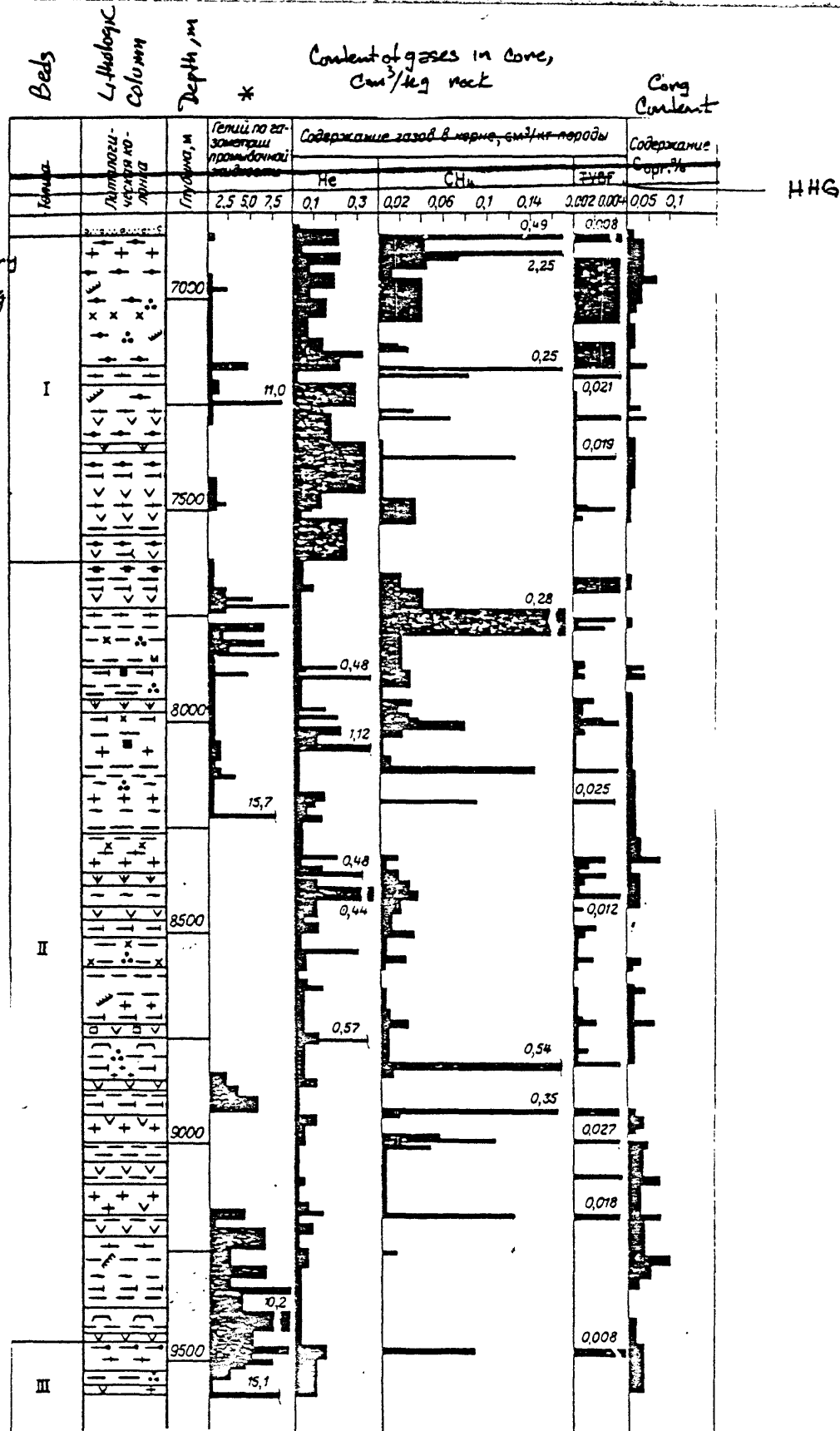
Content of gases in core,  
cm<sup>3</sup>/test rock

No.	CH <sub>4</sub>	H <sub>2</sub> S	Содержание газов в породе,	
			см <sup>3</sup> /кг	содержание С <sub>орг</sub> %
1	63	2,5	77,5	0,1-0,2-0,05-0,1

← C<sub>орг</sub>  
Content, %  
\* H HG



\* Helium from gas mixture  
of circulating fluid, cm<sup>3</sup>/kg



Content of gases in core, →  
cm<sup>3</sup>/kg rock

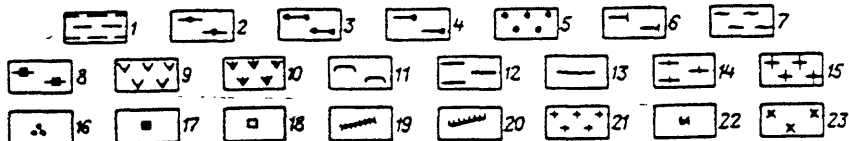
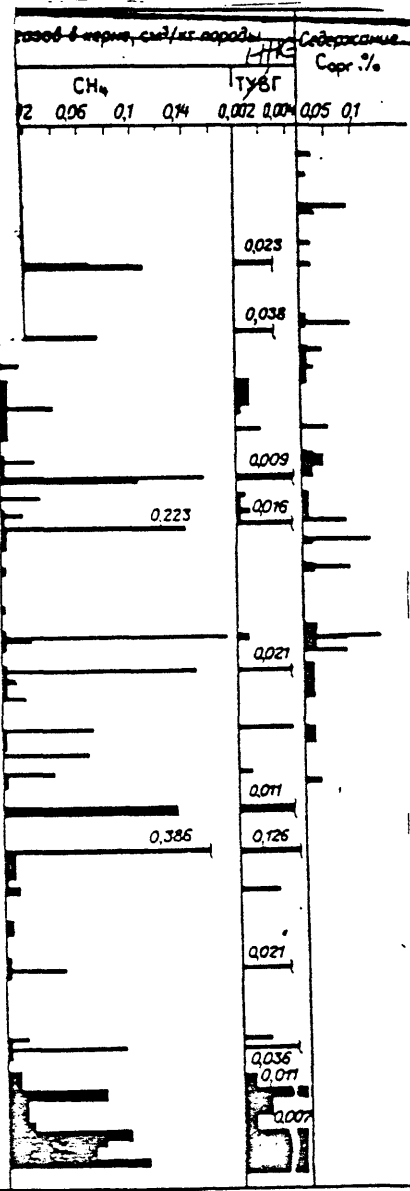


Figure 1.68. Content of helium, methane, HHG, and C<sub>org</sub> in Archean rocks of the Kola Series in well SG-3: 1 - biotite-plagioclase gneiss; 2 - sillimanite-biotite-plagioclase gneiss; 3 - two-mica gneiss with VGM; 4 - two mica gneiss; 5 - garnet-biotite-plagioclase gneiss; 6 - epidote-biotite-plagioclase gneiss; 7 - epidote-biotite-plagioclase schist; 8 - magnetite-amphibole schist; 9 - amphibolite; 10 - amphibolite with cummingtonite; 11 - banded (leucocratic) amphibolite; 12 - biotite-amphibole schist; 13 - phlogopitic rocks; 14, 15 - intrusive formations (14 - plagiogranite and dark mignatite, 15 - plagiomicrocline granite, pegmatite); 16-18 - ore manifestations (16 - sulfide, 17 - magnetite, 18 - ilmenite); 19 - quartz veins; 20 - chloritization; 21 - microclinization; 22 - muscovitization; 23 - migmatized zones.

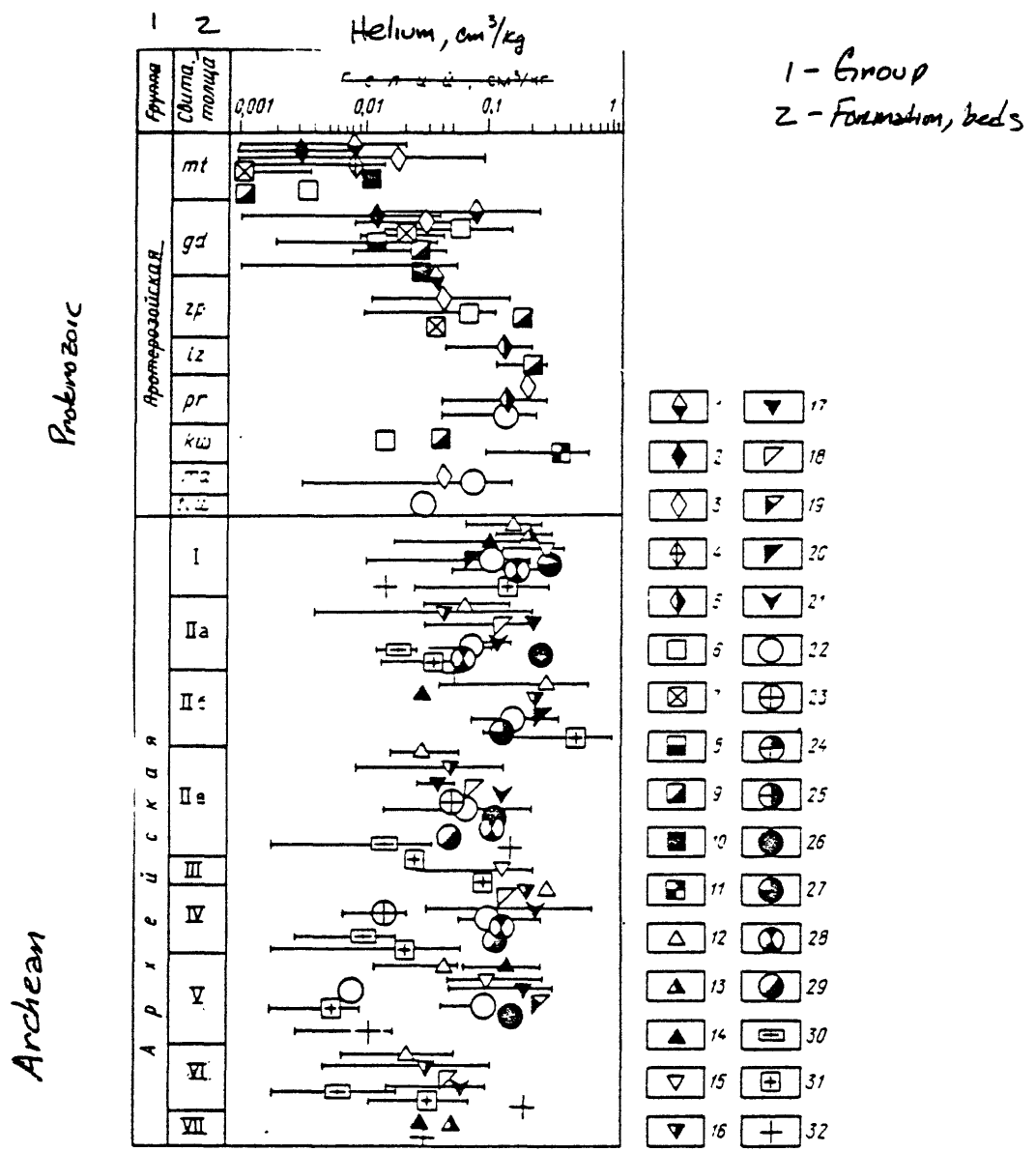


Figure 1.69. Helium content in the rocks of Drillhole SG-3.

Rocks of Middle Proterozoic: 1 - gabbro-diabase, gabbro of differentiated intrusives; 2 - peridotite; 3 - diabase; 4 - picritic porphyrite; 5 - andesitic porphyrite, albitophyre plagioporphyrite; 6 - tuff and tuff breccias; 7 - psammitic metatuffite; 8 - pelitic metatuffites; 9 - metapsammites; 10 - metapelites and siltstone; 11 - carbonate rocks; 12 - biotite-plagioclase gneiss, schist; 13 - biotite-plagioclase gneiss, schist with VGM; 14 - two-mica gneiss, schist; 15 - two-mica gneiss, schist with VGM; 16 - epidote-biotite-plagioclase gneiss; 17 - biotite-amphibole-plagioclase gneiss; 18 - epidote-biotite-amphibole-plagioclase gneiss; 19 - garnet-epidote-biotite-plagioclase gneiss; 20 - biotite-amphibole-plagioclase schist; 21 - epidote-biotite-amphibole-plagioclase schist; 22 - amphibolite; 23 - banded, large and irregularly grained amphibolites; 24 - leucocratic amphibolite; 25 - large and irregularly grained amphibolite; 26 - amphibolite with cummingtonite; 27 - amphibole schist with cummingtonite; 28 - biotite-amphibole schist; 29 - talc-actinolite schist; 30 - plagiogranite and dark migmatite; 31 - microcline granite; 32 - pegmatite. Average helium content - center of rock symbols, range of concentration indicated by length of line.

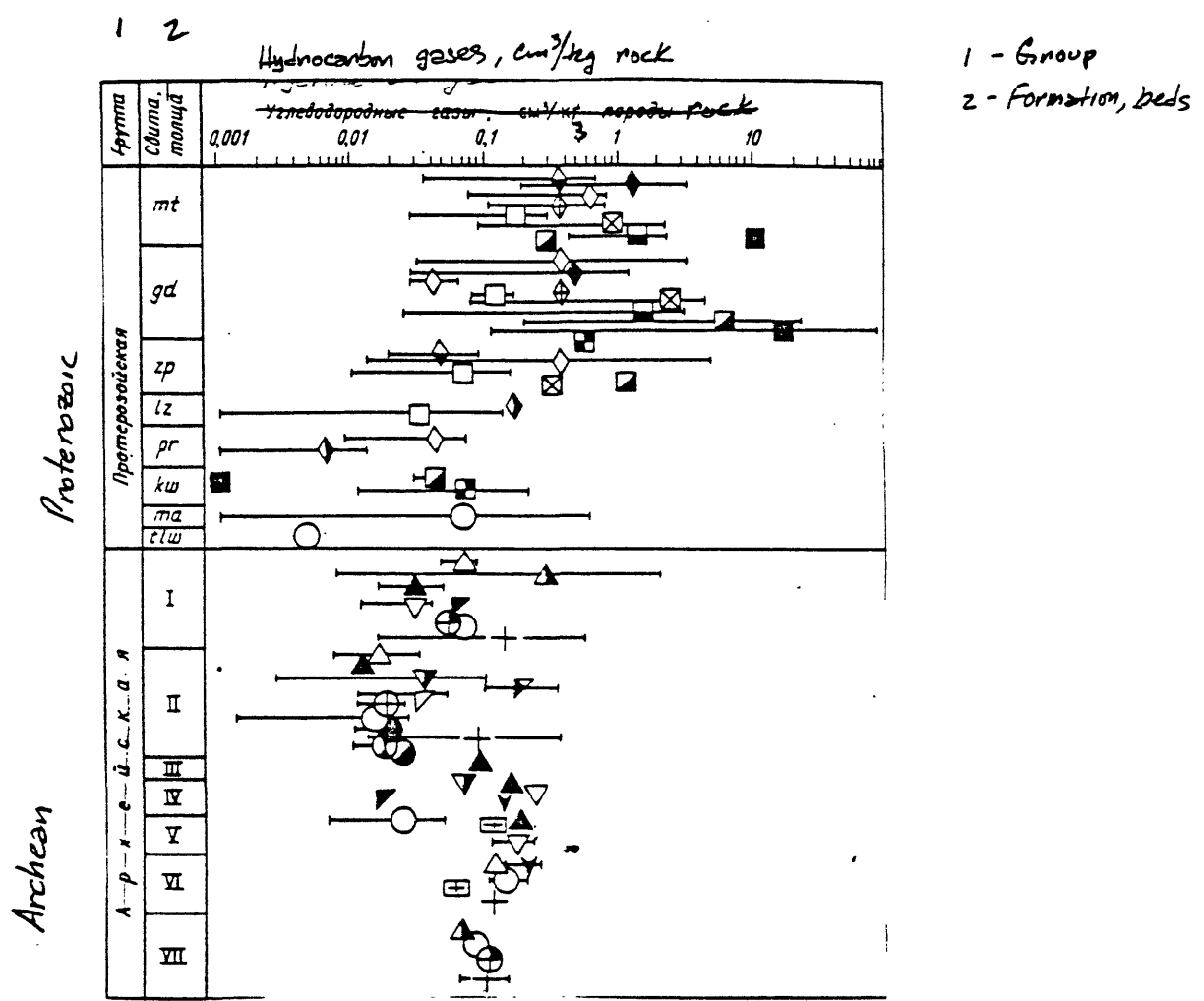


Figure 1.70. Total HG in the rocks of Drillhole SG-3.

Symbol designation same as in Figure 1.72.

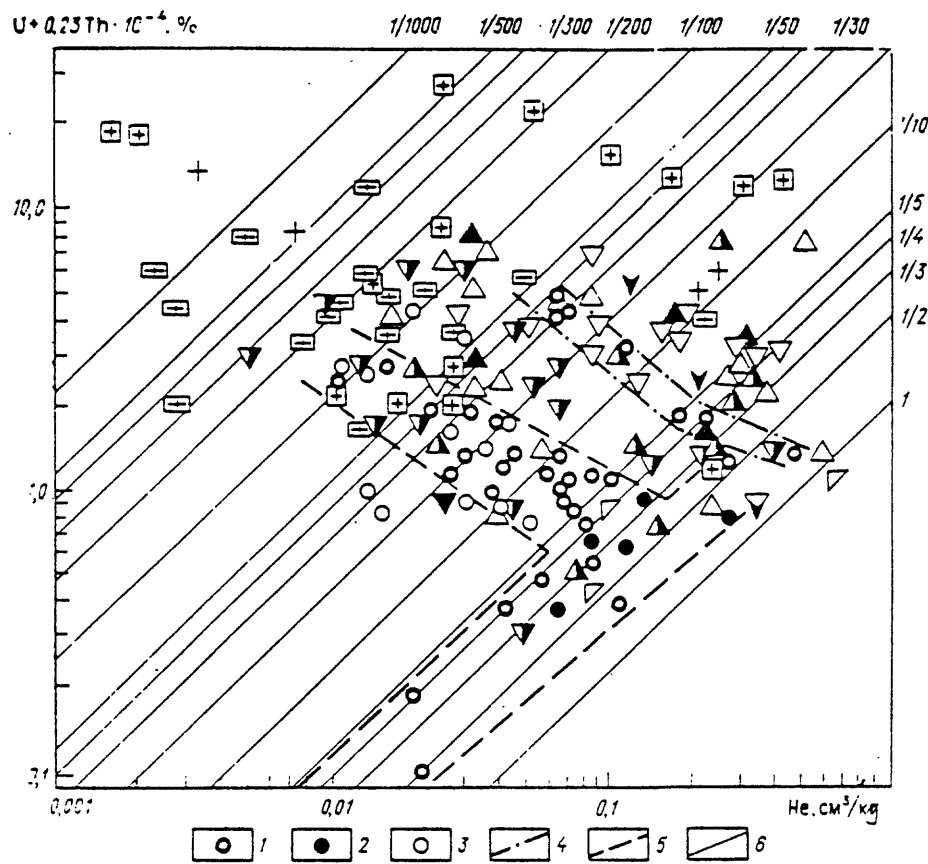


Figure 1.71. Helium content as a function of the concentration of uranium and thorium in amphibolite in rocks of the Middle Proterozoic and Archean complexes in Drillhole CG-3:

1, 2 - amphibolites of the Archean complex, including cummingtonite (2); 3 - amphibolites of the Proterozoic complex; 4 - outline of the field of amphibolites of Series I (6842-7622m) of the Archean complex; 5 - outline of the field of amphibolites of Series II-VII of the Archean complex; 6 - lines of equal coefficients of retention of helium. Remaining rock designation same as in Figure 1.72.

Table 1.29. Average concentration of hydrocarbon gases, nitrogen ( $\text{cm}^3/\text{kg}$ ), and organic hydrogen (%) in metasedimentary rocks of the Zhdanov Formation as a function of sedimentation conditions.

muscovite-chlorite to biotite-chlorite transition zone of the green schist facies at 3180 m; and a minimum HG content in the Archean section in the biotite-plagioclase, biotite-amphibole-plagioclase gneiss, and amphibolite series (7622-9456m) for nearly all rocks.

2. The helium-content profile is the reverse to that of HG. The helium content increases for all Proterozoic rock types down to 4884m (Luchlompol Formation), with a tendency for decreased helium content at 10,600m; and is also observed in the pegmatites and granites. The bulk of the granites, however, fall into the domain of low and medium helium content; minimum values are widespread throughout nearly all <sup>of</sup> the Archean migmatite and plagiogranite series.

3. The helium content significantly depends on depth down to 5 km. At greater depths the predominating factors become the structural-textural properties of the rocks, the mineral composition, the uranium and thorium content, the age of the rocks, and their origin and history of metamorphism.

The reduction in the coefficients of retention of helium in the amphibolites with higher uranium and thorium content suggests that granitizing solutions have been introduced to these rocks. The high magnesium amphibolites with cummingtonite are more resistant to the granitization process and hence helium retention is higher. Plagiogranites and migmatites are more yielding to the recrystallization process of the granitizing potassium-rich fluids and hence fall in the upper left quadrant of the diagram. (fig. I.71).

4. Nitrogen content in the Zhdanov Formation reaches  $20 \text{ cm}^3/\text{kg}$  and correlates with HG and  $C_{\text{org}}$ .

5. The direct correlation between the content of  $C_{\text{org}}$ , HG,  $N_2$ , and the light isotopic composition of hydrogen in HG is evidence of the biological origin of these components; confirmed by the dependence of concentration on facies formation conditions.

6. The results of gas analyses averaged by rock type are plotted as HG -  $C_{\text{org}}$  and HG - He in Figures I.72, I.73; and testify to the joint occurrence of HG with the bulk of the helium in a single system of pores. The partial pressure in a system of connected pores in the earlier metamorphic stages within a single unit is approximately the same, and is preserved as such, after the pores are sealed. The quantity of helium depends on the total porosity and  $C_{\text{org}}$  content. Apparently the preservation of helium as a function of depth and leakage of helium from the Archean basement begins to be significant.

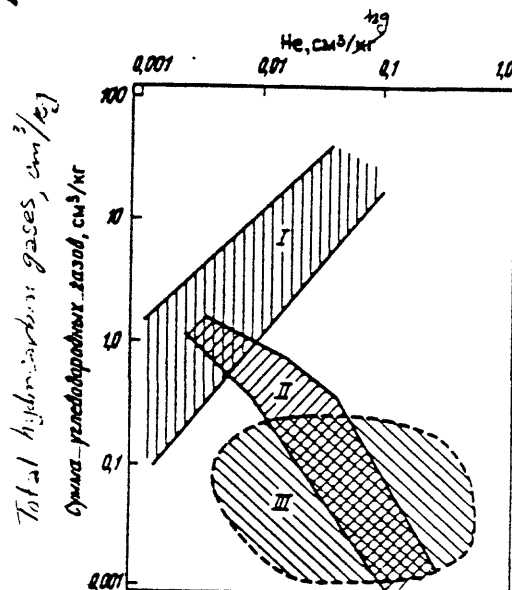


Fig. I.72

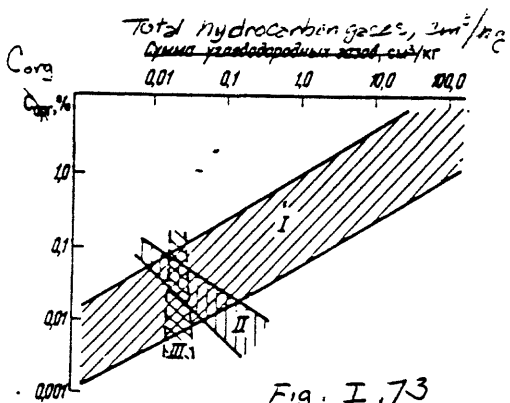


Fig. I.73

Figure 1.72. Relationship of total HG and helium in rocks of Drillhole CG-3:  
 I - field of metasedimentary rocks of the Matertinskiy and Zhdanov Formations; II - field of volcanic rocks of the Proterozoic complex; III - field of Archean rocks.

Figure 1.73. Relationship of total HG and  $C_{org}$  in rocks of Drillhole CG-3:

I - field of metasedimentary rocks of the Proterozoic complex;  
 II - field of Series I, III, V rocks of the Archean complex;  
 III - field of Series II and IV rocks of the Archean complex.

7. A connection is lacking between the average content of total HG and  $C_{org}$  in Proterozoic rocks, and there is a negative correlation between total HG and helium.

8. There is a negative correlation between the total HG and  $C_{org}$  in series I, III-, V of the Archean complex; and no established connection between these components in Series II and IV. This lack of a connection between helium content and total HG is characteristic for all Archean rocks, due to the discrete nature of gas sources and the forms of their occurrence in the rocks.

9. Carbon dioxide and HG are the principal gaseous components of fluid inclusions in quartz, the rock-forming mineral in hydrothermal veins and pegmatites; their content is higher in metasedimentary rocks. For Archean series the principal component is carbon dioxide in quartz of hydrothermal veins and pegmatites, but HG is nearly absent. The granitization process is accompanied by an increasing fraction of carbon dioxide in the fluid phase which participates in the formation of hydrothermal quartz-carbonate and carbonate veins in the Archean and Proterozoic complexes.

Regarding the connection between the gas phase in rocks and ore genesis the following facts are emphasized: 1) helium inflow was detected in the interval 9950-10,500m during well down-time; and during drilling anomalously high concentrations of He and HG in the drilling fluid were associated with high concentrations of helium in the cores. Apparently this interval is a zone of weak ore control and poor fluid permeability; 2) the ore-bearing rocks of the Zhdanov Formation are distinguished by increased HG concentration in rocks similar in age and composition to other regions, which can be used to evaluate volcanic-sedimentary rocks for sulfide mineralization, 3) the inverse relationship between uranium and thorium concentration in Archean rocks and helium retention indicates the later introduction of specific radioactive components (Figure I.71).

#### GEOCHEMISTRY OF ORGANIC MATTER

Geochemical studies of the organic matter in Drillhole SG-3 included quantitative determination of the  $C_{org}$  in a chloroform bitumen extract (CBE), the elemental and component composition, and also structural-chromatographic analyses using infrared spectroscopy (IR), electron paramagnetic resonance (EPR), nuclear magnetic resonance (NMR) and gas-liquid chromatography. Over 500 determinations established the  $C_{org}$  distribution

shown in Figure I.74, whose concentration varied from "traces" to 2% in Proterozoic volcanic-sedimentary rocks, with a maximum in the Zhdanov metasedimentary rocks (phyllites, siltstones, sandstones), and decreased to 0.1%, and 0.01% in diabases, gabbrodiabases, and porphyrites. The concentration ranged from 0.01 to 0.03% in the Archean rocks.

Rock bitumen content was analyzed by bitumen luminescence; however, at high stages of catagenesis the physico-chemical bonding strengths of the bitumenous matter with the surrounding mineral medium sharply increased, reducing the reliability of the determination.

The chloroform extraction data are most interesting (shown in Table I.30) and establish two basic relationships, namely that Proterozoic rocks have a higher CBE than do Archean rocks; and second that the CBE distribution in Proterozoic rocks is characterized by a maximum (up to 0.2%) in the metasediments, and a decrease down to thousandths of a percent for volcanic and volcanogenic sedimentary rocks. The direct correlation between CBE concentration and  $C_{org}$  in purely genetic varieties indicates the syngenetic nature of the bitumenous matter. The CBE components vary stratigraphically, as well according to genetic types of rocks in the Proterozoic.

The elementary composition of CBE is shown in Table I.31, and illustrates the differences in the Proterozoic and Archean deposits in the distribution of hydrogen containing compounds, as well as in their structural properties. The latter is reflected in the C/H ratio.

The CBE components of the metasedimentary rocks possess different structural properties (Figure I.75); oil is represented by oxygen-containing aliphatic and cyclic functional groups. A separate structural type of CBE was detected in Archean deposits; the basic oils are composed of high molecular paraffins.

The following were determined: range of the series of n-alkanes, the location of the maximum concentration in the series and the concentration of "liquid" compounds, the oddness value factor (ratio of total n-alkanes with an odd number of atoms to total even number), the principal differences in the distribution of the CBE oils in the Archean and Proterozoic, and the distribution characteristics of the iso-alkanes beginning with  $C_9$ , (Table I.32, Figure I.76). The predominate component in the CBE oils of the Archean deposits are the n-alkanes; a negligible quantity of n-alkanes were found in the Proterozoic extrusive and intrusive rocks (Figure I.79); and the metasedimentary rocks of the Proterozoic were characterized by an increase in n-alkanes.

## Component composition of CBA, %

Depth, m Глубина, м	Rock Порода	Сорг Сорб %	Не- раст- вори- мый оста- ток, %	CBA ХБА. %	Компонентный состав ХБА %:					Petroleum ether resins Alcohol-benzenes
					ОИ Масла	Петро- лейно- эфир- ные смолы	Бен- золь- ные смолы	Спир- то- бен- золь- ные смолы	Ас- фаль- тены	
Insoluble residue, %										

 Proterozoic Complex  
Протерозойский комплекс

Phyllites, siltstones, sandstones	765—885 887—965 1108,2—1228,2	Туффит Tuft Диабаз Diabaz Филлиты, алевролиты, песчаники	0,04 0,08 0,26	66,7 85,8 79,5	0,008 0,083 0,028	49,4 1,11 35,2	6,8 1,48 9,4	28,3 81,29 11,4	12,7 15,52 31,7	2,8 0,6 12,3
Phyllites with siltstones	1182—1496	Филлиты с алевролитами	0,60	82,0	0,007	42,6	10,8	14,7	22,4	9,5
Gabbro-diabase	1289,4—1305,0	Габбро-диабаз	0,04	71,6	0,084	8,88	8,29	58,9	23,74	0,19
essexite	1284—1413	Эсекситовый	0,02	83,4	0,004	22,7	9,2	14,3	39,3	14,4 *
Hypenbasite	1757,8—1767,6	Гипербазиты	0,13	76,3	0,161	1,74	17,6	76,2	4,46	** Det. T
>	1954,6—1958,3	Энабазиты	0,03	85,5	0,091	4,89	6,13	84,21	4,42	0,35
Intercalated phyllites and siltstones	2154—2291	Переслаивающие филлиты и алевролиты	0,01	80,4	0,005	41,5	9,9	17,4	23,0	8,2 ** Undetected.
Dolomite with carbonaceous matter	2994—3201 3645,8—3650,3	Диабаз Diabaz Диабаз с углеродистым веществом	0,03 0,03	88,3 89,2	0,068 0,056	2,49 3,60	3,38 3,87	84,94 79,26	8,8 12,96	0,39 0,31
Schists often tuffaceous rocks	3752,1—3757,4 3983,8—3987,3 4336—4389 4630,5—4784,2	Туфы Tufts Диабаз Diabaz То же Diffo Сланцы по туфосадочным породам	0,27 0,06 0,03 0,09	74,0 94,4 94,9 88,0	0,095 0,065 0,051 0,185	4,65 2,25 2,43 1,78	4,62 2,02 4,96 3,65	81,54 75,00 86,05 75,53	9,02 20,19 5,68 19,04	0,17 0,54 0,88 ** Det. T
Andesitic porphyrite	4749,15	Андезитовый порфирит	0,04	93,8	0,099	3,28	4,25	64,91	27,56	* Det. T
Ankositic sandstones	4847—4859	Песчаник аркозовый	0,04	96,0	0,059	4,40	7,48	79,11	9,01	* Det. T
Biotite-amphibolite-Plogoclase Schist	6569—6577,5	Биотит-амфибол-плагиоклазовый сланец	0,06	94,0	0,025	4,78	2,58	87,15	6,49	* Det. T
Amphibolite-plagioclase schist	6757,3—6767,3	Амфибол-плагиоклазовый сланец	0,04	96,0	0,016	2,03	2,59	82,03	10,51	2,78

 Archean Complex  
Архейский комплекс

Two-mica gneiss	6933,0—7048,3	Плагиогнейсы двуслюдянные	0,07	96,5	0,014	1,45	2,51	81,16	13,29	1,59
Amphibolite	7642—7656	Амфиболит	Не обн.	Не обн.	0,010	26,1	21,6	48,3	3,4	* Det. T
Biotite gneiss	7937—7944 8313,1—8324,0	То же Diffo Гнейс биотит-титанитовый	0,03	95,3	0,009	0,011 59,99	16,3 16,25	54,1 12,64	7,6 10,10	* Det. T 0,02
Epik-biotite-plagioclase gneiss	9600—9989	Эпидот-биотит-плагиоклазовые гнейсы	0,01	96,4	0,009	21,92	12,95	63,08	0,05	Diffo
Two-mica gneiss	10 144—10 181	Двуслюдянные гнейсы	0,03	98,0	0,011	37,75	11,85	53,37	0,03	

Table I.30 Results of chemical-geochemical analysis of bituminous matter of Kola well 56-3

Sample	Interval, m Интервал отбора проб, м	Rock Порода	Содержание элементов				Element concentration, % and others			
			C	H	S	N O				
Metavolcanic rocks										
Metatuffites										
	771,2—771,9	Tuffaceous silty psammite Туффитовый алевропесчаник	65,49	6,71	1,35	0,00 26,45				
Metapelites and Siltstones										
Metapelites и алевропелиты										
Layered graywacke	1199,0—1199,7	Слоистый гравуакковый алевритовый сланец и але- вропелитовый сланец	71,19	10,21	0,65	0,00 17,95				
siltstone schist and Bilky pelitic schist	1199,8—1200,8	Слоистый граувакковый алевритовый сланец	60,41	8,66	0,0	1,18 29,86				
Layered graywacke	1710,0—1712,2	Тонкослоистый граувакко- вой алевропеллит	64,81	9,79	1,22	0,00 24,18				
siltstone	2163,4—2165,9	Граувакковый алевропеллит <i>Graywacke</i> Silty pelite	55,85	7,03	0,002	0,00 37,12				
thin layered graywacke	2166,9—2167,2	Граувакковый алевролит <i>Graywacke</i> Siltstone	67,68	9,40	0,95	0,00 21,67				
Metapsammites										
	2459,9—2460,5	Silty psammite Алевропесчаник	55,82	8,65	0,00	0,00 35,53				
	2606,3—2608,2	Ankosek psammite Аркозовый песчаник	69,90	10,33	0,00	0,00 19,57				
	2608,8—2610,2	To же Ditto	68,87	9,86	0,61	0,00 20,60				
	4855,6—4862,9	Аркозовый песчаник с гема- тит-серпентитовым цементом	55,94	8,11	0,00	0,00 35,95				
	4863,8—4866,1	Аркозовый песчаник с гема- тит-серпентитовым цементом	56,44	8,14	0,00	0,00 35,42				
Magmatic rocks of basic composition										
	2030,5—2031,2	Gabbro-diabase Габбро-диабаз	61,00	8,23	0,68	0,00 30,07				
	2032,2—2032,5	To же Ditto	70,08	7,46	0,00	0,00 22,46				
	2637,1—2658,7	Amphibolitic gabbro Амфиболитовое габбро	69,93	10,37	0,00	0,00 19,70				
Magmatic rocks of ultra-basic composition										
	370,3—373,8	Peridotite Перидотит	68,82	9,73	0,86	0,00 20,59				
	902,8—903,6	Serpentinite Серпентинит	70,29	8,13	1,28	0,34 20,19				
	1581,3—1582,6	To же Ditto	66,98	8,14	0,00	0,00 24,87				
Ultrabasic magmatic rock										

Table I. 31 Analytical results of the elemental composition of CBE  
in rocks of the Kole Drill/hole SG-3.

Sample interval, m

Element concentration, %

Интервал отбора проб, м	Порода	Содержание элементов, %				
		C	H	S	K	O
<i>Amphibolites</i> <i>Амфиболиты</i>						
schistosic - amphibolite in diabase	6475,7—6485,7	Сланцевые амфиболиты по диабазу	69,86	9,60	0,00	0,00 20,54
	7647,6—7664,1	Переамфиболиты Реда amphibolites	69,90	9,60	0,00	0,00 20,40
	7670,0—7677,5	Amphibolites with sphene Амфиболиты со сфеном	69,41	8,22	0,00	0,00 22,37
	8460,4—8460,8	Амфиболиты Amphibolites	63,60	11,00	0,00	0,00 25,40
	8941,8—8942,5	Сланцевые амфиболиты Schistosic amphibolites	63,60	11,20	0,00	0,00 25,20
<i>Felsic Gneiss</i> <i>Фельсовые гнейсы</i>						
barnet-staurolitic tourmalica gneiss	7120,1—7134,0	Гранат-ставролитовые дву- слюдянные гнейсы	74,00	11,90	0,00	0,00 22,50
vescovitized epidote-biotite gneiss	7771,4—7778,9	(Эпидот-биотитовые гнейсы мусковитизированные	68,89	8,60	0,00	0,00 29,50
	8993,9—8997,9; 8998,0—8999,7	Биотитовые гнейсы Biotite gneiss	60,70	10,20	0,00	0,00 29,50
	8625,6—8628,2; 8637,3	Эпидот-биотитовые гнейсы Epidote-biotite gneiss	63,60	11,30	0,00	0,00 25,10
	9352,4—9355,9	Биотитовые гнейсы Biotite gneiss	70,60	11,20	0,00	0,00 18,20

Table I.31 continued

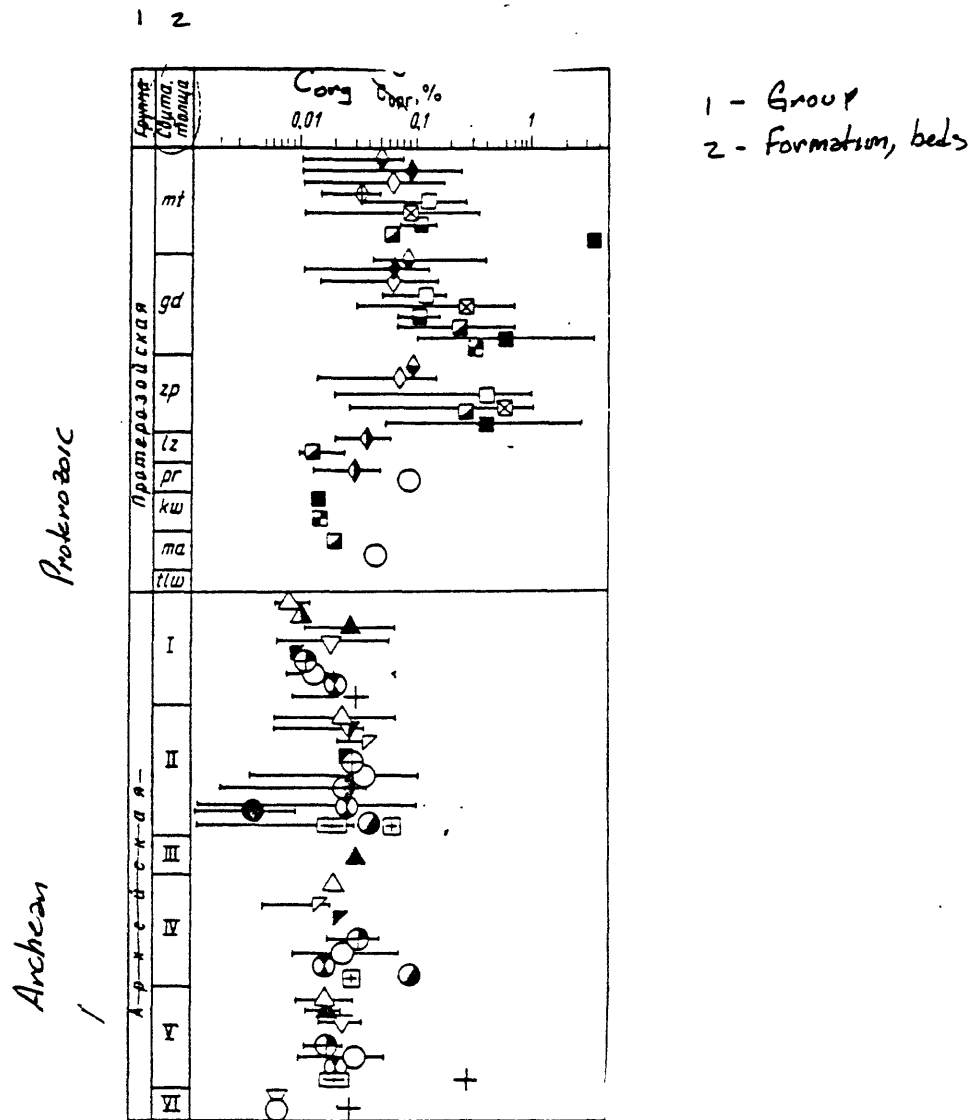


Figure 1.74. Concentration of C<sub>org</sub> in rocks of Drillhole SG-3.  
Symbol designation same as in Figure 1.69.

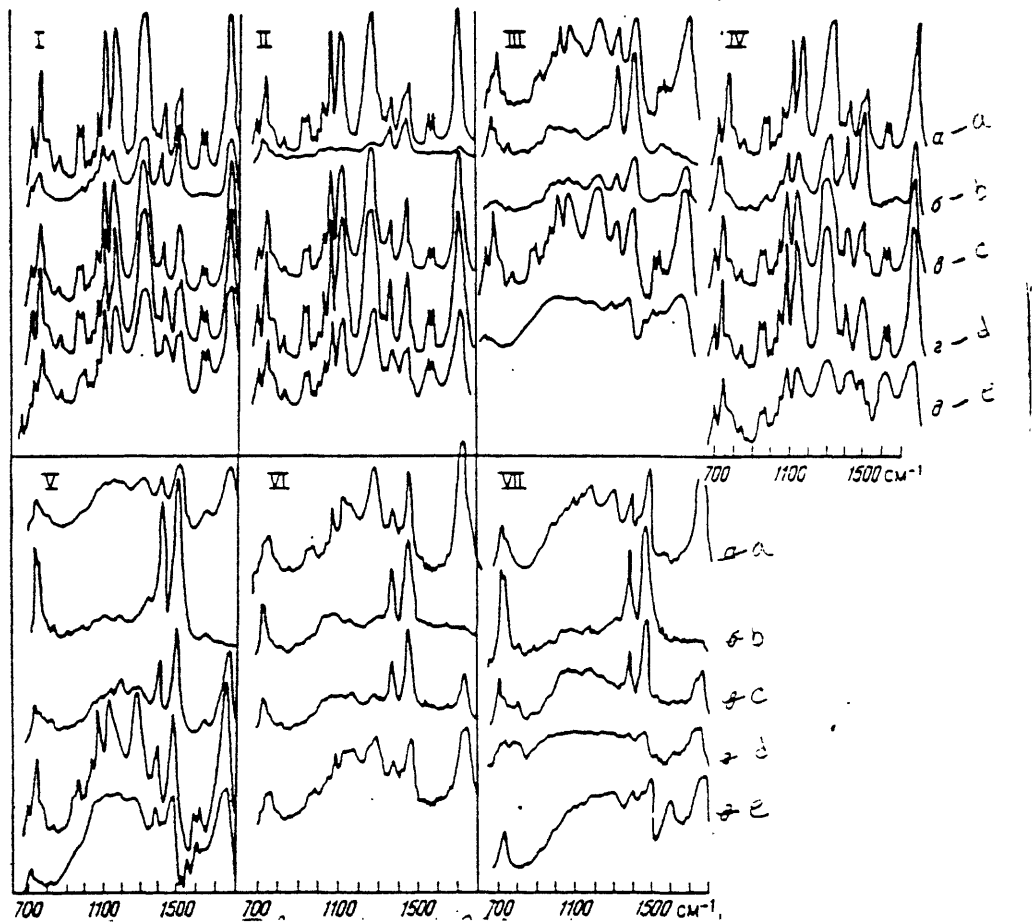


Figure 1.75. IR spectra of CBA and components.

Middle Proterozoic rocks: I - diabase (1954.7 - 1958.4 m);  
 II - tuff (3752.1 - 3757.4 m); III - tuffite (765 - 885 m);  
 IV, V - phyllite with siltstone (1182 - 1496 m), Archean rocks;  
 VI - epidote-biotite-plagioclase gneiss (9600 - 9980 m);  
 VII - biotite gneiss (8313.1 - 8324.0 m); a - CBA; b - oil; c -  
 petroleum ether resins; d - benzene resins; e - alcohol-benzene  
 resins.

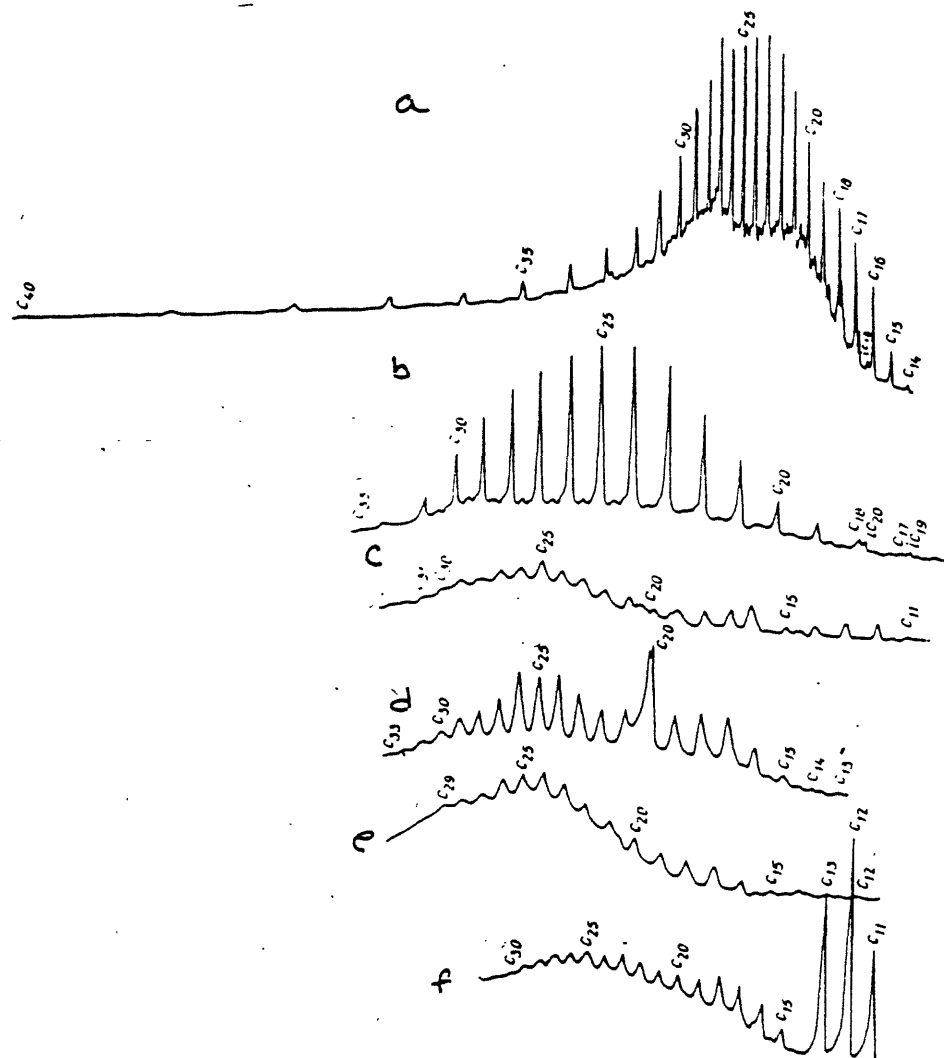


Figure 1.76. Chromatograms of the n-alkanes and iso-alkanes of the CBE oils.

Archean rocks: a - two-mica gneiss (10,144-10,181 m);  
 b - biotite gneiss (8313.1-8324.0 m). Proterozoic rocks:  
 c,d - hyperbasite (1954.6-1958.4, 1757.8-1767.6 m); e - tuff  
 (3752.1-3757.4 m); f - phyllite with siltstone (1182-1496 m).

The results of the geochemical studies indicate that the quantitative distribution, composition, structural properties, chromatographic characteristics of the CBE organic matter depend on the formation conditions of the different genetic types of country rocks. The geochemical sedimentation setting was favorable for the accumulation and preservation of organic matter, which upon transformation generated bituminous aliphatic and cyclic components. Intrusives probably assimilated the organic compounds and transformed them into a variety of organic systems at high temperatures.

Since petroleum was added to the drilling fluid below 7 km, special studies were carried out to determine the contamination effects using gas-liquid chromatography. The petroleum additives had no significant effect on the CBE composition. The possibility of microconcentrations of hydrocarbons forming in intrusive rocks was not excluded; however, this is a problem that can only be solved by superdeep drilling under strictly sterile conditions.

#### HYDROGEOLOGICAL OUTLINE

The main hydrogeological investigations conducted on Drillhole SG-3 focussed on groundwater development conditions and the characteristics of the deep layers of the crust - the ancient metamorphic strata and the role of water in various geologic processes. In addition to investigations conducted on other wells in the Baltic shield, results from geophysical logs, core analyses (petrophysical, geochemical, isotopic, etc.), joint system analysis, gas-liquid inclusions, thermal data etc., were also used in interpretation. Hydrogeological and helium surveys were also conducted along major fault lines.

#### GROUND WATER OF THE PECHENGA

Drillhole SG-3 penetrated a section of the subartesian basin corresponding to ancient Proterozoic secondary artesian basins, structurally related to intermontane basins. The section is separable into two stages; the upper is composed of metamorphosed sediments and volcanogenic formations of the Pechenga complex, and underlying are intensively metamorphosed Archean rocks (artesian basin basement). The average porosity is less than 1%, with a maximum of 2-3%; therefore, the spatial distribution of fluids is governed by fracturing of the water-bearing rocks. A zone of exogenic jointing ranges in depth, but averages 800 m. Ground water is only slightly mineralized, being derived from atmospheric precipitation. Due to very weak exogenic fracturing,

transmissivities rarely exceed  $1-2 \text{ m}^2/\text{day}$ , and are greater only in areas of tectonic disturbances. Multidirectional fractures were discovered at depths of 2.5 - 3 km. From 2.5 to 4.3 km their direction is predominately vertical, but the deeper fractures are widely spaced and oriented horizontally. Below 8.2 km the fractures are again more vertical.

The zones of increased jointing are nonuniform in depth and their thickness ranges greatly. Down to depths of 4.5 - 4.6 km fracture zone thicknesses ranges from 20 to 80 m and are rather sparsely distributed 500-1500m. The rocks outside these zones are nearly impermeable ( $10^{-5}-10^{-6}$  millidarcys). The intervals of increased jointing fall into large zones 500-800 m thick, and enclose 2 or 3 of the local observed maxima. These zones comprise the fracture-vein systems depicted in Figure I.77. The permeability of these zones is comparably small, and formation pressures are low. Three such zones are identified down to 4.5 km; and below this depth individual fracture zone thicknesses increase but their spacing reduces.

The lower part of the section has been named a zone of regional tectonic schistosic development, or more appropriately a zone of regional disaggregation. Its base is at 9 km, and the total thickness exceeds 4 km. The entire zone contains free or gravitational water. A constant inflow of water was observed during drilling. Drillhole testing yielded hydraulic conductivities of  $10^{-7} \text{ m/day}$  at 6170 - 6470 m.

#### GROUND WATER CHEMICAL COMPOSITION

Ground water circulating in the regional fracture zone (exogenic) is of a calcium bicarbonate composition with salinities rarely exceeding 0.5 g/l. The nitrogen and oxygen composition indicates a meteoric origin for these waters.

Ground water in the interval 0.8-5 km is of sodium-chloride composition, slightly alkaline, and salinities increase with depth reaching saturation in some intervals; salinities reach 24 g/l at 900 m, and 51 g/l at 1200-1350 m. In the basal portion there is a relative decrease in sodium, and the water is characterized as predominately the chloride sodium type (little change); however, salinities were significantly higher.

Ground water in the zone of regional disaggregation (4.5-9 km) is not hydraulically connected with the overlying zone; the water instantaneously rose 80 m when this zone was penetrated. Water from 5.3 to 7 km is neutral and slightly alkaline, with a sodium chloride composition. Below 7 km

Well SG-3

RS-2 NE

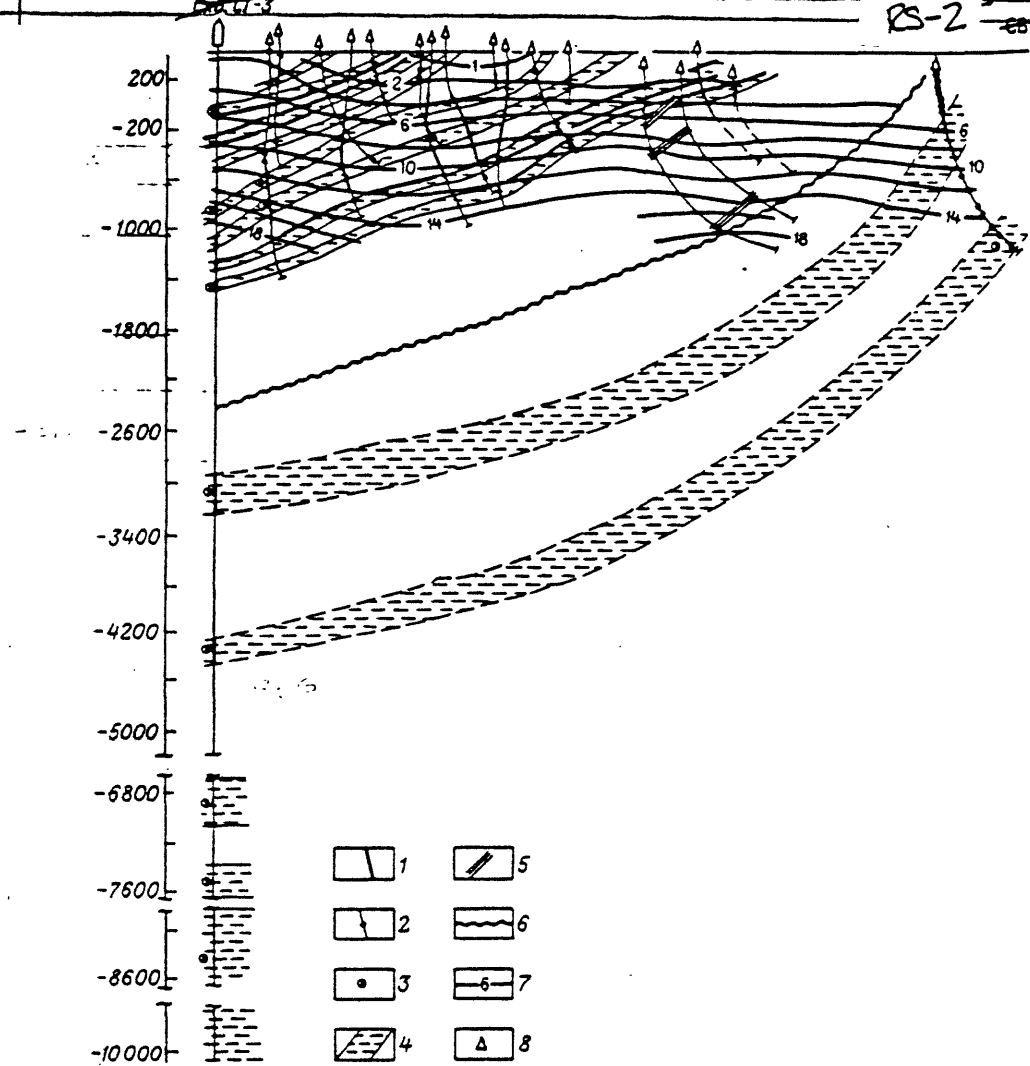


Figure 1.77. General hydrogeological cross-section of Drillhole SG-3 test area:

1 - zones of negative temperature anomalies; 2 - zones of intensive fracturing; 3 - zones of highly mineralized water; 4 - fracture-vein and fracture reservoir systems; 5 - zone of intensive micromovements; 6 - boundary between the III and IV volcanogenic-sedimentary cover; 7 - temperature, °C; 8 - wells.

the situation changed abruptly, water became highly mineralized (saline), was neutral or slightly acidic, and the composition changed to a calcium and sodium-calcium chloride type. The lack of complete analyses of the brine inflow below 8 km made it difficult to identify brine components.

The gas from 0.8 to 2.5 km had significant concentrations of hydrocarbon gases. The hydrogen content increases with depth and predominates from 2.8 to 3 km. Helium content also increases with depth, and at 6 km it is commensurate with hydrogen. The inertness of the helium makes it the best indicator of fluid inflow into the drillhole. Gas analyses of the drilling mud and the gas composition in the intercrystalline pores and fluid inclusions suggest that at 5.5 - 6 km, dissolved carbon dioxide gas begins to be significant; however, gas saturation of ground water, on the whole, is rather low.

#### GROUND WATER AND HYDROPHYSICAL ZONALITY

Gravitational water is distributed throughout the entire thickness of metamorphosed rocks (more than 10 km), marking the first time that ground water was found under such conditions. Based on chemical composition, the water for much of the section was similar to deep metamorphosed marine sedimentary water of the ancient platforms (including the Eastern European), piedmont, and intermontane basins, indicating that the water preserved in the sedimentary rocks was syngenetic with the primary deposits, but underwent a long and complex evolutionary process.

Table I.33 presents the results of isotopic analyses of carbon dioxide and hydrogen in core samples to study the origin of ground water in the metamorphosed rocks. Some depletion in carbon dioxide and the enrichment of deuterium may be due to the fact that a significant part of the water was consumed early in the process of metamorphism in the formation of other hydroxyl-bearing minerals. These waters were most probably initially sedimentary, but then underwent a long and complex evolution.

Several hydrogeologic zones are identified in Table I.34: 1) zone of regional ground water flow (zone of exogenic disaggregation); 2) upper zone of fracture water development (zone of metamorphic compaction); 3) zone of regional tectonic schistosic development and hydraulic disaggregation of the rock; and 4) a lower zone of fracture water (lowest zone of disaggregation).

During progressive metamorphism, water is released from the hydrated minerals (chlorites, epidote, mica, etc.). Chemical bonding of the water is

Depth, m Глубина, м	Lithology Литология	C <sub>2</sub> *Не обн.	C <sub>3</sub> *Не обн.	C <sub>4</sub> *Не обн.	C <sub>5</sub> *Не обн.	C <sub>6</sub> *Не обн.	C <sub>7</sub> *Не обн.	C <sub>8</sub> *Не обн.	C <sub>9</sub> *Не обн.	C <sub>10</sub> *Не обн.	C <sub>11</sub> *Не обн.
765—885	Туффит Tuffite	*	2,2	3,4	2,6	4,3	7,1	10,8	12,9	8,6	
887—965	Диабаз Diabase	.	*Не обн.	2,3	4,8	3,0					
Phyllite with siltstone											
1182—1496	Филлит с алевролитом	15,1	29,1	14,6	0,1	2,1	4,2	5,3	5,5	3,1	
Gabbro-diabase with essexite	Габбро-диабаз эсекситовый	*Не обн.	*Не обн.	*Не обн.	1,4	2,0	2,6	4,5	5,8	4,3	
1289—1305	Гипербазиты — Hyperbasites	1,2	4,2	4,2	0,3	1,4	3,0	6,2	6,3	5,4	
1757—1767	Диабазы Diabase				0,4	2,3	2,1	11,7	4,8	5,3	7,9
1954—1958											
1284—1413	Габбро-диабазы Gabbro-diabase	*Не обн.	1,4	7,1	9,7	8,9					
2154—2291	Пересланывание филлитов и алевролитов	8,6	10,3	5,5	0,4	4,1	4,7	10,6	11,1	5,9	
2994—3201	Диабазы Diabase	*Не обн.	2,1	3,4	5,6	5,5					
Diabase with carbonaceous matter											
3645—3650	Диабазы с углеродистым веществом	.	.	.	.	.	6,5	4,0	6,8	6,0	
3752—3757	Туфф Tuff	.	0,6	0,6	0,9	2,2	3,6	8,8	9,3	8,0	
3983—3987	Диабазы Diabase	.	*Не обн.	*Не обн.	*Не обн.	*Не обн.	3,5	3,4	6,2	4,6	
Schist with tuffogenic-sedimentary rocks											
4360—4389	То же	.	.	.	.	0,7	1,1	4,2	4,2	3,4	
4630—4748	Сланцы по туфогенно-осадочным породам	.	1,4	2,3	1,7	1,2	1,6	3,7	4,2	3,7	
Andesite porphyrite											
4749	Анделитовый порфирит	.	*Не обн.	0,3	0,4	0,5	0,8	1,8	1,6	1,7	
Ankeritic sandstone											
4847—4859	Песчаник арковый	.	.	*Не обн.	*Не обн.	*Не обн.	0,8	4,7	4,3	2,9	
6757—6767	Сланцы Schist	.	.	.	1,1	3,0	3,7	5,4	13,3	15,1	5,5
Biotite gneiss											
8313—8324	Гнейс биотитовый	.	.	*	*Не обн.	*Не обн.	*Не обн.	0,7	1,1	1,9	
Epidote-biotite-plagioclase gneiss											
9600—9989	Эпидот-биотит-плагиоклазовые гнейсы*	.	.	.	0,5	0,8	1,2	1,6	1,9	2,9	
Two-mica gneiss											
10144—10181	Двуслюдянные гнейсы**	.	.	.	0,8	1,4	2,3	3,6	3,8	3,6	
Computed in the sum	Нефть — добавка C <sub>9</sub> , C <sub>10</sub> в буровой раствор	5,4	5,5	4,1	4,7	3,8	4,3	3,2	3,4	2,8	Petroleum additive in oil
	* В сумме учтены C <sub>2</sub> — 2,4, C <sub>3</sub> — 2,2, C <sub>4</sub> — 1,8, C <sub>5</sub> — 1,7, C <sub>6</sub> — 1,6, C <sub>7</sub> — 0,4 %.										
	** В сумме учтены C <sub>2</sub> — 2,1, C <sub>3</sub> — 2,0, C <sub>4</sub> — 1,9, C <sub>5</sub> — 1,6, C <sub>6</sub> — 1,5, C <sub>7</sub> — 1,4, C <sub>8</sub> — 0,4 %.										

Table I.32 Distribution of n-alkanes (%) in oils of CBE from rocks in Kolz Drillhole SG-3.

$C_{\text{Fe}}$	$C_{\text{Si}}$	$C_{\text{Mn}}$	$C_{\text{S}}$	$C_{\text{Al}}$	$C_{\text{Cr}}$	$C_{\text{Ni}}$	$C_{\text{Cu}}$	$C_{\text{Zn}}$	$C_{\text{P}}$	$C_{\text{S}}$	$C_{\text{P}}$	$C_{\text{N}}$	$C_{\text{H}}$	$\Sigma C_{\text{g}-\text{m}}$	$\Sigma C_{\text{H}-\text{m}}$	$\Sigma C_{\text{H}-\text{m}}$	Изогр. чисто пurity, чисто T	
6,6	6,5	6,8	5,2	3,3	5,6	4,6	2,4	2,4	2,3	He обн.	He обн.	He обн.	He обн.	—	—	97,6	20,1	1,3
1,1	6,2	7,1	7,5	10,0	10,2	13,6	9,9	5,9	4,3	2,4	1,5	1,1	.	—	—	90,9	—	1,0
2,1	2,1	2,2	2,3	2,6	2,7	1,8	1,7	1,5	1,4	0,5	He обн.	He обн.	.	—	—	100,0	65,2	1,3
15,4	2,2	5,1	5,6	7,9	7,3	6,2	5,0	2,9	3,3	1,1	.	.	.	—	—	80,6	7,3	1,2
9,1	3,5	4,7	7,0	9,0	8,6	9,4	5,4	4,0	3,2	1,5	1,5	0,8	0,3	—	—	91,0	5,6	1,0
2,1	3,7	5,4	5,4	6,5	9,1	8,1	4,3	2,8	1,4	0,6	He обн.	He обн.	He обн.	—	—	93,1	27,6	1,1
6,8	7,7	9,3	8,4	7,9	8,9	6,0	5,3	4,1	3,8	2,0	1,7	1,0	.	—	—	100,0	1,4	1,3
5,7	4,9	4,1	4,0	3,7	4,5	3,9	3,6	0,9	2,3	He обн.	He обн.	He обн.	.	—	—	98,8	34,0	1,4
3,9	10,7	5,5	10,0	10,4	9,3	9,1	6,0	3,5	2,6	1,9	.	.	.	—	—	90,5	2,3	1,1
6,5	8,0	6,7	9,1	11,0	6,7	7,6	5,5	2,7	6,0	He обн.	.	.	.	—	—	93,1	7,0	1,0
7,6	5,2	5,8	8,0	9,3	8,2	6,4	5,3	4,1	3,2	.	.	.	.	—	—	97,1	8,1	1,1
6,1	7,5	6,4	7,7	11,5	11,5	11,3	8,4	6,5	5,0	.	.	.	.	—	—	99,6	3,5	0,9
1,9	4,2	5,0	8,5	13,4	11,9	12,0	6,9	5,0	5,5	2,1	1,1	0,2	.	—	—	92,0	2,0	1,0
3,2	4,6	3,0	8,9	12,0	12,1	12,3	6,3	4,4	3,8	2,1	0,9	0,3	.	—	—	96,8	8,5	1,0
3,7	9,1	9,7	12,1	11,5	10,6	8,9	7,1	5,7	4,0	2,2	1,4	0,9	0,8	—	—	94,8	2,0	1,2
3,2	6,1	4,6	8,1	11,8	12,2	8,0	6,9	3,6	3,5	1,4	5,3	3,6	4,9	—	—	95,8	—	1,3
2,5	3,9	6,1	6,2	6,6	7,4	5,3	3,2	2,9	4,7	1,3	He обн.	He обн.	He обн.	—	—	97,2	13,5	1,3
2,8	6,3	8,1	11,6	12,7	11,5	10,9	9,6	7,3	5,9	4,7	2,2	0,9	0,4	—	—	98,1	—	1,1
3,8	5,2	3,4	7,2	7,4	7,0	6,5	6,4	4,6	3,0	3,4	3,1	2,8	2,5	89,2	2,6	—	—	1,1
3,8	4,9	5,8	6,2	6,1	5,0	5,7	5,5	4,1	3,5	2,9	2,8	2,4	2,2	87,3	5,1	—	—	1,1
2,7	2,7	2,1	1,5	1,1	0,9	0,6	0,3							61,0	65,0	—	—	1,3

Table I, 32 continued

Table I-33 Results of isotopic analyses of OH<sup>-</sup> groups in minerals

Average chemical composition of Archean paleogneisses and enderbites comprising the basement of the eastern portion of the East European Platform and the calculated composition of the continental crust (% of dry matter)

Oxides окисей	Балтийский щит			Среднее по слову			Балтийский щит			Среднее по слову			Русская платформа			Среднее по слову			Промежуточный слой флюорит-гематит-гипсовые слои				
	1	2	3	4	5	6	7	8	9	10	11	12	13	14	15	16	17	18	19	20	21	22	
SiO <sub>2</sub>	65,05	68,18	67,27	65,27	68,34	66,68	66,91	71,29	65,49	67,23	66,16	70,54	65,18	66,23	66,45	66,10	66,45	66,45	66,45	66,45	66,45	66,45	
TiO <sub>2</sub>	0,68	0,32	0,43	0,60	0,55	0,59	0,52	0,29	0,54	0,46	0,58	0,30	0,56	0,51	0,53	0,50	0,53	0,53	0,53	0,53	0,53	0,53	
Al <sub>2</sub> O <sub>3</sub>	16,55	16,86	16,77	17,19	14,37	15,91	16,28	15,55	16,47	16,19	16,30	15,78	16,94	16,71	15,98	16,20	15,98	15,98	15,98	15,98	15,98	15,98	
Fe <sub>2</sub> O <sub>3</sub>	1,03	0,64	0,75	1,39	1,05	1,21	1,03	0,83	1,43	1,25	1,94	0,72	1,40	1,27	1,55	1,55	1,55	1,55	1,55	1,55	1,55	1,55	
FeO	6,17	2,17	3,33	5,63	4,87	5,28	4,44	1,59	3,90	3,21	4,60	1,60	3,33	2,90	3,73	3,73	3,73	3,73	3,73	3,73	3,73	3,73	
MnO	0,07	0,03	0,04	0,08	0,07	0,07	0,07	0,07	0,03	0,10	0,08	0,06	0,03	0,08	0,07	0,07	0,07	0,07	0,07	0,07	0,07	0,07	
MgO	2,33	1,41	1,68	1,99	1,57	1,79	1,74	0,83	1,87	1,56	2,10	1,76	1,91	1,88	1,89	2,20	1,89	1,89	1,89	1,89	1,89	1,89	
CaO	1,88	2,54	2,35	2,75	3,59	3,12	2,79	3,39	4,59	4,23	4,91	2,98	4,65	4,32	4,55	5,10	4,55	4,55	4,55	4,55	4,55	4,55	
Na <sub>2</sub> O	3,11	5,40	4,73	2,95	3,08	3,02	3,75	5,18	3,92	4,30	3,19	4,55	4,45	4,47	3,88	4,70	3,88	4,70	3,88	4,70	3,88	4,70	
K <sub>2</sub> O	3,05	2,38	2,58	2,07	2,33	2,18	2,35	0,92	1,69	1,46	1,05	1,74	1,50	1,50	1,30	0,62	1,30	0,62	1,30	0,62	1,30	0,62	
P <sub>2</sub> O <sub>5</sub>	0,08	0,07	0,07	0,07	0,18	0,12	0,10	0,11	0,11	0,11	0,11	He-опр.	He-опр.	He-опр.	He-опр.	0,16	0,16	0,16	0,16	0,16	0,16	0,16	0,16
Число проб	69	92	161	25	25	50	211	6	14	20	13	6	41	Undet.	Undet.	Undet.	Undet.	Undet.	Undet.	Undet.	Undet.	Undet.	
Доля разрезе, %	18,7	46,2	64,9	47,4	39,1	46,5	100	He-опр.	He-опр.	He-опр.	He-опр.	He-опр.	82,0	12,3	50,4	62,7	100	He-опр.	He-опр.	He-опр.	He-опр.	He-опр.	

Fraction in section, %

118

Drillhole SG-3 section (1 - meso - and melanocratic, 2 - leucocratic, 3 - weighted average composition), 4-6 - rocks of the Cheremshan Series from Minnibaev Well 20.000 section (4 - garnet-sillimanite-biotite crystallized schists, including the high alumina schists, 5 - boulders of the Kora Series from the Kora River).

associated with the relatively low-hydrated minerals (epidote, micas, etc.). Evolution of the highly hydrated minerals in the main stage of metamorphism led to the generation of solvents and an increase in the volume of gravitational water, which together with primary sedimentary water, is not uniformly distributed within the pore spaces and the system of microfractures along grain boundaries.

Remobilization of the water in the metamorphosed strata controls the processes leading to disaggregation of the rocks and an increase in void volume. First, high pore pressures are responsible for the microfractures at points where the volume of regenerated water is greatest. Second, this water impedes complete compaction during recrystallization, since the release of water from the rocks is difficult due to the low permeability. Third, the metamorphic water is highly aggressive and is able to dissolve certain rock components, increasing their overall void volume.

Hydrogeologic studies indicate extremely low permeabilities ( $10^{-7}$  m/day) in the lower part of the third zone, but it is nevertheless significant since up to now it has been assumed that metamorphic rocks at such depths are impermeable. Because of the extremely low permeability and the great number of isolated voids (microfractures) water has been preserved in the zone of disaggregation for more than one billion years. Thus, analyses of the distribution of water-bearing zones and the nature of the fracture systems led to the conclusion that the source of the fluid in the zone below 4.5 km was mineral dehydration during metamorphic transformation.

Calculations showed that in the interval 4-6.8 km, total water losses comprised  $5.5 \times 10^7$  g/m<sup>2</sup>, or 6.7% of the original rock volume. Analyses based on average mineral composition show that the total volume of the minerals in the transition from the green schist to epidote-amphibole facies comprised 0.96 of the original volume, which combined with the released water is 1.027, or 2.7% greater than the initial volume. To preserve this initial rock volume, water would have to be compressed by 1.7 times requiring pressures of some 30 gPa, corresponding to pressures at mantle depths (90-100 km). An increase in volume can only occur through fracture continuity, since rock tensile strengths are an order of magnitude less than the pressures developing during the release of water. Figure I.79 shows the strong mineral crystal deformation and void development (fracture continuity) from the extremely high hydraulic pressures. Mineral dehydration could not occur otherwise.

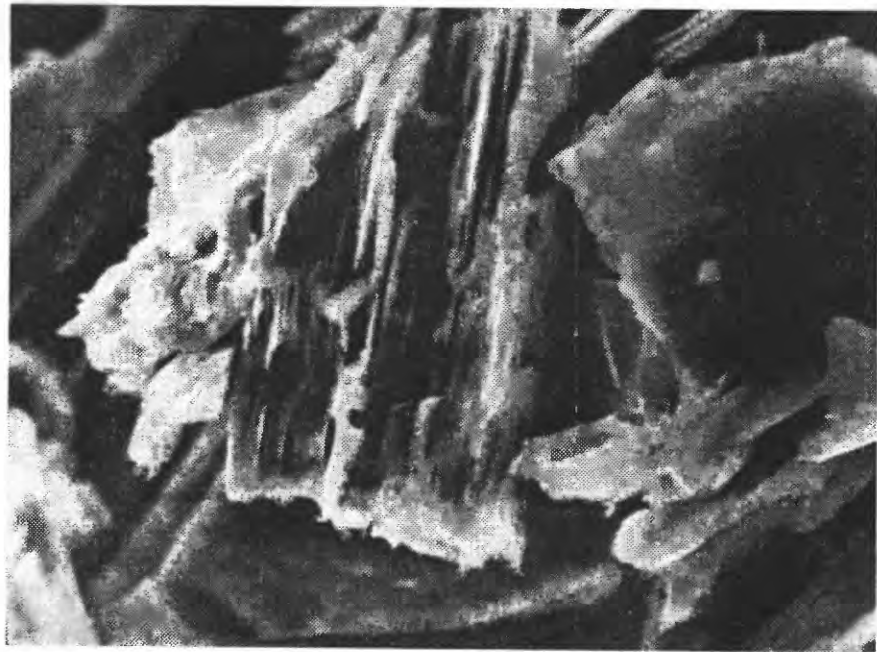


Figure 1.79. Talc-biotite-tremolite schist (8028 m).  
Section, X600. The intercrystalline microfractures are quite  
evident.

Fracture orientation is governed by the spatial orientation of the strain ellipsoid at the time of formation. In a relatively quiet tectonic setting near vertical fractures are formed. If the horizontal stress significantly exceeds the lithostatic load, a known characteristic of the Baltic shield, then fractures may have a horizontal orientation that may open up over time. The regional schistosic development seen in the section of SG-3 is related to this process; the orientation of the schist development is subhorizontal and is independent of stratigraphic boundaries. Inasmuch as high horizontal stresses are typical for deep crustal zones, this phenomenon of regional schistosic development may be detected rather often. Based on the ratio of free and bound water at various stages of metamorphism, hydrogenic disaggregation may likely occur in rocks of epidote-amphibolite and amphibolite facies.

The nearly coincident boundaries of the geochemical zones with the boundaries of the stratigraphic subdivisions and their restriction to definite types of metamorphism suggests that the essential influences on ground water formation is the initial habit of the rocks, the degree of their metamorphic transformation, and contemporaneous metamorphic trends.

The hydrodynamic zones differ from one another not only in their qualitative and quantitative characteristics of fracturing and in transmissive properties and hydrostatic pressures, but also in a range of changes peculiar to each zone in lithostatic pressure, temperature, and gas and chemical composition.

The main mass of ground water was the product of an exogenic water exchange in the zone of regional ground water flow, whereas clearly the water in the lower zones bears an endogenic nature. The total quantity of chemically bound water and the nature of its bonds (highly hydrated in the two upper zones, and a lower hydration in the lower) permits the hydrogeological evolution of the rock masses to be reconstructed. The model of hydrophysical zonality presented in Table I.34, not only explains the nature of the hydrothermal fluids unrelated to intrusions, and allows us to understand the mechanism of regional schistosic development in the zones of disaggregation and the formation of certain types of tectonic disturbances, but also fundamentally changes our perceptions regarding the circulation of ground water in the crust.

### EVOLUTION OF THE CONTINENTAL CRUST IN THE PRECAMBRIAN

Data from the Kola drillhole opened up the possibility to address the problems of Precambrian crustal evolution from the standpoint of a 3-dimensional model where the addition of a known third dimension gives rise to the possibility of reconstructing the geologic process that operated in the past, and evaluating alternative hypotheses regarding the structure and development of the deep crustal zones composed of metamorphosed Precambrian rocks.

### GEOLOGIC MODELS OF THE PECHENGA REGION

The three-dimensional model of the Pechenga structure shown in Figure I.80 (in pocket) was based on drillhole data, gravity-seismic surveys, and wells located in line with SG-3. Based on these data a number of conclusions were drawn regarding the structure of the Pechenga complex. The structure comprises a graben-syncline, bonded on the south by a zone of regional faults with depths greater than 20 km. Gravity surveys yielded a decreasing gravity gradient that repudiated the previously held notion of an overturned north limb, and suggest that the southern regional fault zone is composed of parallel-contiguous reverse faults. The base of the fault zone is "sealed" by a hypabyssal andesitic intrusion. The maximum thickness of the volcanogenic-sedimentary formations of the complex was established in the central part of the graben-syncline, in the vicinity of the Por'itash fault, as being greater than 8 km. Despite the interpretations of surface gravimetric and seismic survey data, the drillhole penetrated a thick granite-gneiss rock mass at 6.8 - 11.6 km, containing many amphibolite bodies comparable to the Kola Series. Geologic and geophysical data also indicated that the Conrad layer could not be explained by either a transformation from more silicic to basic rocks, or by an abrupt metamorphic boundary, or by subhorizontal tectonic zones.

### HISTORY OF THE GEOLOGICAL DEVELOPMENT OF THE PECHENGA REGION

Drillhole SG-3 data have contributed profoundly to our understanding of the historical continental crustal development of the Pechenga region. Development has been subdivided into two great cycles: the Archean (greater than 2.6 by) which includes two stages; 1) sedimentation and volcanism, and 2) folding, metamorphism, and ultrametamorphism; and the Proterozoic (2.6 - 1.1 by) (second cycle), which includes 4 stages of development; 1) subsidence

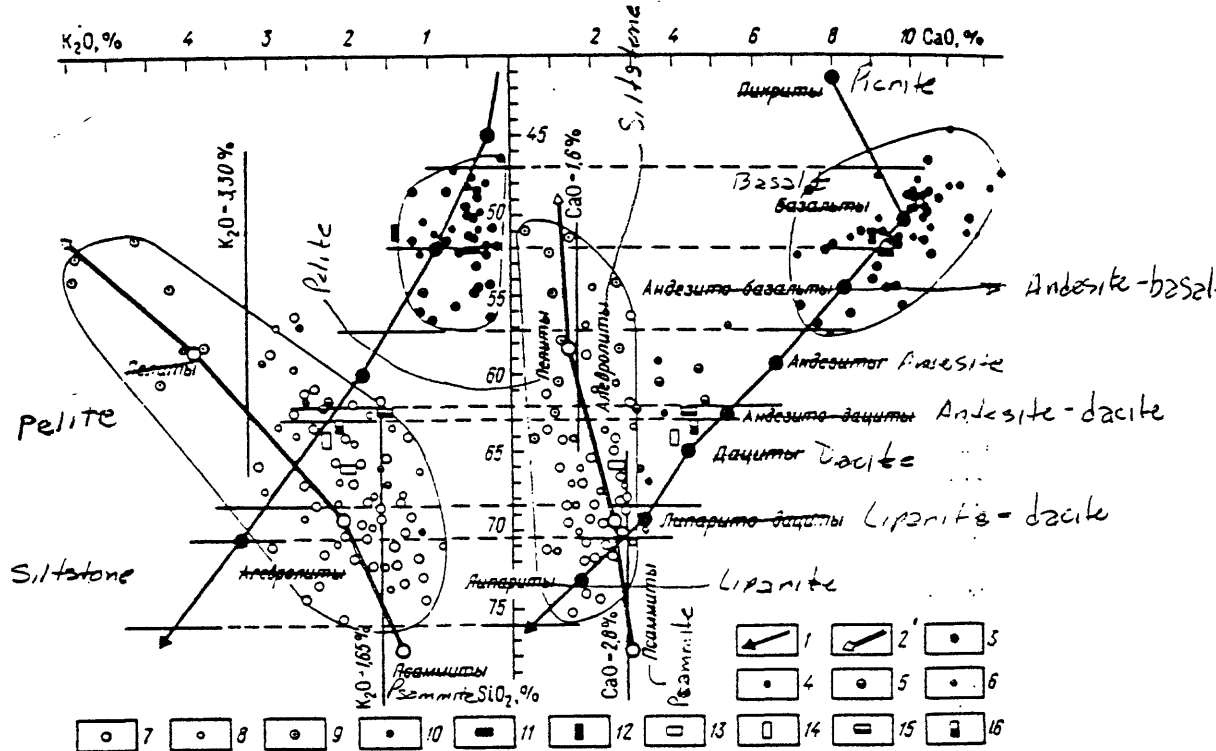


Figure 1.81. Reconstruction of the proto rock composition of the Archean complex from Drillhole SG-3 (odd) and the surrounding surface (even).

1 - trend of magmatic differentiation; 2 - trend of sedimentary differentiation; 3, 4 - amphibolite; 5, 6 - hornblende-biotite paleogneiss; 7, 8 - biotite-plagioclase gneiss; 9, 10 - biotite-plagioclase gneiss with VGM; 11-16 - average composition (11, 12 - rocks of amphibolite group; 13, 14 - rocks of plagioclase group; 15, 16 - rocks of Archean complex).

of the midcontinental mobile belt, 2) andesite-basalt volcanism, 3) picrite-basalt volcanism, and 4) a stage of plicative-rupture dislocation and metamorphism. The structural-metamorphic evolution was consummated by a platform activation stage.

The Archean metamorphic complex (6842-11,622 m) penetrated by Drillhole SG-3, is of mixed composition and has a rhythmic-stratified structure. The preservation of deep rock sections, nearly unchanged by migmatization and metasomatism of the metamorphic rocks, permitted the original compositions to be reconstructed using the petrochemical diagram of Fig. I.81. Using the composition and content of rare earth elements the amphibolites are identified with the volcano-plutonic association of Archean basic rocks of the green schist belts (Figure I.82).

The first Archean stage is characterized by an accumulation of thick sedimentary strata (argillaceous-siliceous) and active volcanism associated with an outpouring of rhyolitic, dacite, and andesitic lavas with minor basalts and ultramafic rocks (basaltic-andesitic formations).

The tectonic structure of the second Archean stage, based on analogous Archean complexes present on the surface, represents a synclinoria zone or an asymmetric-syncline in combination with a dome-shaped structure. Surface observations point to a recurrence of plicative and fracture deformation of the Kola Series from metamorphism and ultrametamorphism; however, Drillhole SG-3 cores failed to distinguish these different-aged tectonic elements. The time of metamorphism for this stage was 2754 + 40 my. Age dating and the products of earliest granitoid magmatism indicate there was a single zonal series of progressive metamorphism and ultrametamorphism of the Kola complex. The Archean cycle culminated with consolidation of the subcrystalline formations (cratonization) and deep faulting.

The Proterozoic cycles are characterized by the formation on the Archean basement of the midcontinental mobile Pechenga-Varzu belt which trends southwest along the entire Kola Peninsula from Norway to the White Sea. Four stages are identified in belt development: 1) subsidence of the belt, 2) andesite-basalt volcanism, 3) picrite-basalt volcanism, and 4) plicative-rupture dislocation and metamorphism.

The first stage was distinctly established on the surface by the development of the Tundra Series in portions of the southern edge of the belt, but radioactive dating could not precisely date the discontinuity between consolidation of the Kola complex and the onset of subsidence. The

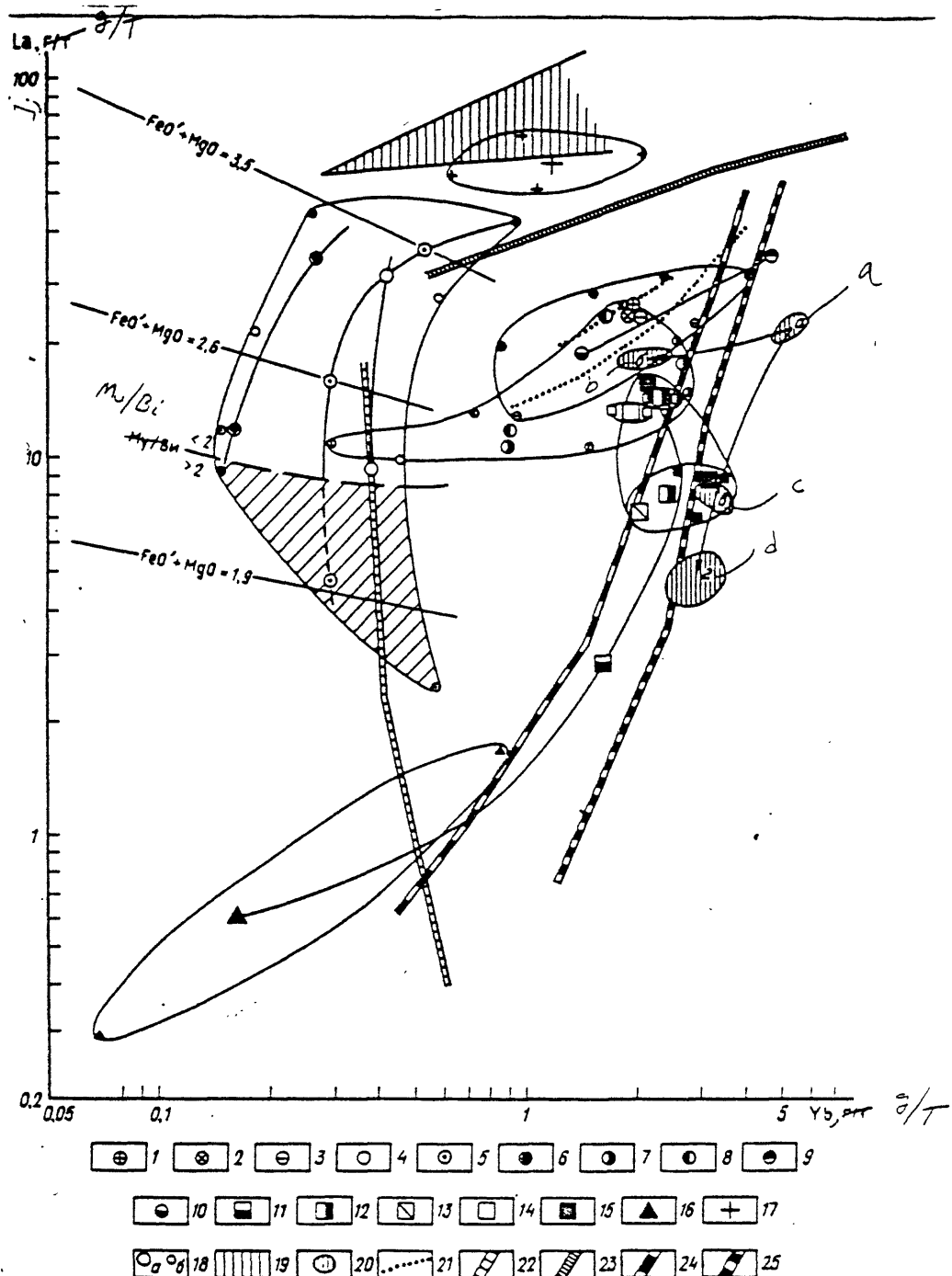


Figure 1.82. Trends in the distribution of La and Yb in rocks of the Archean complex from Drillhole SG-3 and their identification with the main structural-genetic series of the Precambrian and the Phanerozoic: (continued next page).

1 - melanocratic plagiogneiss with VGM; 2 - mesocratic two-mica plagioclase with VGM; 3 - leucocratic two-mica plagioclase with VGM; 4 - biotite plagioclase ( $K_V > 10\%$ ); 5 - biotite plagioclase ( $K_V < 10\%$ ); 6 - biotite gneiss; 7 - leucocratic epidote-biotite plagiogneiss; 8 - mesocratic epidote-biotite plagioclase; 9 - hornblende-biotite schist; 10 - hornblende-biotite-plagiogneiss; 11 - Fe-Ti-amphibolite; 12 - Fe-amphibolite; 13 - Al-Mg-amphibolite; 14 - Si-amphibolite; 15 - gabbro-amphibolite; 16 - talc-actinolite schist; 17 - postfolded porphyry granite; 18 - average (a) and limited (b) concentration; 19 - granitoid, Litsko-Aragub complex (PR<sub>2</sub>), after [18]; 20 - trend of metaextrusive and metaintrusive rocks of the Pechanga Complex (a - metabasalts, b - metaandesite-basalts of the rift-continental stage, c - metagabbro-diabases, d - metabasalts of the rift-oceanic stage); 21-25 - trends (21 - sedimentary differentiation-sand-clay of the Phanerozoic and metapsammite-metapelites PR<sub>2</sub>, after [3], 22 - gabbro-plagiogneiss series of the Early Archean, after [108]; 23 - primary-crustal granitoids of Early Archean Kola Peninsula, after [101]; 24 - intrusive rocks; 25 - extrusive rocks, Early Archean greenstone belts and extrusive series of the Phanerozoic).

paleotectonic conditions during subsidence can only be generally characterized, inasmuch as the rocks of the Tundra Series underwent intensive regional schistosic development and zonal metamorphism, ranging from a sericite-chlorite zone in the greenschist facies to a sillimanite-muscovite zone in the ~~metamorphic~~ amphibolite facies.

The transition from the first to second stage was marked by intensive volcanism under subplatform conditions suggested by the great thicknesses of lava flows, but also by an exceptional uniformity in dip and areal extent of the thin cover of sedimentary rocks. Petrologic and geochemical data show that volcanism began with an outpouring of uniform undifferentiated magmas, whose later evolution and differentiation resulted in an outpouring of trachy-salts (Figure I.84). The mechanism is determined as syntaxis, where basic chamber magma is introduced to the "cool" silicic crust accompanied by melting and assimilation of crustal material and, consequently, modification of the original composition. The subsequent differentiation of the melt resulted in the separation out of andesite.

Between the second and third stages a discontinuity is not so distinct; however, its presence is demonstrated by the development of weathering on the top of the Pittiyarvin Formation, an abundance of magnetite fragments in the Luchlompol sandstones, and a distinct succession of volcanics. Hence, the onset of the third stage was sharply marked by an outpouring of undifferentiated tholeiitic magma, forming a rhythmic tholeiite-basalt formation with an apparent thickness of 1.9 km.

Specifics of the third stage are reflected in the nature of formation of the sedimentary deposits. Thus the Zhdanov Formation has two large distinct sedimentary cycles, as expressed in Fig. I.83. The facies and salt composition of the ground water is indicative of primarily sedimentation conditions.

A detailed reconstruction of the entire succession of tectonic events is impossible; nevertheless, the data permit a new interpretation of the regional structure. Deformation and metamorphism of the Pechenga Complex is related not to the final stage of Middle Proterozoic geosyncline development, but to the protoactivation of Early Precambrian Kola Peninsula structure. The regular variation with depth in structure and texture of metamorphic rocks, the definite orientation in these rocks of quartz, carbonates, mica, and amphibole is evidence that underthrust movement took place along with progressive metamorphism of the Pechenga Complex.

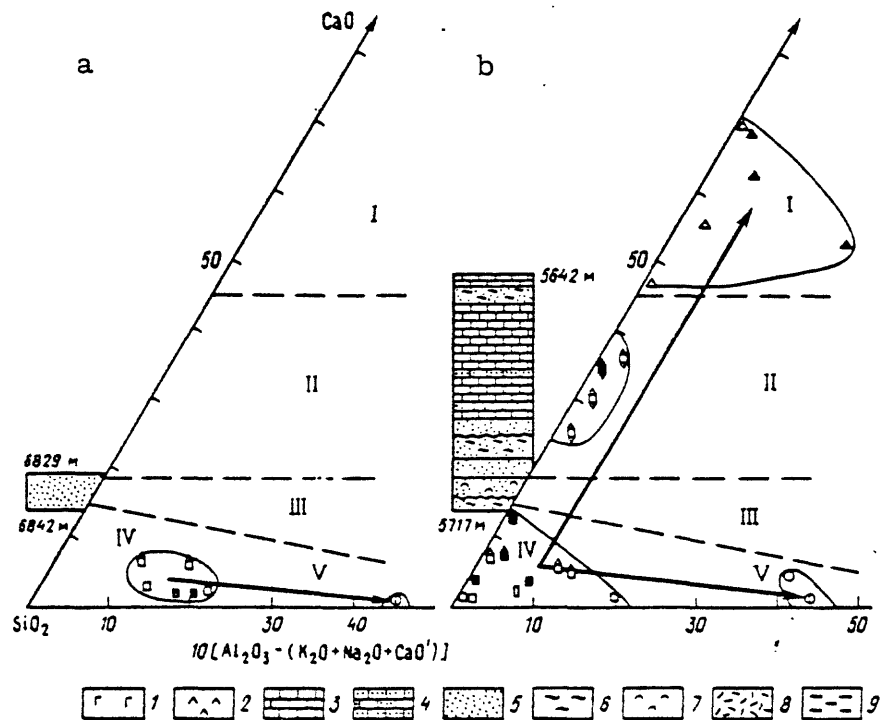


Figure I.83. Lithologic-petrochemical characteristics of the metasedimentary rocks of the Pechenga complex.

Formations: a - Televin, b - Kuvernerin, c - Luchlompol', d - Zhdanov. Rocks: 1 - metaultrabasites, 2 - metagabbro-diabases, 3 - dolomites and limestones, 4 - dolomitic and calcareous metasandstones, 5 - metasandstones and metasiltstones-sandstones, 6 - metasiltstone-sandstones and metapelites, 7 - admixture of carbonaceous material, 8 - metatuffites and metaphyllites, 9 - carbonaceous matter, 10 - sulfates. Rock composition from Drillhole SG-3 (a) and regional surface rocks (b): 11 - sandstone-dolomite and limestones, 12 - dolomitic and calcareous metasandstone, 13 - calcareous metasandstones, 14 - metasandstones, 15 - metasiltstone, 16 - metapelites, 17 - metatuffites, 18 - trends of sedimentary differentiation (I - sandstone-dolomites and limestones, II - dolomites and calcareous sandstones, III - calcareous sandstones, IV - sandstones, V - siltstones and silty pelites).

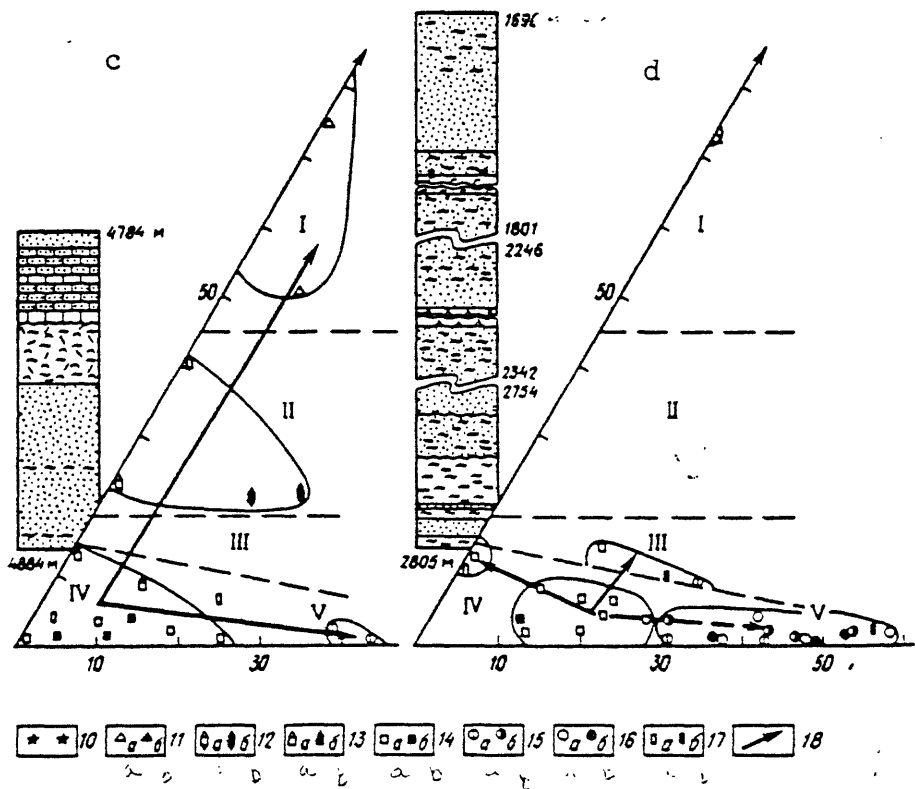


Fig. I.83 continued

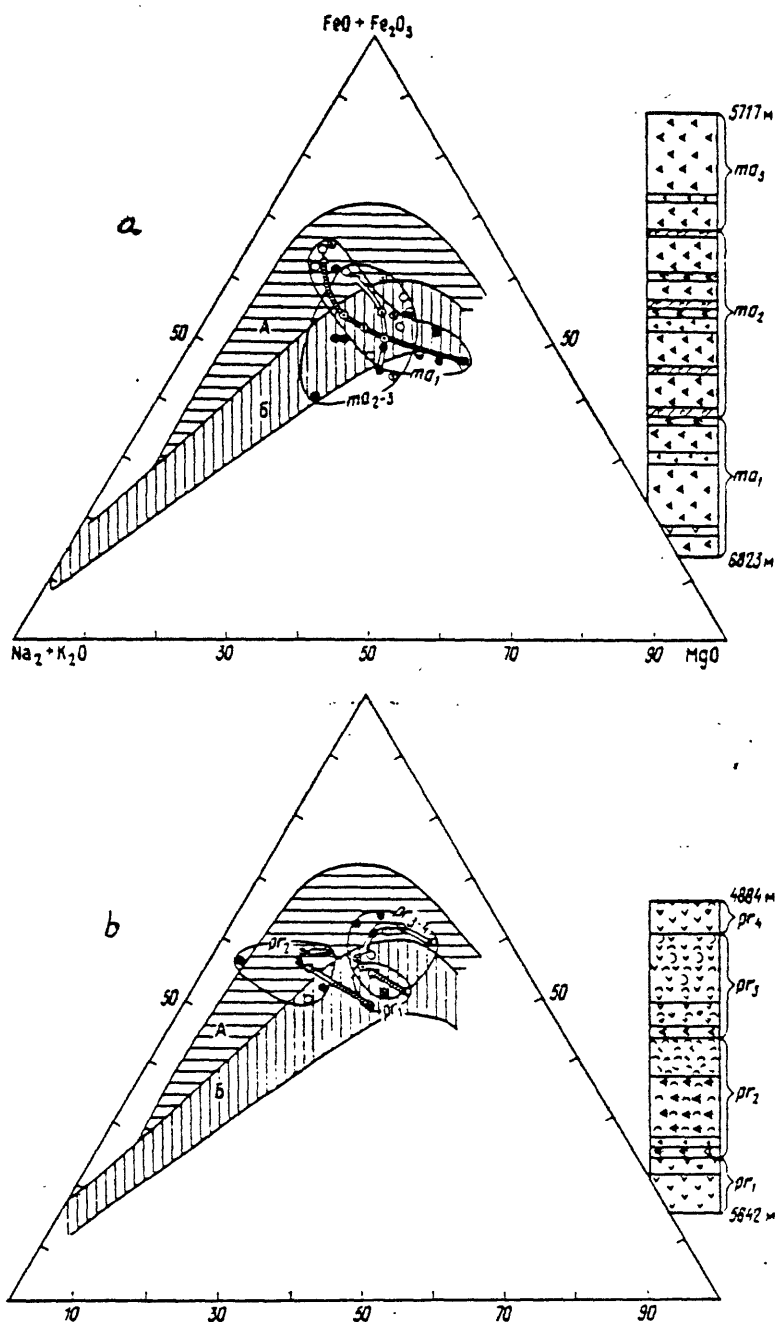


Figure 1.84. Geologic-petrochemical characteristics of metavolcanic rocks of the Pechenga complex.

Formations: a - Mayrvinsk, b - Pirttiyarvin, c - Zapolyarnin, d - Matertin. Principal types of rocks in geologic sections:  
 1 - metapicrites, 2 - metapicrite-basalts, 3 - metabasalts,  
 4 - metatrachybasalts, 5 - metaandesite-basalts,  
 6 - metatrachyandesite-basalts, 7 - metaandesites, 8 - metatuffs,  
 basic (a) and average (b) composition, 9 - metatuffites,  
 10 - metagabbro-basalts, 11 - spilitization. Metaextrusive rock  
 composition (a - average and b - particle values),  
 12 - metapicrite, 13 - metapicrite-basalts, 14 - olivine  
 metabasalts, 15 - differentiated meta basalts, 16 - metabasalts,  
 17 - (missing), 18 - low alkaline metabasalts, 19 - spilites,  
 20 - metatrachybasalts, 21 - metaandesite-basalts,  
 22 - pyroxene-divine metaandesite-basalts, 23 - (missing),  
 24 - metaandesite. Trends metaextrusive rock differentiation,  
 25 - in lower and 26 - in upper parts of volcanogenic

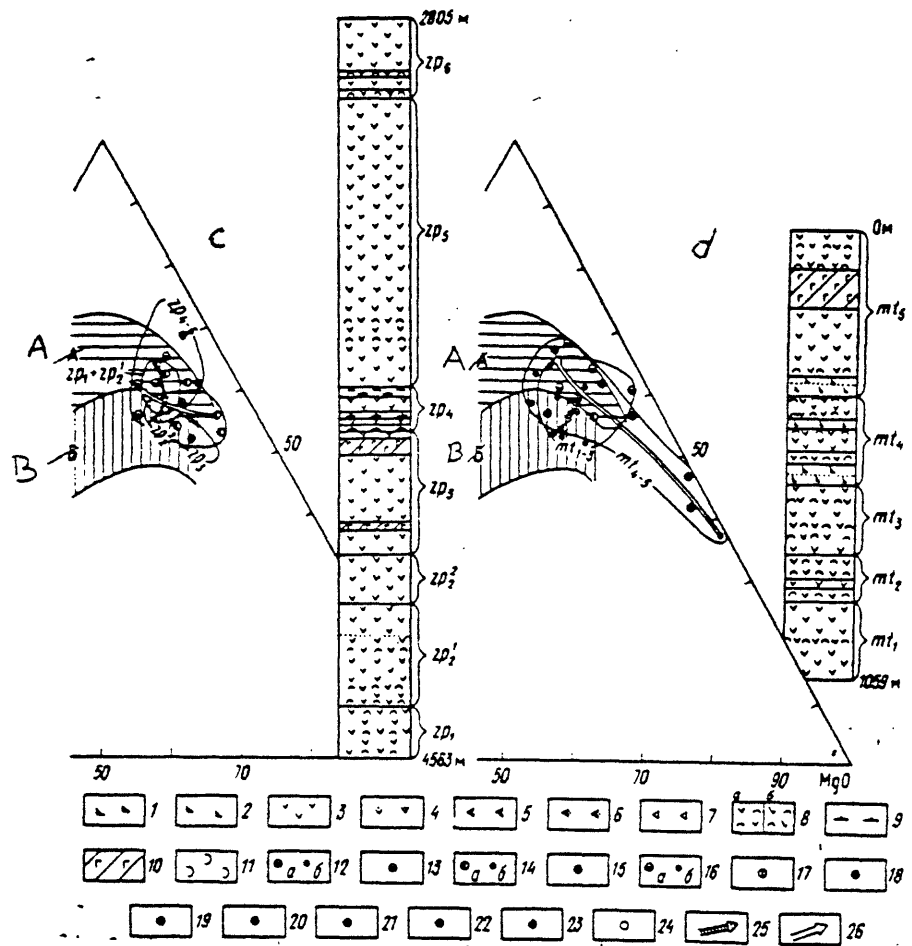


Figure 84 continued

Overthrust movement is associated with a sharp transition from isotropic to anisotropic metamorphic rocks with respect to elastic properties and an interval structure in the zones of regional schistosic development, manifested by a seismic boundary. Outpouring of extrusives was accompanied by low temperature autometasomatic and metamorphic alterations with the formation of hydroxyl-bearing minerals. Progressive metamorphism of the entire complex increased temperatures up to 500-600°C, increasing the pressure and inducing an autoclave effect with the release of synmetamorphic fluids, enriched in chlorine, iodine, barium, strontium, and potassium. This effect resulted in rock deformation and the manifestation of hydraulic disaggregation.

The Luchompol fault was definitely active over a long period of time. The dacite metaporphyrites in the SG-3 section correlate in age and composition with the volcanic-plutonic complex of the southern part of the Pechenga structure (Por'itash fault), and the extrusives formed in the southern basalt-andesite formation are orogenic, yielding the assumption that at depth the Luchompol' fault is connected with the steeply dipping Por'itash tectonic zone, and that this discontinuous dislocation created a disjunctive reverse-overthrust body in the Pechenga structure. It is pointed out, that in the Luchompol' fault and immediate vicinity, the regional schistosic and the metamorphosed sedimentary and volcanic rocks contain anomalously high concentrations of argon and helium, evidently introduced by the fluids.

#### EVOLUTION AND VERTICAL ZONALITY IN MINERALIZATION

Core studies from SG-3 yielded data on the vertical zonality in mineralization in the deep zones of the crust for the first time and established that this zonality was developed in stages. This single section shows all the mineralization processes, related to sedimentation, volcanism, intrusive magmatism, and hydrothermal activity.

Evidence in the Drillhole SG-3 elicits the assumption that the formation of copper-nickel ore deposits in the Pechenga complex was connected with the protoactivation of Early Precambrian crustal structures. The process reached its maximum in the Middle Proterozoic when stabilized continental crustal blocks were broken by large faults.

Based on the data from Drillhole SG-3 it can be assumed that metamorphism took place under a geothermal gradient of 50°- 70° /km. Ultrabasites and copper-nickel ores were metamorphosed under greenschist facies conditions ( $T = 350 - 450^\circ\text{C}$ ,  $P = 0.2 - 0.3 \text{ gPa}$ ).

The types of ore mineralization exposed in SG-3 agree well with the Archean and Early Proterozoic history in the Pechenga region. The Kola Series comprises intensively metamorphosed ferruginous quartzites, iron-titanium ores, copper-nickel mineralization; and the Pechenga Complex includes less metamorphosed pyrite mineralization and copper-nickel deposits. However, this structural scheme clearly compliates the development of low-temperature hydrothermal mineralization which was encountered for the first time in the lower parts of the Pechenga Complex, and subsequently down to 11 km. Although the scale is small, it nonetheless modifies one's notion of the formation of ore-bearing fractured structures. The great stability of the mineral associations in the zones of regressive dislocation metamorphism, low temperature formation of sulfides, and the results of isotopic analyses of sulfur indicate a subcrustal origin for the juvenile hydrothermal fluids.

#### EVOLUTION OF THE EARTH'S CRUST IN THE PRECAMBRIAN

A description of the deep structure and chemical composition of the Precambrian continental crust is one of the fundamental problems of contemporary geology. Any sound solution to this problem should be able to specify the primary evolution in the composition of the ancient complexes from the protocrust to the present continental crust, identify the developmental mechanism, establish the specific fluid regime and P-T conditions for metamorphism in the Archean and Proterozoic, and as a consequence, determine the origins and trends of ore-forming systems.

The fundamental basis for assuming the basaltic composition of the protocrust in the past has been Geoffrey's two-layer model; however, recent interpretations based on deep seismic soundings of the Canadian and Anabar shields, the Eastern European platform and others, disputes the two-layer model since the Conrad surface, the surface that separates the "granite" from the "basaltic" layer, is not present everywhere under the continents.

The Conrad surface was also not detected in the section of Drillhole SG-3, and further seismic data shows that where the "granite" layer is expected, basic metamorphic rocks occur; and conversely, where the "basaltic" layer should be expected, a migmatite-plagiogneiss complex occurs, which to date extends down to 11.6 km.

Data from SG-3 and other deep drillholes into the crystalline basement rocks of the Eastern European Russian platform have for the first time established a factual basis for addressing these problems. A seismic model,

based on these data of the ancient platform crust and the results of studies in the Eastern European Russian platform are presented in Fig. I-85.

Comparisons of SG-3 and other deep drillholes into the basement rocks of the Eastern European Platform elicited a single geologic-geochemical scheme for the structure of the continental crust comprising three layers: granite-gneiss (0-15 km), granulite-gneiss (15-30 km), and a very deep layer (protocrust) (30-40 km). The extrapolation of geochemical trends down to a depth of 35 km suggests that the protocrust was formed from rocks close to sodic dacite in composition.

Well SG-3

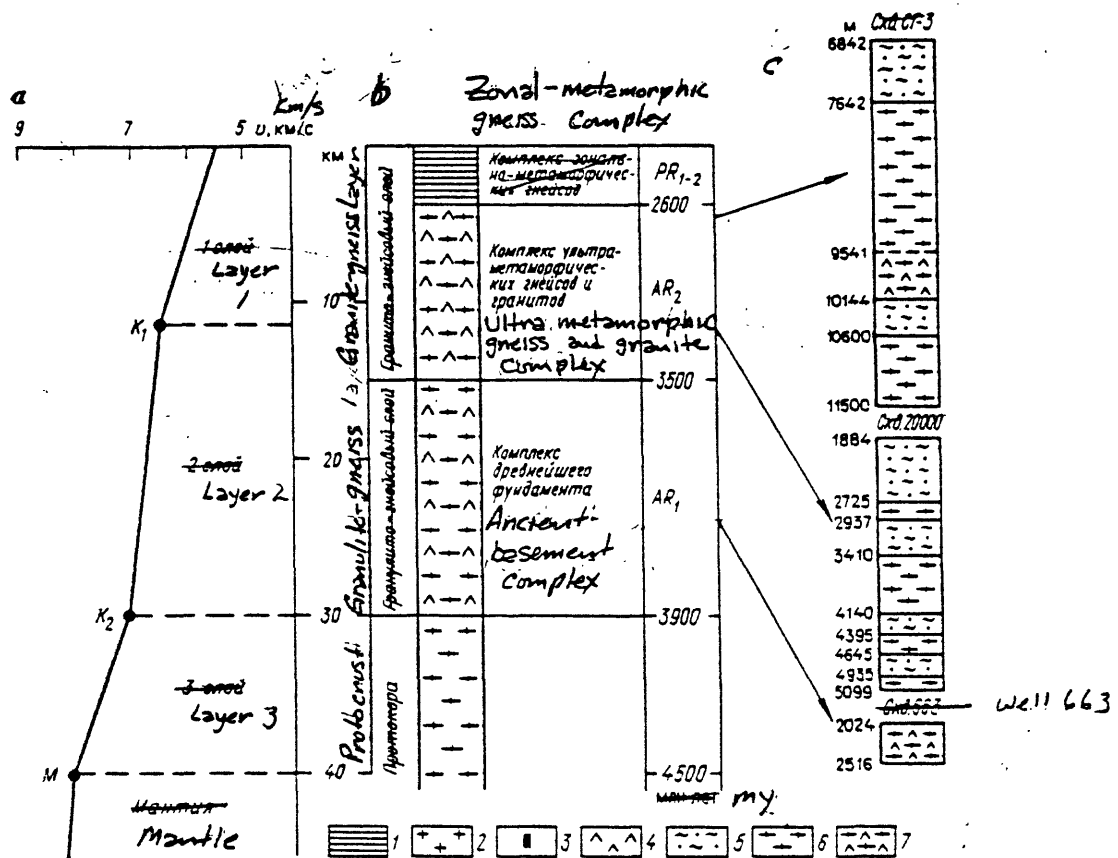


Figure 1.85. Seismic model of the ancient platform crust (a), after [77], and hypothetical (b) and studied (c) deep sections of the Eastern European Platform: 1 - volcanic and volcanogenic-sedimentary metamorphic rocks, 2 - granites, 3 - metaultrabasic and talc-actinolite schists, 4 - amphibolites and two-pyroxene basic crystalline schists, 5 - biotite plagioclase schists, 6 - plagiogneiss and enderbites, 7 - biotite-amphibole plagiogneiss and hypersthene diorite-gneiss.

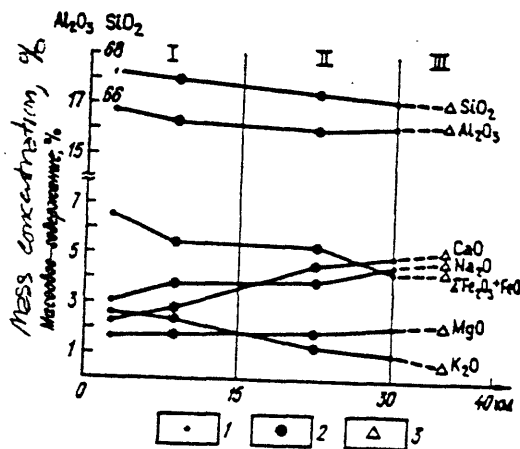


Figure 1.86. Variation in chemical composition of the enderbite-plagiogneiss complexes in a section of continental crust:

1 - average composition of metamorphosed complex, 2 - average composition of the granite - and granulite-gneiss layers,  
 3 - extrapolated average composition of the proto-crust  
 (I - granite gneiss, II - granulite gneiss, III - proto-crust).

## GEOPHYSICS

Geological-technical conditions of geophysical investigations of the drill hole. The diversity of rock types and great length of the hole are important factors in the quality of the geophysical data obtained by the in-hole measurements. In the interval of occurrence of volcanic-sedimentary rocks (2,005-5,000 m), conditions were favorable for such logs; below this, however, particularly in the Archean gneisses and schists, conditions deteriorated. The presence of cavities [caverns in the Russian] to depths of 7,000 m contributed to the complex configuration of the cross section of the hole.

Geophysical programs for study of the drill hole. Emphasis was placed on study of the lithology and composition of the rocks and determination of their physical-chemical parameters and stress state. The various missions and corresponding geophysical logging programs are listed in Table II.1.

Table II.1

Mission	Geophysical Logging program
Subdivision of the section into members and groups of rocks.	Acoustical (AL), laterolog (LL), spectrometric - gamma (SGL), gamma (GL), neutron (NNL-T, NNL-N, NGL), impulse neutron-neutron (INNL), magnetic (ML).
Lithologic-composition study	
Detection of zones of copper-nickel mineralization	Electrical potential (EPM) and gliding contacts (MSC) methods, spectrometric neutron-gamma (SNG).
Determination of interval and formation velocities of elastic waves and attenuation parameters.	AL.
Determination of interval and formation values of electrical characteristics of rocks	Laterolog (LL).
Determination of density rocks	Gamma-gamma (GGD-L).
Determination of effective atomic number of rocks	Selective gamma-gamma (SGGL).
Determination of average life time of thermal neutrons	INNL
Determination of component geo-magnetic field and magnetic susceptibility of rocks; attitude of magnetic complexes	ML

Determination of thermal properties      Thermal logging (TL).  
of rocks

Estimation of values of axial,      AL, GGD-L, LL.  
radial and tangential stresses in  
rocks; subdivision of the mass into  
zones of different direction;  
detection of fracture zones

Formulation of geophysical, geo-      AL, NGL, GL, SGL, ML, LL, GGDL, TL,  
thermal, and geochemical models  
of the section      vertical seismic profiling (VSP),  
gas logging (Gas L).

---

During the first stage of drilling where temperatures were comparatively low, and where hydrostatic pressure was low and did not require a heavy drilling mud, domestic production-line logging apparatus was used. See figure II.1.

The geophysical methods used in the second stage are shown in figure II-2.

Procedure of geophysical investigations. Special procedures had to be used for the in-hole measurements.

1. Depth determinations. At a depth of 11 km the variation in the length of the cable may be 19-20 m. Marker horizons were determined on the logs of each kind, and these were then used as standards for depth( $d$ ).

2. Acoustical log. Measurements have been made to a depth of 11,500 m recording longitudinal and transverse waves. The logs are poor for bottomhole readings, due probably to drilling mud absorbing the signal. When the hole is deepened, the signal for this same interval is better, provided no large cavities are present.

3. Gamma log. A Cs-137 standard was used to calibrate to instrument. Stability of the apparatus was checked by repeat measurements in an andesite porphyry in the 4673-4784 m depth interval.

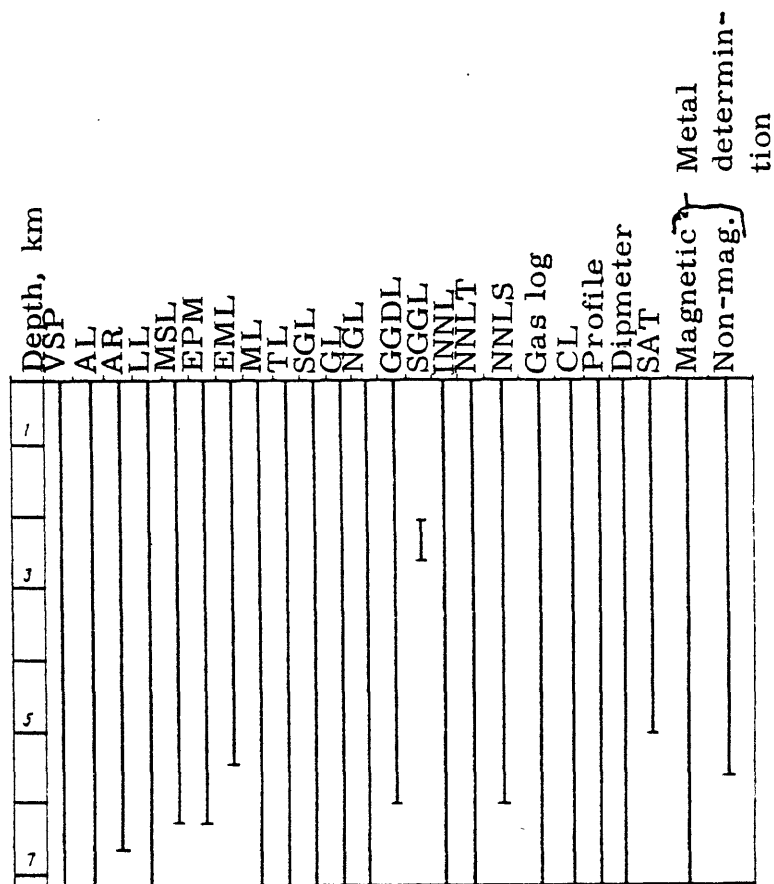


Figure II.1. Geophysical methods used in the first stage.

VSP - vertical seismic profiling, AL - acoustical log, AR - apparent resistivity, LL - laterolog, MSC - method of sliding contacts, EPM - electrical potential method, EML - electromagnetic logging, ML - microlog, TL - thermal log, SGL - spectrometric gamma log, GL - gamma log, NGL - neutron-gamma log, GGDL - gamma-gamma density log, SGGL - selective gamma-gamma log, INNL - impulse neutron-neutron log, NNL-T - neutron-neutron log of thermal neutrons, NNL-S - neutron-neutron log of super-thermal neutrons, Gas L - gas log, CL - caliper log, Profile - profile meter, Dipm - dipmeter, Metal determination: mag-magnetic, non-mag - nonmagnetic.

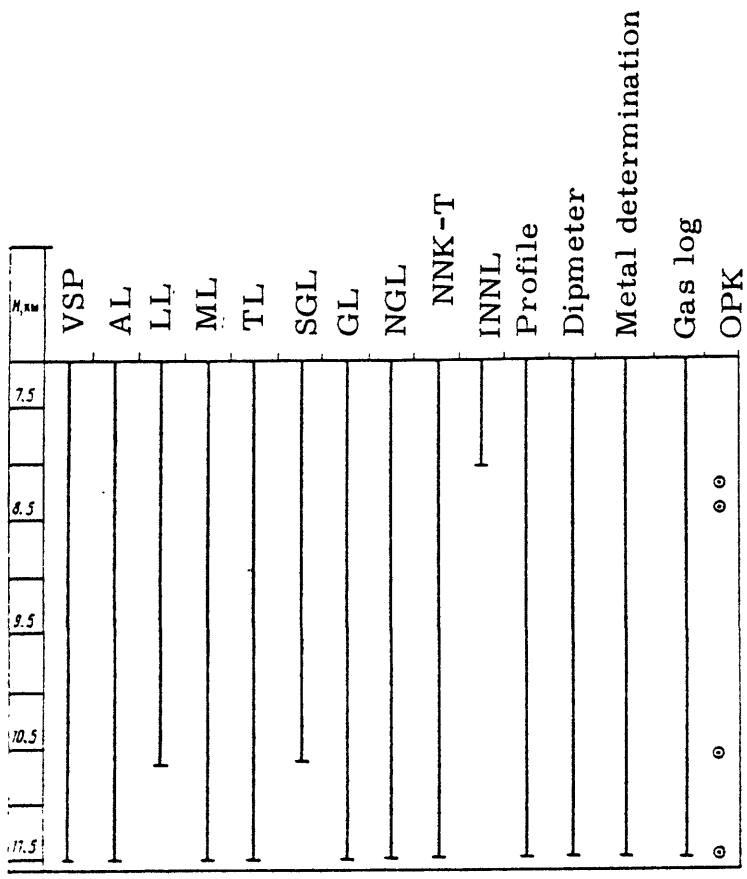


Figure II.2. Geophysical methods used in second stage.

See figure II.1 for abbreviations.

4. Spectrometric gamma log. This log was made at intervals of 100-500 m. It measures K-40, RaC', and ThC' in the rocks.
5. Gamma-gamma density log. A two-probe modification (15 and 35 cm probes) was used to depths of 6,000 m. Below this the column contains abundant cavities, and this method was not used.
6. Selective gamma-gamma log. Used to a depth of 3,000 m, this technique measures the effective atomic number of rocks in ore zones.
7. Neutron-gamma log. This log was run to a dept of 11,440 m. Cavities have a strong effect on the readings; there is a sharp drop in intensity of secondary radiation where cavity diameter is greater than 40 cm.
8. Neutron-neutron log. A pair of probes (30-50 and 40-60 cm) were used for measurements to 11,510 m to study the lithology of the section.
9. Magnetic log. Vertical and horizontal components of the magnetic field and magnetic susceptibility were measured to a depth of 11,500 m.
10. Electrical methods. Various electrical measurements were made to a depth of 10,644 m. The method of sliding contacts (MSC) and the electrical potential method (EPM) were used in the 0-6,000 m interval. These picked up conducting zones including copper-nickel sulfide mineralization. Laterolog was used on farther down the hole.
11. Thermal log (TL). Measurements were made while the thermometer was being lowered and when being raised in the hole. The scale was at 0.25 and 0.5°C/cm. Logs were run to a depth of 11,503 m.
12. Vertical seismic profiling (VSP). A continuous log was made to 11,514 m.

## Prospects and Tasks for Improving Geophysical Logging of Super-deep Holes

Experience gained in logging to 11,514 m is a basis for predicting conditions at greater depths both in SD-3 and other super-deep holes to depths of 15,000 m. Difficulties in logging are related to the high temperatures and pressures. Linear extrapolation of the geothermal gradient ( $0.019^{\circ}\text{C}/\text{m}$ ) gives a temperature of  $266^{\circ}\text{C}$  at a depth of 15,000 m in the Kola hole.

The main thrusts of further logging research are:

1. Increasing the capacity to operate at high temperatures and pressures and extending the life of the in-hole equipment.
2. Improving "without-cable" information systems - independent instruments on the drill stem.
3. Development of multi-strand load-carrying cable.
4. Development of powerful equipment for going in and out of the hole.
5. Development of an optimum system for in- and out-of-hole operations.
6. Development of a system of control of logging parameters.

### Density and Permeability-Porosity Properties of Rocks

Density of the rocks was determined from cores (more than 40,000 measurements), from gamma-gamma density logging, and by in-hole gravimetry. Error does not exceed  $0.01 \text{ g/cm}^3$ . Permeability and porosity were determined only on cores. Error is not greater than 0.1 percent. See Table II.4.

### Acoustical Properties of the Rocks

Acoustical measurements were made on cores as well as by logging. The following parameters were measured on cores: velocity of longitudinal waves along the axis of the core and perpendicular to this axis; maximum, intermediate, and minimum velocity in samples with natural moisture (dry) and the same on water-saturated samples; velocity of transverse waves along the axis of the core and perpendicular to this axis; the coefficient  $K_a$  and the factor A, which are functions of anisotropy of the rock; Youngs Modulus; and Poissant's Ratio.

Results of acoustical measurements on cores. More than 30,000 determinations of longitudinal wave velocity were made and 10,000 of

Table II.4

Rock	Density	Open porosity (%)	Permeability mkm.
Proterozoic 0-4,500 m			
Diabase, gabbro, pyroxene porphyry	3.0	0.40	0.031
Meta-volcanics	2.90	0.45	0.044
Proterozoic, 4,500-6,835 m			
Meta-diabase, meta-andesite	2.89	0.60	0.291
Volcanic-sedimentary (slates)	2.78	0.55	1.252
Archean, 6,835-10,500 m			
Gneisses	2.69	1.19	16,905
Amphibolite	2.93	--	--
Ultra-metamorphosed rocks	2.98	--	--

transverse wave velocity. For the Proterozoic sediments (to a depth of 6,842 m), the average longitudinal wave velocity with natural moisture is 5,670 m/s; for water-saturated - 6,080 m/s. The average value of longitudinal wave velocity for the Archean rocks (6,842 to 11,000 m) is 3,990 m/s.

The idea that velocity for rocks of the same composition increases with depth is not confirmed. Maximum values of velocity are found in the upper part of the section.

On a basis of elastic properties, the section is divided into three parts. The first is to a depth of 4,500 m where the interface corresponds generally with the boundary between the greenschist and epidote-amphibolite metamorphic facies. The principal importance of this boundary is that the primary composition of rocks below it is preserved. The second interface at a depth of 6,842 m is not as pronounced as for other logs. For the main types of rocks, there is a great similarity in velocity values obtained by acoustical logging and by measurements on cores.

#### In-Hole Seismic Investigations

Travel time curves were made of first arrivals and phases of P-waves and travel time curves of phases of S-waves. Vertical seismic profiling data can distinguish strata with thicknesses of 200 to 1,000 m. Average velocity of P-waves is 6,500 m/s and of S-waves, 3,600 m/s. Digital methods were used for more detailed study of the section.

The wave picture of the Kola hole differs qualitatively and quantitatively from that of vertical seismic profiling in platform regions with a thick sedimentary cover. Steeply dipping unconformable interfaces and the large number of faults contribute to complicated seismic conditions. See Fig. II.6.

#### Electrical Properties of the Rocks

Electrical resistivity was measured in the hole by logging ( $\rho$ ) and also on core samples ( $\rho_K$ ). Maximum values were found for diabases, spherulitic lavas, and sandstones, and minimum for silstones and phyllites of the Pechenga Series. Values of  $\rho$  and  $\rho_K$  differ from one another by 1-2 orders. For example, for meta-diabase and spherulitic basalt at depth of 3,200 to 3,600 m,  $\rho_K$  is  $5 \times 10^4$  ohm-m, whereas  $\rho$  is  $4.5 \times 10^5$  to  $5.6 \times 10^6$  ohm-m.

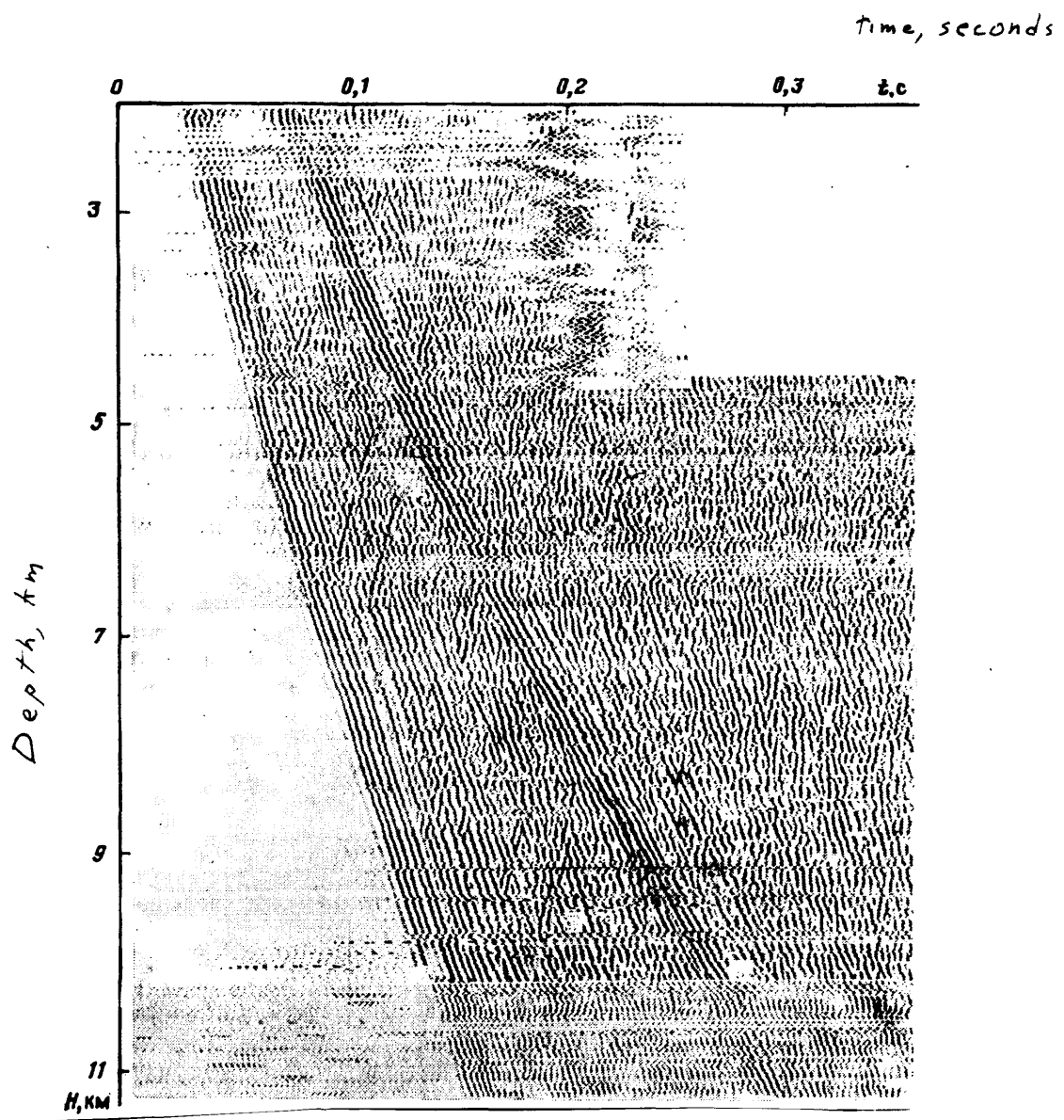


Figure II.6. Wave field of Kola hole.

The predominate frequencies of P- and S- waves vary little with depth and time, indicating low attenuation of waves.

### MAGNETIC PROPERTIES OF THE ROCKS

The magnetic characteristics reflect the concentration and composition of ferromagnetic minerals, their structural stage and relationship to paramagnetic iron-bearing minerals.

The magnetic properties of the rocks of the section of hole SD-3 were determined both under natural conditions and on core samples. In the hole, the components of the total magnetic field vector  $H$  and the magnetic susceptibility  $k$  were measured. On the core, the following magnetic characteristics were studied: magnetic susceptibility  $k$  and anisotropy  $A_k$ ; value and direction of natural remanent magnetization  $J_n$ ; the Koenigsberg factor  $Q = J_n / 0.5 \cdot k$ ; saturation magnetization  $J_s$ , remanent saturation magnetization  $J_{rs}$ ; disturbing field  $H'_{cs}$  of remanent saturation magnetization; and the parameter  $N_t$  (see section on "Results of magnetic-mineralogic analysis of the rocks").

These characteristics were determined on an astatic magnetometer MA-21 and ROK generator ION-1, thermomagnetometer and vibromagnetometer. The procedures of measurement of the magnetic characteristics of the core and processing of the data obtained are sufficiently elucidated in the literature.

The results of study of the magnetic properties of the core recovered from hole SD-3 are given in table II.11.

The most representative material on the core (more than 35,000 determinations) was obtained for magnetic susceptibility, natural remanent magnetization and the Koenigsberg ratio.

### MAGNETIC SUSCEPTIBILITY

This is one of the most important magnetic characteristics of rocks, reflecting their ability to be magnetized in a constant magnetic field  $H$ . The differences in  $k$  through the section in hole SD-3 were rather considerable.

The results of computer processing of the data on the petrophysical intervals showed that 80% of them have a significant difference in  $k$ , with a probability of 95 to 99.9% (limits on both sides), the latter predominating.

In the Proterozoic Pechenga Complex the maximum average values of  $k$  are observed in the meta-trachybasalt schists of the Pirttijärvi formation (4884-5619 m) --  $65 \cdot 10^{-3}$  SI units, and also in the serpentized peridotites of the Zhdanov formation (1541-1678 m) --  $124 \cdot 10^{-3}$  SI units. Relatively high values of  $k$  are typical of the talcized and serpentized picrite

TABLE II.11

## MAGNETIC CHARACTERISTICS OF THE ROCKS IN THE SECTION OF HOLE SD-3

Type of rock	Group of rocks	$\kappa \cdot 10^5$ SI units	$\varrho$	$J_n \cdot 10^5$ , A/m
Proterozoic, depth interval 0-4586 m, zone of sulfide mineralization				
Igneous, tuffs	Diabases	88	3.05	231
	Gabbro-diabases	105	4.1	153
	Ultramafics	6160	2.23	10,612
	Basic tuffs	151	1.79	278
Mean weighted value		561/94*	3.13/3.2*	1017/218*
Tuffogenic-sedimentary	Tuffogenic	108	1.94	50
	Terrigenous, chemogenic	129	7.21	825
Mean weighted value		125	6.05	6.54
Proterozoic, depth interval 4586-5642 m, zone of oxide mineralization				
Igneous, tuffs	Meta-diabase schists	4760	1.2	1,440
	Andesite porphyrites	66	4.1	243
	Ultramafics, tuffs	7067	1.5	7,639
Mean weighted value		4542	1.4	1,507
Sedimentary	Terrigenous, chemogenic	86	1.02	88
Proterozoic, depth interval 5642-6842 m, zone of mixed mineralization				
Igneous	Meta-diabase schists	43	0.4	23
	andesite porphyrites	56	0.2	7
	Ultramafics	45	0.4	22
Mean weighted value				
Archean, depth interval 6842-10,500 m, zone of mixed mineralization				
Gneisses		20	2.0	22
Amphibolites		70	9.1	680
Ultrametamorphics		40	1.4	39
Mean weighted value		46	2.5	70

\*In numerator -- values calculated for all rocks including ultramafic;  
in denominator -- values calculated without ultramafics.

porphyrites of the Materta [Matertinsk] formation,  $(19-38).10^{-3}$  SI units, and the andesite-dacite metaporphyrites of the Luchlompol' formation,  $5.10^{-3}$  SI units. The magnetic susceptibility of all these rocks is ferromagnetic. The value of  $k$  in the metavolcanics of tholeiite-basalt and andesite-basalt petrochemical type varies within narrow limits regardless of the extent of metamorphism (from  $0.5.10^{03}$  to  $1.0.10^{-3}$  SI units) and is ferroparamagnetic. Minimum values of  $k$  are characteristic of the dolomites and metapsammites of the Luchlompol' and Kuvernerinjok formations. Thus the magnetic anomalies in the Pechenga Complex are related either to the ultramafic formations, metamorphosed in greenschist and prehnite-pumpellyite facies, or to metavolcanics of alkalic petrochemical type regardless of the extent of their metamorphism.

The magnetic susceptibility of the Archean complex in the section of hole SD-3 as a whole is lower than in the Proterozoic complex and than the Archean rocks which crop out in the drilling area (fig. II.16). The iron-silicate rocks have maximum values of  $k = (0.6-1.0).10^{-3}$  SI units. The ferromagnetic nature of  $k$  is also typical of the epidote-biotite-amphibole gneisses, schists and amphibolites, migmatized by plagio-microcline granites, for which  $x = (4.6-9.6).10^{-3}$  SI units. These formations as a whole are subordinate and tend to be in the lower part of the section (interval 9541-11,000 m). The background value of magnetic susceptibility is determined by the shadow migmatites and amphibolites [nebulites -?]. In the shadow migmatites,  $k$  increases downhole from  $0.09.10^{-3}$  to  $0.54.10^{-3}$  SI units, and in the amphibolites it varies from  $0.53.10^{-3}$  to  $1.57.10^{-3}$  SI units, the maximum values and greatest spread of  $k$  being observed in the old pre-migmatite amphibolites. In contrast to the dike metadiabasic amphibolites, they are characterized by a log-normal distribution of  $k$ . The great scatter of  $k$  values in these rocks indicates that the magnetite mineralization is superimposed, evidently related to granitization.

From the results of petromagnetic investigations of the Archean rocks to the northeast of the Pechenga structure it was established that in this region there is a systematic relationship between  $k$  and the extent of preservation of the granulite mineral parageneses. High  $k$  are typical of enderbites and charnockites, which in essence are shadow migmatites of the granulite facies. During diaphthoresis of the epidote-amphibolite and amphibolite facies, the magnetite in these rocks disappears or its content is sharply reduced to values typical of similar rocks in the section of hole SD-3, in which the

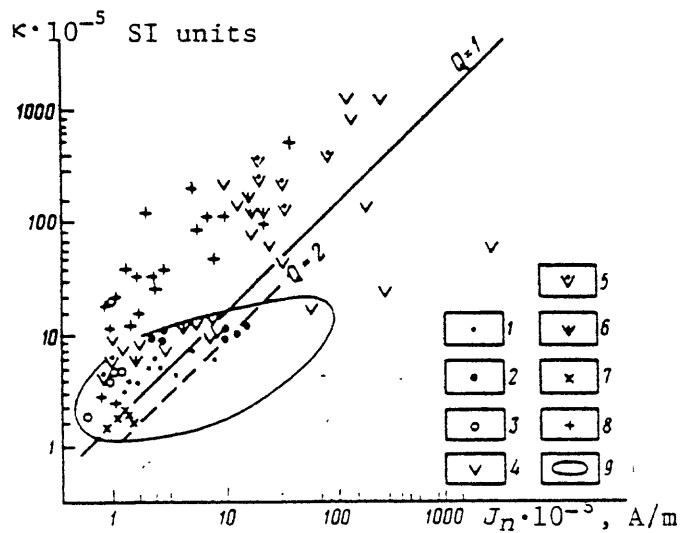


**Fig. III.16.** Magnetic susceptibility of the main Archean rock types in the section of hole SD-3 and of the drilling area as a function of natural remanent magnetization.

On the surface: 1 - biotite gneisses with garnet, 2 - high-alumina gneisses, 3 - biotite gneisses with epidote, 4 - crystalline schists and amphibolites, 5-7 - rocks of granitization series I -- diorites, tonalites, plagiogranites, diaphthorized to various degrees, 8 - rocks of granitization series II, plagiomicrocline granites-granodiorites.

In the hole: 9 - figurative field of rocks of the section in hole SD-3 in the 7-10 km interval (80% of measurements yield  $Q < 2$ ).

maximum extent of appearance of Lower Proterozoic metamorphism-diaphthoresis is recorded for the Archean formations.

If the values of  $k$  measured on core samples are compared with those obtained by borehole magnetometry, it is established that they practically coincide, i.e. the suggestions of some investigators that pressure has a substantial effect on  $k$  is not supported by the results of the investigations in hole SD-3. Thus the conditions of occurrence of the rocks (at least in the upper part of the earth's crust) do not affect  $k$ ; therefore, it is correct to measure it at atmospheric conditions on core samples and to use those values as the true values.

According to the data of statistical treatment of a large number of measurements of magnetic susceptibility, two regularities in its distribution in the section are ascertained (see Table II.11):

-- down-hole from the Proterozoic rocks to the Archean gneisses,  $k_{av}$  decreases systematically from  $10^{-3}$  to  $10^{-4}$  SI units, except for the peridotites of the Zhdanov formation (sedimentary sequence IV,  $k > 10^{-2}$ ) and the magnetite-rich zone of the Pirttijärvi formation (volcanogenic sequence II,  $k > 10^{-3}$ );

-- with depth, the difference between average values of magnetic susceptibility of the igneous and sedimentary rocks evens out. In sequence IV (Zhdanov and Materta formations) it still happens, but beginning with sequence III (Zapolyarna and Luchlompol' formations) and below, the average values of  $k$  in these rocks already are no different ( $k_{av} = 8 \cdot 10^{-5}$  SI units), except for the magnetite zone in volcanic sequence II.

Both regularities are in agreement with the increasing extent of metamorphism with depth -- from prehnite-pumpellyite and greenschist facies to epidote-amphibolite. The process of deep metamorphism on the one hand is usually accompanied by destruction of the magnetic minerals, and on the other by chemical equalization of the composition of the rocks.

The results of comparison of the average values of  $k$  for the petrophysical intervals distinguished indicates the informativeness of  $k$  for lithologic subdivision of the section. The Student t-criterion was used as the statistical criterion of the difference.

The anisotropy of magnetic susceptibility and remanent saturation magnetization  $J_{rs}$  of the rocks varies greatly ( $k_{max/min}$  up to 2.9,  $J_{rsmax}/J_{rsmin}$  up to 2.4), reaching a maximum in the schistose parts of the section of the magnetite zone of the Pechenga Complex and especially in the

Archean gneisses. The great scatter of values of anisotropy is explained in part by the random sampling of the orientation of recovered samples with respect to the directions existing in the earth's crust. The following regularities were ascertained relative to anisotropy: 1) a general increase in anisotropy downward; 2) the anisotropy within a sequence is higher in the sedimentary than in the igneous rocks (igneous rocks 1.05, sedimentary 1.21). Evidently this is related to the greater schistosity of the sedimentary rocks compared to the igneous. This difference levels off with depth, which is consistent with the increase in extent of metamorphism.

Thus, the magnetic anisotropy is paragenetically related to the elastic anisotropy of the rocks -- it increases with depth and extent of regional metamorphism.

#### NATURAL REMANENT MAGNETIZATION $-J_n$

As a result of the fact that the core of hole SD-3 was not azimuthally oriented, it is impossible to analyze in detail the behavior of the total vector  $J_n$ ; only the values of its absolute value value  $J_n$  and the angle between the vector  $J_n$  and the horizontal plane, I, was considered (inclination of the vector  $J_n$ ).

The value  $J_n$  has a lognormal distribution even in the most uniform petromagnetic groups of rocks and depends primarily on the magnetite content and superposed pyrrhotite mineralization of metamorphic origin.

The maximum value of  $J_n$ ,  $21,610 \cdot 10^{-3}$  A/m, was recorded in the serpentized peridotites of the Pechenga Complex, which are rich in magnetite and pyrrhotite.

In the Archean rocks penetrated by the hole,  $J_n$  as a whole is lower than in the Proterozoic formations, but the contribution of remanent magnetization to the total is often much greater than in the rocks of the same type in the Archean complex northeast of the Pechenga structure at the surface, which again is related to the pyrrhotite mineralization typical of most of the section of hole SD-3.

Normal polarity of the  $J_n$  vector predominates in the section of hole SD-3. The average values of inclination I for rocks with relatively high Q (carrying pyrrhotite mineralization) are clustered in the  $30\text{--}50^\circ$  range (fig. II.17). With a decrease in Q the inclination is shifted toward larger angles, i.e. it approaches the inclination of the present geomagnetic field (on the order of  $80^\circ$ ). Thus the less stable rocks were partially or wholly

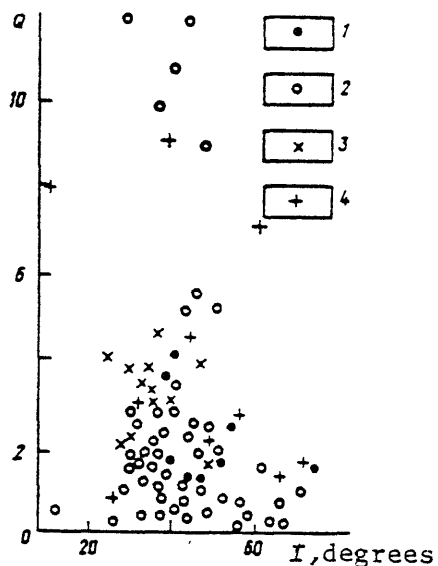


Fig. II.17. Relationship between average values (for the formations) of the suites of inclination of the vector of natural magnetization and the Koenigsberg ratio for the suites: formations:

1 - Materta, Zapolyarnaya; 2 - Zhdanov, Luchlompol' and Pirttijärva, 3 - Kuvernerninjok, Majärva, 4 - Archean formations.

remagnetized under the influence of the present geomagnetic field. Such unstable rocks are most common in the first volcanogenic sequence (Materta suite). The stability of the average inclinations of  $J_n$  of rocks with a high Q throughout the section and their difference from the inclination of the present field and similarity to the inclination of inversely magnetized rocks indicates that such rocks retain ancient remanent magnetization.

As the scatter of values of inclination is not large, it can be presumed that the age of the remanent magnetization  $J_n$  is approximately the same throughout the section.

#### THE KOENIGSBERG RATIO Q

The Q factor is the ratio of natural remanent magnetization to induced, and is very important for interpreting magnetic anomalies. In the section of hole SD-3 it varies from 0.1 to 29 and correlates with the composition of the magnetic minerals: in the zone of pyrrhotite mineralization, high Q are observed, and in the magnetite zone Q is less than 1.5. It should be mentioned that in the sedimentary rocks of the pyrrhotite zone,  $Q_{av}$  as a rule is higher than in igneous rocks, due to the prevalence in the former of magnetically harder material -- antiferromagnetic pyrrhotite. The relatively high  $Q_{av}$  for such ancient rocks indicate that the  $J_n$  is thermoremanent or chemoremanent.

Normal polarity of the  $J_n$  vector predominates in the section. The total thickness of inversely magnetized rocks is about 10%.

According to the data of borehole magnetometry, the zones of pyrrhotite and magnetite mineralization are different. The zones of sulfide mineralization (pyrrhotite) are marked by serrated, sharply angular magnetic anomalies (up to  $5.10^3$  nTl), the anomalies of the horizontal component considerably exceeding those of the vertical (about 1.5 times greater). According to the data of borehole magnetometry, the Q factor is up to 40 units.

The zone of oxide (magnetite) mineralization is marked by more intensive and less angular magnetic field anomalies (up to  $10-20 10^3$  nTl), which correlate very clearly (fig. II.18) with intensive magnetic susceptibility anomalies (up to  $500.10^{-3}$  SI units). The relative contribution of remanent magnetization to the total in this zone is much less than for the zone of sulfide mineralization, the q values in this zone are on the order of 0.1-1.

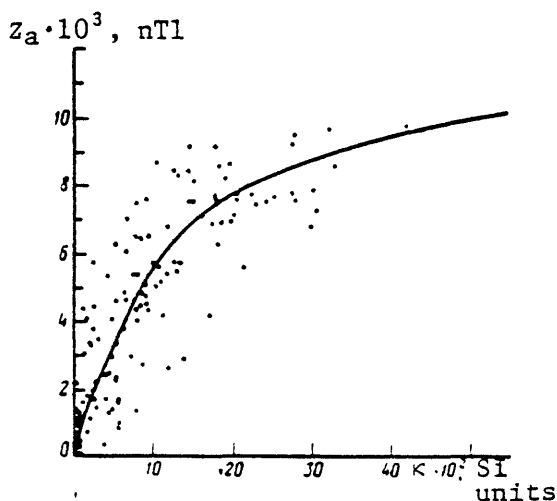


Fig. III.18. Correlation of the vertical component of the magnetic field  $Z_a$  and magnetic susceptibility  $\kappa$  for zones of magnetite mineralization, according to data of borehole magnetometry.

T A B L E II.12  
RESULTS OF INTERPRETATION OF MAGNETIC  
LOGGING DATA

Interval, m	Dip of Azimuth	
	layers of dip	degrees
4600—4616	35	200
4880—5640	65	150
5717—5720	35	150
7628—7633	70	130
9640—9655	50	170

The angles and azimuths of the dip of the magnetic layers are given in table II.12 on the basis of data interpreted from the magnetic logging readings.

The data of table II.12 indicate angular and azimuthal unconformities in the attitude of the zones of magnetite mineralization. The sharp discontinuities manifested in the density, elastic and other properties of the rocks are also observed in the magnetic characteristics.

Results of magnetic-mineralogical analysis of the rocks. The saturation magnetization, determined by the composition and content of ferromagnetic minerals in the rocks, varies widely -- from 0.05 to 15.9 A.m<sup>2</sup>/kg, even in the case of the same rock types and a small sample volume. This suggests an extremely uneven distribution of ferromagnetic minerals, which can only mean superposed mineralization. Low values of  $J_s$  0.2 A.m<sub>2</sub>/kg prevail in volume, especially in the lower part of the section. This fact, together with the data of thermomagnetic analysis -- with the hyperbolic shape of the  $J_s(T)$  curve -- is a sign of low concentration of ferromagnetic minerals and large contribution of paramagnetic iron minerals to the magnetic effect.

According to thermomagnetic analysis and study of the coercivity spectra it is established that two kinds of pyrrhotite are present in the rocks studied: ferromagnetic (monoclinic) and antiferromagnetic (hexagonal) type.

In the thick magnetite zone of sequence II, where pyrrhotite is practically absent, the magnetite concentration varies from 0.5 to 17%, judging from the value of  $J_s$ . The Curie points vary from 580° to more than 600°C. This is related to the monophase oxidation of magnetite and formation of cation-deficient magnetite, which is confirmed by data of X-ray phase analysis. Beneath the magnetite zone, in the Archean rocks at a depth of 7.2-10.5 km, magnetite is present everywhere along with pyrrhotite (according to thermomagnetic analysis,  $T_C = 580^{\circ}\text{--}620^{\circ}\text{C}$ ).

Against a background of general increase in temperature downward from sequence IV to II, from greenstone to amphibolite metamorphism, zones of low-temperature magnetization are observed in the lower part of sequences III, I and the Archean. The observed inhomogeneity probably suggests repeated pyrrhotite mineralization (or recrystallization), in particular low-temperature.

On the basis of these criteria, it is easy to distinguish superposed processes involving the lower part of the gabbro body (depth 1282-1421 m) and the peridotite bodies (550-570 m and 1540-1670 m) and the country rocks

adjacent to them. The oldest generation I of pyrrhotite mineralization is distinguished at depths of 500 m or more (gabbro to 1282 m). The later generation II was superimposed on the lower part of the gabbro (depth more than 1321 m) and underlying country rocks. Variations in the magnetic properties of pyrrhotite as the peridotite body is approached indicate that this body (1540-1670 m) is younger than generation II and correspondingly younger than the gabbro. The pyrrhotite mineralization involving the lower part of that peridotite body and the country rocks adjacent to it is the next generation, III. The pyrrhotite occurring in the peridotite body at a depth of 550 m and in the rocks enclosing it should be assigned to it. Pyrrhotite generation IV is distinguished in the country rocks above the contact with the gabbro body situated at a depth of 1987 m. Toward the contact of this body the magnetic properties of the pyrrhotite do not vary. The exceptionally narrow and intensive  $\lambda$ -peaks of those pyrrhotites suggest that this is the best preserved and possibly youngest mineralization.

From the results of study of the magnetic characteristics of the rocks in the borehole, determined on core samples and from logging data, the following conclusions can be drawn:

- 1) large scatter of  $k$  and  $J_n$  values is found in a small volume of rock, which indicates the superposed character of the mineralization;
- 2) the difference between mean values of  $k$  and  $J_n$  of the sedimentary and igneous rocks evens out with depth; beginning with sequence III, Proterozoic, the average  $k$  values for these rocks are the same;
- 3) the peridotites of sequence IV and the volcanics of Proterozoic sequence II, where high magnetite concentrations are observed, stand out sharply.
- 4) the section is divided into three zones on the basis of magnetic characteristics: depth interval 0-4586 corresponds to the zone of sulfide mineralization. The rocks of this zone are mainly weakly magnetic, the average values of magnetic susceptibility do not exceed  $4.10^{-3}$  SI units, except for intervals of ultramafic rocks. The existence of an intensive magnetic field in the zone is related to remanent magnetization of pyrrhotite and magnetite. The main magnetic mineral of this zone is pyrrhotite, except in the ultramafics, in which magnetite is present in large amount;  
-- depth interval 4586-5642 m corresponds to the zone of oxide mineralization and is characterized by higher magnetic susceptibility of the rocks, up to 0.2-0.3 SI units; magnetite, cation-deficient magnetite, and hematite are present;

-- depth interval 5642-10,500 m is a zone of development of weakly magnetic rocks. The magnetic susceptibility values reach  $(2-4) \cdot 10^{-3}$  only in isolated places; small concentrations of pyrrhotite and magnetite are observed;

5) The average inclination of the  $J_n$  vector with relatively high Q, considerably different from the inclination of the present geomagnetic field, and also the variations in magnetic polarity of the rocks (regardless of their composition and magnetic mineralization) indicates the ancient origin of the natural remanent magnetization. About 20 zones of different geomagnetic polarity are recorded in the section. The average inclination of the  $J_n$  vector of the rocks studied is similar throughout the section and does not correlate with the magnetic anisotropy; thus the age of magnetization of the rocks containing pyrrhotite and magnetite is similar;

6) on the basis of several magnetic properties, several types of magnetic mineralization are distinguished, differing in conditions and time of formation: a) disseminated pyrrhotite mineralization in the sedimentary rocks of sequences III and IV; b) disseminated pyrrhotite mineralization in the mafic igneous rocks of sequences III and IV; c) "ore" pyrrhotite mineralization, later than the first two, confined mainly to the endocontact of a peridotite body and fractures in the sedimentary rocks of sequences IV and III; d) disseminated pyrrhotite mineralization in sequences I and II and the Archean gneisses, evidently relatively the latest (low-temperature); e) mineralization produced by enrichment in magnetite during serpentinization of the peridotites of sequence IV, close in time to the "ore" pyrrhotite mineralization; f) hematite-magnetite mineralization of sequence II, the relative position of which in time is not clear; evidently it occurred before pyrrhotite mineralization of sequences I and II and the Archean rocks; judging from the temperature of magnetization of magnetite (above 500°C), it was produced earlier or at the same time as the amphibolite facies metamorphism;

7) crystallization, transformation and magnetization of the pyrrhotite and magnetite are closely related to the metamorphism of the rocks.

#### RADIOACTIVITY OF THE ROCKS

##### NATURAL RADIOACTIVITY

The natural radioactivity of the rocks of the section in the hole was studied both on core and in the hole. On core, the content of natural radioactive elements (NRE) -- uranium, thorium and potassium -- was

determined. For this purpose the following methods were used: laboratory gamma spectrometry; scintillation gamma-spectrometry; instrumental neutron activation analysis for uranium and thorium; X-ray spectral and X-ray fluorescence analyses; delayed neutron. The average contents of NRE were determined for the rock types ascertained in the petrochemical investigations.

In the hole, the radioactivity of the rocks was determined by gamma logging both in the integral (GL) and spectrometric (SGL) versions.

#### Proterozoic

The rocks of this part of the section fall into four groups on the basis of natural radioactivity.

In the first group there are rocks characterized by very low total natural radioactivity (less than the average clarke contents). On the basis of the GL interval readings, the rocks in this group have a natural radioactivity (intensity of Y radiation  $I_{GL}$ ) averaging  $(7.9-15.8) \cdot 10^{14}$  A/kg. The second group includes rocks in which the total radioactivity (from GL) averages  $(14.3-32.3) \cdot 10^{14}$  A/kg; the third group includes rocks with a natural radioactivity of  $(40.8-79.5) \cdot 10^{14}$  A/kg. The fourth group is characterized by maximally high readings for the middle Proterozoic --  $(79.6-133.4) \cdot 10^{14}$  A/kg (from GL).

The rocks of groups I and IV can be unambiguously distinguished by gamma logging. Radioactivity values of  $(14.3-79.6) \cdot 10^{14}$  A/kg (groups II, III) are typical of rocks of different composition and origin, in connection with which the parameter in question is not informative for subdividing the rocks of those groups.

The possibilities of using natural radioactivity as a parameter for recognizing the rocks of the Middle Proterozoic are greatly increased if gamma logging data are examined together with the contents of the individual NRE in the rocks in specific parts of the section. For this purpose, it is most feasible to determine the natural radioactivity by formations.

In the Materita formation, mainly magnetic rocks of basic composition are developed. The spread of GL readings (including SGL) for them is small. However, the character of the curve is different for individual rocks. For the gabbro diabases uniform GL readings throughout their thickness is typical. In the basalts and diabases, which also are considerably thick, the readings in individual parts of the section increase to  $(14.3-21.5) \cdot 10^{14}$  A/kg, which apparently may be related to the inclusion of small intercalations

of tuffogenic sedimentary rocks in the diabases.

In the GL readings, tuffs of basic composition, picrite and pyroxene porphyrites are hardly different from the diabases and gabbros. but the contacts between these rocks are rather clearly established from GL data.

A high information content of natural radioactivity in subdividing the section is typical of the Zhdanov formation.

In this formation, a group of mafic and ultramafic rocks (group "a") is unambiguously distinguished, in comparison with which the rest of the rocks of the formation differ essentially in radioactivity values.

To ascertain the ultramafics, other methods should be used, including determinations on core and mud. Gamma spectrometric data (SGL) in combination with the readings of other methods provide additional material for distinguishing zones of considerable alteration (serpentine-talc-chlorite-tremolite rocks) in the ultramafics, in which the content of uranium and thorium is higher.

Separation of the sedimentary rocks (group "d") is extremely difficult because of the macro- and microinterbedding of sedimentary formations of different grain size. However, varieties with a prevalence of phyllites are distinguished from essentially siltstone varieties by higher contents of thorium and potassium.

In the Zapolyarna formation, volcanogenic-sedimentary rocks (group "b") which occur among diabases and tuffs of basic composition (group "a") are distinguished on the basis of gamma logging data. The latter can be distinguished on the basis of SGL readings: higher contents of thorium and uranium are typical of the tuffs.

The rocks of the Luchlompol' formation are similar in content of radioactive elements and are the most highly radioactive of the Proterozoic formations. The integral readings of gamma activity of these rocks also are very similar to each other, but on the basis of SGL data these rocks can be clearly divided on the basis of the higher contents of uranium and thorium and relatively low potassium in the andesite-dacite porphyrites compared to the arkosic sandstones.

Subdivision of the rocks of the Pirttijärvi formation can be done on the basis of the total radioactivity values, based on gamma logging data.

The sedimentary-metamorphic formations of the Kuvernerin formation are divided into originally chemogenic-sedimentary and chemogenic with an admixture of clastic-sedimentary material on the basis of gamma logging.

The rocks of the Maärva formation, the most metamorphosed of all the Proterozoic formations, are distinguished from unmetamorphosed rocks of the same composition on the basis of radioactivity values.

#### NUCLEAR-PHYSICAL PARAMETERS

The nuclear-physical characteristics of the rocks in the section of SD-3 were determined *in situ* by the methods of GGL-S [selective gamma-gamma logging], PNNL [pulsed neutron-neutron logging] with thermal and epithermal neutrons.

For conducting borehole investigations of crystalline rocks at considerable depths in the section of SD-3, examples of PNNL and GGL-S apparatus were developed, built and modernized on the basis of standard IGN-4 and DRST-2 instruments.

For the first time ever, measurements were made by a dual-probe PNNL apparatus (probe length 40 and 90 cm) at depths to 8000 m at high temperature ( $T = 140^{\circ}\text{C}$ ) and high pressure ( $p = 100 \text{ MPa}$ ) simultaneously at three time lags (800, 1000, 1300 microsec) and in an interval regime on each probe. Data were obtained on the average life time of thermal neutrons.

The nuclear-physical parameters of the crystalline rocks were determined from the results of chemical analysis of cores.

On the basis of integrated investigations, conclusions were drawn concerning the relationship of  $\tau$  values and effective atomic number of the rock  $Z_{\text{ef}}$  to their mineralogical composition, and a procedure was developed for interpreting the PNNL and GGL-S data.

Fig. II.19 shows  $Z_{\text{ef}}$  as a function of the total content of iron and calcium (Fe+Ca) in the Archean crystalline rocks in SD-3 (at depths greater than 6842 m), and fig. II.20 shows the dependence of the parameter of the macrosection of thermal neutron capture  $Z'c$  to the total content of iron and boron in the rocks -- Fe+B (in equivalent % of Fe content). According to the data of calculations of  $Z_{\text{ef}}$  and  $Z'c$  the Proterozoic and Archean rocks in SD-3 fall into three groups (table II.13), taking into account silicic content and the inverse relationship between the silicon and iron contents (fig. II.21).

The first group includes diabases, gabbro-diabases, essexite gabbros; actinolitized and amphibolized diabases and gabbro diabases; porphyroblastic, plagioclase-amphibole, and magnetite-biotite-plagioclase-amphibole schists and rocks; pyroxene porphyrites, pyroxene metaporphyrites, serpentinized

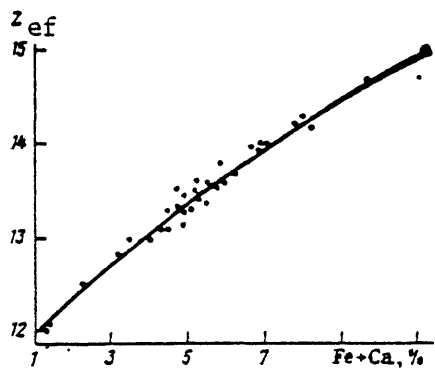


Fig. III.19. Effective atomic number  $Z_{\text{eff}}$  as a function of total content of iron and calcium in the rocks (%Fe).

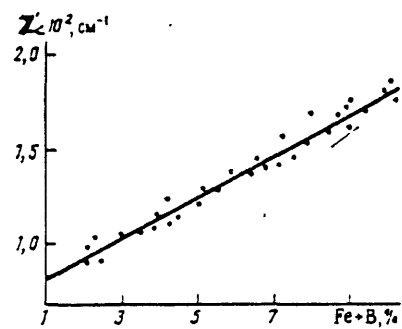


Fig. III.20. Dependence of the parameter of macrocross-section of thermal neutron capture  $Z_c'$  on total content of iron and boron in the rocks  $\text{Fe} + \text{B}$  (%Fe).

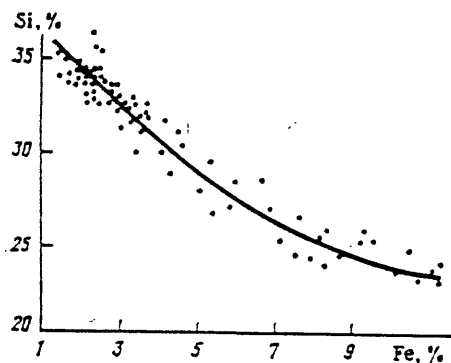


Fig. III.21. Relationship between mass contents of iron and silicon in crystalline rocks.

T A B L E . II.13  
NUCLEAR-NEUTRON PARAMETERS AS A FUNCTION OF ROCK COMPOSITION

Rock group	Rocks	$Z_{\text{eff}}$	$\tau, \mu\text{sec}$
1	Mafic, ultramafic	15-17	110-260
2	Intermediate	13,5-15	260-380
3	Acid	12-14	380-500

peridotites, serpentine-chlorite-talc rocks; amphibolites, plagioclase-amphibole, and magnetite-biotite-amphibole-plagioclase rocks and schists.

The second group consists of rocks of intermediate silicic content, quartz-plagioclase schists with amphibolite, biotite-ampbibole-plagioclase schists and gneisses, leucocratic and melanocratic, with high-alumina material, actinolite-talc rocks, and oligoclasites.

The third group includes andesite-dacite porphyrites, potassic and sodic granites and granite gneisses.

The statistical distribution of the  $z_{ef}$  and  $\tau$  parameters by rock group are also given in fig. II.22. The experimental values of the parameters  $z_{ef}$  and  $\tau$  are defined in the form of continuous histograms down the section of SD-3 using selective gamma-gamma (GGL-S) and pulsed neutron-neutron logging (PNNL).

Thus study of the natural radioactivity and nuclear-physical properties of the rocks on core from SD-3 and logging data made it possible to: establish the content of natural radioactive elements (NRE) for certain types of rock in the hole and enhance the detail of subdivision of the section; distinguish zones of high NRE content related to secondary alteration of the rocks, in particular to granitization; ascertain the regularity of an increase in natural radioactivity with increasing depth; and use data on nuclear-physical properties to determine the petrographic composition of the rocks in the section.

#### THERMAL PROPERTIES OF THE ROCKS

Study of the thermal properties on core samples in the drilling area was necessary to obtain reliable data on the thermal field in the area, and also to predict deep temperatures on the basis of the thermal conductivity equation, where the parameters of thermal conductivity determine the rate of the process of heat transfer to the surface.

Several methods were used to measure the thermal properties of the rocks -- heat conductivity [W/(m.K)], temperature conductivity  $k$  ( $m^2/s$ ) and heat capacity  $C$  [J/(kg.K)]: 1) flat instantaneous source -- to measure  $K, C, k$ ; 2) comparative on plates 40 mm in diameter and 6-10 mm thick; this method was used to measure small samples or when  $\tau$  values were high; 3) dividing rod [bar?] -- in measurements on small samples (plates 21.5 mm in diameter, 3-6 mm thick); 4) noncontact determination of heat conductivity using a moving

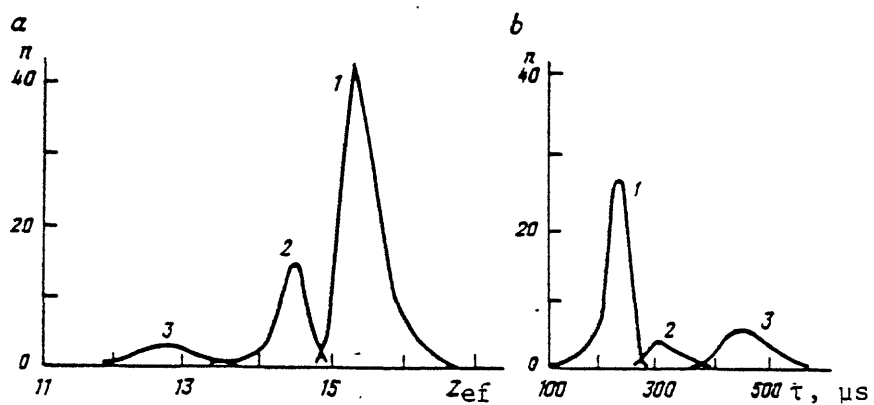


Fig. II.22. Statistical distribution of the parameter  $Z_{ef}$  (a) and  $\tau$  (b) in rock groups 1-3 (corresponding to table II.24).

point source; 5) thermal comparator with two-point probing of surface of sample.

The last four methods are used only to measure the heat conductivity coefficient. On the basis of control measurement (more than 40) made on the same core samples, it was established that the comparability of results of measurement of  $\lambda$  in the 1.5-4.5 W/(m.K) interval for methods 1-4 lies within 3-15%.

For rocks of the Pechenga Complex the thermal properties were measured by methods 1-4 on core samples of all the main rock types, collected to a depth of 6842 m. Core samples in an air-dry state were used. To a depth of 1700 m the samples were taken not only from the super-deep, but also from other holes. The heat conductivity values are given in fig. II.23.

From table II.14 it is seen that the maximum values of heat conductivity for igneous rocks [ $\lambda = 4.27-5.23$  W/(m.K)] were obtained for the andesite porphyrites (group VI) and schists of various compositions (group VII), which can be explained by the high content of minerals with high heat conductivity in the samples: up to 50% chlorite [ $\lambda = 5.2$  W/(m.K)] or carbonate [ $\lambda = 3.6-5.8$  W/(m.K)] in schists and up to 60% quartz [ $\lambda = 7.7$  W/(m.K)] in andesite porphyrites with low (up to 10-20%) content of albite [ $\lambda = 1.9-2.3$  W/(m.K)]. The minimal values are characteristic of amphibolites collected from a depth of more than 5 km [group III,  $\lambda_{av} = 1.38$  W/(m.K)\*] and serpentinized ultramafic rocks of the Zhdanov formation [group IV,  $\lambda_{av} = 1.84$  W/(m.K)].

For core samples of group II ( $H = 2805-4500$  m) the extremes of variation and average values of heat conductivity [ $\lambda_{av} = 3.8$  W/(m.K)] are somewhat higher than for samples of slightly altered rocks taken from lesser depths [ $\lambda = 2.7$  W/(m.K)]. The differences in values obtained in measurements along the axis and perpendicular to it do not exceed 4%. Below 4500 m lies the boundary between the greenschist and amphibolite facies of metamorphism, and the massive rocks of the upper part of the section are succeeded by schistose. The heat conductivity of the metabasic rocks below this boundary is sharply different from the heat conductivity of the rocks of basic composition in the upper part of the section. For the rocks of group III (more than 5000 m deep)  $\lambda$  is sharply lower [ $\lambda_{av} = 2.3$  W/(m.K)], and the values obtained in measurements along the core axis and perpendicular to it differ by 12% on the average. Such substantial reduction in heat conductivity [compared to  $\lambda_{av} = 3$  W/(m.K)] evidently is related not only to the mineralogic conversion of actinolite [ $\lambda = 3.8$  W/(m.K)] to hornblende [ $\lambda = 2.5$  W/(m.K)], but also to

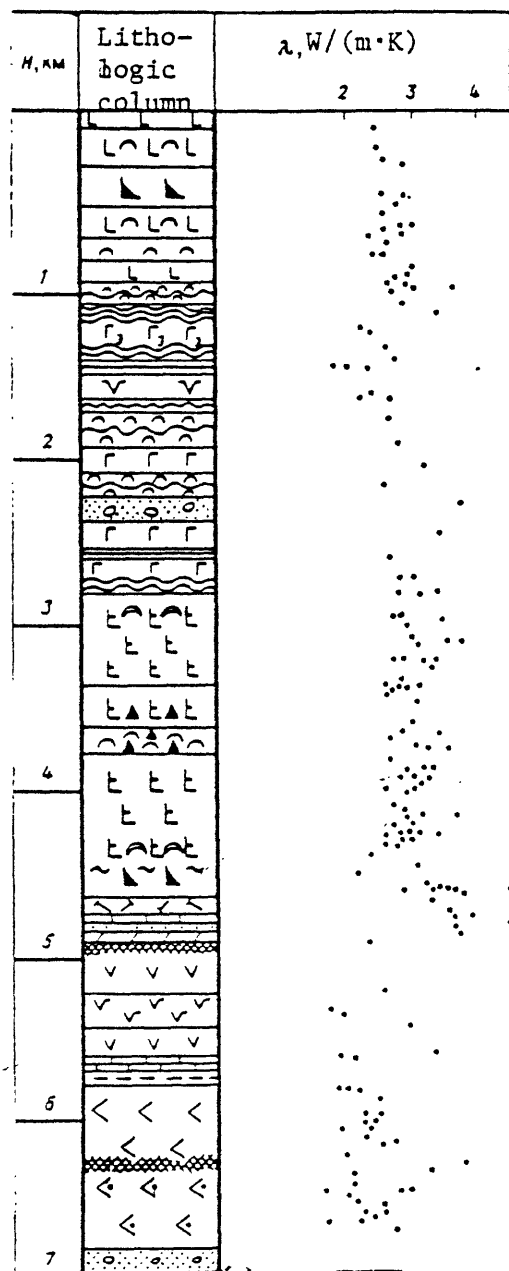


Fig. II.23. Heat conductivity in the Proterozoic section  
For symbols in lithologic column, see appendix at end of  
this chapter.

T A B L E      II.14

LIMITS OF VARIATION AND AVERAGE VALUES OF THE THERMAL PROPERTIES ( $K$ ,  $C$ ,  $\lambda$ ) AND DENSITY  $\sigma$  OF  
SAMPLES OF THE MAIN ROCK GROUPS OF THE PECHENGA COMPLEX

Rock	$\sigma$ , $\text{g/cm}^3$	$K$ , $\text{W/m/K}$	$C$ , $\text{J/gK}$	$\lambda$ , $\text{W/mK}$	No. of samples					
	Limits of variation	Average	Limits of variation	Average						
Gabbroids	2.65—3.12 2.80—3.27 2.92—3.13	3.00 3.01 3.03	0.88—1.43 0.83—1.43	1.09 1.07	630—880 630—1170 670—1090	800 840 840	10 41 24	2.22 2.22 4.22	3.01 3.18 3.68	2.70 2.70 3.00
Metagabbro-diorites								1.38 1.05	3.14 3.89	2.29 2.97
Amphibolites	2.85—3.13	2.92	0.98—1.24	1.09	670—1090	840	24	2.42 1.38 2.05	3.68 3.14 3.89	58 24 15
Serpentinized ultramafic rocks	2.84—3.10	2.93	0.84—1.18	1.03	670—920	800	5	1.84	3.00	2.55
Tuffs	2.80—3.07 2.69—3.05	2.92 2.78	1.01—1.41 1.52	1.15	670—920 840	840	5	2.55 3.26	2.93 4.27	2.74 3.50
Andesite porphyries										6
Schists	2.96—3.01 2.72—2.91 2.72—3.17	2.99 2.84 2.86	1.62 1.03—1.77 —	1.32	750—1000 —	920 —	4	3.0 10 44	5.23 3.66 2.13	6 6 48
Sedimentary and tuffogenic-sedimentary rocks										

textural and structural changes occurring during metamorphism, which corresponds to a change in elastic properties.

For the sedimentary rocks, the highest values of  $\lambda$  were obtained for quartz-mica, arkosic sandstones [ $\lambda = 3.8 \text{ W/(m.K)}$ ] and quartz-mica siltstones [ $\lambda = 3.2-3.5 \text{ W/(m.K)}$ ].

Thus the average values of heat conductivity of the rocks of the Proterozoic complex are  $2.3-3.9 \text{ W/(m.K)}$  (see table II.14). For the volcanogenic rocks of this complex, the correction for moisture<sup>x</sup> is negligible.

Considerable anisotropy of heat conductivity was ascertained (in dry and water-saturated rocks). The maximum values were recorded for profiles oriented perpendicular to the schistosity or linearity, and minimum with values parallel orientation. Heat conductivity anisotropy in gneisses and schists in general is in good agreement with the elastic anisotropy in the same rocks.

On the whole, the results of integrated study of the thermal properties of all rock types in the continuous section of SD-3, which penetrates the major structural-formational zones of the Baltic shield (Pechenga paleo-caldera of Proterozoic age and underlying Archean Kola complex), indicated a zonal distribution.

#### GEO THERMAL INVESTIGATIONS

##### HEAT FLOW AND ITS CHARACTERISTICS

The most important characteristics of the thermal field of the earth's crust are the geothermal gradient  $\gamma$  (GTG), heat conductivity  $\lambda$ , heat flow density (HD) in the near surface zone, and the distribution of sources of radiogenic heat A. The geothermal gradient is determined by measuring temperature after an equilibrium state of the thermal regime is established in the hole. In the case of horizontal beds and steady-state heat conductivity regime, heat flow is determined as the product of the GTG and thermal conductivity of the rocks,  $q = \gamma\lambda$ . Thus the dependability and reliability of heat flow calculation depend on the precision of determination of  $\gamma$  and  $\lambda$ . At present,  $\gamma$  is measured with a precision of about 5%, and  $\lambda$  of 7-10% (for an actual well section). The complexity of obtaining sufficiently precise values of  $\lambda$  is related to the fact that the measurements are not made in situ, but on core samples. In determining  $\lambda$ , the effect of water content of the rocks especially at depth, must be taken into account. At depths of 5-10 km a substantial part of the pores and fractures are closed. The real values of heat conductivity in low-porosity crystalline rocks at depth as a rule are higher than the values obtained under laboratory conditions.

Before drilling SD-3 in the Pechenga structure, 10 holes 470-1675 m deep were studied. The GTG in holes that had been standing for a year or more, heat conductivity of core samples  $\lambda$ , and heat flow density  $q$  were determined.

The values of  $q$  were determined by interval-by-interval averaging of the data on the gradient  $\gamma_{av}$  and heat conductivity  $\lambda_{av}$ . To a depth of 1000 m the average value  $q_{av}$  is  $(26 \pm 2) \text{ W.m}^{-2}$ , in the 1000-2800 m interval it is  $(36 \pm 4) \text{ W.m}^{-2}$ . At a depth of 5000 m the average value of  $q$  drops and falls within  $48-56 \text{ W.m}^{-2}$ . It should be noted that the decrease in  $q$  occurs only from a depth of 6800 m. Very low values of the flow in the upper part of the section (to a depth of about 1 km) can be explained by the effect of several factors: filtration, glaciation not long ago, and denudation.

#### RADIOGENIC HEAT IN THE THERMAL BALANCE OF THE EARTH'S CRUST AND UPPER MANTLE

The heat flow generated due to decay of radioactive elements (RE) in the earth's crust, and the heat flow arriving from the upper mantle, are determined on the basis of an accepted model of the structure and composition of the crust, and also the character of distribution of uranium, thorium and potassium in it. The distribution of the average contents of the RE by rock type and sequence in the section, and also radiogenic heat in the Proterozoic and Archean rocks, are of special interest.

Pechenga Complex. A total of 532 analyses for uranium, thorium and potassium contents were made for the rocks of the Pechenga Complex. The lower formations were sampled in less detail than the upper, in connection with the low core recovery beginning at a depth of 4600 m. However, all the main rock varieties were sampled, and in determining the average contents of RE by formation, the readings of the GL and GL-S geophysical methods were taken into account.

The Materta and Zapolyarna formations, which consist mainly of diabases and metabasic rocks, had the minimum contents of uranium, thorium and potassium, and the Zhdanov and Luchlompol' formations, the maximum. The high RE contents in the Luchlompol' formation are explained by the presence of a body of andesite porphyrite, characterized by a relatively high content of U, Th and K. Low RE contents in the Kuvernerinjok formation are caused by the rather extensive occurrence in it of low-radioactivity carbonate-tremolite schists.

When the average values of the RE in the volcanic flows are compared, a tendency is noted toward a decrease in their content downward from the Materta formation to the Zapolyarny: (to a depth of 4673 m). Below that an increase in

RE contents is recorded. The high contents of RE in the Pirttijärva formation are related to its complex composition: in addition to metabasites, intermediate and silicic effusives are extensively developed here (metaandesites and metaalbitophyres), characterized by high RE contents. In the Majärva formation, which consists mainly of basic effusives, the high RE contents are explained by superposition of processes of foliation, metamorphism and granitization.

Kola Complex. The Kola complex, Archean, was subdivided into sequences by co-workers of the KGRe and VSEGEI on the basis of lithologic criteria, taking into account superposed processes of polymetamorphism. The following features were taken into account in the subdivision: presence of rocks with high-alumina minerals; relative content of biotite-plagioclase gneisses and amphibolites; extent of granitization.

It was presumed that despite the intensive manifestation of superposed metamorphism, the primary details of the rocks are still partially preserved at least in their mineralogical composition. For instance, the presence in the rocks of high-alumina minerals (sillimanite, staurolite, andalusite) unambiguously indicates the original pelitic nature of the metasediments. Six sequences are distinguished on the basis of the features cited.

The average RE contents in the sequences depend to a considerable extent on the degree of granitization of the rocks and the quantitative relationship of granites and pegmatites, silicic and basic varieties.

#### HEAT GENERATION

From the vertical distribution of values of heat generation to a depth of 11,400 m (fig. II.24) it is seen that its character depends mainly on the particulars of lithologic composition of the Pechenga and Kola complexes. A maximum level of heat generation characterizes the tuffogenic-sedimentary rocks ( $1.0\text{-}2.5 \mu\text{W/ms}$ ) and essexite-bearing gabbro-diabases ( $0.7\text{-}1.7 \mu\text{W/ms}$ ), which are developed mainly in the upper part of the section of the series, to a depth of about 2.5 km. Below that, in the region of preferential development of intensively metamorphosed mafic volcanics (in greenschist and epidote-amphibolite facies) the heat generation value falls on the average to  $0.04\text{-}0.08 \mu\text{W/m}^3$ . An abrupt increase in heat generation in narrow intervals at a depth of 3700-4700 m is related to thin intercalations of tuffites and andesite porphyrites, respectively. The peak of heat generation at a depth of 4700 m may be caused (in addition to the lithologic factor) by the thick

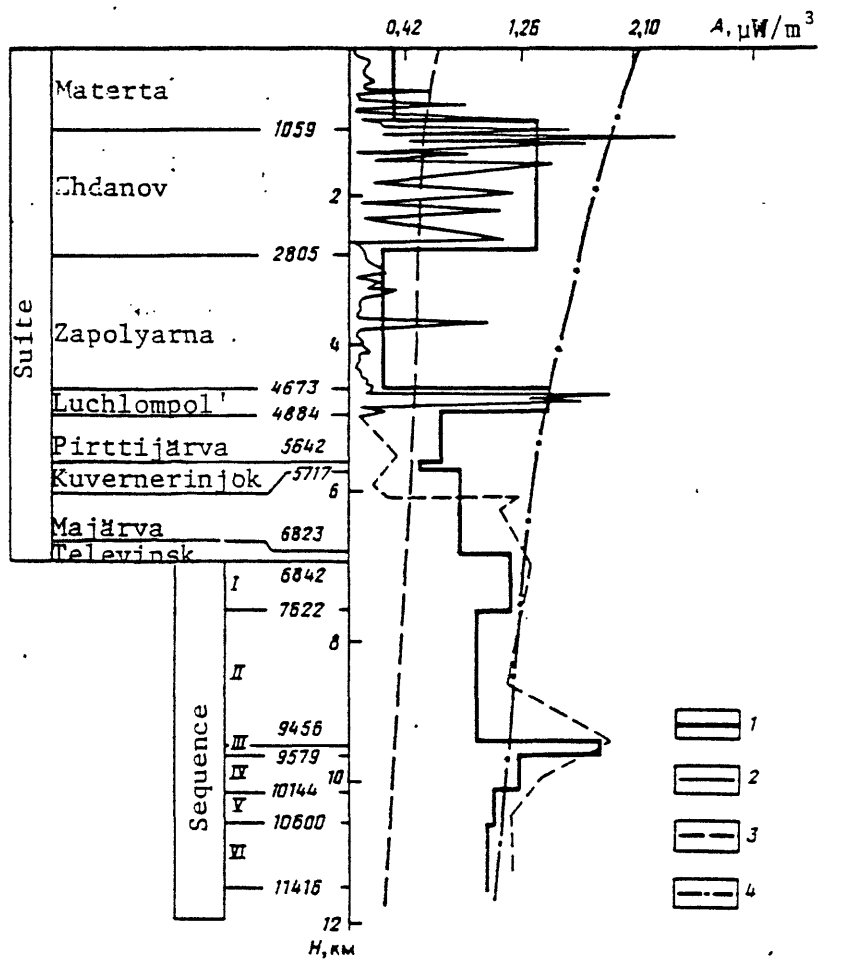


Fig. II.24. Variations in heat generation in the section of SD-3.

1 - heat generation by suites\* and sequences; 2 - variations in heat generation within suites: depth distribution of heat generation: 3 - Ukrainian shield, 4 - Sierra Nevada batholiths.

\* formation

highly permeable zone of the Luchlompol' fault, like the abrupt increase in heat generation at a depth of about 9500 m, where a highly permeable weak zone is recorded in which (on the basis of analysis of the contents of primary helium) it seems possible that elements have been brought in, including radioactive ones.

It is important to note that in the mafic volcanogenic rocks of the Pechenga complex, which are similar in chemical composition but metamorphosed to different extent, the RE contents vary widely (by more than an order of magnitude), which probably is caused by the particulars of the behavior of uranium in the course of progressive metamorphism. The value of heat generation of the volcanogenic sequences of the Pechenga complex is about 0.4, of the sedimentary about  $1.3 \mu\text{W}/\text{m}^3$ .

In the Archean Kola Complex the value of heat generation in the two-mica gneisses (amphibole-plagioclase) with high-alumina minerals is close to the value of that parameter in the sedimentary sequences ( $1.2-1.7 \mu\text{W}/\text{m}^3$ ); in the sequences of the more basic varieties of gneisses (amphibole-plagioclase) with intercalations of amphibolite it is appreciably lower and amounts to about  $0.8 \mu\text{W}/\text{m}^3$ . Thus as a result of the investigations, no systematic decrease in heat generation values with depth was found. The vertical distribution of heat generation is step-wise in character, determined mainly by the mineralogical composition of the rocks.

For comparison, average curves of the deep distribution of heat generation are given for the Precambrian Ukrainian shield and the Sierra Nevada batholiths, which are Mesozoic. The absolute values of heat generation for those regions fall in similar intervals (about  $0.2-2 \mu\text{W}/\text{m}^3$ ) calculated for the Kola hole. It should be noted that the vertical distribution of heat generation in lithologic varieties of the same type, (individually for metabasites and tuffogenic-sedimentary rocks of the Pechanga complex) is close to an exponential distribution law.

#### MODELS OF HEAT GENERATION

In correspondence with present ideas on the structure of the crust in the Pechenga region, it is advisable to consider two models of heat generation.

Model I. According to this model the lower boundary of the "granite-gneiss" layer of the crust runs at a depth of 12.5 km where, according to the data of vertical seismic profiling, there is a discontinuity in the crust which has not yet been unambiguously interpreted. On the one

hand, it may be a region of transition from amphibolite to granulite facies metamorphism, and on the other, it may reflect the lower boundary of distribution of the zone of granitization in the crust.

In this model, the Proterozoic sedimentary-volcanogenic Pechenga (developed to a depth of 6842 m) and Kola complexes can be attentively assigned to the "granite-gneiss" layer. The latter consists (according to the data of the drilling of the Kola hole to a depth of 11612 m) of rocks of varied composition (both silicic and basic). In the drilled part of the section, six sequences of different composition have been distinguished. A uniform lithologic composition of the section is presumed to the distinguished discontinuity (12.5 km). Below that boundary, to a depth of 40 km, there apparently is the "granulite-basite" layer, concerning the composition of which there are different opinions.

This model is based on the idea that this layer consists of metabasic rocks of different metamorphic facies (amphibolites, pyroxene granulites, eclogites). Depending on the proportions of "dry" granulite and water-bearing amphibolite facies in the composition of the layer, heat generation may vary from  $0.2$  to  $0.6 \mu\text{W}\cdot\text{m}^{-3}$ . An average value ( $0.4 \mu\text{W}\cdot\text{m}^{-3}$ ) was used in the model. The calculation of that model shows that the radiogenic heat sources in the crust generate a heat flow of  $23 \mu\text{W}\cdot\text{m}^{-2}$  (the rest of the flow comes from the mantle).

Model II. According to this model it is presumed that the section of the Kola Complex of gneisses, analogous to the section penetrated by the hole, continues to a depth of 15 km, below which (to a depth of 20 km) rocks corresponding in composition to the varieties constituting the Murmansk block are present (the so-called basement of the Kola Complex). This part of the section of the crust (to 20 km), tentatively including the Pechenga complex, is identified with the "granite-gneiss" layer. Below that, to a depth of 40 km, there is the "granulite-basite" layer. In this model (in contrast to model I), two sublayers are distinguished (in depth intervals of 20-30 and 30-40 km) within the "granulite-basite" layer, on the basis of DSS data. The contents of radioactive elements and heat generation in these sublayers are taken on the basis of the clarke values in the rocks of corresponding composition (respectively, gabbro-amphibolite for the upper sublayer and granulite-eclogite for the lower). The radiogenic component of heat flow in the crust calculated for this model differs slightly from the results obtained with model I, being  $26 \mu\text{W}\cdot\text{m}^{-2}$ , which is 45-55% of the total surface heat flow measured in SD-3 ( $49 \mu\text{W}/\text{m}^2$ ). 173

Thus the following are established on the basis of the results of the geothermal investigations.

1. The geothermal gradient increases with depth from 1-1.1°C/100 m in the upper part of the Pechenga complex to 1.7-2°C/100 m in the lower part (at a depth of 6000-7000 m). The variation in the GTG with depth evidently is related to variations in heat conductivity, heat generation and water content of the horizons.

2. In the Proterozoic section heat flow increases with depth in connection with an increase in the content of radioactive elements.

3. The vertical distribution of heat generation (according to the constructed model) varies step-wise with depth, which is caused by the lithology of the rocks.

4. The radiogenic component of heat flow in the crust is 45-55% of the total surface heat flow measured in SD-3.

#### PHYSICO-MECHANICAL PROPERTIES

The physico-mechanical properties of the rocks in the section of SD-3 were determined only on core and were used mainly to solve technological problems of drilling. The following characteristics were determined: static Young's modulus  $E_{st}$ ; static Poisson's ratio  $v_{st}$ ; compressive strength  $\sigma_{cp}$ ; tensile strength  $\sigma_t$ ; resistance to indentation (hardness)  $p_{in}$ ; plasticity  $K_{pl}$ ; and abrasivity  $z$ .

The determination of  $p_{in}$ ,  $K_{pl}$  and  $E_{in}$  (from indentation of die) was accomplished on YMGP-3 and UMGP-4 instruments according to GOST-12288-66. In addition,  $E_{in}$  and  $v_{in}$  were measured on these same instruments in a regime of quasi-uniaxial loading of a cubic sample, with measurement of the deformation over its whole length. Abrasivity  $z$  was determined by the procedure of wearing down the flat rock surface with a steel rod.

The strength characteristics of rocks most widely used are the critical strength under conditions of very simple loading schemes -- uniaxial compression and tension. These characteristics are obtained by splitting off a number of slices  $15 \times 30 \times 100$  mm and subsequently crushing samples (cubes about 15 mm on edge). For each sample at least 15 slices were made, from the results of which the tensile strength was calculated, and at least ten cubes were crushed to determine the compressive strength. The results of the individual determinations in each sample were treated statistically in accordance with the hypothesis of critical distribution [26].

It should be noted that according to the generally accepted procedures, determination of the strength of rocks specifies cutting slices at least 30 mm thick and crushing cubes 40 mm on edge. Inasmuch as it was not possible to use samples that size due to the poor core recovery in SD-3, the feasibility of extending the methods of slicing and crushing the cubes to small samples was checked. As a result of experiments on optically active materials, the predominant action of tensile stresses in splitting slices 10-15 mm thick with wedges was confirmed. Comparison of the results of determination of  $\sigma_{cp}$  for homogeneous pyroxenites showed that the values obtained on very small samples are comparable to those obtained on larger ones (fig. II.25).

The strength characteristics of the core of SD-3 are extremely variable inasmuch as they depend on a large number of decisive factors, including the mineralogical composition, structural-technical particulars of the rocks, fracturing (healed) and microfracturing.

The main factor governing the variations in strength characteristics of the upper part of the Pechenga Complex to a depth of 4500 m is the petrographic-mineralogic composition of the rocks. The critical compressive strength for the rocks of this part of the section varies from 114 MPa in the talcized picrites and peridotites to 219 MPa in the diabases (table II.15), the latter value being the maximum for the whole section in hole SD-3. The critical tensile strength varies from 22 MPa in thin-bedded metasedimentary rocks to 45 MPa in diabase. In the bedded sedimentary rocks, anisotropy of the strength properties is clearly manifested. For instance, in phyllites the tensile strength  $\sigma_t$  is 32 MPa measured perpendicular to the bedding and 40 MPa along the bedding.

In the lower part of the Pechenga Complex (to a depth of 6800 m) the average values of compressive strength  $\sigma_{cp}$ , 160 MPa, are not very different from the corresponding parameters in the upper part. The meta-leucodiabasic amphibole-plagioclase schists have  $\sigma_t = 15$  MPa under tension transverse to the schistosity and 24 MPa along it. Thus the strength of these rocks, which are the commonest in the 4900-6800 m depth interval, is 2-3 times less than in the diabases and metadiabases which constitute a large part of the upper Pechenga subcomplex. Anomalously low strength parameters characterize the chlorite and talc-chlorite metadiabasic and metapicritic schists, lying in the 4500-4673 m interval.

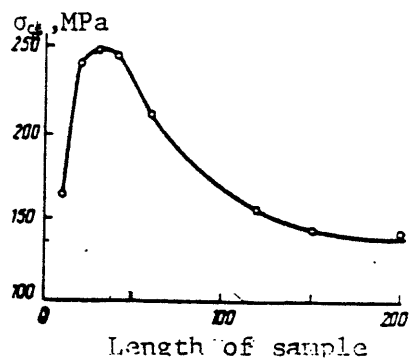


Fig. II.25. Compressive strength of rocks as a function of length of sample.

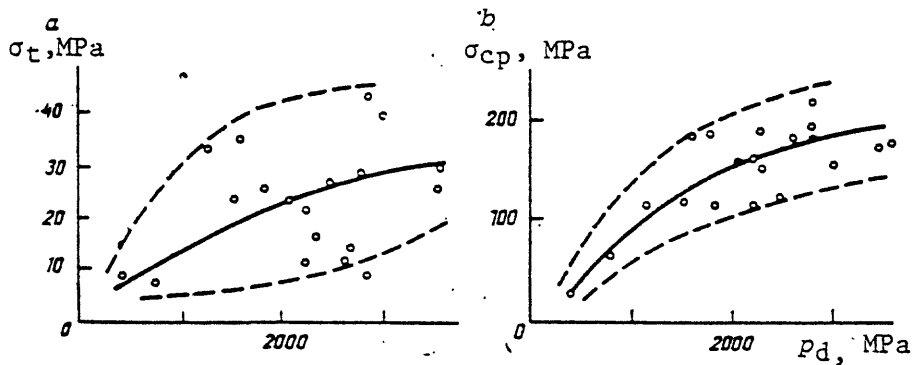


Fig. II.26. Correlation between strength of rocks and hardness to indentation: a - tension, b - compression. Dashed lines designate confidence intervals.

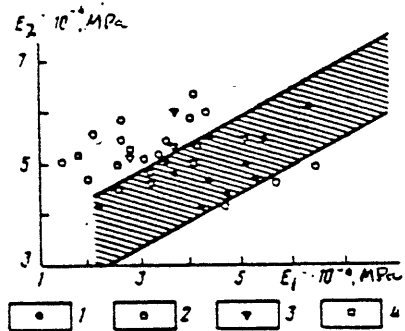


Fig. II.27. Correlation between elasticity modulus upon indentation  $E_{1in}$  and modulus of deformation under uniaxial compression  $E_{2in}$

T A B L E II.17

ABRASIVITY OF ROCKS PENETRATED BY SD-3

Rock	Class	Abrasivity characteristics
Phyllites	I	Below average
Chlorite-sericite and talcized rocks	II	" "
Porphyrites, peridotites, diabases, gabbro-diabases, sandstones, gneisses	IV	Average
Tuff, granites, crystalline schists	V	Above average

TABLE II.15

AVERAGE VALUES OF THE PHYSICO-MECHANICAL PROPERTIES OF THE MAIN ROCK TYPES  
OF THE SECTION IN SD-3

Rock	$\sigma$	$v_p$	$v_s$	$K_a^*$	$E_{dyn} \cdot 10^{-4}$		$\tau_c$	MPa	$\tau_p$	$\rho$	$K_{pl}$
	g/cm <sup>3</sup>	km/s	km/s		MPa		MPa	MPa	MPa		
Pechenga Complex											
Materita suite* (0-1059 m)											
Diabases	3.02 (1987)	6.80 (63)	3.66 (60)	1.02 (63)	10.4 (61)	0.27 (61)	45 (7)	45 (7)	219 (7)	27.8 (24)	2.3 (24)
Tuffs	2.92 (582)	6.48 (34)	3.50 (31)	1.05 (34)	9.1 (31)	0.28 (31)	41 (5)	41 (5)	153 (5)	29.6 (6)	2.7 (6)
Komatiites	3.03 (359)	6.28 (23)	3.23 (23)	1.04 (23)	8.8 (23)	0.29 (23)	26 (4)	26 (4)	114 (4)	17.3 (6)	2.0 (6)
Zhdanov suite† (1059-2805 m)											
Phyllites, siltstones	2.90 (1457)	6.03 (54)	3.41 (50)	1.06 (54)	8.0 (49)	0.20 (49)	32 (7)	40 (7)	183 (7)	15.7 (16)	2.3 (16)
Interbedded sandstones, siltstones, phyllites	2.84 (1297)	5.91 (48)	3.59 (42)	1.10 (48)	8.8 (44)	0.20 (44)	22 (10)	26 (10)	122 (10)	14.9 (31)	2.0 (31)
Tuffs, tuffites	2.88 (325)	6.20 (18)	3.48 (17)	1.08 (18)	8.7 (17)	0.27 (17)	32 (4)	36 (4)	116 (4)	11.9 (4)	2.4 (4)
Amphibolitized and chlori- tized gabbro-diabases	2.98 (1948)	6.24 (52)	3.56 (50)	1.03 (52)	9.3 (50)	0.24 (50)	29 (8)	30 (8)	179 (8)	27.7 (20)	2.0 (20)
Essexite gabbro- diabases	2.84 (552)	5.92 (15)	3.32 (13)	1.02 (15)	8.1 (13)	0.27 (13)	28 (4)	28 (4)	175 (4)	35 (3)	2.0 (3)
Serpentinized peridotites	2.88 (627)	6.29 (17)	3.49 (15)	1.02 (17)	9.0 (15)	0.27 (15)	30 (5)	36 (5)	190 (5)	17.7 (8)	2.3 (8)
Zapolyarna suite* (2805-4673 m)											
Metadiabases, green schists	3.02 (5630)	6.58 (214)	3.76 (216)	1.04 (214)	10.6 (216)	0.23 (216)	30 (35)	31 (35)	175 (35)	35.3 (112)	1.6 (112)
meta-picritic talc-chlorite schists with hematite	2.93 (192)	5.46 (8)	3.35 (6)	1.35 (8)	8.2 (6)	0.22 (6)	6 (1)	10 (1)	29 (1)	3.8 (11)	2.1 (11)
Tremolitized dolomites											
Tuffs, tuffites	2.88 (130)	6.18 (4)	3.66 (3)	1.14 (4)	9.6 (4)	0.24 (3)	10 (3)	46 (1)	126 (1)	24.4 (4)	1.7 (4)
Luchlompol' suite† (4673-4884 m)											
Dolomite and sandy dolomite	2.77 (55)	5.25 (2)	3.41 (1)	1.08 (2)	6.6 (1)	0.05 (1)	— (—)	— (—)	— (—)	13.4 (1)	1.4 (1)
Arkosic sandstones	2.78 (214)	5.22 (11)	3.20 (10)	1.12 (11)	6.6 (9)	0.15 (9)	22 (1)	22 (1)	161 (1)	21.8 (10)	1.8 (10)
Andesite-dacite metaporphyrites	2.75 (259)	5.47 (9)	3.39 (9)	1.11 (9)	7.5 (8)	0.16 (8)	— (—)	— (—)	— (—)	21 (7)	1.9 (7)
Serpentinized peridotites	2.88 (627)	6.29 (17)	3.49 (15)	1.02 (17)	9.0 (15)	0.27 (15)	30 (5)	36 (5)	190 (5)	17.7 (8)	2.3 (8)

\*Formation

Table II.15, continued

Rock	$\sigma$	$v_p$	$v_s$	$K_s$	$E_{dyn} \cdot 10^{-1}$		$\sigma_t$ , MPa	$\sigma_{c\phi}$	$P_{in}$	$K_{pl}$
	g/cm <sup>3</sup>	km/s	km/s		MPa		•t	•t <sub>1</sub>	MPa	
Pirttijärva suite (4884-5619 m)										
Magnetite-biotite-amphibole schists after trachybasalts	2.97 (315)	5.80 (18)	3.50 (13)	1.13 (18)	7.8 (11)	0.18 (11)	—	—	— (21)	2.3 (21)
Magnetite-biotite-plagioclase schists after trachy-andesite basalt	2.86 (244)	5.04 (20)	2.96 (5)	1.14 (20)	6.1 (4)	0.20 (4)	—	—	20.5 (2)	2.3 (2)
Kuvernerinjok suite (5619-5717 m)										
Tremolitized dolomites	2.85 (55)	6.10 (3)	3.12 (2)	1.11 (3)	7.1 (6)	—	—	—	12.2 (3)	3.1 (3)
Meta-diabasic amphibolites										
Carbonate-mica metapsammites	2.74 (87)	5.32 (6)	3.22 (5)	1.10 (6)	6.5 (6)	0.22 (6)	—	—	21.6 (5)	2.0 (5)
Majärva suite (5717-6835 m)										
Amphibole-plagioclase schists after leuco-diabase	2.90 (1895)	5.28 (79)	2.91 (86)	1.14 (79)	6.1 (44)	0.21 (44)	15 (5)	34 (5)	160 (5)	20.4 (78)
Quartz-biotite-plagioclase schists after andesites	2.78 (15)	5.28 (1)	2.88 (1)	1.12 (1)	5.7 (1)	0.23 (1)	—	—	29.4 (1)	1.6 (1)
Meta-diabasic amphibolites	3.03 (122)	5.76 (4)	3.26 (6)	1.08 (4)	7.6 (4)	0.23 (4)	—	—	16.4 (7)	1.8 (7)
Archean Group										
Sequence I, gneisses with high-alumina minerals (6842-7622 m)										
Biotite-gneisses with high-alumina minerals	2.77 (241)	4.29 (12)	2.54 (1)	1.18 (12)	3.4 (12)	0.01 (1)	—	—	12 (10)	3.3 (10)
Migmatite-granites, pegmatites	2.64 (223)	4.34 (5)	—	1.97 (5)	3.5 (3)	—	—	11.5 (1)	117 (1)	22.3 (7)
Sequence II, shadow migmatites, gneisses and amphibolites (7622-9456 m)										
Shadow migmatites, gneiss-plagiogranites	2.65 (5245)	3.99 (40)	1.84 (15)	1.05 (40)	2.02 (15)	0.17 (15)	7 (8)	11 (8)	194 (9)	27.8 (42)
Plagiomicrocline gneiss-granites	2.62 (241)	3.50 (4)	1.83 (4)	1.05 (4)	1.6 (4)	0.20 (4)	—	—	—	375 (4)
Epidote-biotite, epidote-biotite-amphibole gneisses and schists	2.78 (328)	4.34 (4)	—	1.08 (4)	—	—	9.5 (1)	21 (1)	151 (1)	23.1 (4)
Amphibolites	3.02 (417)	4.62 (10)	1.89 (10)	1.13 (10)	2.3 (10)	0.13 (10)	5 (1)	20 (1)	—	25.8 (7)
Sequence III, two-mica gneisses with fibrolite (9456-9541 m)										
Two-mica gneisses with fibrolite	2.72 (98)									

Table II.15, continued

Rock	$\sigma$	$v_p$	$v_s$	$K_s$	$E_{dyn} \cdot 10^{-10}$	$\cdot$	$\sigma_t$ , MPa	$\epsilon_{cp}$	$p_i$ , MPa	$K_{pl}$
	g/cm <sup>3</sup>	kmps			MPa		$\sigma_{t\perp}$	$\sigma_{t\parallel}$		

## Sequence IV, shadow migmatites, gneisses and amphibolites (9541-10,144 m)

Shadow migmatites, gneiss-plagiogranites	2.68 (1118)	4.05 (3)	2.55 (1)	1.06 (3)	1.3 (3)	0.05 (3)	—	—	—	22.8 (5)	2.2 (5)
Shadow migmatites	2.67 (318)										
Epidote-biotite, epidote- biotite-amphibole gneisses and schists, migmatized plagiomicrocline granites											
Amphibolites	3.00 (411)	4.24 (3)	—	1.24 (3)	—	—	—	—	—	17.6 (6)	2.4 (6)
Blastocataclased, chlori- tized shadow migmatites	2.65 (219)	4.98 (2)	—	1.05 (2)	—	—	—	—	—	28.2 (5)	1.8 (5)
Blastocataclased, chlori- tized amphibolites	2.96 (183)	5.96 (3)	—	1.12 (3)	—	—	—	—	—	25 (6)	2.0 (6)

## Sequence V, two-mica gneisses with fibrolite (10,144 to 10,600 m)

Two-mica gneisses with fibrolite	2.70 (1683)	3.02 (2)	—	1.22 (2)	—	—	—	—	—	13.4 (13)	2.1 (13)
Amphibole-biotite gneisses, granodiorites	2.66 (427)	3.30	—	1.06 (1)	—	—	—	—	—	14.3 (2)	2.0 (2)
Gneiss-granites and pegmatites, plagi- microcline	2.62 (93)	—	—	—	—	—	—	—	—	20.9 (3)	1.9 (3)

## Sequence VI, shadow migmatites, gneisses and amphibolites (10,600-11,000 m)

Shadow migmatites	2.64 (594)	—	—	—	—	—	—	—	—	19.5 (2)	1.8 (2)
Epidote-biotite-amphi- bole gneisses, schists	2.97 (43)	3.63 (3)	—	1.11 (3)	—	—	—	—	—	18.9 (1)	1.9 (1)

## Lower Proterozoic-Archean (?)

(Dike?) complex of orthoamphibolites and ultramafic orthoschists (6,842-11,000 m)

Meta-diabasic amphibolites	3.06 (1209)	4.75 (13)	2.25 (4)	1.18 (13)	3.48 (6)	0.20 (4)	13 (2)	18 (2)	182 (22)	26.5 (22)	2.2 (22)
Meta-leucodiabasic amphi- bolites, including cumming- tonites	2.92 (1120)	4.42 (15)	2.65 (3)	1.12 (15)	3.40 (3)	0.04 (3)	11 (3)	23 (3)	190 (3)	22.8 (12)	2.2 (12)
Phlogopite-talc-tremo- lite schists after ultramafic rocks	2.94 (77)	4.27 (4)	1.91 (1)	1.21 (4)	2.6 (1)	0.19 (1)	5 (2)	11 (2)	64 (2)	7.5 (5)	2.1 (5)

Remarks: In parentheses - number of measurements

In the Archean complex the critical compressive strength varies from 64 MPa in the phlogopite-talc-tremolite schists, which are sporadically developed, to 182-194 MPa in the commonest rocks of the section -- shadow migmatites (gneiss-granites) and amphibolites. In the Archean rocks the  $\sigma_t$  values vary from 5 MPa in the phlogopite-talc-tremolite schists, transverse to the schistosity, to 23 MPa in the amphibolites along the schistosity, i.e. they are appreciably lower than the  $\sigma_t$  of the rocks of the Lower Proterozoic.

From Fig. II.26 there is seen a clear correlation of elastic properties of the drill core with critical tensile strength. There also is a relationship between elastic anisotropy and strength anisotropy of the rocks recovered from the hole. This interrelationship is based on the phenomenon of partial disintegration of the core upon decompression. Therefore, the strength indices, at least of the lower part of the section, cannot be used to calculate the true strength of the rocks penetrated by SD-3 *in situ*.

During drilling, information was constantly needed as the rocks were penetrated, especially their strength, which necessitated using a rapid procedure for calculating the strength of the rocks along with determining the critical compressive and tensile strength. The fastest method is determination of the mechanical properties of the rocks under conditions of a volumetrically stressed state using the indentation method.

The mean weighted values of hardness under the die for the rocks of the Pechenga Complex is 2520 MPa (Table II.16), with variations from 380 MPa in the meta-picritic talc-chlorite schists (4578-4673 m) to 3530 MPa in the metadiabases. The values of  $P_{in}$  (indentation hardness) in the metamorphosed tuffogenic-sedimentary rocks (1190-2180 MPa) are appreciably lower than in the metamorphosed magmatic formations (1640-3530 MPa), except for the blastomylonites of greenschist facies, rich in chlorite, mica, talc and serpentine, developed after mafic and ultramafic rocks, which are characterized by anomalously low values of indentation hardness.

The mean weighted value of  $P_{in}$  for the Archean complex is 2230 MPa, i.e. just a little less than that given above for the Proterozoic. The phlogopite-talc-tremolite schists (750 MPa), and biotite and two-mica gneisses with high-alumina minerals (1200 MPa), common in the 6842-7622 interval, have low  $p_{in}$ . The shadow migmatites and amphibolites, most common in the Archean part of the section, have  $p_{in} = 2780$  and 2570 MPa, respectively.

TABLE II.16

AVERAGE WEIGHTED (BY THICKNESS) VALUES OF PHYSICO-MECHANICAL PROPERTIES OF THE ROCKS OF THE SECTION IN HOLE SD-3 BY SUITE, SEQUENCE AND COMPLEX

Suite, sequence, complex	H, m	$\frac{v}{g}$ , m/cm kmps	$v_p$	$v_s$	$K_s$	$E_{dyn} \cdot 10^{-3}$ , MPa	$\sigma_t, MPa$	$\sigma_{cp}, MPa$	$\sigma_{in}, MPa$	$\sigma_{pl}$
							$\frac{\sigma_{t1}}{\sigma_{t1}}$	$\frac{\sigma_{t1}}{\sigma_{t1}}$		
<b>Suite:</b>										
Materta	0—1059	3,00	6,68	3,56	1,03	10,0	0,27	42	42	195 26,8 2,3
Zhdanov	1059—2805	2,90	6,09	3,50	1,05	8,7	0,23	28	32	162 20,4 2,1
Zapolyarna	2805—4673	3,01	6,50	3,73	1,05	10,4	0,23	28	31	164 33 1,7
Luchlompol'	4673—4884	2,76	5,36	3,35	1,11	7,1	0,14	22	22	161 20,1 1,8
Prittijärvi	4884—5619	2,92	5,47	3,26	1,13	7,0	0,19	—	—	— 24,8 2,3
Kuvernerin-jok	5619—5717	2,80	5,79	3,16	1,11	6,9	0,22	—	—	— 16,5 2,6
Majarvi	5717—6835	2,91	5,33	2,94	1,14	6,3	0,21	—	—	— 20,4 2,2
Pechenga sedimentary-volcanogenic complex as a whole	0—6842	2,94	6,08	3,45	1,07	8,7	0,23	—	—	— 25,2 2,0
<b>Sequence:</b>										
I-gneisses w. high-Al minerals*	6842—7622	2,75	4,29	2,54	1,16	3,4	0,01	—	—	— 140 2,9
II-shadow migmatites, gneisses & amphibolites	7622—9456	2,73	4,12	1,85	1,07	2,4	0,16	77	150	1920 283 2,2
III-two-mica gneisses w. fibrolites	9456—9541	2,72	—	—	—	—	—	—	—	—
IV-shadow migmatites, gneisses & amphibolites	9541—10144	2,77	4,26	2,65	1,09	2,8	0,08	—	—	— 226 2,1
V-two-mica gneisses w. fibrolites	10144—10600	2,72	3,20	—	1,20	—	—	—	—	— 153 2,1
VI-shadow migmatites, gneisses & amphibolites	10600—11000	2,65	3,32	—	1,06	—	—	—	—	— 195 1,8
Archean amphibolite-migmatite-gneiss complex (including orthoamphibolites) as a whole	6842—11000	2,73	3,99	2,17	1,10	2,7	0,11	—	—	— 223 2,2

\*All calculations -- orthoamphibolites taken into account.

\*\*Limit of tensile strength  $t$  determined in two directions: perpendicular  $\sigma_{t\perp}$  and parallel  $\sigma_{t\parallel}$  to bedding and schistosity.

\*\*\*Formation

On the basis of correlational analysis (see fig. II.26) it was established that the values of indentation hardness are closely related to the values of  $\sigma_{cp}$  and less closely to  $\sigma_t$ . The correlation coefficient  $r$  in the first case is 0.89, in the second 0.35 (confidence interval at the 1% level of significance  $r = 0.56$ ). In addition, from the results of the analysis it was established that the effect of the decompression factor on the index  $p_{in}$  of the core is secondary, the main role belonging to the mineralogic composition of the rocks. However, it would not be right to completely deny the role of decompression, as the indentation hardness of rocks of the same type at the surface is 20-30% higher than the  $p_{in}$  values measured on core recovered from depths of 7-11 km.

It is known that the ratio of critical compressive and tensile strength characterizes their brittleness (plasticity): the higher the  $\sigma_{cp}/\sigma_t$  ratio, the greater the brittleness and correspondingly the lower the plasticity of the rock. The most brittle rocks have a ratio of  $\sigma_{cp}/\sigma_t = 15-20$ .

The brittleness of the rocks penetrated by the hole to a depth of 6842 m, i.e. to the Archean basement, is low on the whole. Some increase in brittleness is recorded in the lower part of the Pechenga Complex, for instance for the amphibole-plagioclase schists. The brittleness of the rocks recovered from depths greater than 6842 m is still higher. For this part of the section decompression has more effect on the physical properties of the rocks than the mineralogic composition.

The coefficient of plasticity determined by the indentation test is theoretically the value inverse to the brittleness of the rocks. However, no rigid correlation between the coefficients of plasticity and brittleness of the rocks was recorded, as the indices obtained in the indentation test depend to a much greater extent on the mineralogic composition of the core than on the extent of its partial disintegration.

To ascertain the more complete characteristics of the physico-mechanical properties of the rocks of the section in SD-3, data of determinations of  $E_{dyn}$  and  $E_{st}$ , obtained in a regime of quasi-static uniaxial stress of the sample with a measure of deformation along its whole length were compared. The results of the comparison (fig. II.27 [p. 41]) showed that the value of the modulus  $E_{st}$  is less than the value of  $E_{dyn}$  for all rocks of the same mineralogical type, but the character of variation of  $E_{dyn}$  and  $E_{st}$  through the section is practically the same: maximum values of  $E_{st}$ , as of  $E_{dyn}$ , are observed in the upper part of the section (diabases and gabbro-diabases of volcanogenic flows IV and III), where  $E_{st} = (5.0-7.5).10^+ \text{ Mpa}$ .

The  $E_{dyn}/E_{st}$  ratio for the different rock types proved to be different: for diabases and gabbro-diabases it is 2, and for sedimentary rocks 1.7, which is in agreement with the variation in plasticity of the rocks.

To solve technological problems, the abrasitivitiy  $Z$  of the rocks plays a large part.

The average values of abrasitivitiy of the rocks in the section in SD-3 vary from 3 to 48 mg. It is known that the abrasivity of crystalline rocks with respect to steel is larger, the greater the microhardness of the minerals entering into the composition of these rocks. However, in the case of friction additional roughness arises in polymineralic rocks, related to the difference in resistance to abrasion of the minerals, which leads to an increase in abrasivity which is particularly noticeable for clastic rocks. The minimum abrasivity, as would be expected, is that of phyllites, chlorite-sericite and highly talcized rocks ( $Z = 3-16$  mg), the maximum, of granites, amphibolites and crystalline schists ( $Z = 46-48$  mg). Owing to the effect of additional roughness, tuffs, tuffites and sandstones are characterized by high abrasivity ( $Z = 24-44$  mg).

According to the classification of rocks by abrasive properties, the rocks investigated fall into four classes (table II.17).

Thus as a result of study of the physico-mechanical properties of the rocks of the section in SD-3 it is established that:

-- the section consists mainly of elastic-plastic rocks of high strength and average abrasivity;

-- the character of variation of the strength properties through the section is very uneven, due to which serious complications arise during drilling, and routine evaluation of these properties is constantly needed, using a rapid procedure for corrective drilling regimes:

-- the procedure of determining hardness of the rocks by indentation with a flat base best satisfies the requirement for rapidity; the results of hardness determination correlate well with the indices of compressive and tensile strength.

-- the physico-mechanical properties of the rocks depend (by analogy with the acoustic properties) on these factors: petrographic-mineralogic; decompressional (it is of decisive importance in the lower part of the section).

The most informative parameter in estimating the stability of the walls of the hole is tensile strength, which decreases down-hole in jumps, and relative to which anisotropy of the rocks is manifested.

VERTICAL ZONING OF PHYSICAL PROPERTIES OF THE ROCKS AND  
CRUSTAL STRUCTURE FROM THE RESULTS OF STUDY OF THE SECTION AND THE  
AREA OF THE KOLA SUPER-DEEP BOREHOLE

The results of drilling, geophysical investigations, study of core samples recovered at the surface, and also data of geological and geophysical investigations in the immediately adjacent territory provide the possibility of approaching problems of the general structure of the earth's crust in a new way.

One of the most pressing but least studied and debatable problems in earth science is the question of systematic variations in physical properties at great depths. An unambiguous answer to this problem is possible only by using the results of super-deep drilling and petrophysical models (Footnote 1: according to the definition of Ye. V. Karus and L.V. Shierina, a petrophysical model means the distribution at depth of physical characteristics determined in a single hole.) of the section. Study of the petrophysical models is necessary to enhance the precision and uniqueness of ground geophysical surveys.

ELASTICITY-DENSITY MODEL

The main regularity ascertained in studying elastic and density characteristics in the section of SD-3 is the fact that the maximum values of density  $\sigma$  and longitudinal and transverse wave velocities,  $v_p$  and  $v_s$ , and  $\sigma$  also minimal porosity are observed in the upper part of the section. A sharp decrease in  $v_p$ ,  $v_s$  and  $\sigma$  and an increase in anisotropy of the rocks is observed at a depth of 4500 m in a sequence of rocks of the Zapolyarna formation, uniform in composition (fig. II.28). The first discontinuity (depth 4500 m) almost coincides with the boundary between the greenschist and epidote-amphibolite facies metamorphism, the second with the boundary between the Archean and Proterozoic. Below the first boundary schistose rocks occur everywhere.

Attention should be paid to the fact that at the boundary of the upper and lower groups of the Lower Proterozoic, the coefficient of anisotropy of elastic wave velocities increases in a jump, increasing within one member from

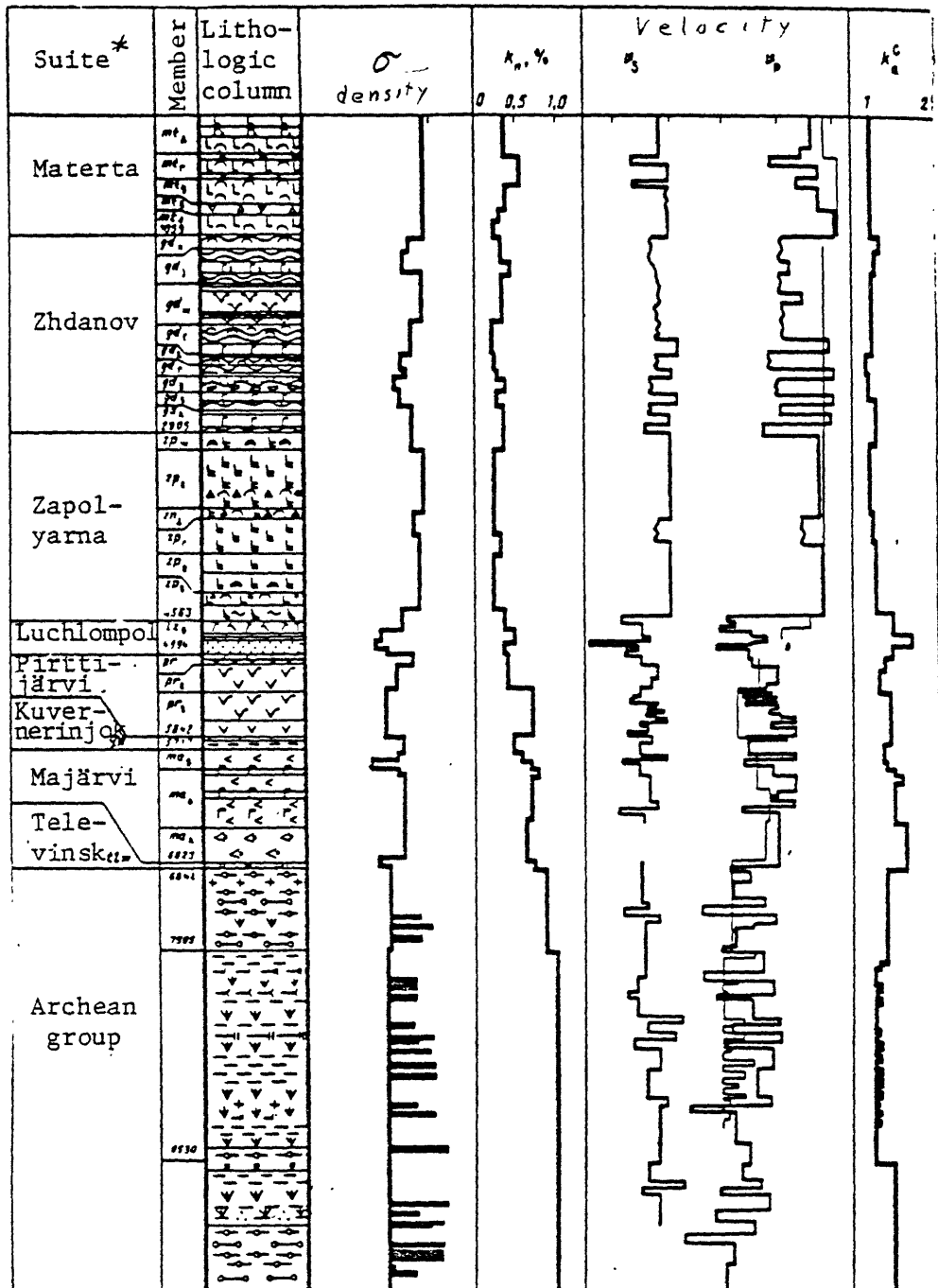


Fig. II.28. Elastic and density properties of the rocks of the section in SD-3  
 For symbols in lithologic column, see appendix.

\*Formation

1.06 to 1.37. Below 4500 m the coefficients of anisotropy vary widely, reaching 1.6, but not one member returns to the values of the upper group of the Middle Proterozoic, i.e. does not exceed 1.05-1.09.

For the section in SD-3, ideas of an increase in velocity with depth for rocks of the same composition were not supported. Such factors as, for instance, progressive and dislocational metamorphism leading to structural alterations in the rocks affect the elastic properties: maximum velocity values are observed in the upper part of the section, i.e. there is an inverted seismogeologic section (velocity inversion).

In the Archean formations there is observed a distinct division in density and velocity of the amphibolites and gneisses, and the upper high-alumina sequence of gneisses is denser than the lower. Below this boundary, no increase in anisotropy of the rocks relative to elastic properties is observed.

#### SEISMOACOUSTIC MODEL

Using modern acoustic logging apparatus in SD-3, a detailed velocity section for longitudinal  $v_p$  and transverse  $v_s$  waves was obtained, vertical time-distance curves of these waves were plotted, effective damping was determined and taking into account the density of the rocks, a seismoacoustic model of the section was compiled (fig. II.29). The main feature of this model is that to a depth of 4500 m, no gradient in  $v_p$  and  $v_s$  velocities is present; below that there is observed a local negative gradient, indicating some decrease in velocity (according to data of acoustic logging and vertical seismic profiling). When the vertical time-distance curves plotted on the basis of the results of these different-in-principle methods of GIS [?] are compared, complete similarity of the data practically throughout the section is obtained, except <sup>for</sup> the very lowest part where the quality of the acoustic logging material is much worse than for the upper part of the section.

It should be mentioned that the sharply expressed zone of inversion (decrease in  $v_p$  and  $v_s$  velocities) is observed from the readings of the GIS method just as clearly as from the data of core measurements. However, due to the effect of the attitude of the rocks on the velocity of propagation of elastic waves, the P values determined from acoustic logs are higher than the results of core measurements, even if the latter are water-saturated (see fig. II.29). For dry samples this difference is still more considerable. From the acoustic logging data, as from the core, the velocity changes abruptly at a depth of 4500 m (from 6.8-7 to 5.5-5.8 km/s).

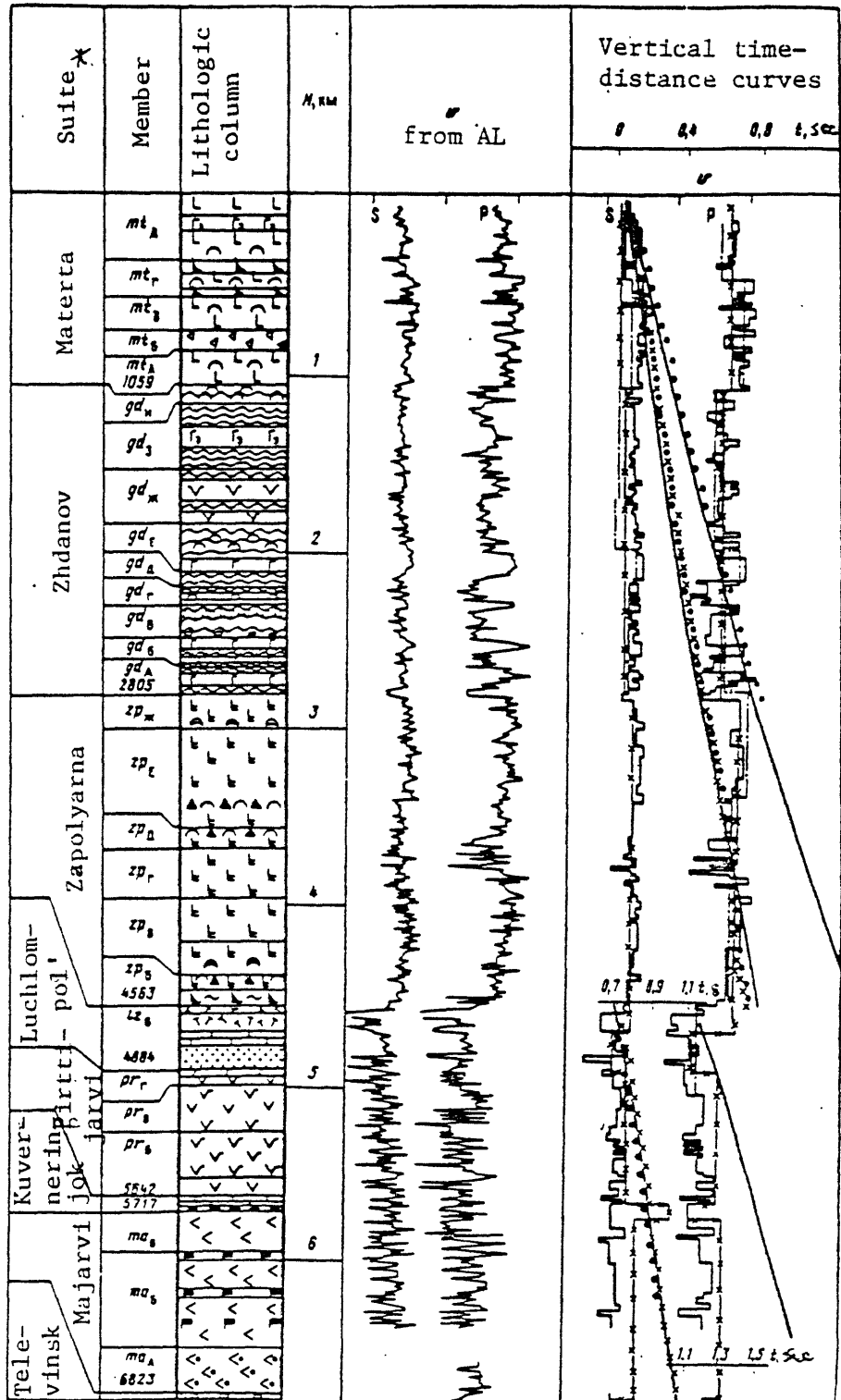


Fig. II.29. Seismoacoustic model of the section in SD-3.

Acoustic logging data: 1 - reliable, 2 - unreliable; vertical seismic profiling data: 3 - VNIIYaGG, 4 - LGI.

## \*Formation

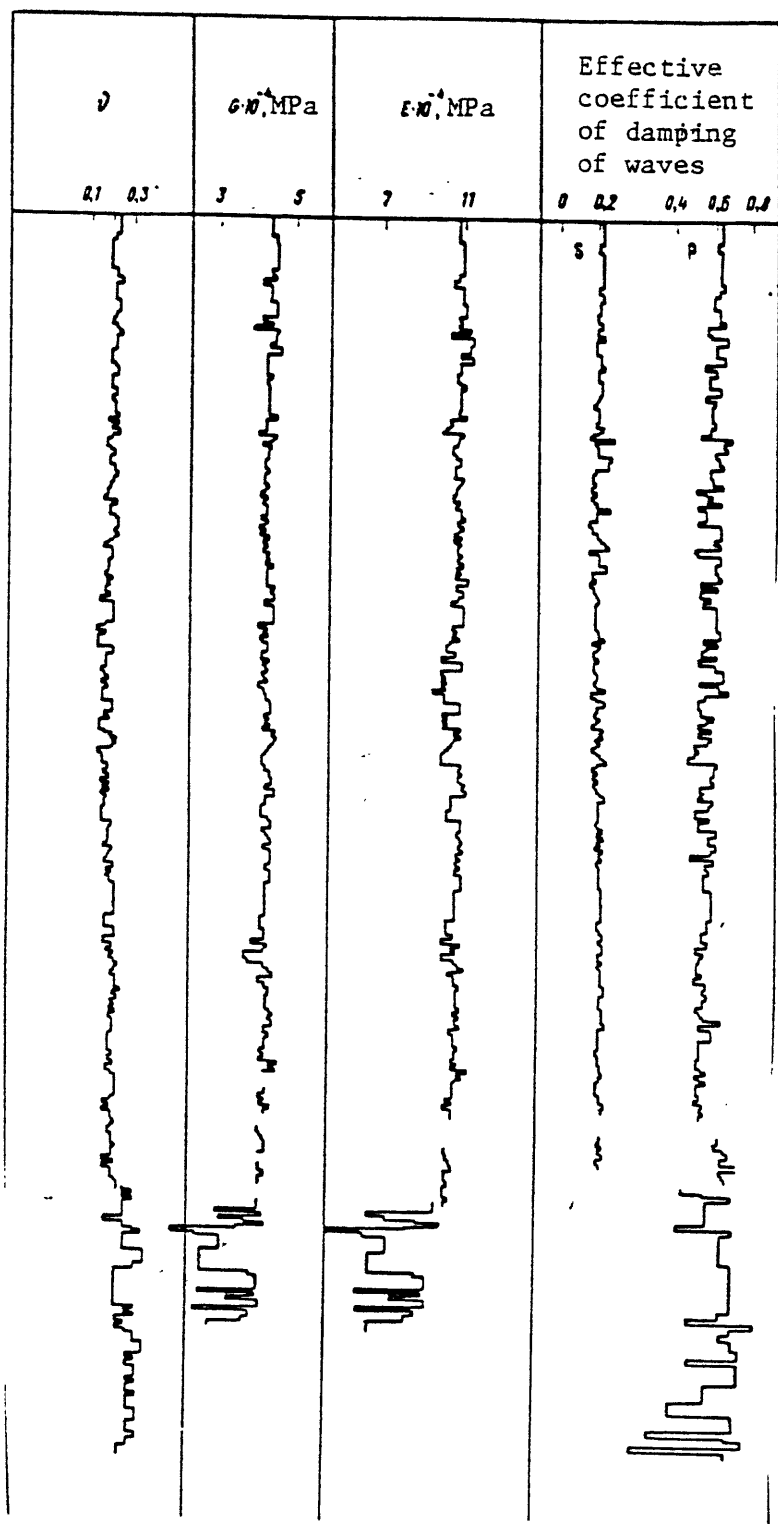


Fig. II.29, continued

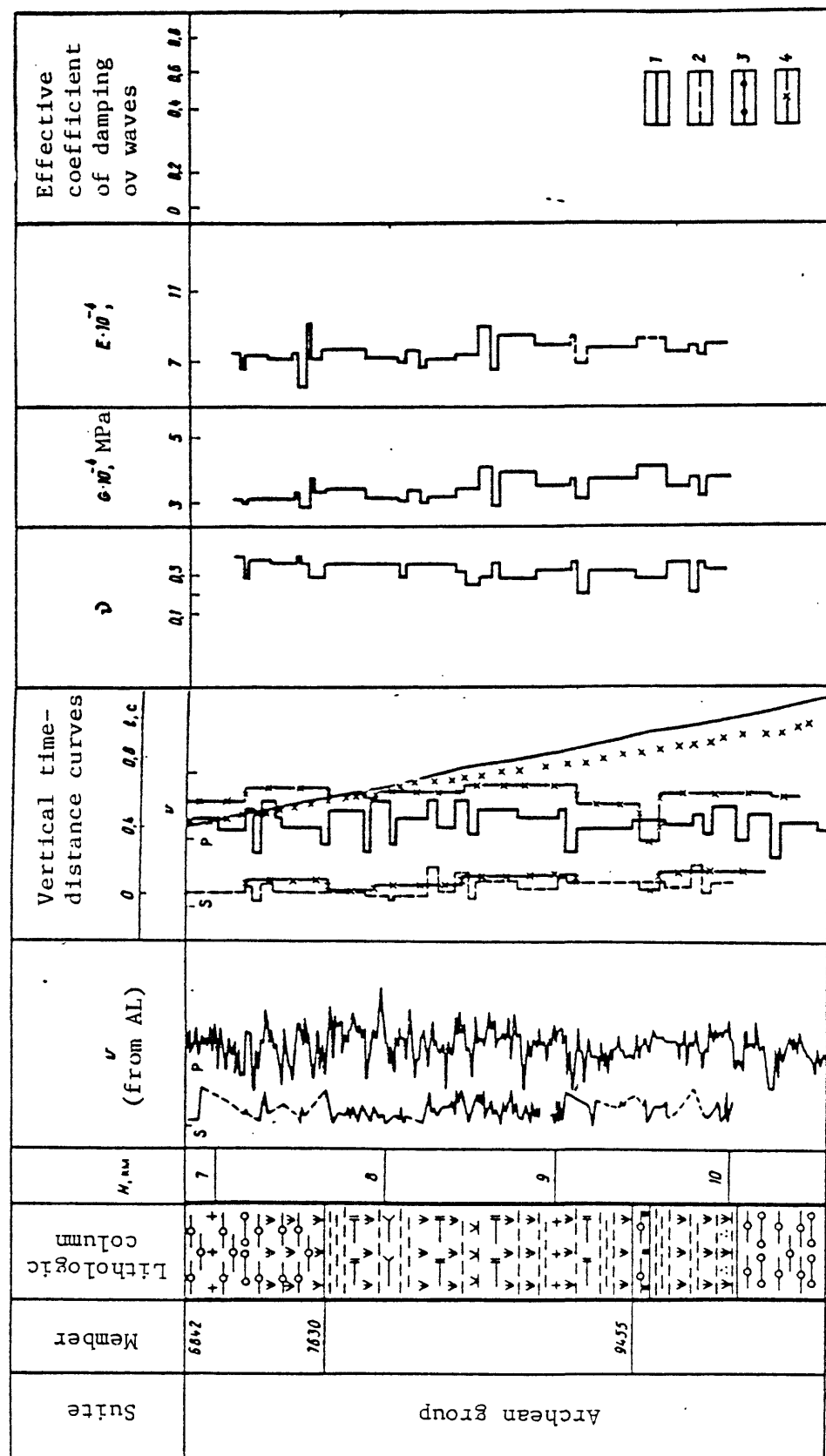


Fig. II.29, continued

Thus, as a result of the investigations made, the presence of a zone of inversion of the elastic (and density) properties of the rocks is demonstrated.

The seismoacoustic model of the section was the basis for experimental determinations and analytical calculations of the complex stress state in the upper part of the crust penetrated by SD-3. The main purpose of these investigations was to calculate the attitude of the rocks, which was needed to solve geological-technical drilling problems. The conclusion obtained concerning the uneven distribution of stress with depth and the presence in the section of a thick (about 3 km) zone of considerable easing of stress (to 40 MPa) (Fig. II.30) is important also for solving geological-geophysical problems, in particular ascertaining the possible nature of deep seismic discontinuities. Fig. II.30 gives the results of study of the temperature gradient and heat flow in SD-3, the stress state and secondary transformations of the rocks. When the results obtained are compared, it is established that the boundaries of abrupt change in the stress state of the rocks (curves II and IV) correspond to stepwise variation in temperature gradient (curve I) and heat flow (curve III) and coincide with the intersections of the section with metamorphic fronts and seismic boundaries, and both have a tendency to smooth out with depth.

Most investigators believe that the causes of redistribution of stresses in the crust are manifold. The results of tectonophysical modeling confirm that idea (see Fig. II.30). However, in the literature it is shown that horizontal tectonic forces are manifested only in the upper part of the crust and do not affect the vertical component of stresses  $\sigma_z'$ . Fig. II.30 gives the variation through the section of precisely that  $\sigma_z'$  component, calculated theoretically (curve IV) taking into account the effect of weak layers, and determined by the full-scale method (curve II). The results obtained by these methods indicate that  $\sigma_z'$  is nonlinearly distributed through the section; there are places both with understressed and overstressed rocks (see Fig. II.30). The principles of redistribution of stresses in all probability is governed by internal processes occurring (or having occurred) in the crust, and primarily by metamorphism of the rocks.

The variation in petrophysical characteristics of the rocks with increasing intensity of metamorphism changes the character of their deformation, and the sharpest changes are recorded in the region of transition from greenschist to epidote-amphibolite facies, where massive textures of

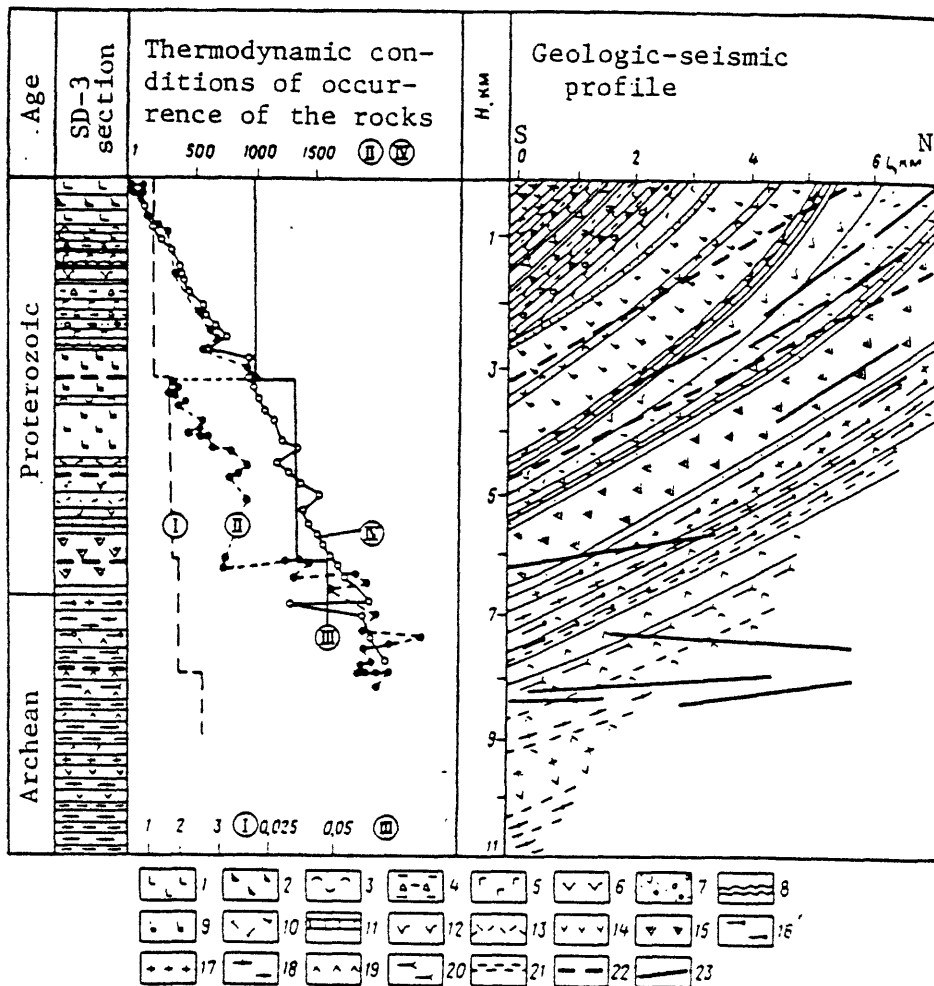


Fig. II.30. Correlation of thermodynamic conditions of occurrence of the rocks with the locations of boundaries of facies (subfacies) of metamorphism and seismic boundaries in the section of Precambrian rocks of the Baltic shield penetrated by hole SD-3.

Indices of curves and corresponding scales of measurements: I - temperature gradient,  $^{\circ}\text{C}/100 \text{ m}$ , II - vertical component of tensor of stresses (full-scale measurement, MPa), III - heat flow,  $\text{W}/\text{m}^2$ , IV - vertical component of stress (analytical calculation), MPa. 1 - diabases, 2 - picrite porphyrites, 3 - tuffs, 4 - tuffites, 5 - gabbro-diabases, 6 - peridotites; 7 - breccias; 8 - siltstones, phyllites, sandstones; 9 - diabases, pillow lavas, actinolitized; 10 - plagioporphyrites; 11 - dolomites, sandstones; 12 - meta-andesites; 13 - orthophyres, albitophyres; 14 - metadiabases; 15 - amphibole schists after basalt and amphibolites; 16 - high-alumina gneisses; 17 - plagiogranites; 18 - biotite-plagioclase gneisses; 19 - amphibolites; 20 - talc-tremolite schists; 21 - biotite-amphibole gneisses; 22 - boundary of facies and sub-facies of metamorphism; 23 - seismic reflecting boundaries.

metabasites are succeeded by schistose textures. In the lower part of the section there is observed intense granitization of biotite-muscovite schist. It is these boundaries which are recorded by geophysical (mainly seismic) methods (see Fig. II.29).

Inasmuch as the variation in properties of the rocks occurring during metamorphism are related to their recrystallization and change in volume, and also to heat flow, those phenomena should be accompanied by redistribution of stresses in the massif. To explain the recorded changes in stress it is necessary to use the regularities found in the variation of physical (mainly elastic and density) properties of the rocks of the section, in particular of its three-layer division.

The calculations show that using the real modulus of elasticity and values of density of the rocks constituting the section, the presence in the section of a zone of unloading equal to 40 MPa can be explained by a relative change in volume of the unstressed middle layer, which should amount to 0.08% all together. That insignificant change in volume can be completely maintained for long geologic time and, as a result, the uneven distribution of the stress state in the section will be retained. The relative increase in volume of the middle layer (dilatation) may also be related to fracturing of the rocks and unevenness of their thermal expansion (due to the change in heat flow). The observed phenomenon in all probability arises under the effect of the enumerated factors related to secondary transformations and accompanying changes in the physical (especially elastic) properties of the rocks. The boundaries of a sharp decrease (or increase) in stress would be recorded by geophysical methods, including seismic (see Fig. II.30).

Thus in this case the nature of deep seismic boundaries is caused by secondary transformations leading to a change in physical properties and in the state of matter of the crust, rather than by lithostratigraphic variability of the rocks.

#### TECTONOPHYSICAL MODEL'

It was shown above that the stress state of the rocks (its distribution by depth) plays a large part in the variations of their physical properties and in the formation of geophysical boundaries in the crust. In order to obtain additional information on stresses in the region of the Kola superdeep hole, tectonophysical investigations were carried out. The object of

tectonophysical analysis was reconstruction of the young and recent tectonic stress fields in the region of SD-3 and prediction of them at depth. To solve the problem, the decomposition method was used, which permits distinguishing the components of the stress field on the basis of a systems approach. They are referred to tectonodynamic systems of different scale.

By tectonodynamic system we mean a systematic genetic model of the relationship of tectonic movements, deformation and stresses occurring in a volume of the lithosphere, the physico-mechanical properties of which can be considered to be uniform at the scale of consideration used. Tectonodynamic systems form a hierarchy closely related to the hierarchy of tectonic deformation (structures). A relationship is established between the size of the area of averaging (size of the base on which the measurements are made) and the depth distribution of stress fields of a given tectonodynamic system.

To reconstruct stress fields, the systematic relationship between orientation of the axes of the principal normal stresses and geometry of the spread in orientation of tectonic fracturing, established theoretically and confirmed by field investigations, seismogeologic data and modeling was used.

The greatest difficulties in reconstructing young and recent stress fields in the region described were related to determination of the age of fracturing. Study of aerophotographs, space photographs, and the topography of a region taking in the whole northwestern part of the Kola Peninsula, made it possible to distinguish faults, clearly manifested in the relief, and thus assumed to be rejuvenated or produced in the young stage of tectonic evolution. Statistical analysis of the relationship between the length of these faults and the average distance between them showed the discreteness of distribution of this parameter, i.e. the possibility of distinguishing the hierarchy of faults in the region, which presumably belonged to tectonodynamic systems of different scale. Plotting of rose diagrams of strikes of these faults, which chiefly have steep dips, showed that the faults of different scale differ both in general strike and in scatter of strikes. This made it possible to suggest that in the area of SD-3 the regional stress field is of strike-slip character with north-northeast orientation of the compressional axis and northwest relative tension (Fig. II.31).

To precisely determine the age of this stress field, the focal mechanisms of earthquakes in the whole Arctic region were analyzed (see Fig. II.32, II.33 a, b), which not only made it possible to predict major faults in the area,

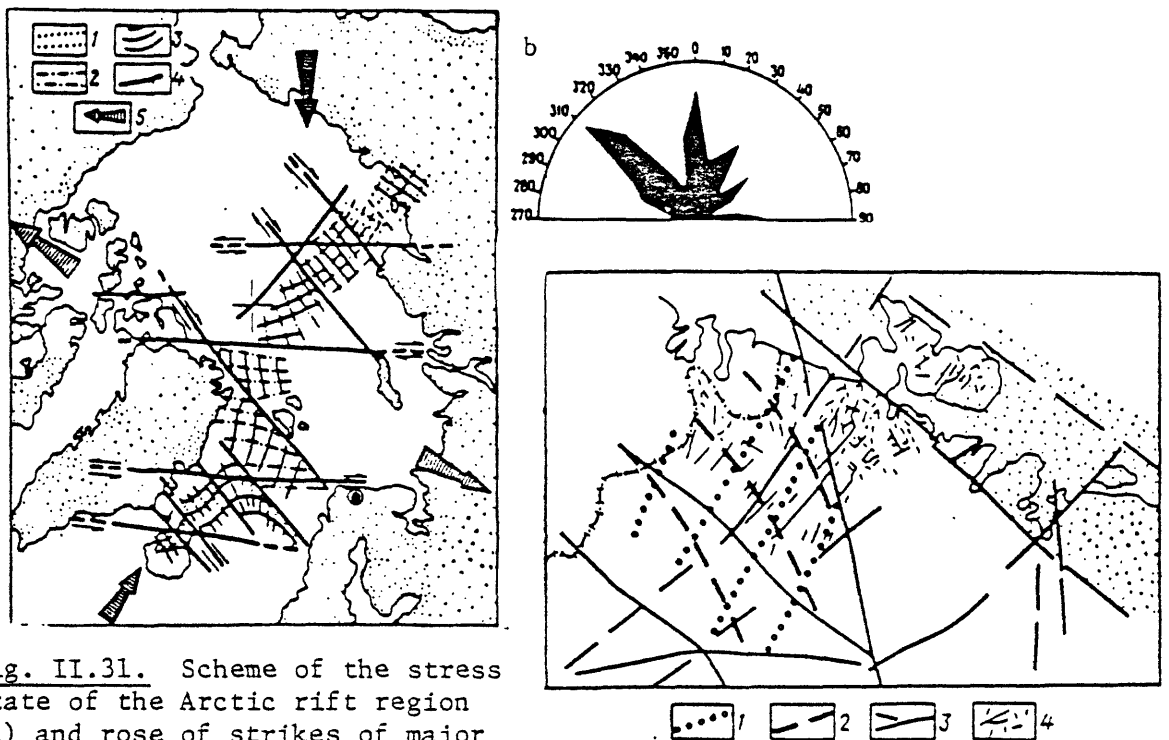


**Fig. II.31.** Scheme of the stress state of the Arctic rift region (a) and rose of strikes of major faults of the Kola peninsula from data of space photographs, geologic surveys and aerial photos.

Trajectories of axes: 1 - tension, 2 - intermediate, 3 - compression; 4 - presumed faults; 5 - direction of compression and tension of the regional field.

**Fig. II.32.** Tectonic stress field in the northwestern part of the Kola Peninsula.

Trajectories of axes: 1 - tension, 2 - compression; 3 - major faults; 4 - minor faults.

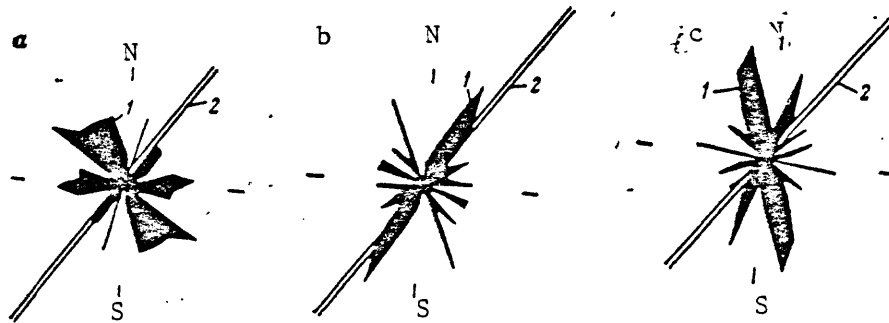


**Fig. II.33.** Roses of strikes (1) of young tectonic fractures in zones of ancient faulting (2).

Joints: a and c = superposed neotectonic, b = "inherited" of young stage.

coinciding with faults established independently on the basis of geologic, geophysical and remote sensing date, but also to confirm the earlier-noted orientation of the axes of principal normal stresses. Thus the present stress field (seismological data) to a substantial extent has inherited the young (at least Holocene) plan of orientation of axes of principal normal stresses in the area of SD-3.

The preliminary results thus obtained made it possible to formulate the task of detailed analysis of the stress field on the basis of a large number of measurements (more than 5000) of tectonic fractures in the Pechenga structure and its immediate surroundings. In the deposits of the Pechenga complex there were distinguished several systems of fractures having different mineral filling. These fractures correspond to old tectonic stress fields. In addition to these, fine hair-like or open cracks devoid of mineral filling occur everywhere in the region investigated. They form systems, in places rather clearly expressed in the present relief, often accompanied by slickensides, and they displace all older fractures having a mineral filling. The systems of these fractures are parallel lineaments readily deciphered on large-scale space photos.

All these signs indicate a young age of the fracturing in question. A large number of measurements of fractures were made on a more or less uniform grid so as to evenly elucidate all deposits of different age and lithology in the Pechenga complex. For each observation point (containing an average of 100 measurements) a local stress field was reconstructed. The points were joined for surface outcrops of individual formations, groups of formations, and finally, for the whole area. Analysis of the sum of data obtained made it possible to bring out the stress fields related to the action of tectonodynamic systems of different rank, i.e. characterizing different depth levels of the crust.

It was established that the lithology of the individual sequences, small faults, dikes, boundaries of zones of differently metamorphosed rocks, etc., considerably affect the character of the local tectonic stress fields. The role of the enumerated factors varies abruptly depending on the structural position and orientation with respect to the external stress field of lower rank. Thus, young fracturing either completely follows the older structural plan, rejuvenating old faults, or cuts across it and does not react at all to earlier formed structural in homogeneities (see Fig. II.33). More detailed analysis shows that the old fractures "revive" if they coincide with the

direction of the principal normal stresses and are generally nor reactivated if their location deviates substantially from the orientation of the young maximum tangential stresses. It must be stressed that the young fracturing (with unfavorable orientation of earlier formed in homogeneities) is not sensitive even to rather large ancient faults, in particular to overthrusts along bedding (see Fig. II.33).

At some observation points young and older fractures were studied separately. A sharp difference in the old stress fields from the young was observed (even in the case of reactivation of movement on old directions), which indicates fundamental reorganization of the structural plan in the neotectonic stage of development and a change in the mechanism of deformation of the crust.

Reconstruction of the stress field on the basis of data of neotectonic fracturing at some points was accompanied by dynamic microstructural analysis of oriented samples, and also by study of thin sections from drill cores. In the vast majority of cases, the old stress fields could be reconstructed using such analysis. Data on twinned carbonates (including those from individual veinlets) and in some cases in plagioclase made it possible to reconstruct the young stress field.

As a result of the investigations, not only could the regional stress field be reconstructed for the Pechenga structure, but also local stress fields corresponding to tectonodynamic systems of three ranks. The third-rank stress field, the shallowest one forming the upper tectonophysical layer, is characterized by vertically oriented compressive axes and subhorizontal orientation of the other two axes. The deeper second tectonophysical layer has a subvertical orientation of relative tension. The deepest layer is characterized by a strike-slip field of tectonic stresses and corresponds to the region of action of a tectonodynamic system of first rank.

The results obtained made it possible to construct a tectonophysical model of the area of SD-3 (Fig. II.34).

In the Lower Proterozoic deposits, stress fields of three ranks were distinguished, differing mainly in size of averaging areas and characterizing different depth levels in the crust. Examination of these fields showed that a "lens" of less viscous deposits of the Pechenga Complex, differing from the enclosing sequence of Archean age in petrophysical properties, was subjected to flattening deformation, accompanied by quasi-plastic upward bending of the material and its own local stress field, which is characterized by subvertical

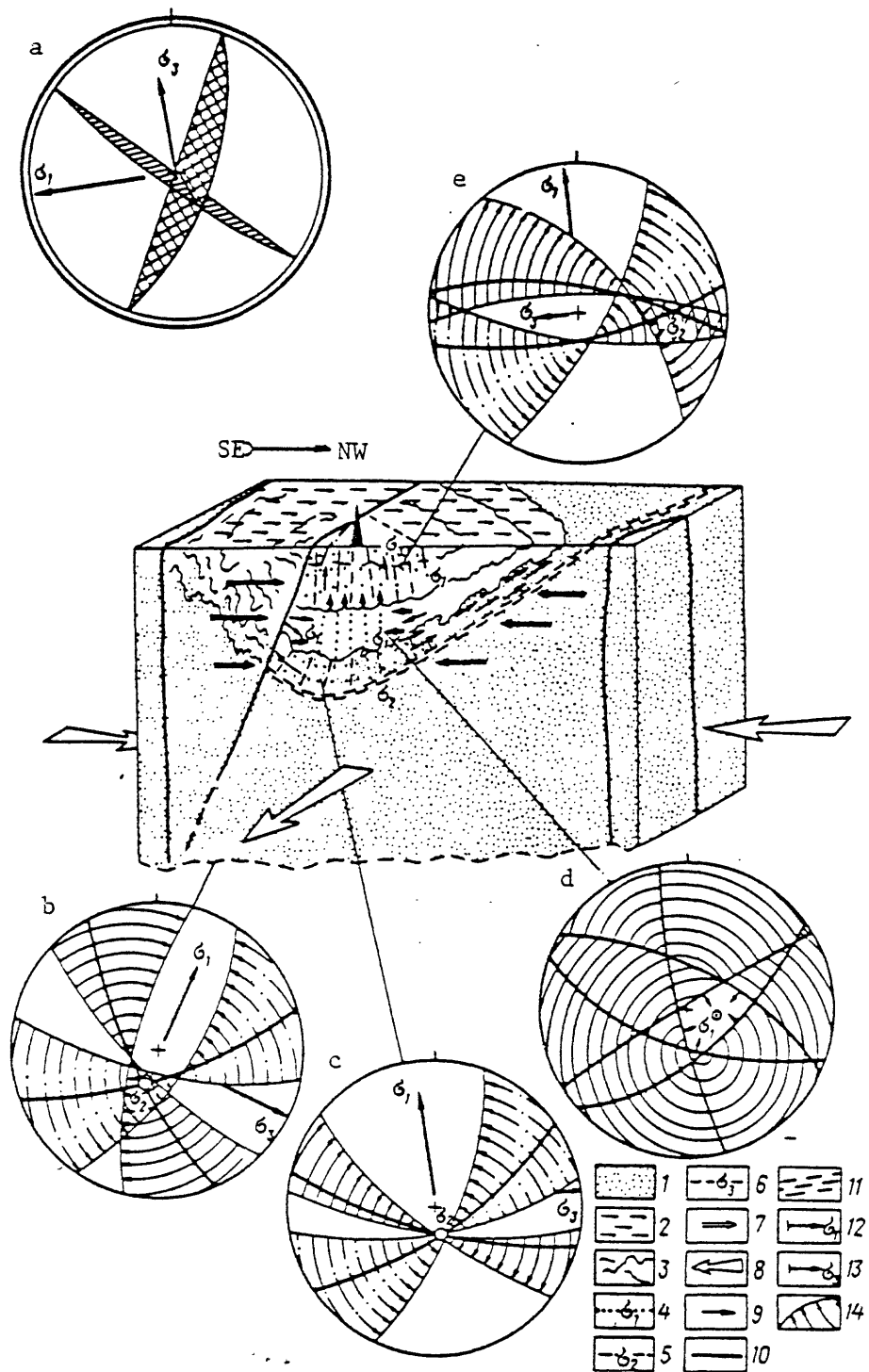


Fig. II.34. Tectonophysical model of the area of the Kola superdeep borehole.

Block diagram. Outcrops of rocks: 1 - Archean, 2 - Lower Proterozoic, 3 - marker horizons; orientation of stresses: 4 - relative tension, 5 - intermediate type, 6 - compression; orientation of external forces: 7 - local level, 8 - regional level; 9 - direction of movement of deformed material; 10 - suture faults; 11 - zones of foliation.

Circular diagrams (arrows indicate north). Orientation of stress axes: 12 - tension, 13 - compression, 14 - planes of fractures (arcs), directions of scatter in their orientation (arrows), modal orientation of fractures (heavy arcs). Diagrams of stress fields: a - Arctic basin, b - regional Pechenga structure, c - in Archean part of section, d - for de-stressed zone, e - for upper part of section.

orientation of the axis of relative distension and more or less uniform compression horizontally (see fig. II.34,d). In this case some increase in volume of the deformed sequence should occur. In the upper and lower parts of the "lens" of Lower Proterozoic rocks the boundary conditions are acutely disturbed, which causes a change in the mechanism of deformation. The sharp change in rank of tectonic stress field both on shorter and on longer bases on which the reconstruction of the stress state is made, is evidence of this.

The squeezed-out rocks of the middle and lower parts of the section described act as a "soft stamp" on the more brittle deposits of the upper part of the Lower Proterozoic formations, causing transverse bending in them in a vertical direction and an additional local stress field with vertical axis of compression and subhorizontal relative tension (see fig. II.34,e). The rank analysis of the stress field shows that the boundary between the tectonophysical layers would run at depths of the order of 3500-3800 m.

The described mechanism of formation can really arise only in the case of slippage due to horizontal compression of the base of the deformed "lens" of deposits of the Pechanga Complex on the older formations. Actually, the construction showed that at the boundary of the Lower Proterozoic and Archean deposits (depth on the order of 6800 m) there is a new change in the tectonic stress field. This field is of strike-slip character with subhorizontal orientation of both the compressional and relative tension axes (fig. II.34,c) and indicates displacement of the material layer-wise along the boundary of the complexes of different age. It can be expected that at depths of the order of 13-15 km a zone of displacement and separation into layers will be observed, depicted in the figure and kinematically corresponding to an overthrust along the bedding. Petrostructural investigations of the Archean deposits from the lower part of the section showed the possibility of distinguishing two successive (in time) stress fields, one of which corresponds to the stage of formation of the schistosity and is characterized by a compression axis oriented normal to it. The other, the younger, stress field is reoriented so that the plane of schistosity is parallel to the area of action of maximum tangential stress, i.e. the idea of displacement of material along layering is confirmed by the data.

Analysis of the stress fields of different rank suggests that there is clearly expressed horizontal layering of the crust, related not to extensive manifestation of horizontal displacements in it, but to a change in local conditions and mechanisms of deformation of different deep horizons.

Thus in tectonophysical respects the Pechenga structure is a region of pressure characterized by high confining pressure at depth, produced by compression and some increase in volume of the rocks in the middle part of the section penetrated by the hole. At the base and top of this layer special boundary conditions arise, leading to reorientation of the tectonic stress field and subhorizontal layering of the crust, which is recorded by seismogeologic methods.

Thus on the basis of geophysical investigations of the section of SD-3 and systematic measurements of the physical properties on core samples, geophysical and petrophysical sections (models) of the structure of the upper part of the crust, including seismoacoustic and magneto-electrical (magnetic and electrical properties according to measurements in the hole and on samples) models, a model of the natural radioactivity of the rocks (from logging data and measurements on samples), and an elastic-density model were constructed. Analysis of the vertical zoning of physical properties of the rocks and crustal structure in the section of SD-3 and the area around it made it possible to establish the following:

The seismoacoustic model reflects in detail the distribution of elastic wave velocities, modules of elasticity and effective sampling in the section. The quality of acoustic logs was markedly lower at a depth of more than 4500 m in connection with an increase in cavities in the hole and in its average diameter. Below 4500 m a zone of low elastic wave velocities was noted, which is traced in the rocks of the Pechenga (to 6842 m) and Kola (to the bottom of the hole) complexes. The zone of low velocities stands out relative to the upper high-velocity part of the Proterozoic Pechenga complex and primarily reflects a sharp drop in elastic wave velocity with depth.

## APPENDIX

Conventional symbols for lithologic columns

Symbols	Rocks	
	Proterozoic group	
	Phyllites	Biotite-amphibole-plagioclase schists after diabases
	Siltstones	Melanocratic plagioclase-amphibole rocks
	Sandstones, metamorphosed sandstones	Picrite porphyrites
	Sandstones, gritstones, conglomerates	Magnetite-biotite-plagioclase schists after andesites with intercalations of magnetite-amphibole-plagioclase schists after andesites
	Metam. sandstones, gravelly sandstones, fine-fragmental conglomerates	Magnetite-biotite-plagioclase schists after andesites & metamorphosed andesites & trachy-andesites
	Sandy limestones, dolomites, metamorphosed	Serpentinized peridotites, serpentinites, talc-sericite rocks
	Calcite, calcite-dolomite, talc-tremolite marbles	Gabbros
	Quartz-mica-carbonate & quartz-mica schists, metamorphosed quartzites & sandstones	Essexite gabbros
	Basic tuffs: a = pelitic, b = psammitic; metamorphosed	Dacite-andesite porphyrites
	Lava-tuff breccia and fine basic tuffs	Achean group
	Tuffogenic phyllites, sandstones	Biotite-plagioclase gneisses
	Actinolitized lava-breccias, tuff-lavas and tuff-breccias	Biotite-plagioclase gneisses with high-alumina minerals (garnet, staurolite, andalusite, sillimanite)
	Talc-chlorite & carbonate-chlorite schists after ultramafic & mafic tuffs & effusives	Two-mica gneisses, schists w. high-alumina minerals
	Sericite schists, metamorphosed weathered layer	Biotite-amphibole-plagioclase gneisses
	Diabases, actinolitized diabases	Amphibolites
	Actinolitized pillow-lava diabases	Amphibolites with cummingtonite
	Porphyroblastic actinolitized diabases	Metaultramafics and biotite-amphibole schists
	Magnetite-amphibole-plagioclase schists after diabase	Porphyritic biotite granites
	Amphibole-plagioclase schists after diabases	Sulfide impregnation
		Magnetite impregnation
		Zone of cataclasis

## DRILLING

### Technological and Scientific Basis for Choosing of the Drilling Equipment

This section contains the main results of scientific studies of the principal problems of superdeep drilling in crystalline rocks with continuous coring.

#### Parameters of Drilling

Theoretical determination of the major parameters of drilling was based on the analytical function  $T_{np} = t(h_{cp} v_{cno} v_M)$ . Optimum combination of these factors results in minimum time of drilling.

$T_{np}$  - Useful time of drilling

$h_{cp}$  - Average drilled interval during one round trip

$v_{cno}$  - Speed of round trip

$v_M$  - Mechanical speed of drilling

#### Design of the Well

Information on characteristics of rocks adequate for design of the Kola well were not available. The technology that permits corrections during drilling was applied. Essence of the method was as follows. After permanent casing of the drilled interval, a temporary casing that can be withdrawn is fixed on the surface. Then the drilling resumes. If new casing is required, the temporal case is withdrawn and the drill hole is widened.

#### Stability of Rocks around the Drill Hole

Different components of the stress field have been theoretically assessed. Expected behaviour of rocks around the drill hole depending on depth and their physical characteristics are shown in Fig. III.5., where  $G_{nm}$  = hydrothermodynamic stability,  $H$  = depth.

## Permissible Parameters of the Spatial Trajectory of the Well

Calculations show very tough requirements to the parameters of inclination of the deep wells, especially in their upper intervals. See Figure III.6.

### Method and Regimes of Drilling. Prognosis of Indices of the Wear and Tear of Bits

Calculations showed significant advantages of turbodrilling over rotary drilling at depths over 10 km. Optimum frequency of rotation appeared to be 100 to 200 rotations per minute. Thermostable reduction turbodrill has been found to be the best bit when temperature exceeds 150°C.

### Drilling Device

Calculations have been done to develop light alloys with required properties for the drilling pipes. At the top of the pipe string, steel piping 1.5 to 2 km long is recommended; then aluminum below this. Analysis showed strength requirements for the tool joints.

### Drilling Mud

Analysis of the drilling conditions revealed certain advantages of drilling and with coarser clay particles; kaolinite rather than bentonite should be the base for the drilling mud.

### Coring

Sticking of core in the core holder is the major problem of successful coring, especially in fractured rocks. Technological requirements for the coring tool that can decrease sticking are discussed.

### Control of Technological Parameters of the Drilling Process

It is proposed that bottom well information be obtained by a hydraulic telemetric system.

### Drilling Rig

Hoisting capacity of the drilling rig must be not less than 4000 kH. For casing of crystalline rocks at great depths specially designed (using foreign models), built-in, round trip mechanism of large hoisting capacity can be used. Required characteristics of the pump are: Hydraulic power 930-1100 kilowatts, maximum pressure of supercharging 35-40 MPa. These and other technological requirements were considered during design of the rig "Uralmash-15000." A three-step system can provide adequate cleaning of the drilling mud.

## SURFACE DRILLING EQUIPMENT AND SERVICES

### Drilling Equipment and Electric Drive

To depth of 7,000 m the well has to be drilled by the rig "Uralmash-4E" and deeper by the rig "Uralmash-15000."

### Controlling System for Technological Purposes

The controlling system consists of several subsystems: Control of mechanical drilling, round trip, and flush, and control of the main parts of the drilling equipment.

### Services

Services on the well consist of two complexes: One to service major operations for drilling and logging and another to support organization of the drilling process. The first is located on the platform of the rig and adjoining building. The second includes repairing shops, warehouses, stores for core, etc.

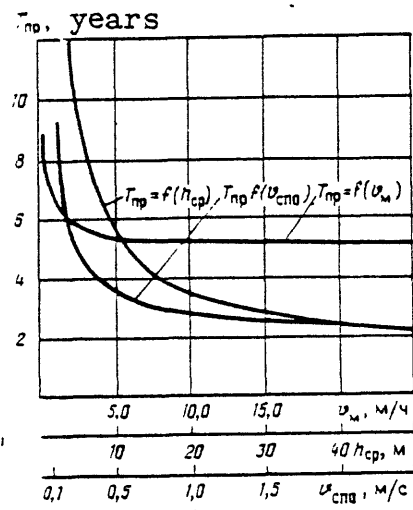


Figure III.1.--Dependence of  $T_{np}$  on basic parameters.

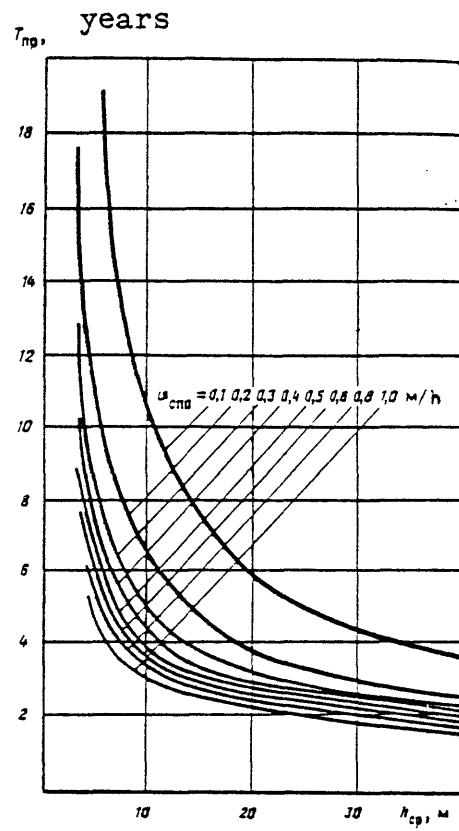


Figure III.2.--Dependence on  $T_{np}$  on  $H_{cp}$  if  $U_M = 2.5$  meter/hour.

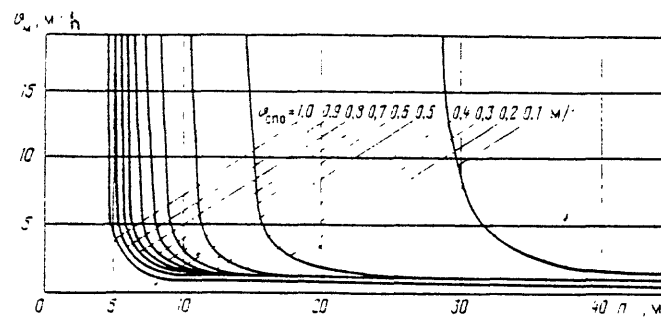


Figure III.3.--Graph for choosing of basic parameters with  $T_{np} = 5$  years.

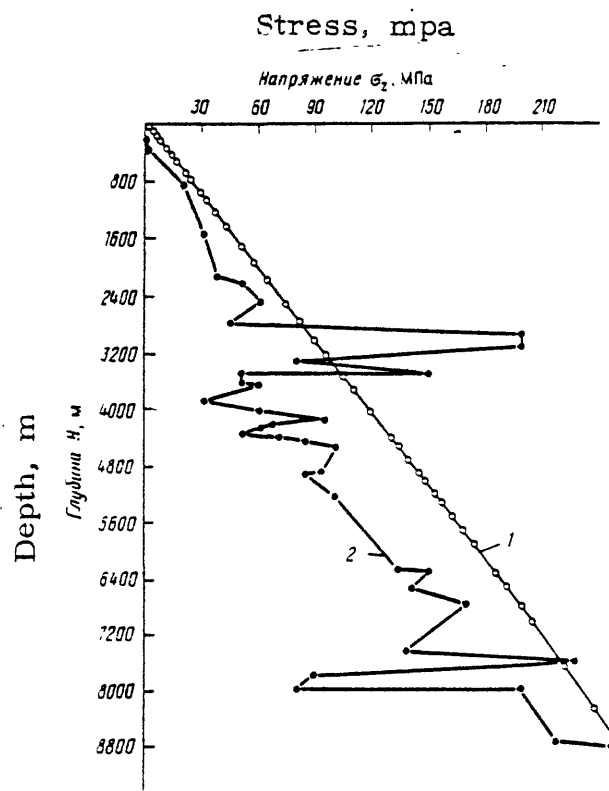


Figure III.4.--Dependence of stress ( $\sigma_z$ ) from depth (H). 1 - Calculation on lithostatic load , 2 - Calculation on elastic characteristics of rocks.

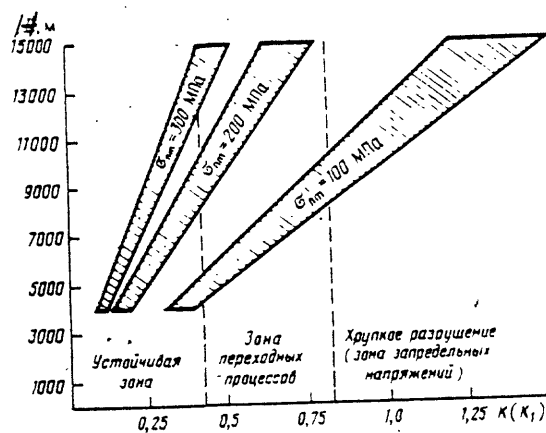


Figure III.5.--Relationship of stability of rocks around the drill hole on H and  $G_{lm}$

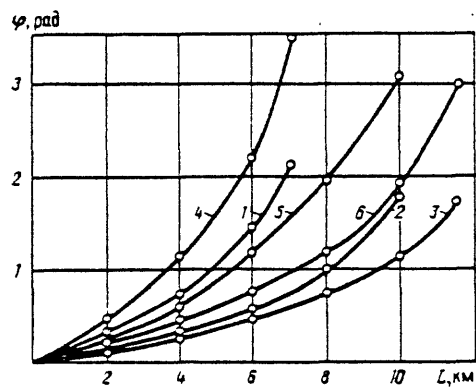


Figure III.6.--Dependence of permissible change of the total angle of inclination ( $\varphi$ ) from depth of a well. 1, 2, and 3 - depths of 7, 10, and 11.5 km with  $T = 300 \text{ kH}$  ( $T$  - friction between the drilling string and walls of the hole). 4, 5, and 6 - the same with  $T = 600 \text{ kH}$ .

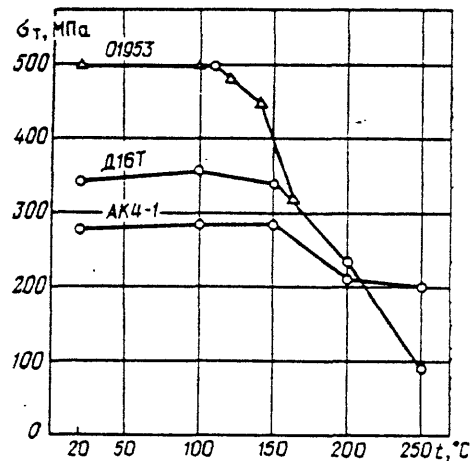


Figure III.7.--Dependence of strength of aluminum pipes on temperature (heating for 100 hours).

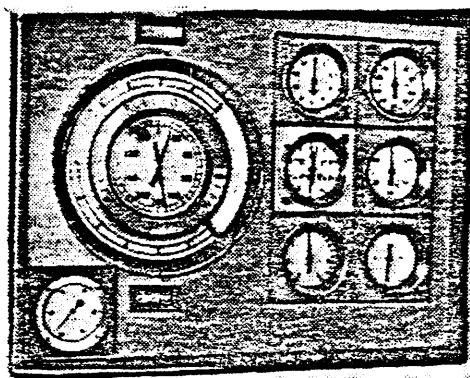


Figure III.17.--Apparatuses on the stand of the driller.

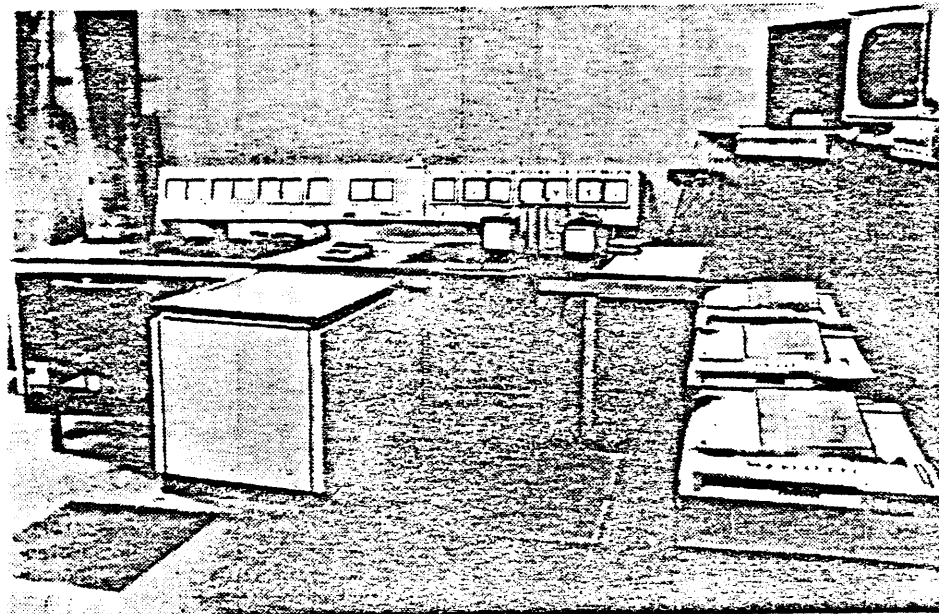


Figure III.18.--Room of the controller.

## Drill Bits

Several types of drill bits shown on the pictures were used during drilling with coring. The bit in Fig. III.21 was specially designed for this well, others were modernized. All the bits are used for rotary drilling except of ISM-214,3/60T (Fig. III.28) that is designed for turbodrilling with coring. Figs. III.30 through III.34 show reamers (to increase the diameter of the hole), and Fig. III.35 demonstrates the design of the centralizer.

## Equipment for Coring

Three types of coring mechanisms have been specially designed for drilling of the superdeep well. Two of them are shown in Figs. III.36 and III.37.

Turbodrilling with coring scientifically approved for the superdeep well required a significant amount of research and design work. The main aims were to decrease the rotation frequency with maintenance of the high torque characteristics, to increase the thermal stability, and improve reliability.

## Highly Durable Drill Pipes

Drill pipes made of light alloys (LBTVK0147) and steel joints (ZLK-178) (Fig. III.46) are used for deep and superdeep turbo and rotary drilling. Traperziform threads specially developed for the well are used in joints. Steel drill pipes (TBVK-140) (Fig. III.47) are used in difficult and complicated conditions of drilling.

## Drill Muds

Several types of drilling muds were used in the superdeep well. Changes in the composition of muds were necessary because of increasing depth of the well and rise of temperature.

## Telemetric System of Indication of Rotation

### Frequency of Bottomhole Motors

The system was developed in the Kola Exploration Expedition and applied from the depth of 9745m. It includes a downhole generator of impulses GIZ.03 and well head receiving device UNP-1. The most important part of the system that requires high reliability is a downhole generator working in conditions of high temperatures, high pressure, chemically active environment, and strong vibrations.

## Equipment of the Well Head

The superdeep well was drilled in crystalline rocks and no significant flow of formation liquids was expected. Thus, the equipment of the well head was simplified. This equipment permitted drilling of the advancing hole, reverse circulation, turning and change of the string, and different auxiliary operations.

## Assemblage of the Lower Part of the Drill Pipe

Depending on the particular purposes and technical conditions, different assemblages of the lower part of the drill pipe were used. The most important

was the requirement for maximum coring and maintenance of the verticality of the hole.

#### Technical Means for Preventive Maintenance

With increasing depth of the bore hole, the preventive inspection becomes more and more complicated. Usual procedures become less effective or useless all together. Special technical situations developed that can result in a breakdown, including the drill pipe float valve, mechanical and hydraulic downhole catchers for metal, mechanical, and hydraulic disconnectors of the drill pipe.

#### Composite Interpretation of the Technical-Economical Results of Drilling

This section considers the main regularities of the process of drilling depending on the bore hole depth. An integral index that changes with geological and technical conditions of drilling is applied. Data that characterize the affect of new technology on efficiency of drilling are analyzed. Analysis of the drilling process discloses interrelations between main indices of drilling and geological conditions, permits the development of models of drilling at great depths, and improves technology for further drilling of the Kola well and new wells in analogous situations.

#### Technical-Economical Assessment of the Drilling Process

This section analyses the main indices that reflect efficiency of drilling: penetration rate, penetration per run, round trip time, time of auxiliary work. Time of penetration changed from 21.7% of total time at

0-2000m to 3.1% at 10,000-11,500m. Penetration rate varied between 1.3 and 2.5 m/hour.

#### Major Tendencies of Changes of Drilling Indices With Depth

##### Drillability

Traditional methods of assessment were difficult to apply because the penetration rate and penetration per run were deliberately decreased in potentially complicated zones. In intervals from 0 to 5000m, the drillability worsened with depth and the coefficient of drillability  $K_i$  decreased from 1 to 0.46. In Archaen rocks at 6,000-11,000 the coefficient increased 1.5-2 times compared with the interval of 0-6,000m probably due to changes in the structure of the rocks.

##### Cavity Formation in the Drill Hole

Logging showed that cavities were formed only during drilling, and they hardly grew with time. Destruction of rocks had a brittle character. Another important factor is a fractured structure of crystalline rocks widely present in the superdeep well along its entire length. The largest cavities formed in zones of tectonic contacts between different formations.

##### Temperature in the Drill Hole

To obtain a real measure of temperature, experimental works were carried out during circulation with specially designed autonomous thermometers

at depths of 6015, 6275, 6950, and 10909m. The difference in temperatures of mud moving up and down does not exceed 40°C; distribution of heat flow with depth is linear; <sup>the</sup> equilibrium zone of the temperature gradient in mud column was found at 5000m; the time of restoration of the thermal regime in the well is not more than 50 hours.

Variation of performance of bottomhole motors with increasing depth. During drilling of the well significant difficulties were met because of fast wearing out of bearings in turbines in the first stage of drilling. In the second stage, the lower rotation rate increased the time between ~~repairs~~. At greater depths and temperatures (over 140-150°C) however, the rubber and glues appeared to be of insufficient quality, and this resulted in short working periods of motors before wearing out.

#### Wearing of Drill Pipes

Major wearing of drill pipes occurred during round trips. The approach was developed to calculate wearing of drill pipes depending on total length of round trips. The results were used to establish succession of checking of pipes and changing their place in the drill pipe string.

#### Dynamics of Change of the Resistance Force

Specifics of drilling in crystalline rocks result in increased resistance force measured as increase of excessive loading on the drilling hook and in different cross sections of drilling string during pulling out of the string and the torque during rotation. Changes of resistance force with depth has an

exponential character close to linear in the upper intervals and with maximum increase beginning at 1000m from the bottom of the hole. Cuttings at the bottom significantly affect the resistance force.

#### Wearing of Wire Line

Data on wearing of the wireline are shown in Table III.27.

#### Core Recovery

Of the 11,500 m total depth of the drill hole, 9325.2 m were drilled for core recovery. Total length of recovered core is 3700.1 m, or 40.1 percent of the total where core recovery was sought.

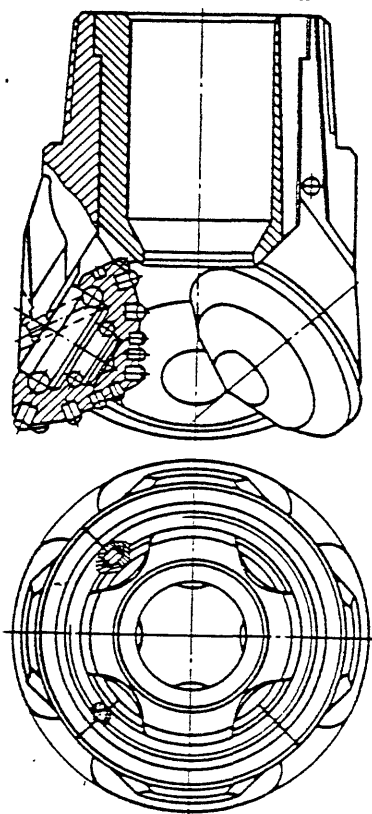


Figure III. 21. Drill bit KC-212, 7/60 TKZ (2B-K212.7/60TKZ

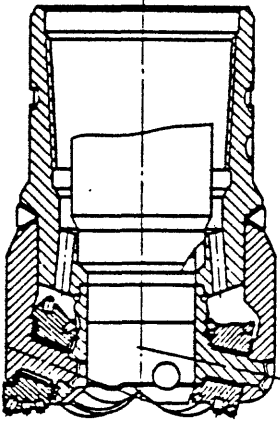


Fig. III. 22

Drill bit 21H-D212.7/80TKZ

Рис. III.22. Бурильная головка  
21Н-Д212.7;80ТКЗ

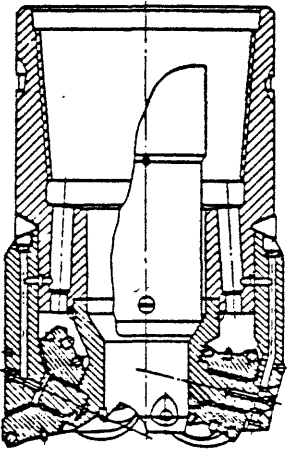
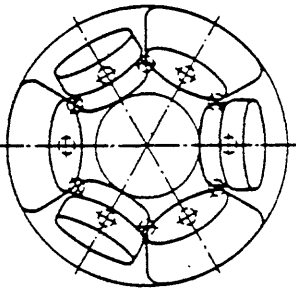
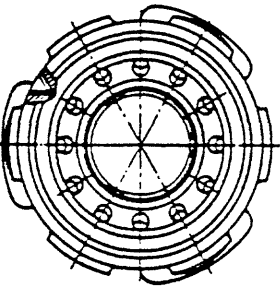
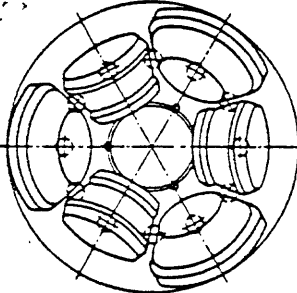
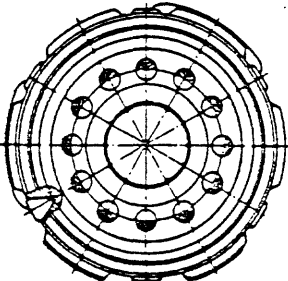


Fig. III. 23

Drill bit KC-212.7/60TKZ-H (25Н-K212.7/60  
TKZ)

Рис. III.23. Бурильная головка  
KC-212.7,60TKZ-H (25Н-K212.7/60TKZ)



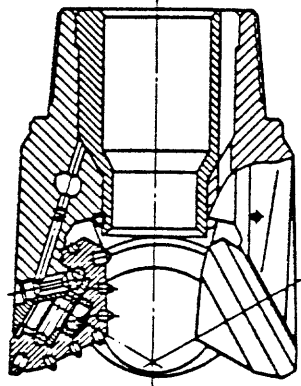


Fig. III.24

Рис. III.24. Бурильная головка  
KC-212.7/60TK3-NY

KS-212.7/60TKZ-NU

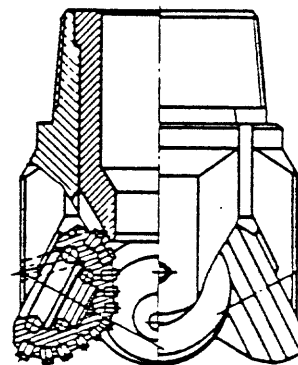


Fig. III.26

Рис. III.26. Бурильная головка  
1Н-K214/60TZ

1Н-K214/60TZ

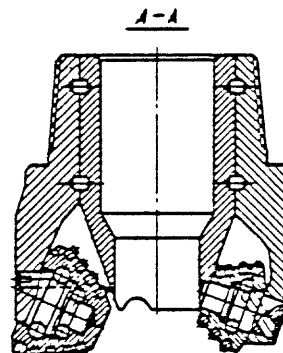
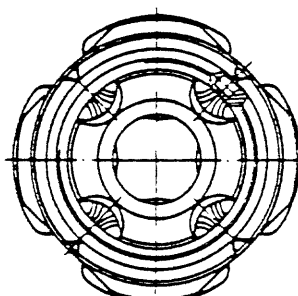
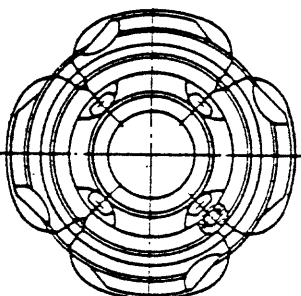
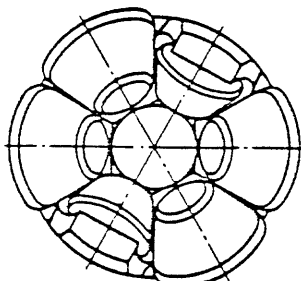
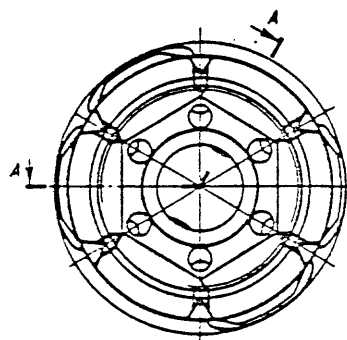


Fig. III.25

Рис. III.25. Бурильная головка  
15N-K214/60KZ

15N-K214/60KZ



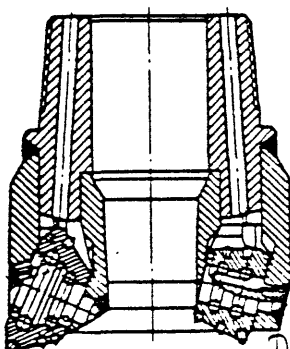


Fig. III.27

Рис. III.27. Бурильная головка 20Н-К214 60К

Drill Bit 20 N - K21-60K

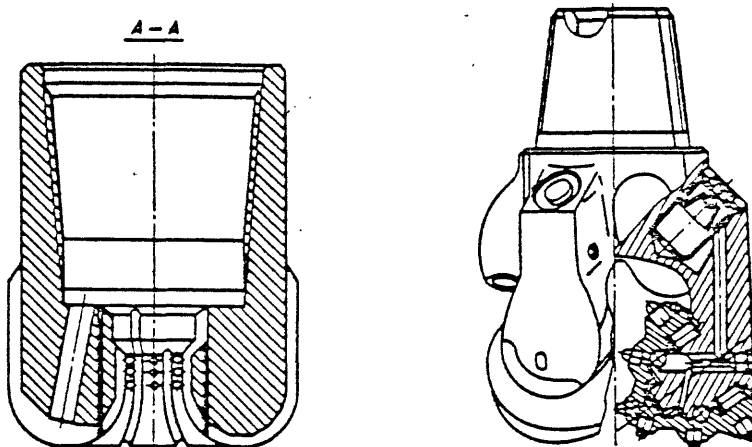
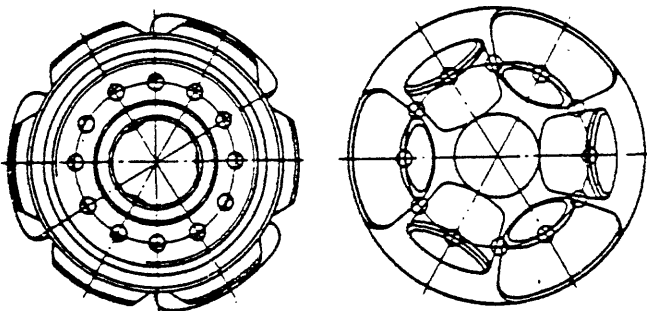


Fig. III.29

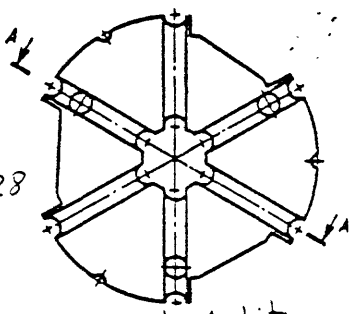


Fig. III.28

Рис. III.28. Бурильная головка НСМ-214,3/60Т  
ISM - 214,3 / 60T

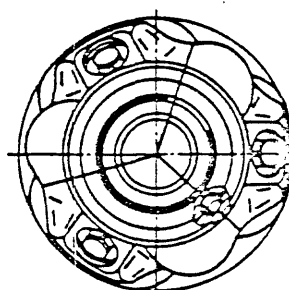


Рис. III.29. Трехшарочечное долото III-215.9TKZ-ГНУ

Tricore bit  
III-215.9TKZ-GNU

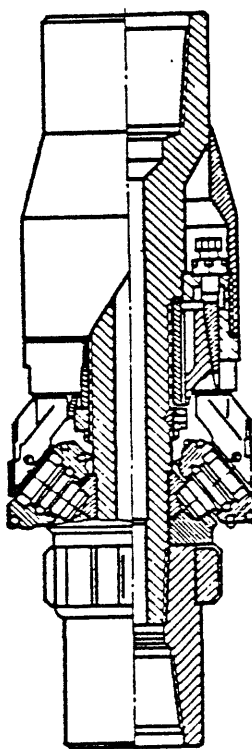


Fig. III.30

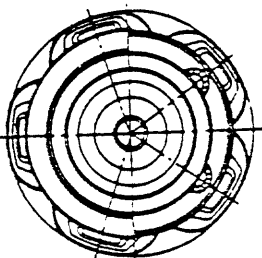


Рис. III.30. Расширитель  
4РШ-295,3/215,9ТК3

- Reamer  
4 RSh - 295,3/-215,  
9 T K Z

Technical characteristics of 4RSh-295,3/215,9TKZ	
Техническая характеристика	
minimum diameter of the hole	Diameter $D_1$ of the reamer
High	Диаметр расширителя, мм . . . . .
Difference in height between cones no more than, mm	Наименьший допустимый диаметр расширяемой скважины, мм . . . . .
	Высота расширителя, мм, не более . . . . .
	Разновысотность шарошек, мм, не более . . . . .
	Диаметр центрального отверстия, мм . . . . .
	Допустимая осевая нагрузка, кН . . . . .
	Масса, кг, не более . . . . .
	Mass, kg, not more than . . . . .
	Permissible axial load, kN . . . . .
	Diameter of the central hole, mm . . . . .

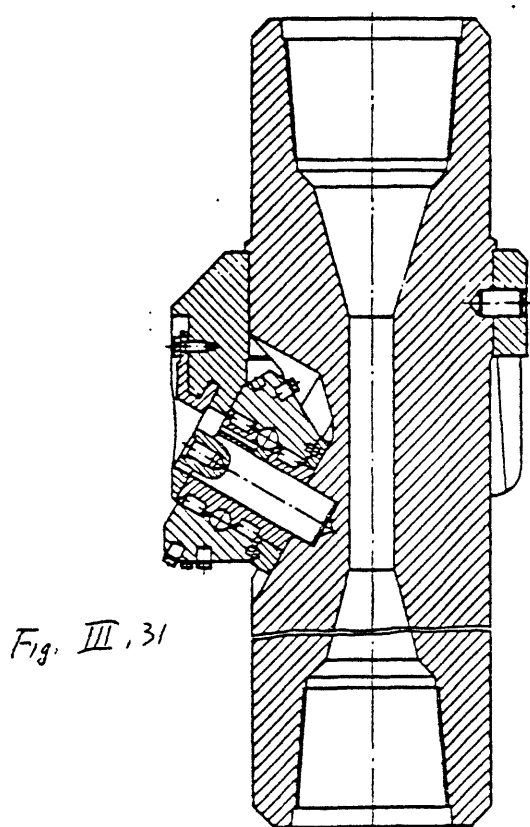


Fig. III.31

Рис. III.31. Расширитель РДУ-394

reamer  
РДУ-394

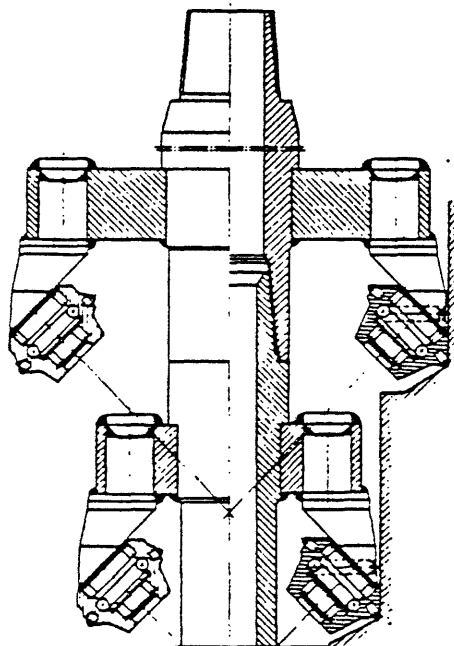


Fig. III.32

Рис. III.32. Расширитель РД-445.640

reamer  
РД-445.640

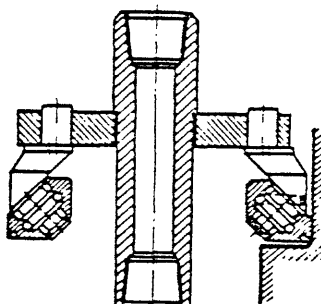


Fig. III.33

Рис. III.33. Расширитель РД-920

reamer  
RD-920

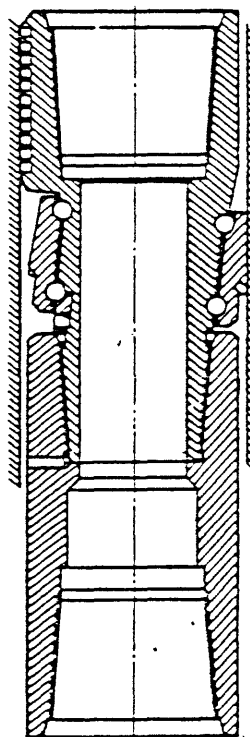


Fig. III.34

Рис. III.34. Расширитель РОП-9В→

reamer ROP-9V

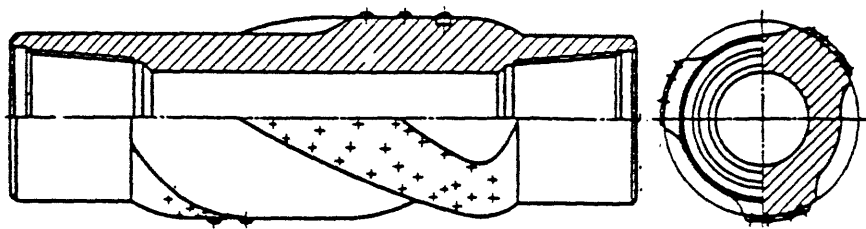


Fig. III.35

Рис. III.35. Центризатор ЦС-212,7СТ

Centralizer TsS-212,7ST

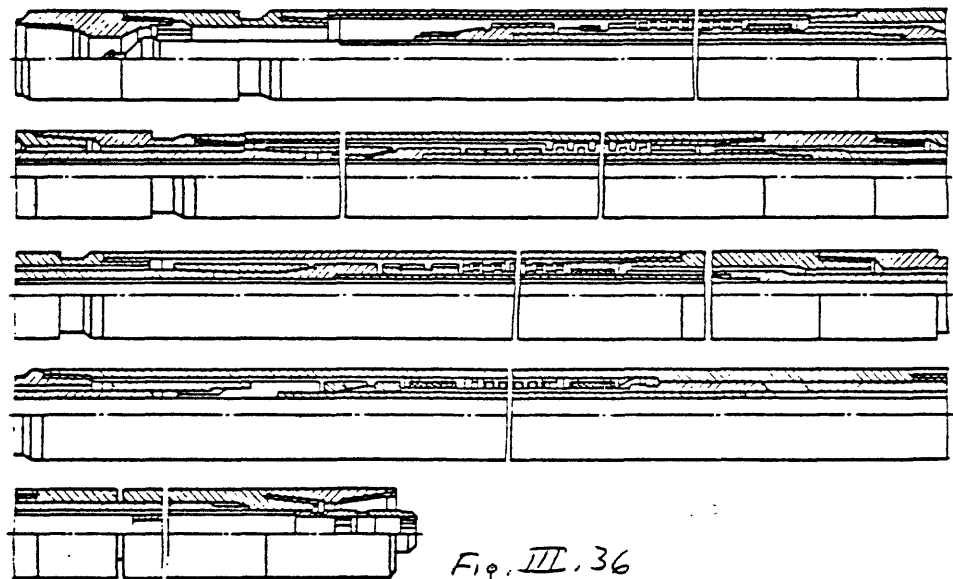


Fig. III.36

Рис. III.36. Турбодолото КТД4С-195-214/60-80

Turbobit КТД4С 195-214  
60-80

Technical characteristics of KTD4S-195-214/60-80  
Техническая характеристика КТД4С-195-214/60-80

1. Length, m	Ф. Длина, м . . . . .	25,92
2. Number of sections	6. Число турбинных секций . . . . .	3
3. Length of sections, m	7. Длина секции, м . . . . .	7,955
4. Length of spindle rod, m	8. Длина шпинделя, м . . . . .	4,415 (4,922)
5. Number of the steps of the turbine	9. Число ступеней турбины . . . . .	315
6. Steps in one section	10. В том числе в одной секции . . . . .	105
7. Steps in the basic section	11. Число ступеней пяты . . . . .	30
8. Number of supports	12. Число средних опор . . . . .	11
9. Among them	13. В том числе:	
10. In one section	14. в одной секции . . . . .	3
11. In spindle rod	15. в шпинделе . . . . .	2
12. Diameter of the body	16. Диаметр корпуса, мм:	
13. External	17. наружный . . . . .	195
14. Internal	18. внутренний . . . . .	165
15. length of the core barrel, m	19. Длина керноприемника, м . . . . .	25,835
16. External diameter of the core barrel, mm	20. Наружный диаметр керноприемной трубы, мм:	
	21. съемной . . . . .	83
	22. несъемной . . . . .	105
	23. removable	
	24. nonremovable	

Continued next page.

19	Внутренний диаметр керноприемной трубы, мм:	
20	съемной . . . . .	70
21	нестъемной . . . . .	86
22	Присоединительные резьбы:	
23	к бурильным трубам . . . . .	3-147
24	к бурильной головке с 60-мм керном . . . . .	3-161
25	к бурильной головке с 80-мм керном МК150×6×1:8 . . . . .	
26	Масса керноприемного турбодолота, кг . . . . .	4450
	Рабочая характеристика турбодолота (Working characteristics)	
27	Расход жидкости, л/с . . . . .	28—36
28	Мощность, кВт . . . . .	84—178
29	Частота вращения, об/мин . . . . .	480—600
30	Крутящий момент на валу, Н·м . . . . .	1450—2380
31	Перепад давления, МПа . . . . .	6.6—10.8

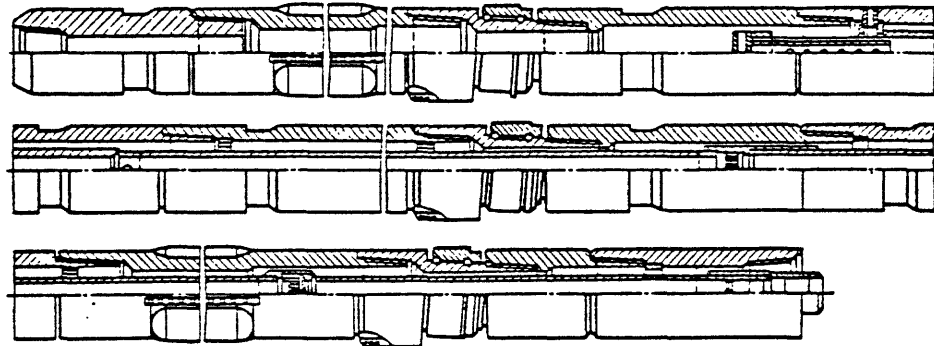


Fig. III.37

Рис. III.37. Керноотборный снаряд КДМ-195-214/60  
Coring system KDM-195-214/60

### Technical characteristics KDM -195-214/60

#### Техническая характеристика КДМ-195-214/60

- 1 - Liquid flow rate, l/sec
- 2 - Permissible load, kN
- 3 - Frequency of rotation per minute
- 4 - Joining threads
- 5 - Upper
- 6 - Lower
- 7 - Diameter, mm, of
- 8 - Drill bit
- 9 - Centrator
- 10 - Body of the section
- 11 - Core
- 12 - Length of the system with 2 sections
- 13 - Length of the core in 2 sections, m

1	Расход жидкости, л/с	20—40
2	Допустимая нагрузка, кН	160—200
3	Частота вращения, об/минн	60—600
4	При соединительные резьбы:	
	5 верхняя	3-117
	6 нижняя	3-161
7	Диаметр, мм:	
	8 бурильной головки	212—214
	9 центратора-калибратора	212—214
	10 корпуса секции	195
	11 керна	60
12	Длина снаряда в двухсекционном исполнении, м	18,58
13	Керновместимость в двухсекционном исполнении, м	15,5

Bottom hole motors (turbines)

ЗАБОЙНЫЕ ДВИГАТЕЛИ

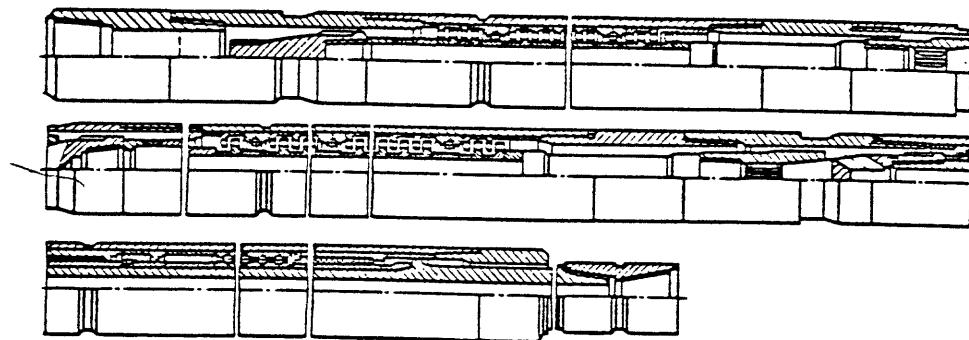


*Fig. III. 38*

Рис. III.38. Турбобур А7Ш

Turbobit A7SH

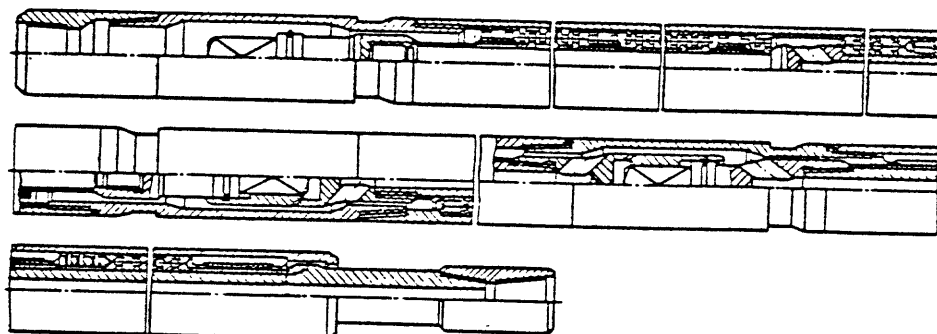


*Fig. III. 39*

Рис. III.39. Турбобур А7ГТШ-1

Turbobit A7GTSH-1

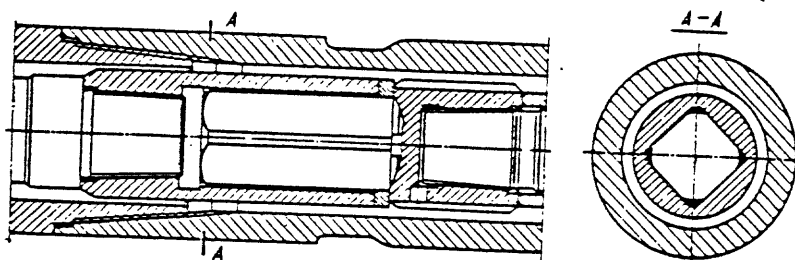


Рис. III.40. Соединение валов турбобура и шпинделя

Joining of the shafts of the turbobit and spindle

*Fig. III. 40*

Fig. III.41

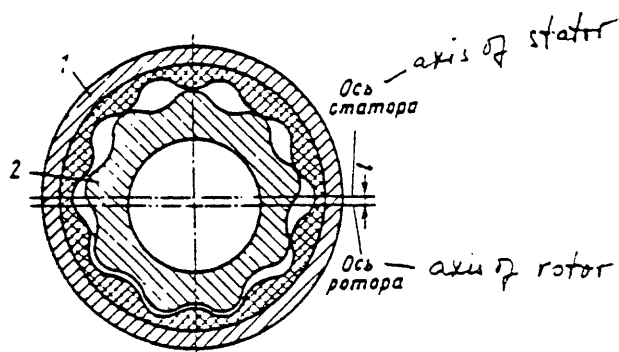


Рис. III.41. Поперечное сечение винтового двигателя  
Cross section of the spiral (scroll) pump

Fig. III.42

Technical drawings of three views of the D2-172M spiral bottom-hole motor, showing its internal structure and components.

Рис. III.42. Винтовой забойный двигатель Д2-172М  
Spiral bottom-hole motor D2-172M

Fig. III.43

Characteristics of the spiral bottom-hole motor D2-172M

$p$  - pressure,

$n$  - frequency of rotation

Net-power

jet-Efficiency

(liquid is water, flow rate  $Q = 23 \text{ l/sec}$ )

On the horizontal axis is torque

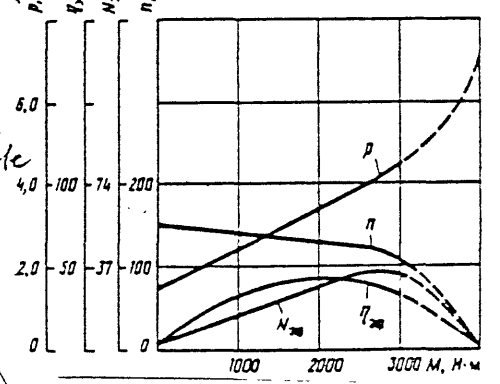


Рис. III.43. Характеристика винтового забойного двигателя Д2-172М:  
 $p$  — давление;  $n$  — частота вращения;  $N_{\text{净}}$  — мощность;  $\eta$  — к. п. д. (промывочная жидкость — вода, расход  $Q=23 \text{ л/с}$ )

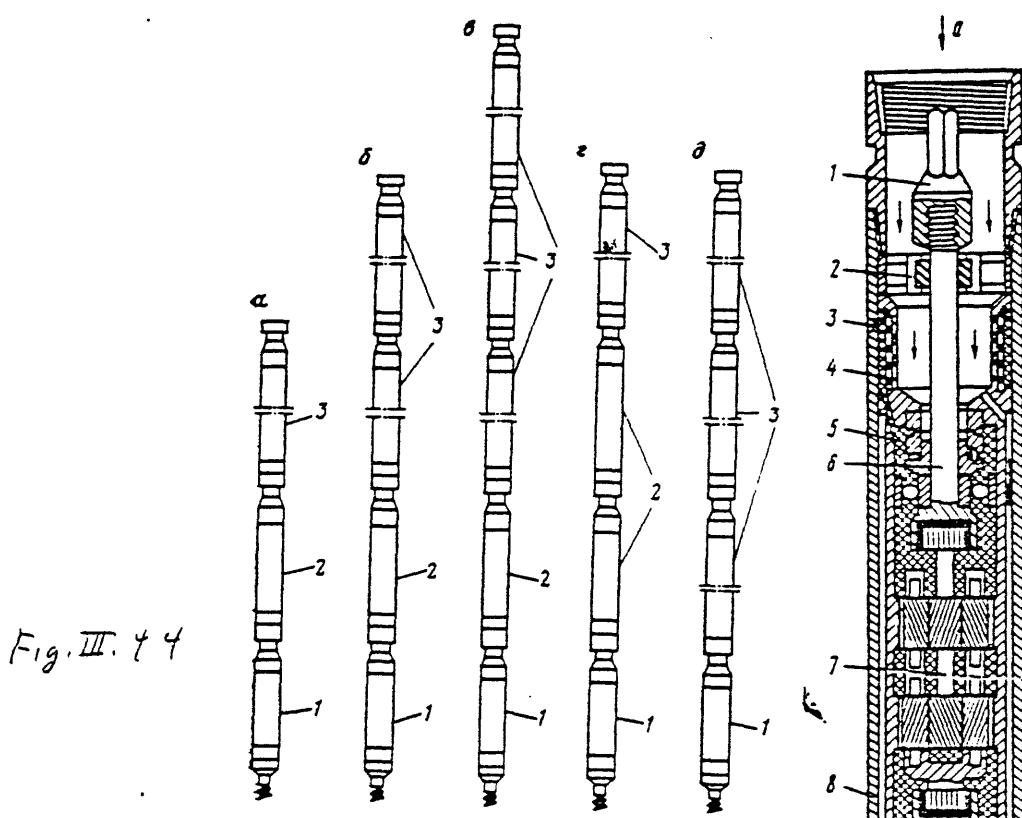


Fig. III.44

Рис. III.44. Варианты компоновки двигателя с использованием редукторной вставки РМ-195  
Variations of assembly of the motor with reduction insert RM-195

Fig. III.45

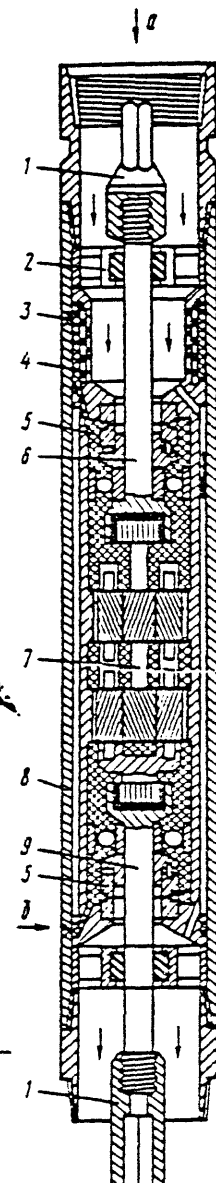


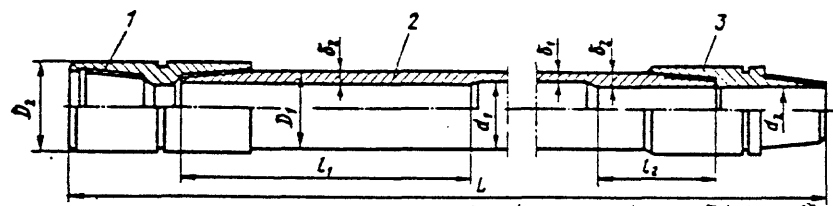
Рис. III.45. Редуктор турбобура РМ-195:  
a - буровой раствор; б - масло

Reducer of the turbobit RM-195  
a - drilling mud, b - oil

Вариант компоновки двигателя (см. рис. III.45)	Секция турбобура	Число ступеней турбины	Редуктор / РД	Длина компоновки, м	Масса компоновки, кг	Переводное отношение	Flow of component		Крутящий момент, Н·м	Максимальная мощность, кВт	Нормальная мощность, кВт	Предел запасания, МН	Коэффициент полезного действия, %
							шага	частоты вращения, об/мин					
a	1	109	1	13,7	2600	3,69	24-28	150-175	2200-3020	35-55	2,2-2,9	-	64
б	2	218	1	21,2	+000	3,69	20-28	125-175	3080-6040	+1-110	3,1-6,1	-	64
в	3	327	1	28,6	5+00	3,69	18-20	115-125	3740-4620	+5-61	3,7-4,6	-	64
г	1	109	2	17,2	3260	11,76	20-28	35-48	5230-10250	20-52	1,6-3,2	-	59
д	3	327	-	25,9	+740	-	24-30	560-700	1960-3060	115-225	6,5-10,0	-	70

Примечание. Энергетические данные турбобура соответствуют жидкости плотностью 1 г/см<sup>3</sup>.

Table III.12

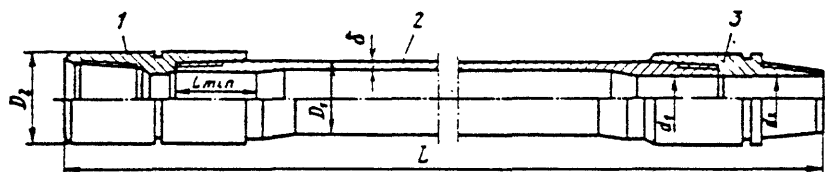


Drill pipe LBVK-147 with joints ZLK-178

Рис. III.46. Бурильная труба ЛБВК-147 с замками ЗЛК-178:  
1 — муфта; 2 — труба; 3 — ниппель

1 - Coupling, 2 - pipe, 3 - nipple

Fig. III.46



Drill pipe TBVK-140 with joint ZSK-178

Рис. III.47. Бурильная труба ТБВК-140 с замком ЗШК-178:

1 — муфта; 2 — труба; 3 — ниппель

1 - Coupling, 2 - pipe, 3 - nipple

Fig. III.47

Fig. III. 48

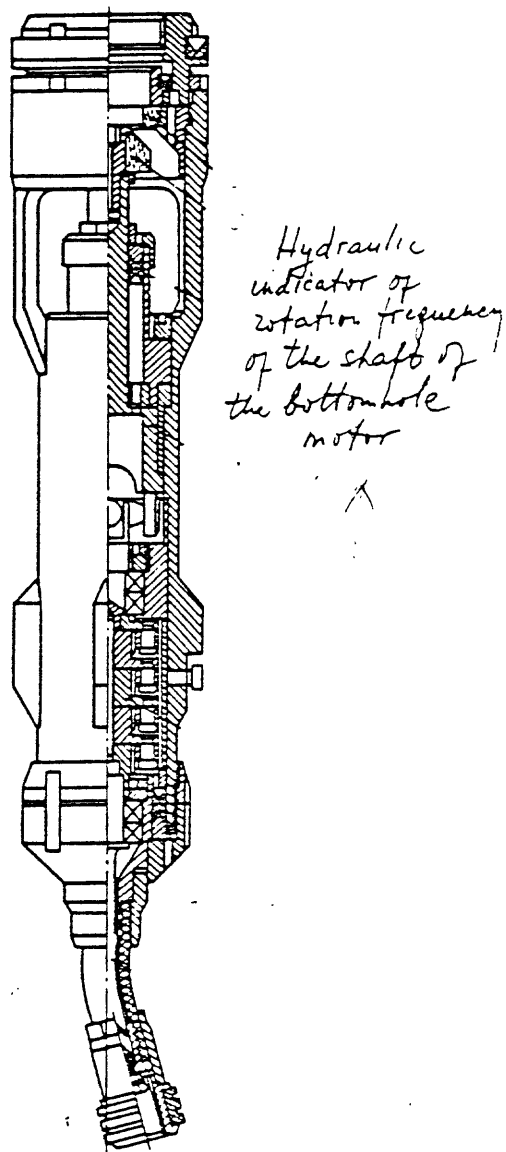


Рис. III.48. Гидравлический индикатор частоты вращения вала забойного двигателя

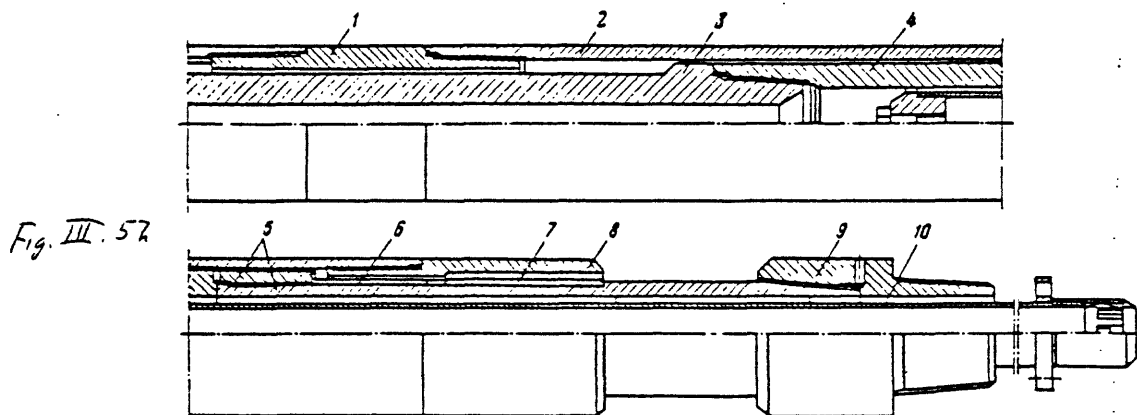


Fig. III.52

Рис. III.52. Керноприемная надставка КН-2 к турбобуру  
core barrel extension KN-2 to the turbobit

Fig. III.53

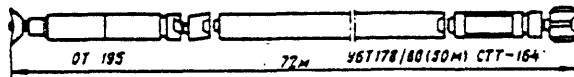


Рис. III.53. Компоновка для борьбы с кривизной ствола скважины активного типа

1 - nut, 2 - body,  
3 - lead disk  
4 - circulation pipe  
5 - lower reducer

### Device of pendulum-kind assembly

Рис. III.54. Конструкция маятниковой компоновки:  
1 - поджимная гайка; 2 - корпус; 3 - свинцовый диск; 4 - циркуляционная труба; 5 - нижний переводник

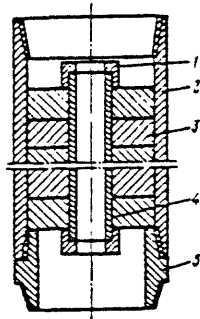


Fig. III.54

Fig. III.55

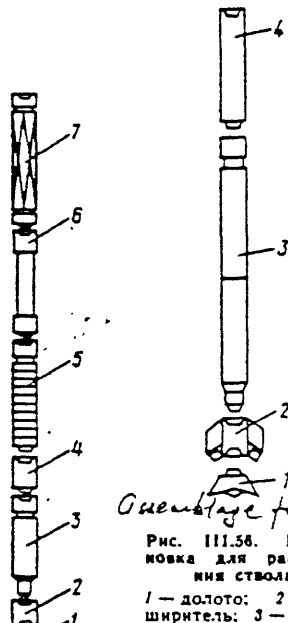


Fig. III.56

### Assembly for dilatation of the hole

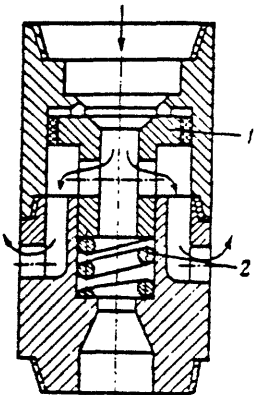
Рис. III.56. Компоновка для расширения ствола:

1 - долото; 2 - расширитель; 3 - турбодрill  
4 - УВТ

### assembly for drilling of a new hole

Рис. III.55. Компоновка для забуривания нового ствола:

Fig. III.57



Drill pipe float valve

Рис. III.57. Перепускной клапан бурильной колонны

Fig. III.58

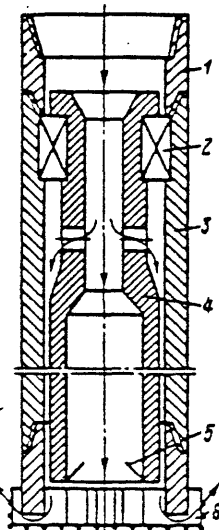


Рис. III.58. Механический забойный ловитель металла  
Downhole metal catcher

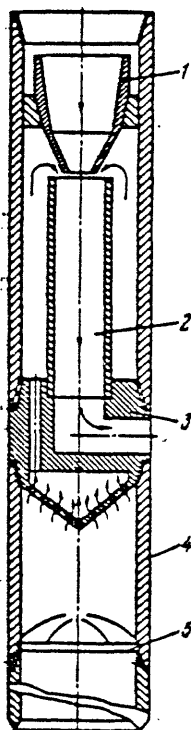


Рис. III.59. Гидравлический забойный ловитель металла  
Hydraulic downhole metal catcher

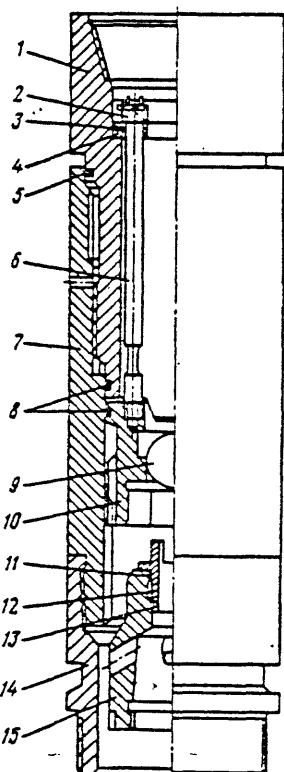


Рис. III.60. Разъединитель бурильной колонны РБК-195  
Disconnecter of the drill pipe RBK-195

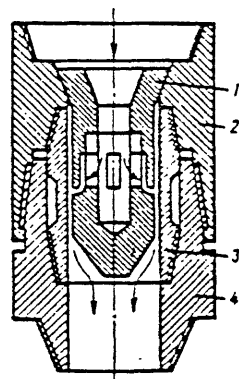


Рис. III.61. Гидравлический разъединитель бурильной колонны ГРБК-195

Hydraulic disconnect of the drill pipe GRBK-195

Fig. III.59

Fig. III.60

Fig. III.61

Table III.18

ТАБЛИЦА III.18

Глубина замера температуры, м Depth of temperature measurement, m	Температура, °C Temperature, °C		Длина спущенной бурильной колонны, length of drill pipe, m
	статическая static	динамическая dynamic	
890	34.6	—	—
299	45.1	—	—
3470	51.5	—	—
4000	58.6	—	—
4540	67.4	—	—
4850	75.0	—	—
6015	93.2	82.5 *	—
6275	97.5	90.6 *	10 600
6510	110.5	103.6 *	10 160
6950	1116.6	109.5 *	10 160

\* Расход промывочной жидкости 32–34 л/с.  
Flow of mud 32–34 l/sec

Table III.19

ТАБЛИЦА III.19

Глубина замера температуры, м Depth of temperature measurement, m	Температура, °C Temperature, °C	
	статическая static	динамическая dynamic
3 960	56.8	43.0 *
6 350	98.2	89.0 *
7 800	123.0	—
8 230	131.0	123.0 *
10 425	167.8	161.0 *
10 909	181.0	147.6
10 909	181.0	146.6
10 909	185.4	—
after 14½ hours of interruption После 42 ч остановки		
10 909	185.4	150.6
10 100	132.0	—

\* Температуру замеряли после промежуточных промывок (15–20 мин); расход промывочной жидкости — 34 л/с.

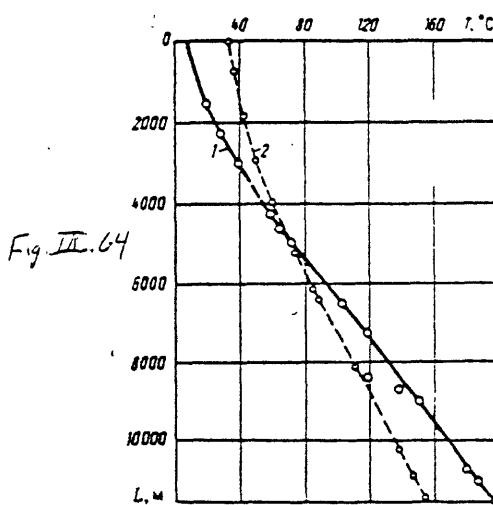


Fig. III.64

→ Рис. III.84. График распределения температуры в стволе скважины:  
1 — статической; 2 — динамической, уставновившейся при  $Q = 32$  л/с

Chart of distribution of temperature in the well bore  
1—static, 2—dynamic at flow of 32 l/sec

↓ Рис. III.85. Восстановление температуры во времени  
Restoration of temperature with time

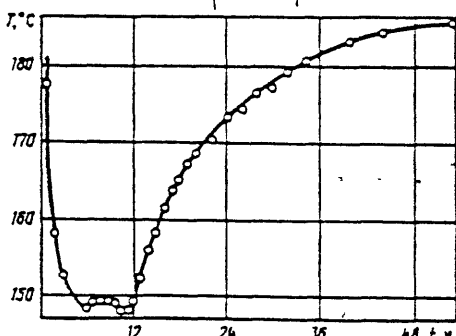


Fig. III.65

Table III.16

Interval of drilling Интервал бурения, м	Average hardness of stamp Г, МПа Средняя твёрдость по штампу, МПа	Number of runs Число рейсов	Average penetration per run m	Average time of penetration hours	Frequency of rotation, rev/min Частота вращения, об./мин	ТАБЛИЦА III.16		Coefficient коэффици- ент $K_1$						
						rotation, mm Углубление за оборот, мм	calculated расчетное							
Loading $P_1 = 80 \pm 20$ kN														
0—1000	—	—	—	—	—	—	—	—						
1000—2000	1800	7	7.6	2.44	350	0.31	0.149	1						
2000—3000	1870	11	6.3	3.37	300—500	0.3	0.082	0.55						
3000—4000	3260	17	4.0	2.62	300—500	0.179	0.083	0.55						
4000—5000	2860	11	4.2	3.01	300—500	0.179	0.077	0.51						
5000—6000	—	—	—	—	—	—	—	—						
6000—7000	2000	24	8.0	2.34	350—450	0.283	0.163	1.09						
7000—8000	2320	6	8.1	1.91	350—450	0.227	0.183	1.23						
8000—9000	2370	11	6.0	1.71	300—400	0.227	0.203	1.36						
9000—10 000	2300	3	15.0	3.2	300	0.227	0.262	1.76						
Loading $P_1 = 20 \pm 20$ kN														
0—1000	2390	12	7.2	3.06	500—700	0.057	0.068	1						
1000—2000	1710	19	7.5	3.75	600	0.07	0.055	0.82						
2000—3000	2110	17	6	3.38	500—800	0.065	0.031	0.43						
3000—4000	—	—	—	—	—	—	—	—						
4000—5000	2250	10	3.6	2.92	650	0.060	0.032	0.47						
5000—6000	2210	10	8.8	6.94	500	0.050	0.044	0.65						
6000—7000	2000	13	8.4	4.01	500	0.065	0.078	1.15						
7000—8000	1700	10	9.6	5.57	500	0.07	0.099	1.45						
8000—9000	2510	8	6.8	2.99	500	0.057	0.08	1.18						
9000—10 000	2410	6	8.1	2.38	600	0.057	0.094	1.4						

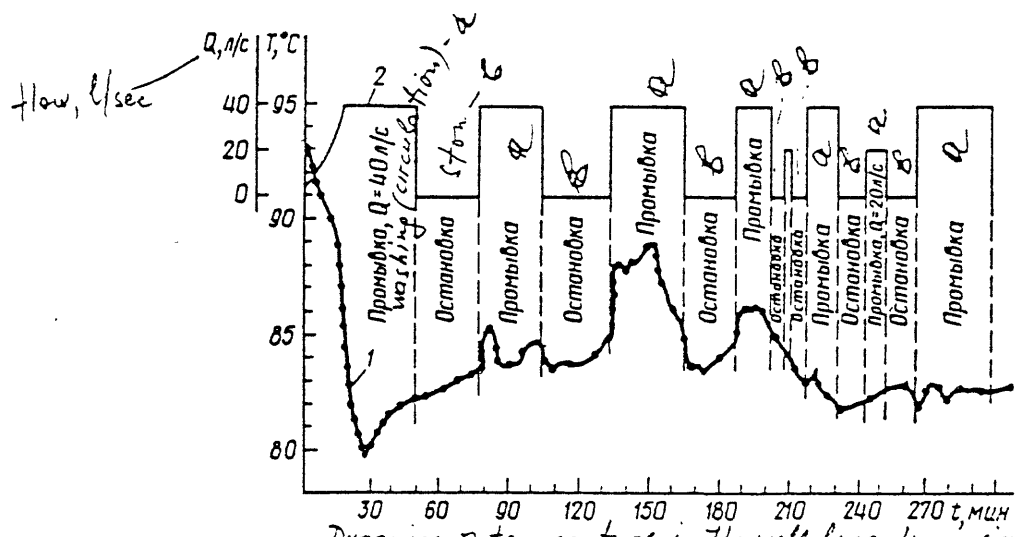


Fig. III.66

Рис. III.66. Динамика температуры в скважине при промывках (глубина 6015 м):

1 — температура; 2 — расход жидкости  
1 — Temperature, 2 — mud flow

a — circulation; b — at rest.

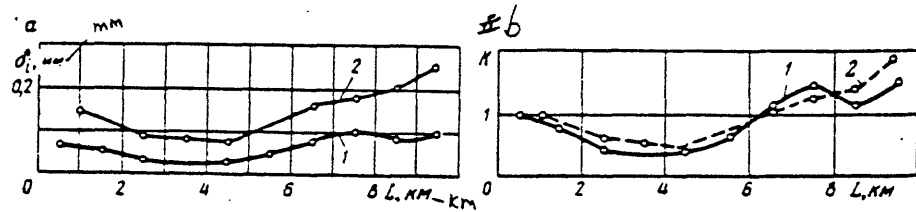


Рис. III.62. Зависимость углубления за один оборот долота (буримости)  $a$  и коэффициента буримости  $b$  от глубины скважины:  
1 — нагрузка  $20 \pm 20$  кН при  $n = 300 \div 700$  об/мин; 2 — нагрузка  $80 \pm 20$  кН при  $n = 300 \div 500$  об/мин

Fig. III.62

Penetration per one rotation of a bit  
(drillability)  $a$  and  
coefficient of drillability  
( $b$ ) versus depth of  
the well

1 - Loading  $20 \pm 20$  kN  
at  $500 \div 700$  wt./min  
2 - Loading  $80 \pm 20$  kN at  
 $n = 300 \div 500$  rotation  
per minute

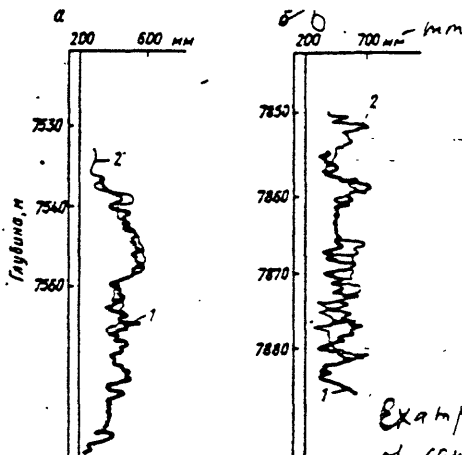


Fig. III.63

Examples of dynamic  
of changes of caves  
in time

a - For interval  
7530-7580 m, 1 - May 8  
2 - August 14  
b - For interval  
7850-7880 m, 1 -  
March 1, 2 - June  
30

ТАБЛИЦА III.17

Interval of measured height, m	Volume of well bore, m <sup>3</sup> , at bottom of casing, m <sup>3</sup> , in		Interval of measured height, m		Volume of well bore, m <sup>3</sup> , at bottom of casing, m <sup>3</sup> , in		Interval of measured height, m		Volume of well bore, m <sup>3</sup> , at bottom of casing, m <sup>3</sup> , in		Interval of measured height, m		Volume of well bore, m <sup>3</sup> , at bottom of casing, m <sup>3</sup> , in		Interval of measured height, m		
	1976 r.	1977 r.	8.V	4.II 1979 r.	12.II 1981 r.	13I — 06.III	1978 r.	2.IX 1978 r.	30.X 1978 r.	27.II 1979 r.	15.VII 1979 r.	6.X 1979 r.	17.VI 1980 r.	5.III 1980 r.	25.XII 1983 r.	14.IV 1984 r.	8.X 1982 r.
0—2000																	
2000—2100	3,59		4,26	4,31	4,32	5,55	7 500—7 500			11,74	13,04						
2100—2200	4,89		5,31	4,87	5,04	7 600—7 700			11,79	13,44							
2200—2300	4,78		5,1	4,83	5,19	5,56	7 700—7 800			9,29	11,22						
2300—2400	5,14		5,47														
2400—2500	5,26		5,6	5,24	5,56	7 800—7 900			10,28	12,45							
2500—2600	4,82		5,18	4,87	5,3	7 900—8 000			8,99	7,17	8,47						
2600—2700	4,56		4,6	4,37	4,78	8 000—8 100			10,78	6,48	10,9						
2700—2800	5,32		5,76	5,39	6,04	8 100—8 200			10,29	10,23	10,3						
2800—2900	4,52		4,56	4,81	4,99	8 200—8 300			10,63	9,51	9,35						
2900—3000	4,15		4,26	4,25	4,27	8 300—8 400			8,86	7,76	8,49						
3000—3100	4,15		4,3	4,25	4,18	8 400—8 500				6,68	6,19						
3100—3200	4,18		4,33	4,35	4,43	8 500—8 600			10,69	10,69	10,15						
3200—3300	4,23		4,48	4,37	4,14	8 600—8 700				5,01	5,35						
3300—3400	4,12		4,41	4,29	4,09	8 700—8 800						5,76					
3400—3500	4,09		4,34	4,26	4,17	8 800—8 900						8,37					
3500—3600	4,01		4,67	4,27	4,18	8 900—9 000						7,52	7,96				
3600—3700	4,30		4,83	4,57	4,66	9 000—9 100						7,72	7,11				
3700—3800	4,37		5,1	4,49	4,57	9 100—9 200						9,47	9,19				
3800—3900	4,25		4,79	4,56	4,5	9 200—9 300						7,72	7,46				
3900—4000	4,1		4,48	4,25	4,23	9 300—9 400						7,73	7,54				
4000—4100	4,1		4,45	4,23	4,14	9 400—9 500						8,00	8,55				
4100—4200	3,85		4,45	3,89	4,14	9 500—9 600						6,85	10,84				

Table III. 17 continued

4200—4300	4.13	4.71	4.32	4.05	9 600—9 700	6, 61
4300—4400	4.03	4.87	4.64	4.34	9 700—9 800	7, 9
4400—4500	4.32	4.95	4.67	4.51	9 800—9 900	9, 7
4500—4600	6.56	8.29	7.08	8.37	9 900—10 000	5, 84
4600—4700	7.62	10.81	8.38	8.3	10 000—10 100	5, 89
4700—4800	4.14	4.87	4.47	4.23	10 100—10 200	6, 82
4800—4900	5.66	7.26	5.49	5.87	10 200—10 300	6, 19
4900—5000	6, 56	8.19	6.82	7.18	10 300—10 400	6, 63
5000—5100	5.11	6.24	5.19	5.46	10 400—10 500	6, 55
5100—5200	5.39	6.24	5.57	5.62	10 500—10 600	8, 07
5200—5300	6.14	8.76	6.63	6.29	10 600—10 700	9, 16
5300—5400	6.78	8.39	7.35	7.58	10 700—10 800	8, 28
5400—5500	5.02	5.85	6.01	5.69	10 800—10 900	8, 50
5500—5600	4.39	5.10	4.75	4.52	10 900—11 000	7, 68
5600—5700	4.48	5.35	4.74	4.6	11 000—11 100	9, 10
5700—5800	5.09	6.78	5.43	5.31	11 100—11 200	7, 40
5800—5900	6.72	10.40	8.74	6.14	11 200—11 300	6, 84
5900—6000	7.37	9.78	8.3	11 300—11 400	7, 21	
6000—6100	4.98	6.15	5.47	11 400—11 500	7, 25	
6100—6200	5.37	6.97	6.02			
6200—6300	6.39	9.56	7.59			
6300—6400	5.19	7.74	6.19			
6400—6500	6.48	8.91	8.03			
6500—6600	4.39	7.21	5.10			
6600—6700	5.18	7.54	5.99			
6700—6800	5.39	8.81	6.67			
6800—6900		7.74	11.16	9, 61		
6900—7000		6.44	10.46	7, 64		
7000—7100		7.54	10.57	8.63		
7100—7200		11.91	16.18	12.45		
7200—7300		9.59	10.72	9.28		

Аналитическая  
 характеристика  
 работы  
 АЛТГИ-РМ  
 в  
 Бытовых  
 условиях

Table III, 20

ТАБЛИЦА III, 20

Диагноз Л.О.П.Г	Интервал		Интервал 7:00—7:16 ч		Интервал		Интервал 7:16—8:28 ч		Интервал		Интервал 8:28—8:54 ч	
	Проколка, м	Число рейсов переборки периода часов	На один рейс		Проколка, м	Число рейсов периода часов	На один рейс		Проколка, м	Число рейсов периода часов	На один рейс	
			Межре- монтный период, ч	время ме- ханическо- го бурения,			Межре- монтный период, ч	время ме- ханическо- го бурения,			Межре- монтный период, ч	время ме- ханическо- го бурения,
ЗА714С	—	—	—	—	113,7	15	7,6	2,1	20,0	54	—	—
ЗА7Ш	168,0	16	10,5	4,9	27,7	308,3	50	6,2	21,9	—	5,5	2,7
ЗА7+шил.2	—	—	—	—	—	80,8	11	7,4	1,7	35,1	—	—
ЗА7Г+шил.2	—	—	—	—	—	—	—	—	—	48,3	7	—
ЗА7ГТИ	—	—	—	—	—	—	—	—	—	189,7	31	—
ЗА7ГТИ-1	—	—	—	—	—	—	—	—	—	—	—	—
4А714И	—	—	—	—	—	—	—	—	—	101,1	11	—
Л2-172М	—	—	—	—	—	—	—	—	—	—	7,2	—
А714-РМ	—	—	—	—	—	—	—	—	—	—	6,7	15,0
А7ГТИ-РМ	—	—	—	—	—	—	—	—	—	171,7	17	—

Диагноз Л.О.П.Г	Интервал		Интервал 9:11—9:51 ч		Интервал		Интервал 9:51—10:38 ч		Интервал		ПРОДОЛЖЕНИЕ ТАБЛ. III, 20	
	Проколка, м	Число рейсов	На один рейс		Проколка, м	Число рейсов	На один рейс		Проколка, м	Число рейсов	На один рейс	
			Межре- монтный период, ч	время ме- ханическо- го бурения,			Межре- монтный период, ч	время ме- ханическо- го бурения,			Межре- монтный период, ч	время ме- ханическо- го бурения,
ЗА714С	—	—	—	—	—	—	—	—	—	—	—	—
ЗА7Ш	41,1	7	5,9	3,5	—	—	23,7	—	5	5,7	—	10,9
ЗА7+шил.2	—	22	8,1	2,9	—	—	66,1	—	9	7,3	—	35,3
ЗА7Г+шил.2	178,0	—	—	—	—	—	—	—	—	—	—	—
ЗА7ГТИ	—	—	—	—	—	—	—	—	—	—	—	—
ЗА7ГТИ-1	—	—	—	—	—	—	—	—	—	—	—	—
4А714И	200,6	21	9,6	2,7	—	—	30,8	—	—	—	—	—
Л2-172М	220,6	22	10,0	3,5	—	—	30,9	—	—	—	—	—
А714-РМ	29,8	6	5,0	2,4	—	—	13,4	—	—	—	—	—
А7ГТИ-РМ	114,8	14	8,2	4,2	—	—	25,7	—	88	8,8	—	22,4

Table III.21

Number of pipe sets (from bottom)	Interval 7000-7700 м (100 рейсов)			Interval 8500-9200 м (120 рейсов)			Interval 9600-10700 м (95 рейсов)		
	Номер комплекта (счет ведется от з а б о я)	Положение комплекта, км	Условная работа, кН·км Conditional	Относительный износ, %	Положение комплекта, км	Условная работа, кН·км	Относительный износ, %	Положение комплекта, км	Условная работа, кН·км
1	7,5	60 000	1,10	8,75	168 000	2,8	10,00	180 500	3,2
2	7,25	87 030	1,2	8,50	193 800	3,2	9,75	213 040	3,8
3	7,0	98 000	1,2	8,25	217 800	3,4	9,50	252 700	4,6
4	6,75	168 750	2,6	8,00	384 000	4,3	9,25	360 290	5,8
5	6,5	195 000	3,1	7,75	492 900	4,8	9,0	444 600	6,5
6	6,25	231 000	3,4	7,50	576 000	5,9	8,75	548 620	8,2
7	6,00	252 000	3,8	7,25	582 900	7,3	8,50	557 170	9,1
8	65,75	258 750	4,6	7,00	596 400	10,6	8,25	595 650	9,6
9	5,5	269 000	5,3	6,75	639 900	12,2	8,00	615 600	9,8
10	5,25	299 250	6,0	6,50	702 000	13,5	7,75	677 350	10,1
11	5,00	293 000	6,2	6,25	705 000	13,0	7,50	662 620	10,3
12	4,75	289 750	5,4	6,00	698 400	12,6	7,25	654 310	9,7
13	4,50	288 000	5,1	5,75	690 000	12,0	7,00	651 700	9,5
14	4,25	276 000	5,2	5,50	679 800	11,4	6,75	641 250	8,6
15	4,00	264 000	5,0	5,25	667 800	11,0	6,50	636 020	8,2
16	3,75	247 500	4,3	5,00	660 000	11,2	6,25	623 430	8,0
17	3,50	238 000	4,1	4,75	644 100	10,8	6,00	621 300	7,4
18	3,25	237 250	3,6	4,50	626 400	9,5	5,75	617 260	7,1
19	3,00	222 000	2,4	4,25	601 800	8,7	5,50	606 100	6,7
20	2,75	209 000	2,2	4,00	585 600	8,2	5,25	588 520	6,2
21	2,50	192 500	2,0	3,75	571 500	6,3	5,00	584 250	5,6
22	2,25	180 000	1,6	3,50	554 400	5,6	4,75	577 600	5,2
23	2,00	162 000	1,2	3,25	530 400	4,8	4,50	566 020	5,0
24	—	—	—	3,00	511 200	3,9	4,25	549 100	4,6
25	—	—	—	2,75	488 400	2,8	4,00	539 600	4,1
26	—	—	—	2,50	453 000	2,6	3,75	527 250	3,9
27	—	—	—	2,25	415 800	2,1	3,50	508 720	3,2
28	—	—	—	—	—	—	3,25	481 650	2,8
29	—	—	—	—	—	—	3,0	447 450	2,4
30	—	—	—	—	—	—	2,75	413 390	2,2
31	—	—	—	—	—	—	2,5	384 750	2,0
32	—	—	—	—	—	—	2,25	350 550	1,9
33	—	—	—	—	—	—	2,0	311 600	1,8

Data on usage of drill pipes on the first stage of  
drilling (to 7263 m)

ТАБЛИЦА III.22

СВОДНЫЕ ДАННЫЕ ПО РАСХОДУ БУРИЛЬНЫХ ТРУБ НА ПЕРВОМ ЭТАПЕ БУРЕНИЯ СГ-3  
ДО ГЛУБИНЫ 7263 М

Показатели Indices	ЛБТ-147x11 ЛБТ-147x11	ЛБТ-147x13 ЛБТ-147x13	ЛБТ-147x15 ЛБТ-147x15	СБТ СБТ
pipes used				
Использовано труб и т	19 025 310	4314 77	1525 25	7659 288
Отбраковано или переведено в нижний класс по причине: поворота в трубной резьбе и т	4 277 68	4314 77	— —	— —
износа замковой резьбы и т	14 748 242	— —	— —	7959 288
износа тела или утолщения, и Средняя наработка труб, рейс Расход металла на 1 м про- ходки, кг	— 365 42,3	— 150 32,0	1525 108 52,4	— — 40
<i>average work number of pipe Usage of metal per 1 m of penetration</i>				

Примечание. В расход труб на 1 м проходки не включены 4277 м ЛБТ 147x11 мм и  
2260 м ЛБТ 147x13 мм из-за малой наработки и массового выхода их из строя в результате  
поворота замков в трубной резьбе.

Data on usage of drill pipes on the second stage of drilling  
(7263-11500 m)

ТАБЛИЦА III.23

СВОДНЫЕ ДАННЫЕ ПО РАСХОДУ БУРИЛЬНЫХ ТРУБ НА ВТОРОМ ЭТАПЕ БУРЕНИЯ  
СГ-3\_8 ИНТЕРВАЛЕ 7 263-11 500 М

Показатели	ЛБТВК-147 (Д167) ЛБТВК-147	ЛБТВК-147 (Ш1953) ЛБТВК-147	ЛБТВК-147 (АКУ-1) ЛБТВК-147	СБТ СБТ
pipes used	(Д167)	(Ш1953)	(АКУ-1)	
Использовано труб и т	19 200 306	15 100 256	5900 89	7700 252
Отбраковано или переведено в нижний класс по причине: износа замковой резьбы и т	4 922 77	15 100 256	— —	1550 50
износа тела или замка и т	9 644 153	— —	5900 89	6150 202
эррозионного размыва, и Средняя наработка труб, рейс Расход труб на 1 м проход- ки, кг	4 434 291 72	— 367 60	— 250 20,9	— 470 59,3

The same

ТАБЛИЦА III.24

Номер станин Number of stand	Длина буриль- ной колонны. Length of the string,	Loading at the hook, кН Нагрузка на крюке, кН		Расчетный вес колонны, кН Calculated weight of string, kN	Скорость подъема, м/с Speed of pulling out	Силы сопро- тивления, кН Resistance forces, kN
		по прибору measured	с учетом к. п. з. тяговой системы with correction of slack and traction system			
268	9990	2600	2670	1550	0.3	1120
265	9866	2680	2760	1510	1.0	1250
260	9681	2600	2670	1450	1.0	1220
255	9495	2500	2560	1390	1.0	1170
250	9308	2360	2410	1330	1.0	1080
245	9121	2220	2250	1270	1.0	980
240	8934	2120	2140	1200	1.0	940
235	8749	2040	2060	1160	1.0	900
230	8564	2000	2010	1130	1.0	880
225	8378	1900	1900	1100	1.0	800
220	8193	1830	1830	1070	1.0	760
215	8006	1750	1740	1040	1.0	700
210	7818	1680	1660	1020	1.0	640
205	7633	1620	1600	990	1.0	610
200	7445	1560	1530	960	1.0	570
195	7258	1500	1470	930	1.0	540
190	7074	1460	1420	910	1.0	510
185	6889	1400	1360	880	1.0	480
180	6705	1340	1290	860	1.0	430
175	6514	1300	1250	830	1.0	420
170	6333	1260	1200	810	1.0	390
165	6145	1240	1180	780	1.0	400
160	5960	1160	1090	760	1.0	330
155	5772	1120	1050	740	1.0	310
150	5587	1080	1010	740	1.0	300
145	5400	1050	970	690	1.0	280
140	5212	1030	950	670	1.0	280
135	5027	990	910	650	1.0	260
130	4840	950	860	620	1.0	240
125	4654	910	820	600	1.0	220
120	4463	880	790	580	1.0	210
115	4277	850	750	560	1.0	190
110	4090	820	720	530	1.0	190
105	3902	790	690	510	1.0	180
100	3715	760	660	490	1.0	170
95	3528	710	600	470	1.0	130
90	3343	680	590	440	1.0	130
85	3163	660	550	420	1.0	130
80	2980	630	510	390	1.0	120
75	2798	600	480	370	1.0	110
70	2616	580	460	340	1.0	120
65	2434	550	430	310	1.0	120
60	2250	510	380	290	1.0	90
55	2069	480	350	270	1.0	80

ТАБЛИЦА III.27

Длина каната, м Length of wire line, m	Интервал бурения, м Interval of drilling, m	Число выполненных рейсов Number of runs	Средняя наработка талевого каната, кН·км Average work of wire line, kN·km	Расход талевого каната, м Usage of wire line, m	
				на один рейс per run	на 1 м проходки per 1 m of penetration
8 850	7 284—8 010	200	495 620	44,3	12,2
13 084	8 010—9 025	219	425 920	59,7	13,0
10 806	9 025—9 993	157	487 800	68,8	11,2
13 406	9 993—11 059	180	490 100	74,5	12,6
3 192	11 059—11 514	36	516 880	88,7	7,00
49 338	7 284—11 514	792	489 870	62,3	11,7

## СОРИНГ

(a) Interval of drilling, m	Интервал бурения, м . . .	0—500	500—1000	1000—1500	1500—2000	2000—2500	2500—3000	3000—3500	3500—4000	4000—4500	4500—6179—6202
(b) Average length of a column of core	Средняя длина столбика, см	13,4	11	17,4	13,1	17,1	13,9	23,9	19,7	17,8	8,9
a	Интервал бурения, м . . .	6202—6300	6300—6403	6403—6411	7233—7299	7324—7410	7410—7508	7508—7558	7637—7647	7706—7809	7813—7902
b	Средняя длина столбика, см	6,7	6,6	7,8	5,9	3,9	4,5	3,6	4,9	3,8	4,3
a	Интервал бурения, м . . .	7902—8007	8007—8101	8101—8190	8202—8302	8302—8400	8400—8494	8522—8589	8618—8701	8710—8803	8803—8901
b	Средняя длина столбика, см	8	6,5	2,8	5,2	7,3	6	5	4,5	8,3	8,9
a	Интервал бурения, м . . .	8901—9003	9003—9103	9103—9202	9202—9299	9303—9404	9404—9510	9510—9610	9610—9682	9902—10 000	
b	Средняя длина столбика, см	3,7	3,9	4,3	2	1,8	2,7	2,2	2,2	2,5	2,2
a	Интервал бурения, м . . .	10 001—10 105	10 105—10 202	10 202—10 301	10 301—10 360	10 424—10 502	10 502—10 608	10 608—10 703	10 703—10 760		
b	Средняя длина столбика, см	2,5	1,9	2	1,8	1,7	1,9	0,7	0,6		

## Соринг

ТАБЛИЦА III.28

Интервал бурения, м Interval of drilling, m	Номер участка locality	Number of runs	Number of runs	Проходка, м penetration, m	Вынос керна		Average per run, m В среднем за рейс, м	
					m	%	penetration проходка	вынос керна coreing
0—1 059		108		942	386	41,0	8,7	3,6
1 059—2 805	1	239		1674	913	54,5	7,0	3,8
2 805—4 673		265		1570	940	59,7	5,9	3,5
Итого:		612		4186	2239	53,4	6,8	3,7
4 673—5 624		80		644	103	16,0	8,1	1,3
5 642—6 823	2	125		865	260	30,1	6,9	2,1
6 823—7 263		35		334,7	46,8	14,0	9,6	1,3
Итого:		240		1843,7	409,8	22	7,7	1,7
7 263—7 943	3	39		291,3	103,8	36,3	7,5	2,7
8043—9008,4		105		742,5	308,1	41,4	7,1	2,9
Итого:		144		1033,8	413,9	40	7,2	2,9
9008,4—10 028		104		835,8	248,3	30	8,0	2,4
10 028—10 772	4	56		612,2	163,9	26,8	10,9	2,9
10 772—11 500		61		723,7	225,2	31,1	11,9	3,7
Итого:		221		2171,7	637,4	29	9,8	2,9
Всего		1217		9235,2	3700,1	40,1	—	—

straight circulation  
through core barrel

ТАБЛИЦА III.29

Показатели indexes	КДМ-195-214/60 КДМ-195-214/60						КТД4-195-2М/60-80 КТД-195-2М/60-80	
	Прямая промывка через грунтоноску			Обратная промывка Reverse circulation		Без про- мывки, грунтонос- ка заполне- на смазкой		
	обыч- ную и usual	конус- ную cone- shaped	шлифо- ванную пластин- ными polished	корпус диаметром 195 мм, обычная грунтонос- ка, расход 1-2 л/с.	корпус диаметром 203 мм, обычная грунтонос- ка, расход 6-8 л/с			
① Число рейсов	11	9	5	29	8	6	4	
② Общая проходка, м	75,4	64,8	47	238,5	75,3	39,1	28,3	
③ Общий вынос керна, м	9,84	12,2	16,7	95,25	39,85	15,9	5,65	
④ Проходка за рейс, м	6,83	7,2	9,4	8,2	9,4	6,5	2,0	
⑤ Вынос керна за рейс, м	0,89	1,35	3,34	3,3	5	2,65	1,4	

Body diameter 203 mm,  
Usual core barrel, flow  
6-8 l/sec

Body diameter 195 mm,  
usual core barrel,  
flow 1-2 l/sec

① Number of runs (roundtrips)

② Total penetration

③ Total core recovery

m

%

④ Penetration per run, m

⑤ Core recovery per run, %

Core did not come to the case

ТАБЛИЦА III.31

Интервал бурения, м	Керн не поступал в камеру						Керн поступал в камеру -Core came to the case					
	в интервале in interval			за рейс per run			в интервале in interval			за рейс per run		
	N	H, м	L <sub>K</sub> , м	H, м	I, м	вынос керна, % plugs	N	H, м	L <sub>K</sub> , м	H, м	I, м	вынос керна, % - coring %
7469,4—7943,0	19	142,4	45,6	7,5	2,4	32	6	49,6	30,8	8,3	5,1	62
8043,0—8465,8	23	154,2	33,4	6,7	1,5	22	10	72,2	57,3	7,2	5,7	79
8506,5—9008,4	10	71,6	22,4	7,2	2,2	31	10	103,9	79,5	10,4	8,0	77
9008,4—9344,4	26	197,3	34,3	7,6	1,3	17	11	77,9	57,2	7,1	5,2	73
9344,4—9651,0	20	234,4	34,8	11,7	1,7	15	4	45,6	23,6	11,4	5,8	51
Total Итого	98	799,9	170,5	8,2	1,7	21	41	349,2	248,4	8,5	6,1	71

Примечание. Обозначения те же, что и в табл. III.30. — The same as in Table III.30

in interval

per run

KU-195

KU-195

MA6-MA5-214/60, SKU-195/80

MA6-MA5-214/60, SKU-195/80

MA6-MA5-214/60, SKU-195/80

MA6-MA5-214/60, SKU-195/80

Interval borehole, m drilling, m	KU-195				KU-195				KU-195				KU-195						
	B интервал				За речь				B интервал				за речь						
	N	H, м	L <sub>k</sub> , м	h, м	N	H, м	L <sub>k</sub> , м	h, м	N	H, м	L <sub>k</sub> , м	h, м	N	H, м	L <sub>k</sub> , м	h, м			
7469.4—7943	1	5,1	3,2	5,1	3,2	61	14	99,3	29,5	7,1	2,1	30	25	192	76,3	7,7	3,1	40	
8 043—8465,8	2	12,6	2,2	6,3	1,1	17	13	72,6	25,8	5,6	2,0	35	33	226,4	90,7	6,9	2,8	40	
8506,5—9008,4	11	83,9	27,6	7,6	2,5	33	25	170,2	50,8	6,8	2,4	35	20	175,5	101,9	8,8	5,1	58	
9008,4—9344,4	1	9,7	2,65	9,7	2,65	27	4	33,7	2,1	8,4	0,5	6	37	275,2	91,5	7,5	2,5	33	
9344,4—9 651	—	—	—	—	—	—	—	—	—	—	—	—	24	280	68	11,7	2,4	21	
9 738—9 910	1	7,3	0,4	7,3	0,4	5	6	47,3	2,2	7,9	0,4	5	8	66,9	30,5	8,4	4,2	50	
9 918—10 028	—	—	—	—	—	—	—	—	—	—	—	—	22	104,4	55,8	4,8	2,5	54	
10 028—10 136	—	—	—	—	—	—	—	—	—	—	—	—	12	106,3	26,3	8,9	2,2	25	
10 136—10 243	—	—	—	—	—	—	—	—	—	—	—	—	10	100,9	41,6	10,1	4,2	41	
10 248—10 360	—	—	—	—	—	—	—	—	—	—	—	—	8	102,7	34,6	12,8	4,0	31	
10 427—10 622	—	—	—	—	—	—	—	1	12,7	0	12,7	0	0	14	174,3	39,7	12,3	3	24
10 656—10 772	—	—	—	—	—	—	—	4	31,3	0,6	7,8	0,15	2	7	82,1	26,7	11,7	3,8	33
10 633—10 792	—	—	—	—	—	—	—	—	—	—	—	—	12	132,2	34,3	11	2,9	26	
10 800—11 003	—	—	—	—	—	—	—	—	—	—	—	—	12	147,2	37,1	12,3	3,1	25	
11 003—11 254	—	—	—	—	—	—	—	—	—	—	—	—	14	180,3	49,2	12,9	3,5	27	
11 254—11 499	—	—	—	—	—	—	—	—	—	—	—	—	16	185,4	73	11,6	4,6	39	

Причины. N — число речек; H — общая проколка; L<sub>k</sub> — средняя проколка на речке; h — плюс кернок; t — средний проникновение керна в речке.

N — number of runs; N — number of rivers; H — total penetration; L<sub>k</sub> — coring; h — average penetration per river;

t — average coring per run

0 2 4 6 км

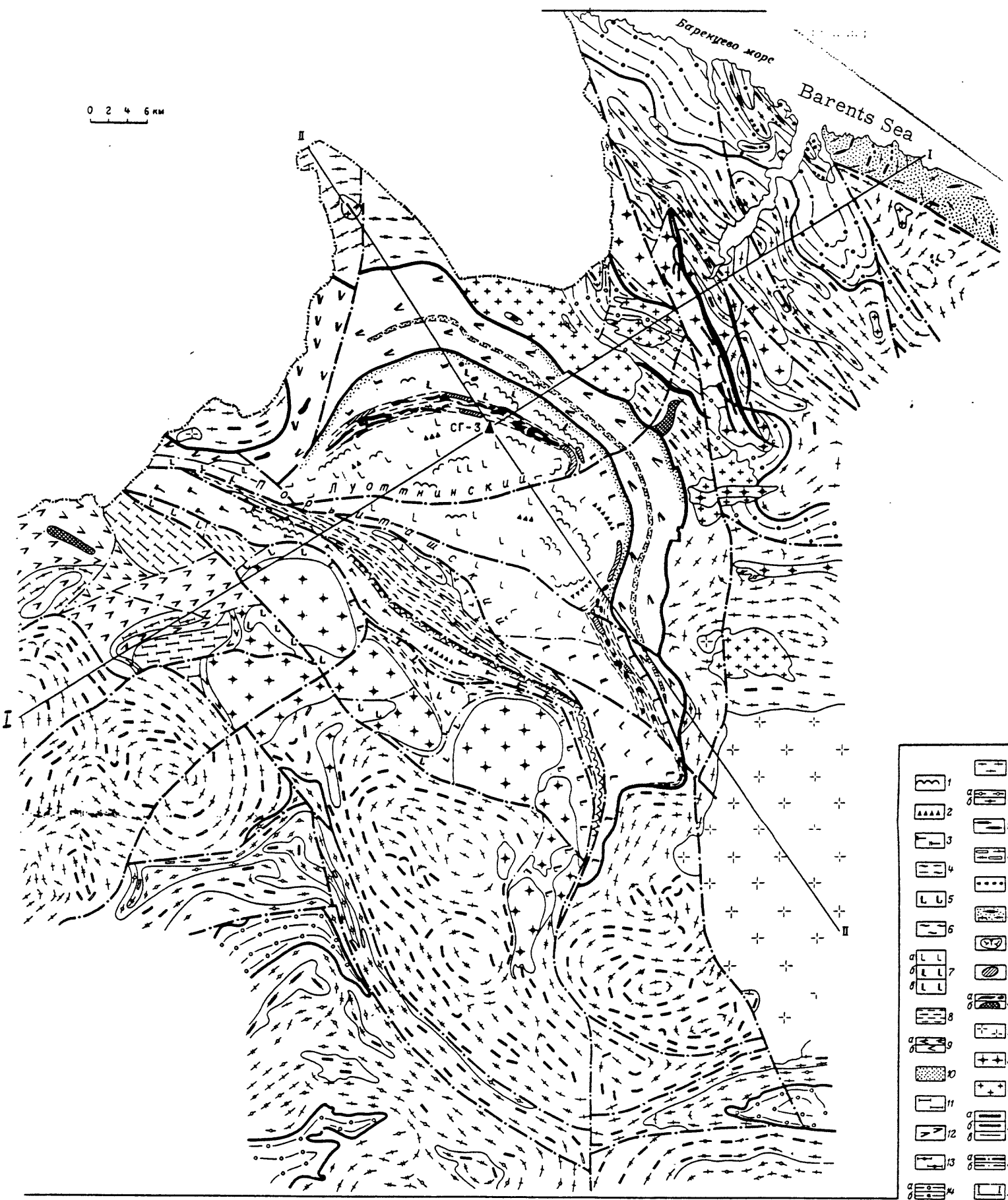


Figure I.8

Figure I.8. Geological map of the Pechenga region (after Lanev, Nalivkina, Rusanov, and Suslova).

Pechenga complex (Lower Proterozoic): 1 - tuffs and sedimentary-tuffaceous rocks of different composition and shales; 2 - volcanites of basite-hyperbasite and hyperbasite composition and shales. Southern zone, the Por'itash beds - Shovnyy tectonic block: 3 - andesitic, andesite-basaltic metaporphyrites-schists and actinolitic amphibolites; 4 - argillaceous tuffites, phyllites, siltstones, sandstones and shales; Russel beds - block of granite domes 5 - amphibolite and amphibole-plagioclase schists with tholeiitic basalts; 6 - varied gneisses and schists with argillaceous material in sedimentary and tuffogenic-sedimentary rocks. Northern zone, nickel series: 7 - metamorphosed tholeiitic basalts (a - diabases, b - metadiabases and greenschists, c - amphibolites and amphibole-plagioclase schists); 8 - argillaceous phyllites, tuffites, siltstones, sandstones; Luostarinskiy Series: 9 - metamorphosed trachybasalts. trachyandesites, andesite-basalts (a - metadiabases, metaleucodiabases, metaandesites, greenschists, b - amphibolites, amphibole-biotite-plagioclase and biotite-plagioclase schists); 10 - metasandstones, metaconglomerates, quartzetic-sandstones, dolomites; Tundra series (Lower Proterozoic - Upper Archean): 11 - Tal'inskaya suite - mica-chlorite-actinolite feldspathic and mica-quartz-feldspathic schists and gneisses, frequently with granite; 12, 13 -

Kaskamskaya suite (12 - amphibolites, frequently with granite, 13 - biotite-garnet-amphibole-feldspathic schists and gneisses). Kola-White Sea complex (Archean), Kola series, upper formation 14 - biotite-plagioclase gneisses with VGM (a - without cordierite, b - with cordierite); middle formation: 15 - biotite-plagioclase and amphibole-biotite-plagioclase gneisses and migmatites; 16 - biotite-plagioclase gneisses with VGM (a - without cordierite, b - with cordierite); 17 - amphibole-biotite-plagioclase gneisses with pyroxene and pyroxene-amphibolites and amphibole crystalline schists; 19 - quartz-magnetite schists; lower formation (Basement complex): 20 - amphibolites, pyroxene-amphibole-plagioclase schists, gneisses, granite gneisses, chainockite and enderbite. Intrusive formations: 21 - andesite-dacite (diorites); 22 - diabases and gabbro-diabases; 23 - differentiated basite-hyperbasites (a - gabbro-wehrlites, b - gabbro-norites); 24 - microcline granites; 25 - microcline-plagioclase granites, granodiorites and diorites; 26 - plagiogranites and migmatites; 27 - geologic boundaries (a - complexes, b - formations, series); 28 - principal tectonic disturbances; 29 - block diagram section line.

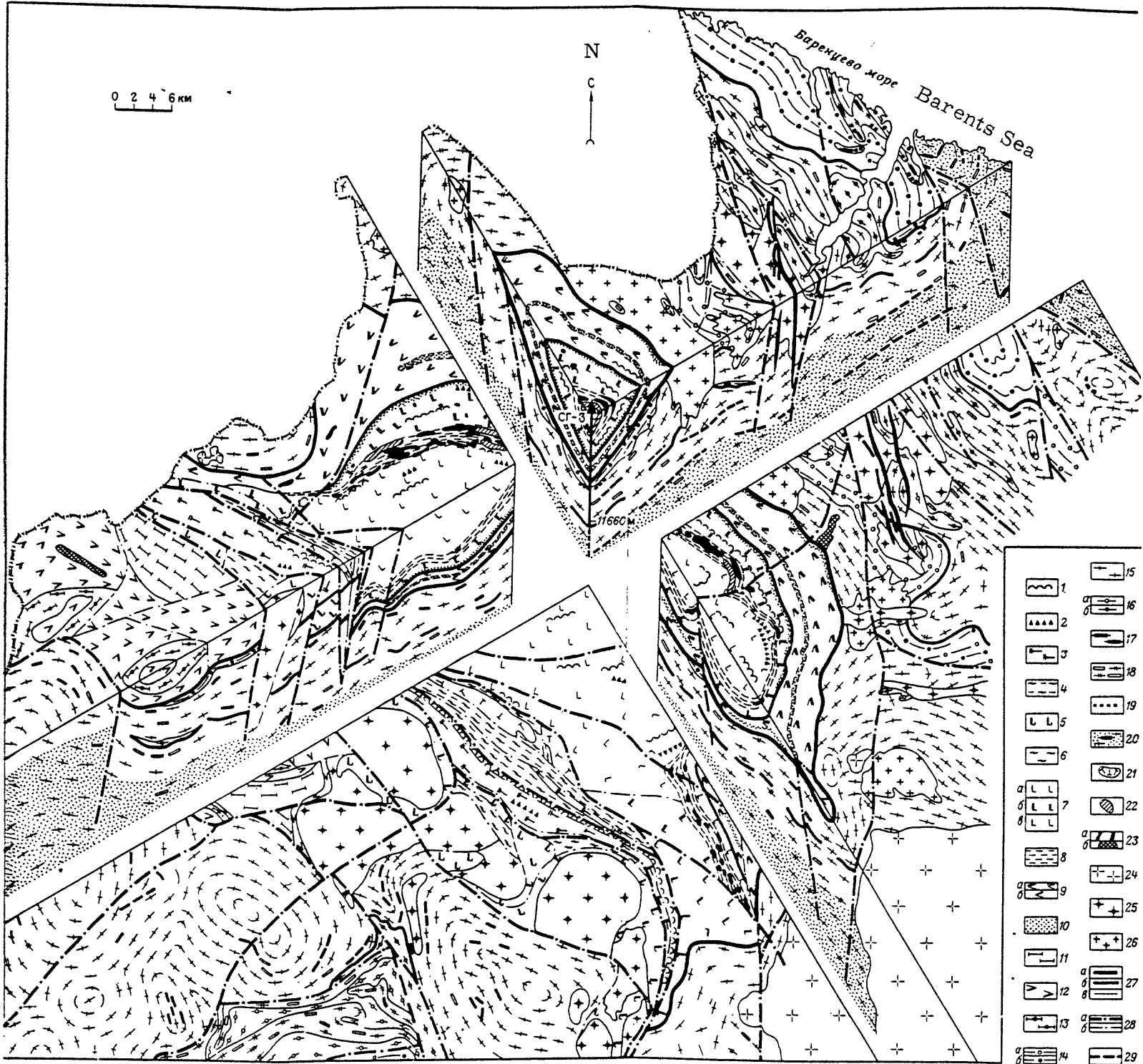


Figure I. 80

Figure I.80. Geologic block diagram of SG-3 drillhole region

Pechenga complex (Lower Proterozoic): 1 - tuffs and sedimentary-tuffaceous rocks of different composition and shales; volcanites of basite-hyperbasite and hyperbasite composition and shales. Southern zone, Por'itash Formation - Shovnyy tectonic block: 3 - andesitic, andesite-basaltic, basaltic metaporphyrites-schists and actinolitic amphibolites; 4 - argillaceous tuffites, phyllites, siltstones, sandstones and schists; Russel formation - block of granite domes: 5 - amphibolites and amphibole-plagioclase schists with tholeiitic basalts; 6 - varied gneisses and argillaceous schists and sedimentary and tuffogenic-sedimentary rocks: Northern zone, nickel series: 7 - metamorphosed tholeiitic basalts (a - diabases, b - metadiabases and greenschists, c - amphibolites and amphibolite-plagioclase schists); 8 - argillaceous phyllites, tuffites, siltstones, and sandstones; Luostarinskaya series: 9 - metamorphosed trachybasalts, trachyandesites, andesite-basalts (a - metadiabases, metaleucodiabases, metaandesites, greenschists, b - amphibolites, amphibole-biotite-plagioclase and biotite-plagioclase schists); 10 - metasandstones, metaconglomerates, quartzitic-sandstones, dolomites; Tundra series (Lower Proterozoic-Upper Archean): 11 - Taljinskaya suite - micaceous-chlorite-actinolite-feldspathic and micaceous-quartz-feldspathic schists and gneisses, frequently with granite; 12, 13 -

Kaskamskaya suite (12 - amphibolites, frequently with granite; 13 - biotite-garnet-amphibole-feldspathic schists and gneisses). Kola-White Sea complex (Archean), Kola series, upper formation: 14 - biotite-plagioclase gneisses with VGM (a - without cordierite, b - with cordierite); middle formation: 15 - biotite-plagioclase and amphibole-biotite-plagioclase gneisses migmatites; 16 - biotite-plagioclase gneisses with aluminiferous minerals (a - without cordierite, b - with cordierite); 17 - amphibole-biotite-plagioclase crystalline schists; 18 - amphibolites and amphibole crystalline schists; 19 - quartz-magnetite schists; lower formation (Basement complex): 20 - amphibolites, pyroxene-amphibole-plagioclase schists, gneisses, granite gneisses, charnockite, enderbite. Intrusive formations: 21 - andesite-dacites (diorites); 22 - diabases and gabbro diabases; 23 - differentiated basite-hyperbasites (a - gabbro-wehrlites, b - gabbro-norites); 24 - microcline granites; 25 - microcline-plagioclase granites, granodiorites and diorites; 26 - plagiogranites and migmatites; 27 - geologic boundaries (a - complexes, b - formations, series); 28 - principal tectonic disturbances; 29 - conversion points and boundaries of divergent waves (PS).